Evaluation and Optimization of Sol-Gel Coatings for Oil and Gas Applications

Tiphaine Muguette Emilienne Lutzler

Submitted in accordance with the requirements for the degree of

Doctor of Philosophy

The University of Leeds

Institute of Functional Surfaces

School of Mechanical Engineering,

November 2018

The candidate confirms that the work submitted is her own, except where work which has formed part of jointly-authored publications has been included. The contribution of the candidate and the other authors to this work has been explicitly indicated below. The candidate confirms that appropriate credit has been given within the thesis where reference has been made to the work of others.

Thesis related publications

Journal papers

Lutzler, T., Charpentier, T.V.J., Barker, R., Soltanahmadi, S., Taleb, W., Wang, C., Alejo-Rodriguez, A., Perre, E., Schneider, H., Neville, A., *Evaluation and Characterization of Anti-Corrosion Properties of Sol-Gel Coating in CO_2 Environments.* Materials Chemistry and Physics, 2018. **216**: p. 272-277.

Key conference presentations

Lutzler, T., Charpentier, T., Pfeifer, S., Schneider, H., Neville, A., *Evaluation and optimization of sol-gel coatings for oil and gas applications*, 57th Corrosion Science Symposium, Swansea, United Kingdom, September 2016

Lutzler, T., Charpentier, T., Pfeifer, S., Schneider, H., Neville, A., *Evaluation and optimization of sol-gel coatings for oil and gas applications*, European Corrosion Congress 2016: Advances in linking science to engineering, Montpellier, France, September 2016

Lutzler, T., Alejo-Rodriguez, A., Charpentier, T., Schneider, H., Neville, A., *Improvement of sol-gel coatings and their anti-corrosion properties by doping with Titanium precursors*, 58th Corrosion Science Symposium/ Electrochem 2017, Birmingham, United Kingdom, September 2017

Lutzler, T., Alejo-Rodriguez, A., Charpentier, T., Schneider, H., Neville, A., *Improvement of sol-gel coatings and their anti-corrosion properties by doping with Titanium precursors*, European Corrosion Congress 2017/ 20th International Corrosion Congress , Prague, Czech Republic, September 2017

Acknowledgements

I would like to express my deepest gratitude to my supervisors, Professor Anne Neville and Doctor Thibaut Charpentier, for giving me the opportunity to work with them, their amazing and continued support, encouragement, advice and patience throughout my study period.

A special thanks to the EPG-AG team in Henriville for providing financial support and the opportunity of this PhD study.

Many thanks to the technical and administrative staff of the Mechanical Engineering Department: Fiona, Mick, Jordan, Andrew and Paul for their involvement and contribution. Besides, I would like to also thank my colleagues of the iFS for their expertise and technical support.

I also appreciate the support from my friends in Leeds and abroad, these several years would have been different and even more difficult without them: Audrey, Marion, Magalie, Justine, Sue, MX, Kevin, JinA and the others. Special thanks to Marjorie and Adam for helping me so much during the writing-up of the thesis.

Last but certainly not least, I would like to thank my parents. Their endless love and support allowed me to keep moving forward. Without their encouragement, I would not have been able to finish this study. (Also thank you so much for the care packages of French food, very much needed). Merci.

To S.B.

Abstract

Corrosion is a major oilfield flow assurance problem with coatings being commonly used by industry as a barrier to electrochemically active species. In recent years, studies on sol-gel materials have drawn an increased interest, gaining more recognition as an alternative to conventional coatings due to many promising properties.

In this project different sol-gel coatings were developed and studied in order to optimize their physicochemical properties with particular attention to their corrosion resistance. To evaluate the protective properties metal coupons (stainless steel and carbon steel) coated with inorganic/hybrid, organic and hybrid/composite coatings were subjected to a mildly corrosive environment at first. Then the focus of the second batch was on non-functionalised inorganic/hybrid coatings and other inorganic/hybrid coatings with the same sol-gel structure and composition but in addition doped with a titanium precursor. The doped coatings were prepared by hydrolysis of a titanium butoxide through the sol-gel process. The purpose of this batch was to evaluate the advantages of titanium butoxide and the influence of its concentration on its properties. In the final batch the focus was on the link between parameters such as curing process and solvent used during the sol-gel mechanism to the corrosion behaviour. The purpose was to investigate the effect of the solvent as well as the curing process on the anti-corrosion properties of the different coatings.

Several methods, chemical and mechanical, were used throughout the project to identify and analyze the results obtained and improved the coatings. The EIS data could be linked to the corrosion progress while being compared to the evolution of spectra from FTIR data. The impedance spectroscopy also gave information on the water intake. The substrate proved to have an influence on the adhesion of the coating as opposition to the amount of precursor added. The doping with a titanium precursor led to coatings with improved anti-corrosion properties but only within a certain percentage range (between 0% and 6% but less than 10%). There seem to be a limit to the amount of titanium allowing the anti-corrosive properties to protect the substrate.

Table of Contents

List of Tables

List of Figures

List of Abbreviations

AC: Alternating Current

AEAPS: 3-(2-Aminoethyl)aminopropyl trimethoxysilane

APS: 3-Aminopropyl trimethoxysilane

BTSTS: Bis-[3-(triethoxysilyl)-propyl]tetrasulfide

BuOH: Butanol

C_c: Coating Capacitance

CE: Counter Electrode

C_{dl}: Double Layer Capacitance

Ceramer: Ceramic polymer

CPE: Constant Phase Element

CVD: Chemical Vapour Deposition

DC: Direct Current

EDL: Electrical Double Layer

EDX: Energy Dispersive X-Ray Spectroscopy

EIS: Electrochemical Impedance Spectroscopy

EtOH: Ethanol

FIB-SEM: Focus Ion Beam- Scanning Electron Microscope

FTIR: Fourier-Transform Infrared Spectroscopy

GPTES: Glycidoxypropyl triethoxysilane

GPTMS: 3-Glycidoxypropyl trimethoxysilane

IEP: Isoelectric Point

IpOH: Isopropyl Alcohol

MAPTS: γ-Methacryloxypropyl trimethoxysilane

MTEOS/MTES: Methyl triethoxysilane

MPTMS: γ-Mercaptopropyl trimethoxysilane

MTMS: Methyl trimethoxysilane

NHE: Normal Hydrogen Electrode

OCP: Open Circuit Potential

Ormocer: Organic Modified Ceramic

Ormosil: Organic Modified Silicate

PHS: Diethylphosphonatoethyl triethoxysilane

PTMS: Phenyl trimethoxysilane

PVD: Physical Vapour Deposition

PZC: Point of Zero Charge

R_c: Coating Resistance

RE: Reference Electrode

R_{ct}: Charge Transfer Resistance

R_p: Polarization Resistance

R_s: Solution resistance

SCC: Stress Corrosion Cracking

SEM: Scanning Electron Microscopy

TEOS: Tetraethyl orthosilicate

TMOS: Tetramethyl orthosilicate

TWL: Total Weight Loss

VTMS: Vinyl trimethoxysilane

WE: Working Electrode

Chapter I. Introduction

1.1 Introduction and Background of the Research

Metallic materials are widely used in many industrial fields (e.g., automotive, aeronautics, marine, petroleum industry, etc.) but can corrode when exposed to an aggressive environment. Corrosion is one of the main contributors of material loss in our society. Corrosion is partly responsible for about 25% of failures experienced in the oil and gas production industry, while more than 50% of failures are associated with sweet (presence of CO_2) and sour (presence of H_2S) corrosions in pipelines [1]. This major risk in oil and gas production requires the understanding of the failure mechanism and procedures for assessment and control [2]. Fluid flowing from oil and gas pipelines has a combination of chemicals such as (but not limited to) CO_2, H_2S, organic acids, bacteria and water. These constituents are among the major causes of corrosion in pipeline [2].

In some cases metals used for construction purposes are inadequate when exposed to the atmosphere. With the help of a coating, a longer period of time is required for corrosion to form on the substrate. Thus it is important that the coating material is selected for an application in a specific environment. Actual studies are working on the improvement and enhancement of the lifetime against corrosion and coatings can help to manage corrosion.

Several methods are known to control corrosion [3]. The selection of the substrate is important as the corrosion resistance of a metal depends on its corrosion behaviour as well as the environment (chemical composition, temperature…). Inhibitors are chemical compounds which allow lessening the corrosion rate of a material when added to a liquid or a gas. Protective coatings are well-known and used for corrosion protection (e.g., sol-gel, epoxy resins) as they create a physical barrier between the metallic substrate and the environment.

Inhibitors are sometimes used in addition to coatings in order to avoid corrosion but they are not used in the current project and thus will not be developed. Other common types of coatings used in oil and gas environment are shown in Table 1.1.

Table 1.1 Main coatings used for corrosion protection [4, 5]

Type of coating	Property	Drawback
Fluoropolymer	Corrosion protection/extension of component life	Can be damaged during the assembly of fasteners in the field and high melt viscosity
Epoxy	Corrosion resistant/ high impact and chemical resistance	Expensive and relatively brittle if epoxy phenolic
Sol-gel	Scratching/abrasion resistance and thermal stability	Porosity
Polyurethane	Chemical resistant/ Water and humidity resistant	Adhesion

Sol-gel technologies were developed during the past 50 years as an alternative for the preparation of glasses and ceramics at considerably lower temperatures. Sol-gel synthesis becomes, however, much more interesting for highly advanced ceramic materials [6-8]. Sol-gel coatings were created after the issue of chromate coatings, proved as really effective for corrosion protection but it was discovered that hexavalent chromium compound, the chemical most widely used in the immersion bath process, is highly toxic. Sol-gel process generally consists of thin films deposited on solid substrates from a liquid solution (sol) turning into a gel. These thin films find their application for different fields such as modifying the reflectivity of the substrate's surface, altering its rigidity or modifying its surface chemistry [9].

Design can also help to reduce corrosion problems, cost and time. Corrosion generally occurs in cracks or fissures, spaces where the corrosive element becomes more damaging. These areas can be eliminated or minimized in the design process [3]. The use of coatings is particularly recommended in aggressive environment. Ceramic films can be used to improve the resistance against high temperature oxidation and corrosion of metals. Among the different ways of controlling corrosion, the sol-gel process is a less expensive, simple and non-hazardous method for processing ceramic coatings with control over the composition and the microstructure [10]. A more generic approach to enhance corrosion resistance is to apply protective films or coatings such as paint. Coatings are often used as a protective layer over the metal substrate to prevent the substrate from oxidizing, acting as a barrier, hindering the flow of current which is essential to link the areas of anodic and cathodic activity on the substrate [11]. This mostly takes place if the coating wets the surface of the substrate and then adheres well in the presence of electrolyte and water. Coatings do not really stop oxygen sufficiently to make its

concentration at the surface rate limiting, and they do not completely stop water ingress into coatings. However, an efficient coating which acts as a barrier slows the penetration of water and electrolyte while remaining in place at the substrate/coating interface.

That is why the sol-gel process has been more and more used in the last decades. It is essential not to forget the properties of both the substrate and coating as well as the properties of the final combination. Therefore the choice of the substrate and of the coating has a considerable interest and must be fully taken into consideration.

The close control of parameters of the sol–gel reactions leads to the design of new advanced materials with interesting properties for many applications. Materials with different compositions can be easily obtained in the form of glasses, fibres, ceramic powders and thin films [12].

There is an increasing technological need to protect metallic structures in aggressive environments such as acidic or oxidizing environments. Metallic materials are widely used in all kinds of industrial fields (i.e. automotive, aeronautics, marine, petroleum industry) but can corrode in aggressive environments. Several methods are known to control deterioration [6, 13]. In that regard, the protection of metallic materials is one of the most promising applications of sol-gel coatings. The close control of parameters of sol-gel reactions leads to the design of new advanced materials with interesting properties for many applications. Sol-gel synthesis offers a great potential for corrosion protection for advanced ceramic materials [6].

By means of a coating, a longer period of time is required for rust to form on the substrate. Therefore it is important that the proper coating material be selected for application in a specific environment.

For a coating to be effective, it must isolate the base material from the environment. The service life of the coating depends on the thickness and the chemical properties of the coating layer. To be effective, the coating’s durability must be greater than that of the base metal or it must be maintained by some means [14].

Surface preparation, which includes cleaning and pre-treatment, is the most important step in any coating operation. In order to have good adhesion, the surfaces must be free from any lose particles or corrosion products. The choice of cleaning method depends on the substrate and the size and shape of the object. To improve coating adhesion, pre-treatments are applied after cleaning [14].

1.2 Objectives of the Research

The aim of this study is to understand the structure-property relationships in order to establish the link between the coating processing parameters, the sol-gel coating compositions and corrosion behaviour. Different coatings from the sponsor company EPG-AG were studied in order to evaluate this link between their properties: hybrid/composites, organic and inorganic/hybrid silica sol-gel coatings, with or without doping (titanium butoxide in the precursor) and with different curing processes. This study also presents results for different types of coatings deposited on different substrates. The properties of both the substrate and coating are studied and corrosion as well as erosion-corrosion.

The main objectives are:

- To study the coatings of this project, which are established coatings for automotive applications, in order for them to be applied in another field.
- To link the structure of the coatings to the properties in terms of corrosion rates using surface characterisation techniques
- To use impedance spectroscopy to probe the metal/coating interface, understand the corrosion mechanism and investigate the corrosion behaviour of the coating systems in a saline environment
- To study the effect of several parameters; metal substrate, coating composition, curing process and especially the use of titanium butoxide as a dopant, on the corrosion behaviour of the coating systems.

1.3 Outline of the Thesis

This thesis is composed of nine chapters.

The second chapter includes Fundamental Theories, discussing the different types of corrosion that can happen, electrochemical reactions and how electrochemical corrosion methods work as well as the theory about the sol-gel process.

Chapter three, Literature Review, presents the subject area, its background and a summary of the current research status. It is divided into sections relevant to our subject; corrosion of coatings and the methods to evaluate this, the sol-gel coatings

literature around structure-property relationships and the general processing parameters that may affect corrosion.

The fourth chapter is Experimental Procedures and Characterisation Techniques, describing the different batches of samples, experimental techniques, methods and procedures used in this study. The pre and post-test examination procedures are also explained in this chapter. Experiments are carried out to assess the evolution of the corrosion on different types of substrates with or without coatings. Further characterisation of the materials is presented here.

Chapter five, Characterisation and Properties of the Coatings Prior to Corrosion Tests, presents results about characterisation of the samples before immersion, the samples being analysed before any experiment to obtain information on their chemistry and properties. Several analytical methods are used to present their properties.

The sixth chapter, Resistance to Corrosion and Erosion-Corrosion, presents the experimental results of the electrochemical experiments performed on the samples. The behaviour of the samples of the different batches are presented and explained with the mean of impedance plots and equivalent circuits which can be used to fit the data and thus give numerical values.

Chapter seven, Characterisation and Properties of the Coatings After Experiment, presents the results of analyses done on the samples after the immersion experiments and displays the evolution of the corrosion or of the coatings of those same samples.

Chapter eight provides a detailed Discussion as a direct response to experimental results. The principal sections in this chapter are the relation between the different methods of experiments and analyses done on the samples and the links that can be made between them. It sets out the major contribution from the thesis and links the results from this thesis with the wider literature.

The Conclusions obtained from this study are then summarised in chapter nine. Some concluding remarks are presented.

Chapter II. Fundamental Theories

2.1 Presentation of the Chapter

This chapter introduces the principles of corrosion, the theory with the different types of corrosion most likely to occur. Then the thermodynamics and kinetics are explained to present the reactions of the mechanism. In a second part the sol-gel process is presented with an explanation about the different stages and equations and then the types of sol-gel coatings.

2.2 Theory of Corrosion

Corrosion can be described as the degradation of materials due to chemical or electrochemical reactions with the environment, leading to deterioration of the metal and its properties. The reactions can be chemical, electrochemical, physical or a combination [3, 15, 16]. The materials can be metals, ceramics or polymers and the environments can be aqueous or non aqueous, liquids or gases. However corrosion is often referred to metallic materials and the current project is about protecting pipelines in oil and gas industry. The aftermath of corrosion in oil and gas industry, especially pipelines consists mainly of environmental damage, health and safety risks, production shutdown, excessive repair and replacement costs [17]. It occurs most of the time in the presence of hydrogen sulphide gas (H_2S), which is qualified as sour corrosion or in the presence of carbon dioxide gas (CO_2), referred to as sweet corrosion.

There are five primary methods of corrosion control: material selection, coatings, inhibitors, cathodic protection and design [3].

Regarding the selection of materials and substrates, each metal and alloy has its unique corrosion resistance behaviour (for example high resistance for noble metals or low corrosion resistance for active metals). Moreover, the environment in which the metal is exposed has a strong influence on its corrosion resistance and depends on the chemical composition, temperature, velocity etc. In oil and gas industry, an acceptable rate of corrosion would usually be fixed and the purpose of the experiment would be to equal the actual corrosion resistance of the material and the

corrosivity of the environment to the defined corrosion rate (or have a lower value) [3].

The conductivity of a solution is a measure of its ability to transport current. A high conductivity solution easily transports current, whereas a solution with low conductivity transports current much less effectively. The conductivity is inversely proportional to resistivity; that is, if conductivity increases, resistivity decreases.

Various solutions exhibit a wide range of conductivities. Seawater is a highly conductive solution and has a very low resistance to transporting current (typical value of conductivity is 5 S/m) [18]. Distilled water, on the other hand, is a very low-conductivity solution and has a high resistance to the transport of current (typical value of $5.5.10^{-6}$ S/m) [18]. Distilled water, having a lower conductivity, is thus much less corrosive than sea water [3].

In general, as the concentration of dissolved species in the solution increases, the conductivity increases, and as the conductivity of the solution increases, the corrosion of metals in that solution increases.

2.2.1 Presentation of Different Types of Corrosion

Corrosion can be divided into general corrosion (around 25% of the cases) and localised corrosion. General corrosion is often measured with methodologies such as weight loss, electrochemical or non-electrochemical techniques. The determination of the severity and the extent of the localised corrosion involves the use of inspection tools or even microscopic techniques. The main types of corrosion encountered in oil and gas will be presented as seen in Figure 2.1 and Figure 2.2.

The corrosion rate can be deduced from the relation of the corrosivity of the environment and the corrosion resistance of a material [3].

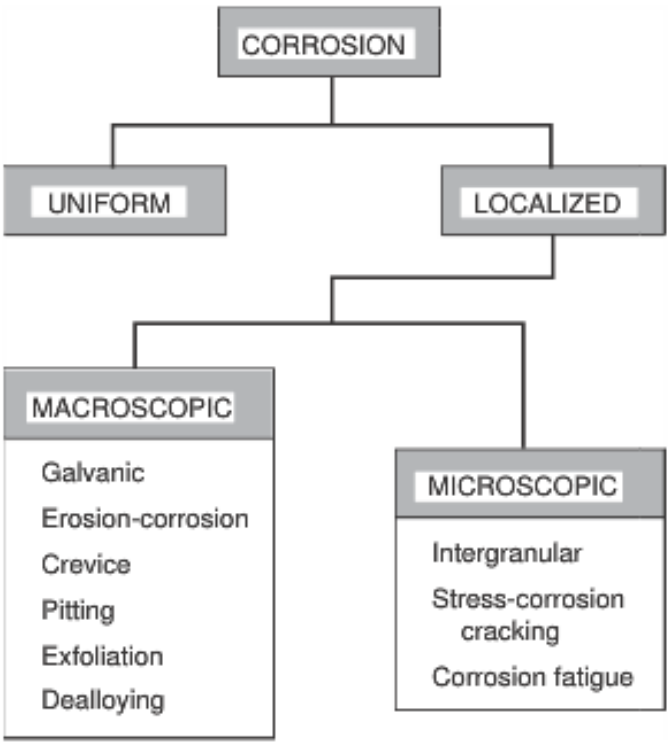

Figure 2.1 Macroscopic versus microscopic forms of corrosion [19]

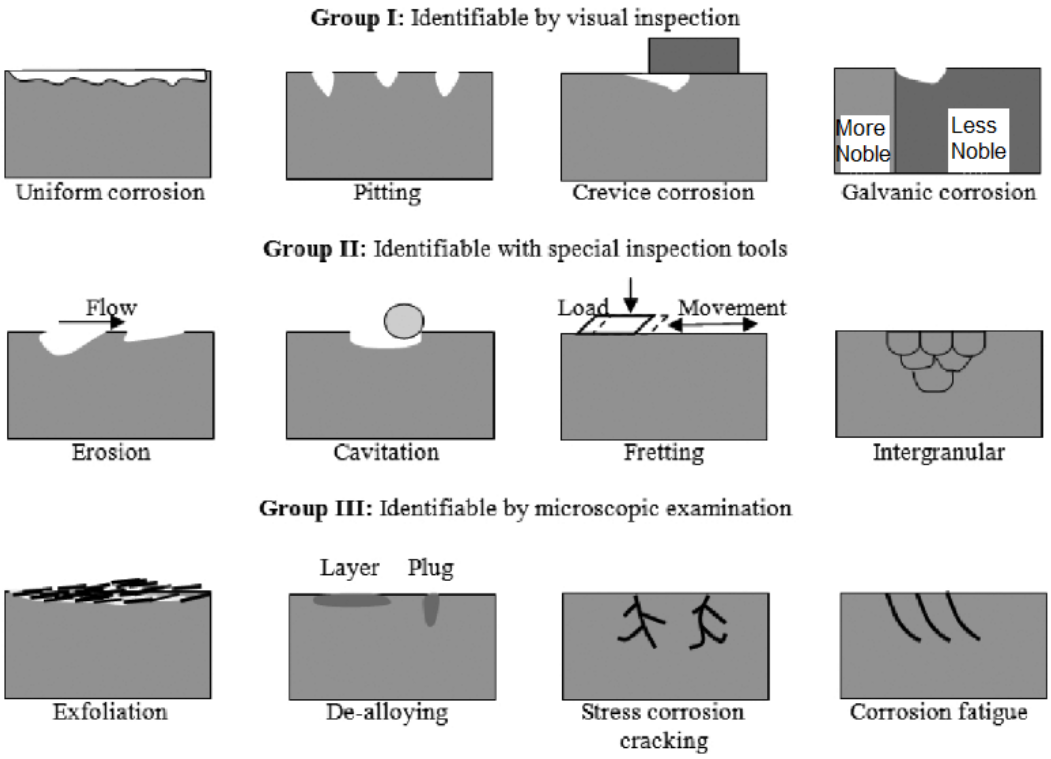

Figure 2.2 Main types of corrosion damage [20, 21]

The metal substrate itself can behave in three different ways when immersed in an environment: immune, active and passive [3]. Stainless steels are known for their good corrosion resistance in many corrosive environments, but in the presence of chloride ions are susceptible to localized corrosion [22]. Steels have different behaviours depending on their nature. Under static conditions, stainless steels show low corrosion rates as opposed to medium carbon steels that corrode at high rates. This can be explained through the high chromium content which generates the formation of a passive film that protects the metal against corrosion. While being in an environment more aggressive (for example with the presence of solid particles), the protective film of the stainless steels fails to keep its integrity which results in increased corrosion rates but which are, still much lower than the rates of the medium carbon steel [23].

The immune behaviour means that there is no reaction between the environment and the metal hence no corrosion on the substrate. Metals known to display this immunity are called noble metals (example: gold, silver and platinum). Immune behaviour results from the metal being thermodynamically stable in the particular environment; the corrosion reaction does not occur spontaneously [3].

The behaviour of a metal is described as active when it corrodes in the solution: the metal dissolves in solution, producing non-protective corrosion products. Corrosion or dissolution of the metal continues in this solution because the corrosion products do not prevent subsequent corrosion. Active corrosion is characterized by high weight loss of the metal [3].

The passive behaviour is when the metal reacts while or after being immersed in the solution and the metal does corrode. However, an insoluble, protective corrosion product film is formed. These corrosion products thus form a protective barrier on the alloy surface and prevent the electrochemical interaction between the environment and the metal [24, 25]. This thin protective film, also referred to as a passive film, slows the reaction rate to very low levels. The corrosion resistance of the metal in this case depends on the integrity of the protective film. However the metal can regress to an active behaviour if the passive film is broken or dissolves [3].

Iron can be found in the states of immunity, passivity and corrosion on water depending on the pH and the applied potential. Its different states are presented in Figure 2.3.

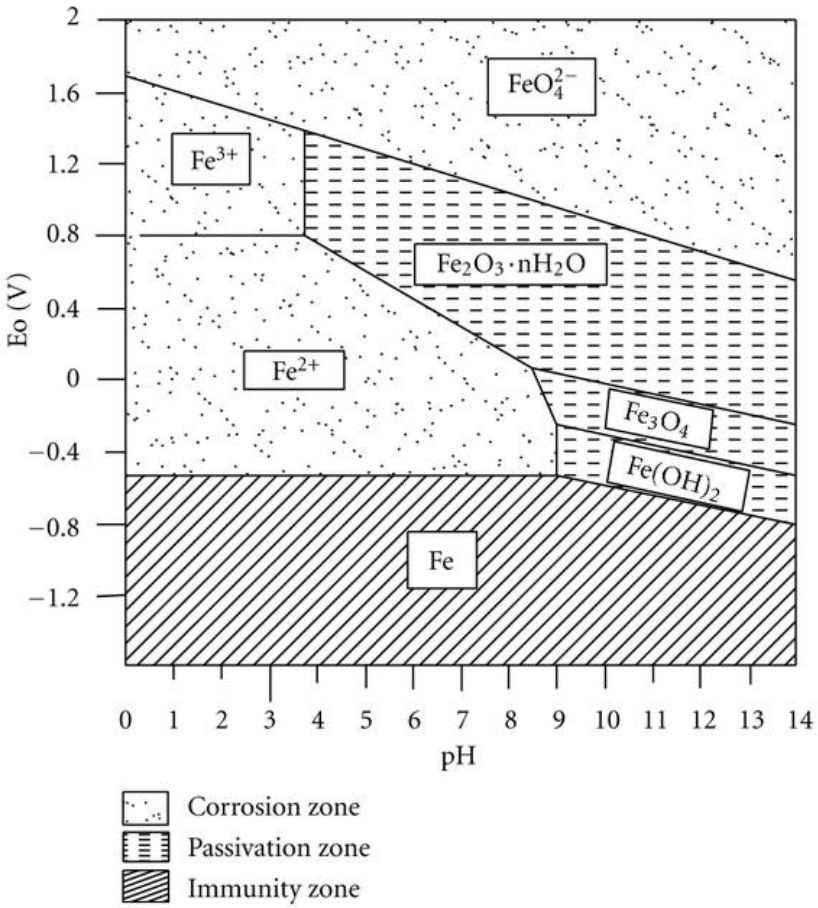

Figure 2.3 Pourbaix diagram of Iron [2]

- General/Uniform Corrosion

The most common form of corrosion in the oil and gas industry occurs when the metal comes in contact with an aqueous environment and rusts. It can occur equally or with equivalent intensity over the entire exposed surface causing a uniform mass loss of the material. General corrosion is observed when the exposed metal (or alloy) surface is entirely corroded in an environment because of a uniform penetration and rate of the electrolyte. All metals are affected (although passive materials are subjected to localized form of attack) [3, 25-30]. It usually is easier to be measured (with methodologies such as weight loss, electrochemical or non electrochemical techniques) and predicted, making important failure relatively rare. In most cases it can be controlled by cathodic protection or use of coatings [3, 21, 26, 31, 32].

- Localized corrosion

Localized corrosion implies that specific parts of an exposed surface area corrode in a suitable electrolyte, at much higher rate than over the rest of the surface. This form of corrosion is more difficult to control than general corrosion. All metals are affected, although passive materials, such as stainless steel or Ni-Cr alloys are normally subjected to localized forms of attack. The susceptibility of metals to be subjected to localized corrosion as well as its rate is linked to the quality of the passive film [3, 25, 27-29].

- Galvanic Corrosion

Galvanic corrosion occurs when a metal or alloy is electrically coupled to another metal or conducting non-metal in the same electrolyte, two dissimilar materials being in direct electrical contact in a corrosive environment. The two metals, which have different potentials in a conducting electrode, result in the more anodic metal being the one subjected to galvanic corrosion. In this case, in opposition to the other forms of corrosion where the anodic and cathodic sites are separated, the anode and the cathode exist on the same surface. This type of corrosion can be encountered on surfaces where the chemical composition is not homogeneous and it the basis for sacrificial cathodic protection systems [3, 25, 27-29].

Knowledge of the galvanic series of metals/alloys is important in preventing galvanic corrosion attack. Figure 2.5 lists and arranges the pure metals according to their relative potentials in a given environment.

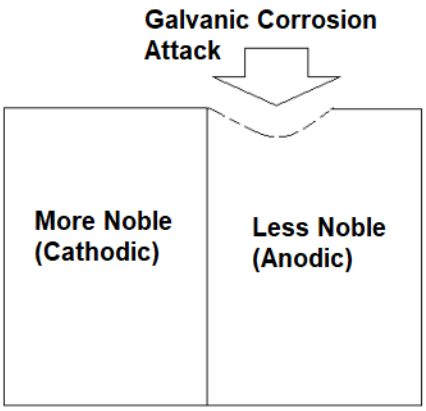

Figure 2.4 Illustration of galvanic corrosion [33]

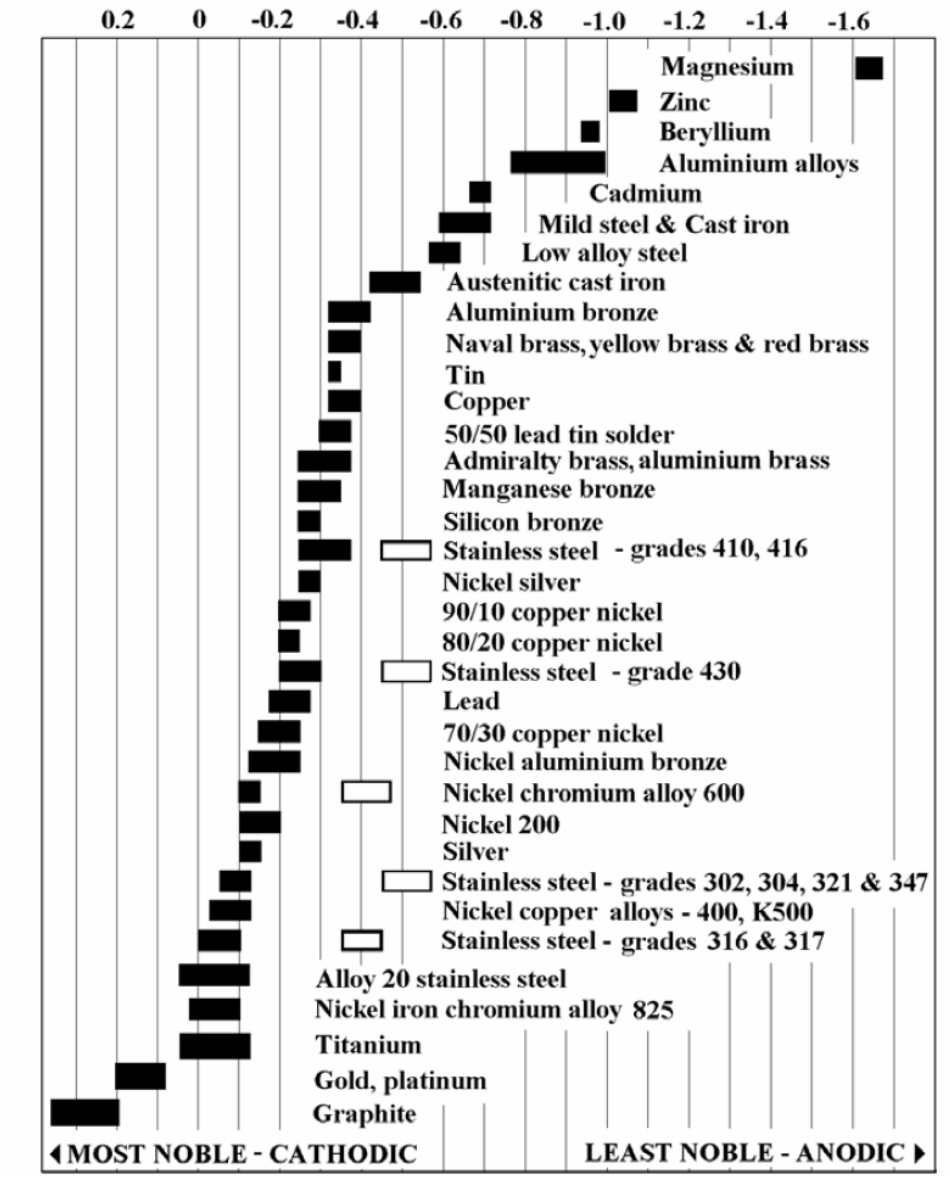

Figure 2.5 Galvanic series of metals and alloys [34]

- Pitting Corrosion

Pitting corrosion is an extremely localized corrosion mechanism that causes destructive pits, which attack areas of metal surfaces where there are surface scratches, an emerging dislocation or a compositional heterogeneity. Pits can either be isolated from each other or close together. Pitting occurs when one area of a metal becomes anodic or when highly localized changes in the corrosive environment in contact with the metal, for example pits or crevices, cause accelerated localized attack. It is a local dissolution, leading to the formation of pits in passivated metals or alloys exposed to electrolytes containing aggressive anions. It is aggravated with increasing temperatures. Pits are generally small and often remain undetected. The pit part becomes the anode while the intact surface

becomes the cathode of the electrochemical cell [3, 25, 27-29]. Pits can be of different shapes, as presented in Figure 2.6.

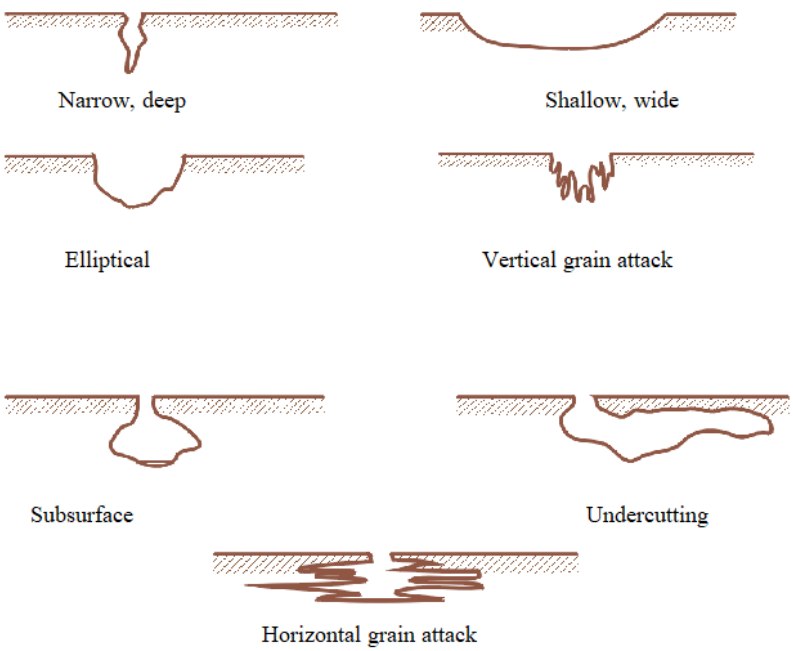

Figure 2.6 Common pit shapes [35]

- CO_2/ sweet corrosion

Carbon dioxide is an important corrosion factor in oil and gas production environments. Carbon dioxide dissolves in water to form a weak acidic oxide which reacts with iron. This type of corrosion is referred to as “sweet corrosion”.

It is responsible for most types of general corrosion in oil and gas pipelines. The characteristics of CO_2 corrosion of carbon and low alloy steel are much more complex than for other weak acids primarily because of the semi-protective nature of corrosion products formed on the steel surface. These products include $FeCO_3$ and Fe_3O_4, and undissolved Fe_3C in some cases. Velocity may disrupt the protective nature of the corrosion products via a mechanical erosive effect or via a mass transfer effect involving dissolved iron ions. The oil and gas industry is currently using a wide selection of corrosion resistant alloys to solve the difficult corrosion problems associated with corrosive downhole environments. The applicability of each alloy depends upon the severity of the environment and the strength requirements [36, 37].

The corrosiveness of the water saturated CO_2 environments is dependent upon the CO_2-partial pressure (pCO_2), water composition, temperature, flow conditions and

presence of hydrocarbon liquids. Weight loss, pitting and crevice corrosion are the primary concerns in these environments. CO_2 corrosion has been successfully mitigated by use of effective corrosion inhibition programs or corrosion resistant alloys depending on the severity of the environment.

Many deep wells have encountered oil and gas with high levels of CO_2 in the gas phase. The CO_2 is readily adsorbed in any water present, which reduces the pH and increases corrosivity. The relative effect on pH depends on the partial pressure of CO_2, temperature, and the presence of buffers in the water phase. In oil wells, the pH of the water is often buffered by bicarbonates available from the produced water, which is produced along with the oil. By contrast, any water present in gas wells is most likely a result of water condensation from the water saturated gas phase. In this case buffers are not available to modify the pH [36].

The corrosion process depends on two main aspects: thermodynamics and kinetics. The study of thermodynamics indicates the spontaneous direction of the corrosion reaction, predicting the possibility of corrosion. Kinetic calculations quantify the corrosion rate and gives information about the degradation of metals.

Figure 2.7 shows the distribution of the types of corrosion encountered by a company:

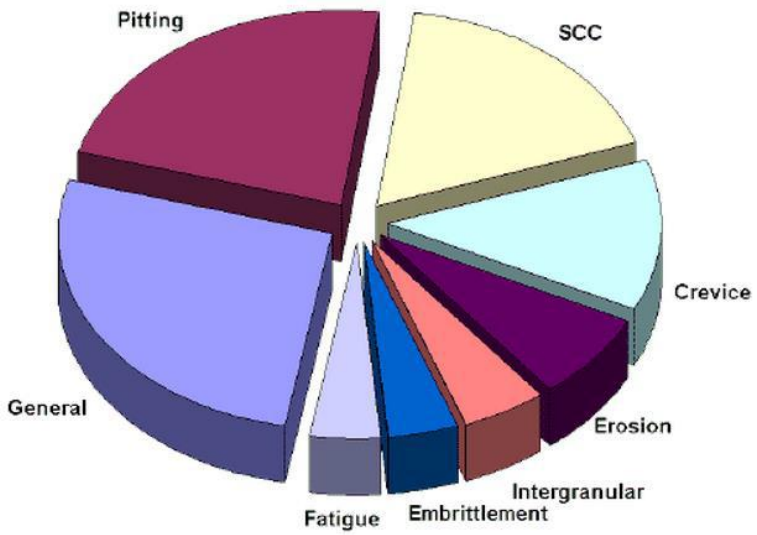

Figure 2.7 Example of distribution of corrosion types [38]

- Erosion

When a solid particle impacts a surface, it can scar the surface. The structures of these defects depend on many parameters including surface material, particle size, and impact angle. The mechanism of erosion changes depending on the ductility of the surface. The erosive particles can cause high degradation rates of the material as they can damage a stable passive film on the surface of the material [1, 39, 40].

Mechanical erosion and electrochemical corrosion are in nature two different mechanisms of material loss in erosion–corrosion. The former is a result of various mechanical forces produced by fluid and the latter is produced by electrochemical dissolution. They are normally controlled by very different parameters [41].

2.2.2 Thermodynamics of Corrosion

A metal submerged in an electrolyte is called an electrode. The metal and electrolyte together are electrically neutral, and no measurable external current flows to or from an electrode in the absence of an external applied voltage.

Corrosion is an electrochemical process involving mass transfer and charge transfer which require the presence of four key elements to occur:

- a cathode, metal or another electronic conductor, whose surface provides sites for the environment to react [42]
- an anode, the corroding metal
- a metallic conductor, electrical connection between the cathode and anode to allow the flow of electrons between them [42]
- an electrolyte in contact with both the cathode and anode providing a path for ionic conduction [42]

The cell is composed of an anode and a cathode connected through the electrolyte and through the metal. As all natural phenomena, corrosion will occur spontaneously it is thermodynamically favourable; this is described by the thermodynamics of the corrosion reaction in which every element tries to minimize its energy state.

In order to ensure electroneutrality, charge transfer half reactions take place in opposing direction, are usually in separated spaces and happening at different

electrodes which are immersed in the solution in a cell [43]. Corrosion is a loss of material due to the electrochemical interaction with the environment. The electrochemical reactions involve electron transfer which means that one of the most effective corrosion control technique is to electrically isolate the anode from the cathode [31, 44].

The electrodes are connected via ionic transport by conducting route both located in the solution, as well as externally so that charge can be transported. The electrolytic path in Figure 2.8 enables the transportation of the metal ions from the anode to the cathode. When this occurs, a reduction reaction takes place as shown in Equation (2.1). The electrons required by this reaction are produced by the reaction of oxidation at anodic area and provided via the metallic path, as shown in the figure as well, before being consumed at the cathodic sites [45-47]. This is achieved through reducible species in the electrolyte adsorbing onto the metal surface and removing the electrons. When all four elements are present the developed measured potential is called the free potential or E_{corr} [32]. Corrosion is often described chemically as the dissolution of the anode due to an oxidation process by which a metallic ion leaves the metal surface into the electrolyte (solution). The metal surface is charged by the excess electrons as presented in Equation (2.2) and Equation (2.3).

$$M^{n+} + ne^- \rightarrow M$$

$$2H^+ + 2e^- \rightarrow H_2 \quad (2.1)$$

$$O_2 + 2H_2O + 4e^- \rightarrow 4OH^- \quad (2.2a)$$

$$O_2 + 4H^+ + 4e^- \rightarrow 2H_2O \quad (2.2b)$$

With M being the symbol for metal and n the valency of the metal.

Reduction described in Equation (2.2a) happens in neutral or alkaline conditions while (2.2b) happens in acidic conditions.

$$M \rightarrow M^{n+} + ne^- \quad (2.3)$$

As shown in Equation (2.1) the solution contains other species that could go through the reduction process instead of the metal ion on the anode. The pH is what dictates which reaction will be more likely to occur such as the hydrogen evolution in acidic conditions or the hydroxide creation in basic environments. In the case of corrosion of metal components, both anodic and cathodic reactions occur on the surface of a single component at the same time [2].

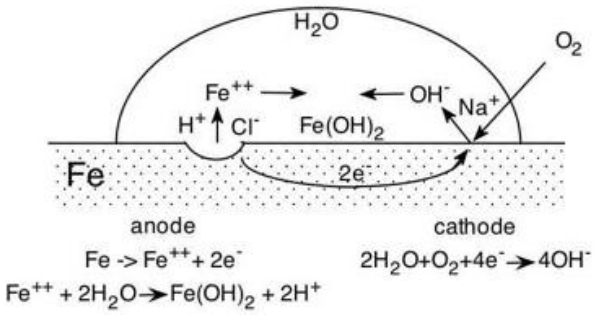

Figure 2.8 Schematic of the corrosion mechanisms for iron [48]

The cathode does not normally corrode. Cathodic reactions are possible depending on which reducible species are present in the solution and strongly depend on the pH of the solution.

The electrode reactions are heterogeneous and take place in the interfacial region between the electrode and the solution. It corresponds to the region where charge distribution differs from that of the bulk phases. At each electrode, charge separation can be represented by a capacitance and the difficulty of charge transfer by a resistance [2, 49]. Regarding the nature of the electrode reactions, they are heterogeneous and take place in the interfacial region between electrode and solution, the region where charge distribution differs from that of the bulk phases. The electrode process is affected by the structure of this region. The corrosion current is thus formed by the flow of electrons between the corroding anode and to the cathode. The global rate of metal dissolution is influenced by the formation of corrosion products, their solubility in the electrolyte and the formation of passive films [2, 16].

In the case of experiments, most electrochemical accelerated tests use a three-electrode system as presented in Figure 2.9.

A potentiostat is used to control the potential of the working electrode versus a stable reference electrode submerged in an electrolyte. The external current only

flows between the working electrode and the counter electrode (or auxiliary electrode) [31].

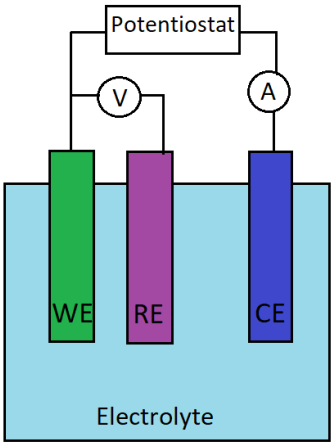

Figure 2.9 Three-electrode cell

The working electrode (WE) is the material to be tested.

The reference electrode (RE) has a stable and known potential.

The counter electrode (CE) ensures that the current does not run through the reference electrode.

The basis of electrochemical accelerated test techniques is to change the potential of the working electrode and monitoring the current which is produced as a function of time or potential through the three-electrode system. Some of these techniques are: Linear Polarisation Resistance, Tafel Plot, Potentiodynamic Scanning, Cyclic Polarisation and Electrochemical Impedance Spectroscopy (EIS) or AC Impedance which will be studied here. Other methods are used in the electrochemical area but have to be applied on the metal itself without any coating.

Uncertainties or errors in measurement can be minimised by taking data when the test electrode is at steady state, correcting uncompensated solution resistance, using appropriate scan rate to collect data, choosing correct test electrode data, counter electrode area, etc. [30].

Electrochemical impedance is usually measured by applying an AC potential, not DC voltage, to an electrochemical cell and by measuring the current through the cell. The difference between AC and DC voltage is that a given DC voltage has a constant magnitude, and its polarity is either anodic or cathodic. An AC voltage cycles from peak anodic to peak cathodic amplitudes [30].

For the AC impedance, a small-amplitude sinusoidal potential perturbation is applied to the working electrode at a number of separated frequencies. Each frequency produces values of resistance and capacitance which can provide information on the corrosion behaviour and its rates but also an insight into the corrosion rate-controlling mechanisms at the material surface within an electrolyte (especially in the presence of material coating) [1, 50]. This method allows the creation of quantitative data that connects to the quality of a coating on a metal substrate. EIS is a very sensitive method which detects the condition of a coated metal. Thus, the response can express the changes in the coating before any visible damage occurs. However this method is not an absolute measurement. In order to monitor and measure the quality of the coating, the process while measuring EIS must be stress induced. It also will allow the estimation of a coating failure rate. EIS itself is a non-destructive measurement, so it can be used to track the evolution of the coated sample. In most cases, it is possible to identify the cause of coating failure [51].

For the cell itself and the measurements of the impedance, assimilation to electrical circuits is needed, but first the electrical double-layer needs to be explained.

When a metal is submerged in an electrolyte, its metal ions leave the structure and their electrons behind in the metal. Water molecules next surround metal ions and the hydrated ions are free to move away from the metal. The surplus of electrons cause a negative charge on the metal surface which attracts positively charged metal ions [30]. The water layer around ions prevents most of them from making direct contact with excess surface electrons and thus being reduced to metal atoms. Positive ions in the electrolyte are also attracted to the negatively charged metal surface. Then the electrolyte layer adjacent to an electrode surface contains water molecules, ions from the metal and bulk electrolyte, and has a different chemical composition than the bulk electrolyte. The negatively charged surface of a metal and the adjacent electrolyte layer are collectively referred to as the Electrical Double Layer (EDL) [15, 30].

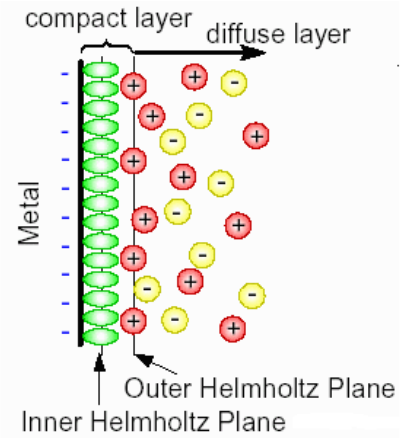

Figure 2.10 Electric double layer [15]

The EDL, as presented in Figure 2.10, separates the metal surface and the solution. It behaves as a capacitor, which means that there is a rise in potential across the interface, between the metal and the test solution. The metal also resists transferring excess electrons to the electrochemically active ions, which in addition allows the EDL to behave as a resistor [30].

Figure 2.11 presents a simple electrical circuit which can be used to represent the properties of the EDL:

Figure 2.11 Equivalent circuit model

C_{edl} is a capacitor (F). It represents the capacitive behaviour of the EDL

R_{ct} is the charge-transfer resistance (Ω) and can be compared to corrosion resistance

R_s is the solution resistance (Ω).

The thermodynamics of corrosion are influenced by the chemical and electrochemical processes of the surface and interfacial energy of the material [26-29]. Most pure metals are active and try to react with elements from the environment. Metals are unstable and can corrode when the opportunity is given. They try to lower their energy by spontaneously reacting to form solutions or compounds with greater stability [42]. According to thermodynamic laws, a strong tendency for high energy states to revert to low energy states also applies to the

metal/environment relation. For these metals to go back to their natural state, they have to possess a negative Gibbs free energy (-ΔG) which is the change in free energy of the metal and environment combination brought about by corrosion [42]. The energy must be negative in the case of a spontaneous reaction. For corrosion reactions to take place spontaneously, the thermodynamics of the system must be favourable. In order to determine if a reaction is thermodynamically favourable, the equation of Gibbs free energy is considered:

$$\Delta G = \Delta G° - RT\ln\frac{[a_{products}]}{[a_{reactants}]} \quad (2.4)$$

Where: a is the chemical activity of products and reactants

ΔG: Gibbs free energy (kJ.mol^{-1})

ΔG^{0}: standard free energy of the cell (kJ.mol^{-1})

R: ideal gas constant (J.mol^{-1}.K^{-1})

T: temperature (K)

F: Faraday's constant (C. mol^{-1})

If ΔG has a positive value, then energy will be required to make the reaction take place.

However, if ΔG has a negative value, then the reaction occurs spontaneously.

When it comes to the EDL, the potential which cross it is presented in Equation (2.5).

$$\Delta G = (-nF)E \quad (2.5)$$

With: ΔG: Gibbs free energy (kJ.mol^{-1}) associated with the oxydo-reduction equation

n: number of electrons exchanged

F: Faraday's constant (C. mol^{-1})

E: potential difference between the two half cells at non-standard conditions (V)

Even after the formation of the EDL metal atoms continue to leave the metal network meaning that corroding metals are not at equilibrium. In order to re-organize the original conditions of the EDL, more metal atoms are leaving the lattice, which is caused by electrochemically active species diffusing from the bulk electrolyte to the metal surface and discharge the EDL at the point on the metal surface where electrons are removed. As long as the electrochemically active species diffuse to the metal surface and remove electrons, the EDL is considered to be on a stable state and the corrosion reaction proceeds in the forward direction [30].

Physically separating two oppositely charged planes produces an electrical capacitor. Consequently, charge (metal ions and electrons) separation gives an EDL capacitor-like behaviour. A metal also resists transferring its excess electrons to electrochemically active species. Consequently, the EDL has both capacitive and resistive properties and these properties are similar to those for a simple electrical circuit composed of a capacitor and resistor in parallel. An electrical potential can also be produced by the charge separation in an EDL. This potential can be measured as a difference between two metal electrodes, or a metal and reference electrode [30].

If the oxidized and reduced species involved in an electrode reaction are in equilibrium at the electrode surface, the Nernst equation can be applied. The electrode reaction is known as a reversible reaction since it obeys the condition of thermodynamic reversibility. The Nernst equation mathematically relates EDL composition to electrical potential:

$$E = E° - \frac{RT}{nF} \ln \frac{[a_{products}]}{[a_{reactants}]} \quad (2.6)$$

Where: a is the chemical activity of products and reactants

E: measured potential (V)

E^0: potential at standard conditions (V)

R, T, n and F represent the same parameters as in Equation (2.4)

Chemical activity is equal to activity coefficient γ, times concentration of a species in moles/litre. So Nernst' equation can be rewritten as:

$$E = E° - \frac{RT}{nF} \ln \frac{[\gamma_{products}]}{[\gamma_{reactants}]} \quad (2.7)$$

This equation shows that the potential is determined by concentrations of both metal ions and electrochemically active species in the electrical double layer [30].

The major factor in corrosion is the environment in which the metal is studied [48]. To present a summary of the thermodynamics of a metal and its associated species in such environment, potential – pH diagrams can be used (also known as Pourbaix diagrams as presented in Figure 2.3). They do not define the kinetics of the corrosion reaction but the thermodynamics prediction of corrosion reaction can be drawn from these diagrams [48] which are based on the Nernst equation. They relate the corrosion and electrochemical behaviour of most metals in their given environment. The potential and the pH of these diagrams are the most important variables that govern the behaviour of metals in their environment, indicating how they react at a particular potential and pH condition. It shows which reaction will occur and which products will form during any reaction at the potential-pH condition [25].

2.2.3 Kinetics of Corrosion

Thermodynamics describe the tendency of a system to corrode but do not give information about the speed of the corrosion reaction. Kinetics of the corrosion reaction when considered, give information about which reactions can occur [48].

A chemical process can be simplified as:

Reactants → Products

where an activation barrier (activated complex) created during the reaction process is to be overcome before the formation of the products [39]. From the thermodynamic point of view, this activation barrier has a higher energy level compared to the reactants' as presented in Figure 2.12.

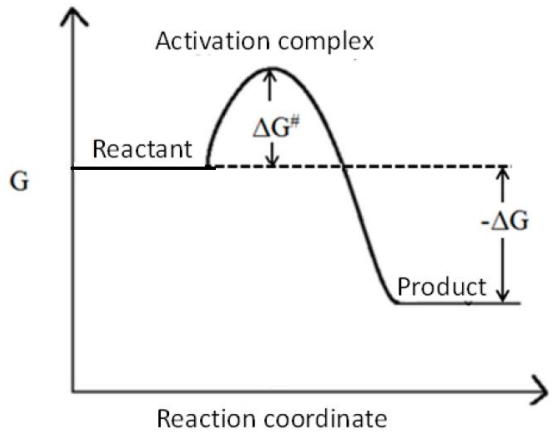

Figure 2.12 Energy profile adapted [52]

As it can be seen, a difference of energy (activation energy $\Delta G^{\#}$) exists between the initial position and the activation complex. This energy determines the rate of a chemical reaction.

For a corrosion reaction, the corrosion rate v is defined in (2.8).

$$v = kc \tag{2.8}$$

With: c: concentration of reactants (mol)

k: constant of reaction derived from Arrhenius equation presented in (2.9)

$$k = Ae^{(\frac{\Delta G\#}{RT})} \tag{2.9}$$

With k: rate constant

A: pre-exponential factor

$\Delta G^{\#}$: activation energy (J)

R and T have been defined in Equation (2.4)

The rate of the reaction partly depends on the activation energy. A higher activation energy decreases the reaction rate.

The Nernst equation studied in the precedent part does not express a relationship for electrical current. Electrical current is important because corrosion current can be converted into a rate of metal penetration by corrosion. The current flowing during any corrosion reaction is related to the corroding area and is referred to as the corrosion current density. At equilibrium, the sum of the anodic and cathodic currents is zero and the deviation from this equilibrium is called polarisation, with η the symbol for overpotential. The overpotential is the difference the equilibrium potential and the resultant potential.

The polarisation includes three components that can be defined as:

$$\eta_{ap} + \eta_{cp} + iR \qquad (2.10)$$

with η_{ap}: activation polarisation

η_{cp}: concentration polarisation

i: current (A) or ($A.cm^{-2}$)

R: resistance (Ω)

iR element (called Ohmic drop) describes the polarization as a result of the applied current

The activation polarisation describes the charge transfer kinetics in the electrochemical processes. It is predominant at small polarisation currents or voltages [3, 44]. It is a manifestation of the relative changes in the activation energies for dissolution and deposition, when equilibrium is disturbed and refers to the situation where some steps in a corrosion reaction control the rate of charge or electron flow.

The concentration polarisation describes the constraints of mass transport connected to electrochemical processes. It is prevailing for large polarisation currents or potentials [44]. It refers to the situation when the progress of an electrode reaction is determined by restrictions either in the rate of supply of reactants or in the rate of removal of products.

The Butler-Volmer equation relates electrical current to changes in metal potential caused by an external power source and is used as a representation of the polarised surface:

$$i = i_{corr}\left[e^{\left(\frac{-\alpha n F \eta}{RT}\right)} - e^{\left(\frac{(1-\alpha) n F \eta}{RT}\right)}\right] \quad (2.11)$$

R, T, n and F represent the same parameters as in Equation (2.4)

i: external current density flowing to or from an electrode because of an applied potential ($A.cm^{-2}$)

i_{corr}: corrosion current density that occurs when the electrode is at its OCP

α: charge transfer barrier having values that ranges from 0 to 1 ($A.cm^{-2}$)

η: test electrode overpotential and difference between electrode OCP and applied potential (V)

$e^{\frac{-\alpha n F \eta}{RT}}$: is for anodic current while $e^{\frac{(1-\alpha) n F \eta}{RT}}$ is for cathodic current

The concentrations of species at the interface depend on the mass transport of these species from bulk solution, often described by the mass transfer coefficient k_d. A reversible reaction corresponds to the case where the kinetics of the electrode reaction is much faster than the transport. The kinetics is expressed by a standard rate constant, k_0, which is the rate constant when $E = E'_0$. So the criterion for a reversible reaction is $k_o >> k_d$.

By contrast, an irreversible reaction is one where the electrode reaction cannot be reversed. A high kinetic barrier has to be overcome, which is achieved by application of the overpotential and in this case $k_o << k_d$.

Some reactions, known as quasi-reversible, present an intermediate behaviour between reversible and irreversible reactions. This is due to the overpotential having a rather limited value, leading to extra potential reactions which can be reversed. The potential-dependent expression for the rate constant of an electrode reaction is, for a reduction:

$$k_c = k_0 e^{\frac{-\alpha_c nF(E - E_0')}{RT}} \quad (2.12)$$

And for an oxidation:

$$k_a = k_0 e^{\frac{\alpha_a nF(E - E_0')}{RT}} \quad (2.13)$$

In these equations α_c and α_a are the cathodic and anodic charge transfer coefficients and are a measure of the symmetry of the activation.

The result of those equations is shown in Figure 2.13. This figure represents the densities of anodic current and cathodic current as well as the resulting current density. The current is composed of the two currents, anodic and cathodic, and for an overpotential η=0 both currents have the same absolute value which make the resulting current being null.

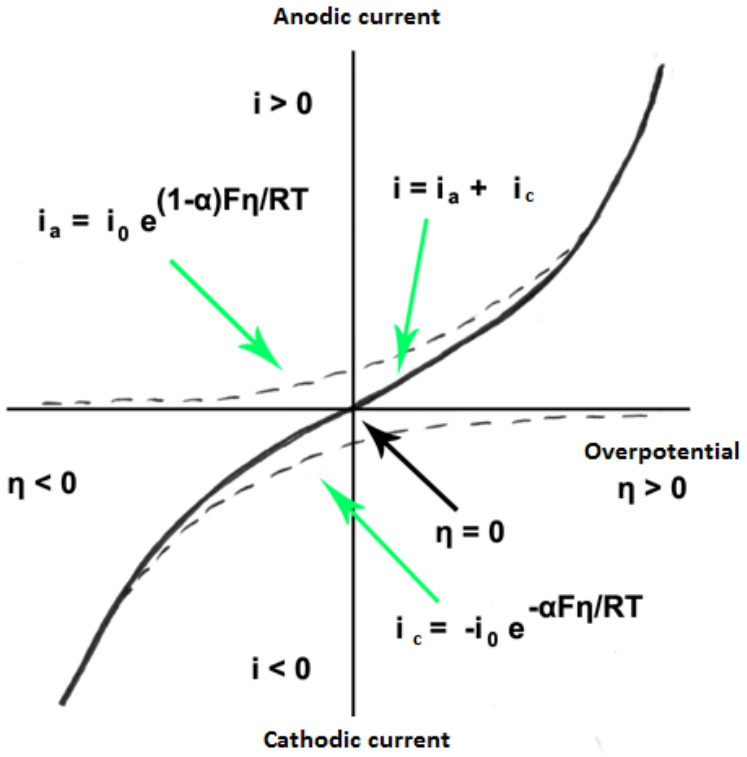

Figure 2.13 Curves of current density as a function of overpotential [21]

2.2.4 Factors Affecting Corrosion

The corrosion can be affected or stimulated depending on some conditions of the environments itself.

- pH of the environment and water chemistry

Depending on the location of pipelines, the composition of water present in oil and gas industry installations differ (for example fresh water or seawater [21]) and can vary from very simple to more complex with numerous species [53]. The main component of seawater is sodium chloride. When increasing its concentration, the corrosion rate tends to increase as well. Divalent ions such as iron ions, in certain conditions, can react with carbonate species when these are present in the system to form corrosion products. The presence of dissolved gas (H_2S or CO_2 for instance) or the presence of acetic acid would also start corrosion on the metal [53].

The pH of the environment would influence the composition of the water leading to influence the electrochemical reactions [54]. An increase of the pH would lead to a reduction of the corrosion rate due to the formation of protective layers.

- Temperature

Temperature is a crucial parameter influencing the evolution of corrosion and its rate [54, 55]. When the pH is low, precipitation processes are limited and the corrosion rate tends to increase with the temperature [53]. In some studies [54, 56] the temperature was observed to influence the concentration of iron ions, a decrease in its value for an increase in temperature. Kermani [54] also showed in his study that the corrosion rate increases with temperature but at low temperatures (<70°C). Above 90°C, the general corrosion rate decreases (intermediate temperatures being between 70°C and 90°C) which can be due to the formation of protective corrosion product.

- Microstructure

The composition of steel and its microstructure are part of the factors affecting the corrosion [54]. This parameter also concerns alloys which are not homogeneous and often composed of at least two different phases but not studied in this project.

The corrosion on coatings will be fully developed in Chapter III (Part 3.3. Corrosion of a Coated Sample).

2.3 Sol-gel Process

The sol-gel process can be defined as a chemical synthesis method initially used for the preparation of inorganic materials such as glasses and ceramics [57] or as a colloidal route used to synthesize ceramics with an intermediate stage including a sol and/or a gel state [6]. It allows a production of equilibrium compositions to be done using simple, non vacuum methods, which are generally less expensive than methods which require a vacuum [58].

The sol-gel process concerns the development of inorganic networks through the formation of a colloidal suspension (sol) and gelation of this sol to form a network in a continuous liquid phase (gel) [59]. A sol is a colloidal suspension of solid particles in a liquid, while an aerosol is a colloidal suspension of particles in a gas and an emulsion is a suspension of liquid droplets in another liquid. Those three kinds of colloids can be used to make ceramics by generating polymers or particles. Those solid particles are denser than the surrounding liquid in order to have the forces responsible of dispersion greater than gravity so the sol can exist. The size of the particles is between 2nm and 0.2µm [60]. The sol-gel method is complex. The difficulty of its chemistry is due to the metal and the double role of water (as ligand and solvent in the case of aqueous solution). There is also a certain number of parameter to take into account as they have to be fully controlled, such as reaction parameters: hydrolysis and condensation rate of the metal oxide precursors, pH, temperature, method of mixing, rate of oxidation, nature and concentration of the anions. Figure 2.14 allows the explanation of the sol-gel process step by step by first defining colloids and polymers, then the gel-point of gelation and the drying as well as the final post-processing treatments.

Coatings act as barriers and their protective properties generally improve with the increase of their film thickness (without imperfections); or in the case where they are applied in multiple layers. Coatings can act to release inhibitor materials that passivate the substrate or block the corrosion reactions. Some coatings use soluble organic inhibitors, but these often leach out the film too rapidly to give long term protection.

In the case of a coating developed with a metal pigment more electroactive than the substrate it is deposited on, then the coating can provides cathodic protection to this substrate. This type of coating provides protection for damaged areas.

However, because the metal pigments can be oxidized by atmospheric exposure, they should be kept through an overcoat of the coating [57].

The sol-gel process is similar to the process for creating polymeric materials, and more precisely an oxide macromolecular network will be created during the hydrolysis and condensation steps defined in a few pages. The interest in gels is not only associated to their physicochemical properties but also and especially to the important opportunities of the colloidal state in the field of the development of materials.

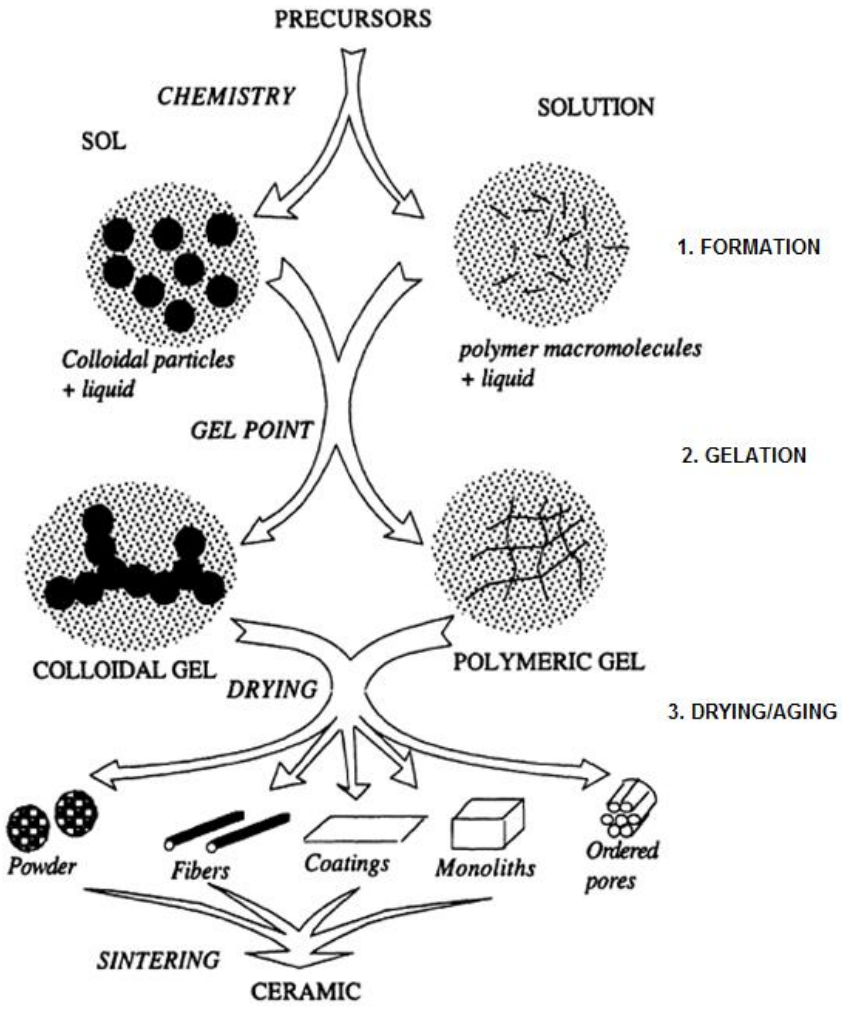

Figure 2.14 Simplified chart of sol-gel processes [6]

All the products that can be obtained from this process are shown in Figure 2.15.

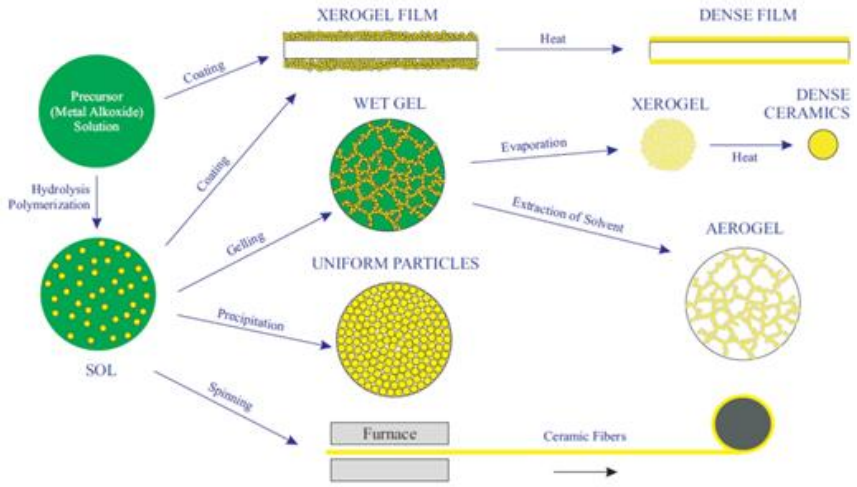

Figure 2.15 Various products which can be obtained through sol-gel process [61]

The most important advantages of sol–gel process are: low equipment costs, low processing temperature (thus the degradation of involved elements such as organic inhibitors due to the temperature is minimized), good homogeneity, use of compounds that do not introduce impurities into the final product as initial substances thus making it ‘‘green’’, waste-free technology. These advantages make the sol–gel process one of the most appropriate technologies for preparation of thin, nanostructured films. Sol–gel technology has been significantly improved in the past 20 years [22]. The sol-gel process has been an effective way for applying hard, corrosion resistant, erosion resistant ceramic coatings such as Al_2O_3, TiO_2, SiO_2, ZrO_2, which are mostly used as functional sensor films and membranes [62] and corrosion resistant films on structural components [63]. The main cost of this process comes from the need of high sintering temperature. However it is relatively lower than other methods, for example plasma sprayed, CVD (Chemical Vapor Deposition) and PVD (Physical Vapor Deposition) coating processes [64]. Although the sol-gel coatings provide many advantages and are promising materials having high strength characteristics, they have low crack properties at the same time (they tend to crack if their thicknesses are more than several microns). This is one of the major factors hindering the wide-scale applications of these materials in various areas [65]. The crack resistance properties can be improved by suitable coating preparation and deposition, which are the main factors used to control the quality, property and characteristic of the coatings. Unlike most ceramic coating techniques, sol-gel coatings are applied as low viscosity solutions and thus can be used to smooth over rough surfaces.

2.3.1 Nanoparticles and Colloids

Colloids are a combination of solids in liquid or liquid in liquid, all of these containing distinct particles dispersed to various degrees in a liquid medium. The colloids have properties depending on the size of the particles. The particles are larger than atomic dimensions but small enough to exhibit Brownian motion. Nanoparticles are particles between 1nm and 100nm in size. A colloid is a suspension in which the dispersed phase is so small that gravitational forces are negligible and interactions are dominated by short-ranges forces, such as Van der Waals attraction and surfaces charges. Industrial products such as inks, paints, reinforced plastics can be considered as mixtures of colloidal components. A particle is defined as a small object that behaves as a whole unit with respect to its transport and properties [66]. The nanoparticles are usually used in the sol-gel field for the nanoscale powders application. The colloidal dispersions are constituted of charged particles dispersed in an electrolyte solution. The simplest definition is that it is a two-phase system where one phase (the dispersed phase β) is dispersed in the second phase (the continuous phase α) as illustrated in Figure 2.16. At least one of the dimensions of the dispersed phase lies between 10 Å (1 nm) and 10 000 Å (1 mm) [6, 67].

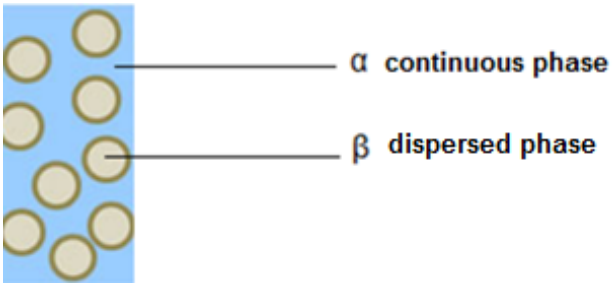

Figure 2.16 Schematic representation of a colloidal dispersion

Consequently, colloidal particles are generally much larger than the molecules of the dispersion medium.

In many practical cases, the system may be rather more complex. There may be more than one type of dispersed phase present, and any of the phases (dispersed or continuous) may be multi-component. Usually, there is a definite difference between the dispersed phase and the dispersion medium; network colloids excepted since in this case both phases consist of interpenetrating networks on the colloidal scale. Gels are a typical example [68]. Particles are localized objects, rigid and

compact. Their size and charge are significantly greater than those of the ions present in the electrolyte. Immersed in water, the particles will behave like polyions. In order to respect the electroneutrality, the charge of the polyions is exactly compensated by the presence of ions of opposite charge, which are called counter-ions. In the case where salt is added to the dispersion, there will also be free ions without direct interaction with the particles. These ions are called co-ions and take in all the ions of the same sign as well as colloidal particles. There are two types of species: colloidal particles of huge size compared to an ion, surrounded by counter ions responsible for the electric neutrality and free ions i.e. not associated to colloidal particles. In a practical way, an operation of separation through centrifugation, ultrafiltration or osmotic compression allows the isolation of the dispersive environment, providing access to the concentration of free ions in equilibrium with the dispersion. A colloidal dispersion is separated in two phases: an electrolyte solution and a concentrated dispersion [6, 59, 67].

An important aspect of the study of colloidal dispersions is the understanding of their stability. There are several types of systems: suspensions (solid–liquid dispersions), emulsions (liquid–liquid dispersions) and foams (gas–liquid dispersions). The colloid stability of these systems depends on the equilibrium of interaction forces such as Van der Waals attraction, double-layer repulsion and steric interaction [69].

The solid particles in the colloidal precursors can be metals, metal oxides, metal oxy-hydroxides, or other insoluble compounds. The degree of aggregation or flocculation of the colloidal precursor can be adjusted to vary the pore size and the drying characteristics of the resulting gel [70].

2.3.2 Sol

Sol-gel coatings can be used as barrier coatings to prevent corrosion and to suppress the cathodic reaction by limiting the diffusion of the electrolyte, oxygen and water and chloride ions to the coating/metal interface [71]. It also limits the transport of electrons off the metal interface.

Sol-gel formation occurs in four stages:

1. Hydrolysis
2. Condensation and polymerization of monomers to form chains and particles
3. Growth of the particles

4. Formation of networks from clusters of polymers; those networks extend throughout the liquid medium resulting in thickening which forms a gel.

In fact both the hydrolysis and condensation reactions occur simultaneously once the hydrolysis reaction has been initiated [57].

The first step of the sol-gel process consists in selecting the precursors of the wanted materials. It is the chemical reactant that, by its chemistry, leads the reaction towards the formation of either colloidal particles or polymeric gels. It contains the cation M present in the final gel [6]. There are different categories of precursors: metal alkoxides, metal salts, any other solution containing metal complexes, inorganic or metal-organic according to Brinker and Sherer [59]. In the case where the future material is composed of several components, different precursors can be combined which lead to others reactions therefore different products. This allowed the creation of a new type of sol-gel coatings: organic-inorganic hybrids coatings. The choice of the solvent (water or organic liquid) also depends on the choice of the precursor [6] and can even have an influence on the final thickness of the coating [72].

Metal alkoxides and metal salts are more used because they react readily with water. Metal alkoxides ($M(OR)_n$ where R is an alkyl group) are commonly employed as high purity solution precursors in the sol-gel process. Many metal alkoxides can be made to react with water through a series of hydrolysis and condensation steps to yield largely amorphous metal oxide or oxy-hydroxide gels. Such reactions have been used to cast shapes, spin fibers and deposit coatings. The volatile alcohol produced by the hydrolysis is easily removed during processing [70]. The most widely used metal alkoxides are the alkoxysilanes. When alkoxides are used as the starting materials, the formation of ceramic coatings is based on hydrolysis and condensation, as shown in Equation (2.14) to Equation (2.16) [59]. In the first reaction, an alkoxide and water are placed in a mutual solvent and a suitable catalyst is added. Hydrolysis of the metal alkoxide bond (M-OR) results in the formation of a metal hydroxyl bond (M-OH), as shown in Equation (2.14) by replacing the alkoxide ligands with hydroxyl ligands:

$$\mathrm{M(OR)_x} + \mathrm{H_2O} \leftrightarrow \mathrm{(RO)_{x-1}M-OH} + \mathrm{ROH} \tag{2.14}$$

In the next step is shown the condensation reaction involving the hydroxyl ligand and an alkoxide ligand:

$$(\mathrm{RO})_{x-1}\mathrm{M}-\mathrm{OH}+(\mathrm{RO})_{x}\mathrm{M}\leftrightarrow(\mathrm{RO})_{x-1}\mathrm{M}-\mathrm{O}-\mathrm{M}(\mathrm{RO})_{x-1}+\mathrm{ROH} \qquad (2.15)$$

or between two hydroxyl ligands,

$$(\mathrm{RO})_{x-1}\mathrm{M}-\mathrm{OH}+\mathrm{HO}-\mathrm{M}(\mathrm{RO})_{x-1}\leftrightarrow(\mathrm{RO})_{x-1}\mathrm{M}-\mathrm{O}-\mathrm{M}(\mathrm{RO})_{x-1}+\mathrm{HOH} \qquad (2.16)$$

An example with silica is shown in Figure 2.17.

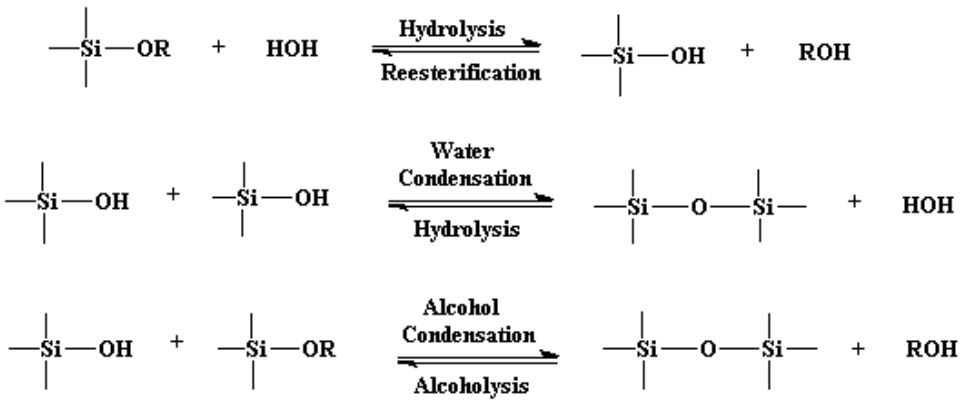

Figure 2.17 General reaction scheme for the sol-gel process with silica [73].

In the case of aqueous or organic solvents, the precursors are hydrolysed and condensed and then form inorganic polymers composed of M-O-M bonds [73]. For inorganic precursors (salts), hydrolysis proceeds by the removal of a proton from an aquo ion to form a hydroxo (-OH) or oxo (=O) ligand [70, 74].

This results as the formation of a metal-oxygen-metal bridge, which is the centre of the oxide ceramic structure. In solution, the rates, extents and even the mechanisms of the reactions shown in the precedent equations are profoundly affected by the electro- negativity of the metal, size of the alkyl ligand on the metal, solution pH,

type and concentration of solvent, concentration of water, temperature, and pressure. Each, in turn, can affect the course of structure (hence property) development in the gels and ceramic materials made from this point. This multitude of variables provides the great flexibility in material structure and properties which can be achieved with sol-gel processing. For example, depending on the quantity of water and catalyst, hydrolysis can either be fulfilled (all OR groups replaced by OH) or stop while the metal is only partially hydrolyzed [59].

Stabilization due to electrostatic repulsion is due to formation of a double layer at the particle. The surface of a particle is covered by ionic groups, which determines the surface potential. Counter ions in the solution will cover this layer, shielding the rest of the solution from the surface charges. For hydroxides the surface potential will be determined by reactions with the ions hydrogen H^+ and hydroxide OH^- . Thus, the surface potential is pH dependent and it is proved with the previous Equation (2.14) to Equation (2.16).

$$M - OH + OH^- \rightarrow M - O^- + H_2O \quad (2.17)$$

$$M - OH + H^+ \rightarrow M - OH_2^+ \quad (2.18)$$

For hydrous oxides, the charge-determining ions are H^+ and OH^- (Equation (2.17) and Equation (2.18)). Those ions organize the charge on the particles by the protonation or deprotonation of the MOH bonds on the surfaces of the particles [59]. The ability with which protons are added or removed from the oxide depends on the metal atom.

The kinetics of hydrolysis and condensation can be influenced by many parameters. Moreover, the systems are more complex than represented by the simplified equations presented before. Many species are present in the solution and hydrolysis and polycondensation occur at the same time. The important parameters are temperature, nature and concentration of electrolyte (acid, base), nature of the solvent, and type of alkoxide precursor [59, 75, 76] .
As the pH modifies the kinetics and the mechanisms of the reaction, Figure 2.18 to Figure 2.21 presented both cases of acidic and basic pH [59].

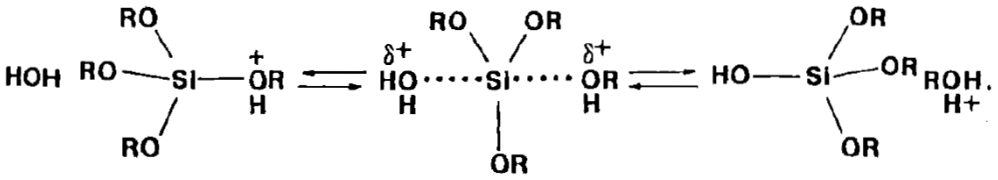

Figure 2.18 Hydrolysis in an acidic environment [59]

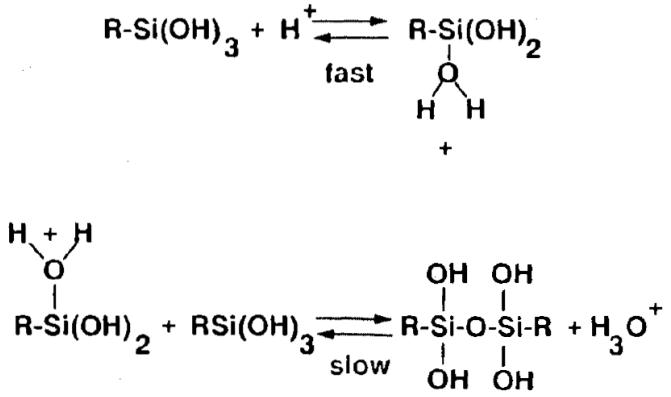

Figure 2.19 Condensation in acidic environment [59]

Then for a basic environment:

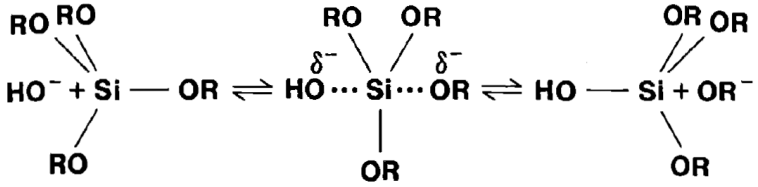

Figure 2.20 Hydrolysis in a basic environment [59]

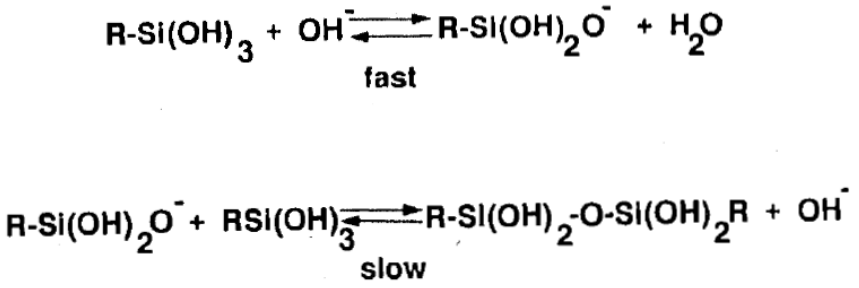

Figure 2.21 Condensation in a basic environment [59]

2.3.3 Gelation, Aging and Drying

After the polymerization, another step takes place: the gelation. A gel is a solid phase of interconnected particles containing liquid [77]. If the solid network is made of colloidal sol particles the gel is said to be colloidal. If the solid network is made of sub-colloidal chemical units then the gel is polymeric. The gel comes into being when the homogeneous dispersion known as sol becomes solid. This process, gelation, prevents the development of heterogeneities within the material. The sol can be transformed into a colloidal (or polymeric) gel by going through what is called a gel-point. It is at this point that the sol suddenly changes from a viscous liquid to a solid phase called gel. The monomers are able to form bonds and each are capable of making more than one, the size of the resulting molecule which can be then formed is in theory limitless. If this molecule reaches macroscopic dimension so that it is able to develop itself all over the solution, the substance is said to be a gel which means that the gel point is the time at which the last bond of the large molecule is formed, completing it. A gel can be described as a substance that contains a solid frame, itself enclosing a liquid phase [59]. The continuity of the solid structure gives elasticity to the gel. Gels can also be formed from particulate sols. Attractive and dispersive forces make them agglomerate and form a network [6, 59]. The gelation step makes the gel process irreversible. The gelation process may be reversible if other interactions are involved.

According to the kind of precursor chosen, the time of preparation of sol-gel coating can take up to a few days: indeed, if it is a silicon alkoxide, which is not sensitive to hydrolysis, gelation can take place within several days; but it can be enhanced by catalysis [78].

Aging is the process of change in structure and properties after gelation and would result in further condensation reaction and consequently the formation of a stronger network, which would resist the capillary force and prevent the formation of a dense sol-gel coating. Aging a gel before drying it helps to strengthen the network which will allow reducing the risk of cracks. When a gel is maintained in its pore liquid, its structure and properties continue to change long after the gel-point [75].
Aging was found to have a significant influence on the corrosion protection of the sol-gel coatings. Chou [79] studied the effect of aging on coatings and information from passivation. The differences obtained between the passivation region and passivation current density indicated that a coating from aged sols is less effective in corrosion protection than a coating from fresh sols. One possible explanation is that

the coatings made from a fresh sol had low porosity and/or a larger thickness than those of the coatings from an aged sol. It is unlikely to obtain thicker coatings made from fresh sol, since the viscosity of a sol increases with the aging time due to the continued condensation reaction. Aging led to an extended condensation reaction, which resulted in the growth of larger silica polymers and the formation of a stronger gel network [79].

Three processes can occur separately or simultaneously during aging of the silica gels: polycondensation, syneresis and coarsening [75]:

Polycondensation reactions continue to occur within the gel network as long as adjacent silanols are close enough to react. This increases the connectivity of the network and its fractal dimension (as explained earlier in 2.3.2 Sol).

Syneresis is the spontaneous shrinkage of the gel and resulting expulsion of liquid from the pores. In the case of alcoholic gel system, the shrinkage of the gel network is usually associated to the formation of new connection of silicon-oxygen-silica bonds through condensation reaction [75]. The syneresis contraction rate increases with concentration of silica in the sol and with temperature. When organic solvents are present they may form hydrogen bonds with the silanol groups which prevent condensation and slow syneresis [75].

Coarsening is the irreversible decrease in surface area through dissolution and reprecipitation processes. It is due to selective dissolution and precipitation with the gel network. Time, temperature and pH are variables that can effectively alter the aging process [75].

Finally, after the different steps, the final one is the drying. The process of drying of a porous material can be divided into several stages. The material starts by being reduced by an amount equal to the volume of liquid that evaporates and the liquid-vapor interface remains at the exterior surface of the body. The second part begins when the body is too solid to shrink anymore and the liquid retreats into the interior, leaving air-filled pores near the surface. Evaporation continues to take place as a continuous liquid film flows to the exterior, even as air invades the pores. Eventually, the liquid becomes isolated into pockets and drying can proceed only by evaporation of the liquid within the body and diffusion of the vapor to the outside. Drying produces a pressure gradient in the liquid phase of a gel, which leads to differential shrinkage of the network [59]. The most obvious characteristic of a dried gel is its

porosity. This aspect provides gels with properties that cannot be obtained with conventional ceramics [59].

There are several types of drying which lead to several types of gel. A xerogel is the brittle solid obtained when the gel is dried by evaporation under normal condition. This increases the capillary pressure that causes shrinkage of the gel network [6]. The xerogel is often reduced in volume by a factor of 5 to 10 compared to the original wet gel. If the wet gel is dried under supercritical condition, there is no interface between liquid and vapor, so there is no capillary pressure and relatively little shrinkage [59]. This process is called supercritical (or hypercritical) drying and the product is an aerogel. This is mostly air, having volume fraction of solid as low as ~ 1% [59]. Most gels are amorphous (non-crystalline), even after drying, but many crystallize when heated.

Depending on the connection between the liquid and the solid network, there can be different types of gel. An hydrogel (or aquagel) is a gel where the liquid is mostly composed of water. If the liquid phase is largely composed of an alcohol then the gel is an alcogel [6].

Chapter III. Literature Review

3.1 Presentation of the Chapter

This chapter introduces the literature review about different types of coatings: organic, inorganic and hybrid with a focus on silica sol-gel coatings and their physical and mechanical properties. Methods of application are presented before introducing the corrosion of the coated samples and the method of impedance chosen to be studied.

3.2 Organic, Inorganic and Hybrid Coatings: Definitions, Properties and Methods of Application

In aggressive environments, the coating must be an efficient barrier to prevent the diffusion of species and it has to withstand severe conditions. There are several important properties for sol-gel coatings in this field: a good adhesion between the coating and the substrate, chemical and heat resistance as well as chemical inertness and low permeability. It has been reported that sol–gel coatings have been successfully applied to improve corrosion and wear resistance in metals [80, 81]. Cracks in coatings help the penetration of corrosive material into the material. Therefore, the thermal expansion coefficients of the coating material and the material to be coated need to be similar to prevent crack formation during the heat treatment.

One of the main limitations of sol-gel coatings concerns their thickness, which can lead to the failure of the coating when too large [82]. Indeed, in the case of sol-gel coatings, a thicker coating does not mean a better protection. Greater thickness should establish an efficient physical barrier against steel corrosion, thus making it more difficult for the electrolyte to access the substrate surface. The degree of cracking depends on the type of coating, its composition and the heat treatment procedure [82, 83].

Thicker coatings (for example those which can be obtained at high temperature process) are more susceptible to the developments of cracks and lack of uniformity. This can be harmful regarding the corrosion protection if these cracks reach the substrate [84, 85]. Coatings obtained from gels subjected to the action of ultrasound and from aged gels are less susceptible to cracking [59]. Cracks in coatings being in

service in aggressive water media are particularly harmful. Cracks which appear during high temperature oxidation are less dangerous [83]. An undesirable aspect of the coatings produced by the sol–gel technique is their brittleness and lack of elasticity: under plastic deformation they crack easily and delaminate [86].

3.2.1 Precursors

The structure of the precursor can influence the structure of the deposited film [87]. There are mainly two types of precursors: silicates and non-silicates [59]. The transition metal alkoxides, especially Ti and Zr, are used as molecular precursors to glasses and ceramics [59]. These systems can be differentiated from silicates by a more important chemical reactivity resulting from the lower electronegativity of the metal and its ability to display several coordination states. This means that coordination expansion occurs spontaneously upon reaction with water or other nucleophilic reagents [6, 59].

The possible structures of the solution precursors range from weakly branched polymeric species to uniform particles that may or may not be aggregated [59].

There can be nanoparticles (for example TiO_2 nanoparticles) or microparticles within the sol-gel matrix. Microparticles have been used to improve the mechanical properties (including scratch-resistance, abrasion resistance etc.) [88-92]. Nanoparticles have other advantages for coatings materials such as better adhesion and decreasing coating thickness. The particles combine the matrix by enhancing the reactions of active surface groups of these particles and the sol-gel functional groups [88].

3.2.2 Organic Coatings

Organic coatings have been used for a long time to protect metals against corrosion in atmospheric conditions. The primary function of organic coatings in corrosion protection is to isolate the metal from the corrosive environment. In addition to forming a barrier layer to stifle corrosion, the organic coating can contain corrosion inhibitors [3].

The main advantages of organic systems are that they are mechanically flexible and tough, but have poor abrasion and thermal resistance. Organic coatings have been

used for a long time to protect metals against corrosion in atmospheric conditions or for the protection of structures against marine corrosion. Organic components in sol-gel films lead to improved corrosion protection properties due to formation of thicker crack-free films compared to the inorganic ones, their thickness being able to reach as high as several hundreds of micrometers. The use of these components is limited by their thermal weakness and by their mechanical properties which, although superior to those of polymers, are not as good as those of ceramics [83]. Moreover, the organic component leads to the decrease of wear resistance and mechanical properties of the sol–gel coatings in hybrid coatings for example [93, 94]. The main constituents responsible for the creation of well-adhering adhering film (membrane) are organic compounds: polymers, oligomers, monomers, or mixtures [95].

The types of organic coatings can be summarized as follow [95]:

- Primers: adhesion to the substrate, corrosion protection
- Topcoats, with high resistance to external factors, such as: enamel and paints
- Adhesive cements: materials with a suitable consistency coatings used for surfacing
- Resins: epoxy, polyamides, silicones…

The epoxy resins will be of particular interest for this project. The organic coatings do not go through the sol-gel process and are thus not called organic sol-gel coatings but organic coatings.

3.2.3 Inorganic Sol-Gel Coatings

Historically, the first type of sol–gel pre-treatments are inorganic oxide sol-gel derived films. Inorganic sol–gel coatings for corrosion protection of different metallic substrates were developed and investigated in several works [96-98]. The sol–gel derived inorganic coatings which are prepared using low temperature for the drying stage usually present better barrier properties against wet corrosion than fired sol-gel films, due to the formation of less defective layers [72, 99, 100]. However, the barrier properties of these coatings are not faultless and efficient enough to obtain a good protection against corrosive species. This can be due to the formation of non-compact coatings with high amount of micropores. On the other hand inorganic sol-

gel coatings provide a good adhesion layer between metallic substrate and organic coatings [96, 101].

When the sol-gel process was first created, hydrolysable precursors were used which lead to the development of pure inorganic coatings. These coatings had to be cured necessarily at higher temperatures close to 600°C-1000°C [102]. Moreover, these coatings were quite thin with thicknesses ranging from few hundreds of nanometres to a maximum of 1µm [103]. Coatings were hard and able to provide good wear and corrosion resistance, in addition to other specific properties depending on the precursors employed. However, coatings could be deposited only on high melting metal or alloys, glass, and ceramics [78]. The coatings were brittle, limiting the application segment of the novel process.

Inorganic systems have excellent abrasion resistance and high density, but are brittle and require high processing temperatures. Inorganic sols not only strengthen adhesion on metal substrate, but also improve comprehensive performances of polymer [12].

There are different types of inorganic coatings such as [104]:

- Hydraulic cement used to coat pipes inside and out, especially those buried under sea water
- Ceramics and glass, used in the same principle as hydraulic cement but with the purpose of conferring resistance to heat or attack by hot, high velocity gases
- Chromate filming

3.2.4 Hybrid Sol-Gel Coatings

Hybrid films combine properties of the organic polymeric material and properties of the ceramic. The sol-gel processing not only allows for materials to have any oxide composition, but it also permits the production of new hybrid organic-inorganic materials which do not exist naturally. It was to overcome the limitation of pure inorganic sol–gel coatings [57]. Hybrid coatings can be prepared over a continuous compositional range from almost organic to almost inorganic [63]. The properties of these coatings can be changed regularly to form an optimum coating [105]. The inorganic components provide enhanced mechanical properties such as the increase of scratch resistance, durability and adhesion to the metal substrate [66,

72]. The organic component increases density, flexibility, and functional compatibility with organic paint systems [106]. Hybrid coatings can be divided in two categories. First the organic molecules or polymers are embedded in an inorganic matrix [103]. The inorganic network is generated as a result of hydrolysis and condensation while the organic compound that is added occupies the pores in the inorganic network. The interactions between the two parts are regulated by hydrogen bonding and van der Waals forces. The second category consists of organic and inorganic components which are strongly linked through iono-covalent bonds [103].

An advantage of the organically modified sol–gel systems is the possibility to prepare thick, crack-free coatings [107]. Montemor [108] described in a review different functional coatings and especially siloxane-modified epoxy coatings deposited on steel [109-112] which significantly improve their properties. This type of hybrid coating is of particular interest for this project.

Hybrid coatings can easily form a thicker layer in micrometer scale without cracks while the temperature needed for the curing process is much lower. The polymer sol–gel network can be strengthened by the distribution of inorganic particles in the hybrid matrix. Moreover the hybrid sol–gel system has much more flexibility in adaptation of anti-corrosion additives, such as inhibitors, pigments, etc., so the overall corrosion protection ability of the sol–gel system can be considerably improved [57, 113].

Hybrid coatings thus have the advantages and properties of both inorganic and organic components.

The synthesis of hybrids can be performed by mixing an inorganic sol with an organic phase and carrying out the sol hydrolysis and condensation reactions in the presence of a preformed organic polymer [105, 107]. Such composites usually cannot provide effective long term stability during weathering. The precursors with already covalent or complex bonded organic groups are used for synthesis of the hybrid sol–gel systems in the second class of hybrids. Strong chemical bonds form between organic and inorganic parts in the final hybrid materials [72, 114]. Figure 3.1 presents a limited selection of the precursors, organo(alkoxy)silanes and metal alkoxides for sol-gel derived hybrid materials.

Inorganic sols in hybrid coatings increase the adhesion to the substrate by forming chemical bonds between metals and hybrid coatings but also improve the performances of polymer in the coatings. Regarding the corrosion protection of the

metallic substrate, the organic constituents of the hybrid coatings are selected to repel water, to form dense thick films and reduce the porosity of the coating [12, 115].

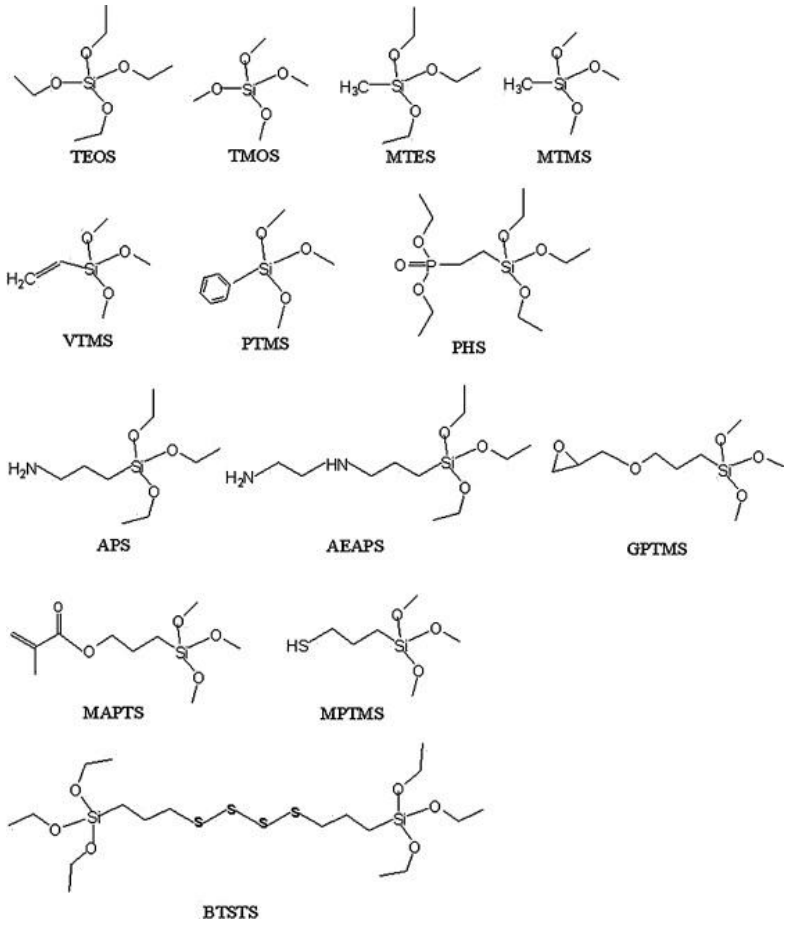

Figure 3.1 Organo(alkoxy)silanes and metal alkoxides serving as precursors for sol-gel derived hybrid materials [57, 116]

In a review written by Figueira et. Al [117] it was demonstrated that the most used precursors for metal substrates are TEOS, GPTMS and MAPTS.

3.2.5 Silica

In this project, most of the samples are silica inorganic/hybrid sol-gel coatings. Due to their chemical and thermal durability, silica (SiO_2) coatings are of interest for protection of metals against oxidation and acid corrosion at temperatures T >300°C [100]. They are a rapidly expanding technology due to their main advantages [118]. Silicon alkoxides are not very sensitive to hydrolysis. Gelation may take place within

several days when pure water is added. Therefore hydrolysis and condensation rates of silicon alkoxides are currently enhanced by acid or base catalysis [74, 119].

However, the protective function of these coatings is limited by lack of adhesion between coating and metal and crack formation during the thermal densification at temperatures around 500°C [100, 120]. To improve the adhesion of films on a metal surface, prior to ceramic deposition the metal surface should be treated. As a result of this treatment, a bond between the substrate and the ceramic coating is formed [120]. The physical, chemical and mechanical properties of ceramic films formed on metallic surfaces are dependent on the physical and chemical properties of the gel precursor solutions. They are also dependent on the parameters of the dipping process, the drying and densification processes. The protective ability of the coating can be influenced by a change in one of the parameters of the process which in turn can modify the physical and chemical properties of the gel precursor solution or dipping process [121]. The corrosion protection accorded by the sol-gel coatings is affected by the coating thickness. Although those coatings provide many advantages, they tend to crack if their thickness is more than several microns [122].

Generally, ceramics and ceramic coatings with good passivity, low conductivity (some with silica alumina or magnesia components have an electrical conductivity at room temperature as low as 10^{-17} – 10^{-21} Ω^{-1} cm^{-1}) or insulating properties and good tribological properties show good corrosion resistance in aggressive media. Therefore, ceramics oxide films and coatings like TiO_2, Al_2O_3, ZrO_2, SiO_2, etc. can be applied on metals to improve their surface properties [81, 123].

Since silane sols offer very good adhesion performance together with high environmental compatibility, silane pre-treatments are also widely used as adhesion promoters for organic coated metals to replace the traditional metal surface pre-treatment (for example chromate conversion coating), which are considered toxic and hazardous to the environment [12].

The use of organofunctional silanes can improve the mechanical properties and adhesion to specific organic paint systems in comparison to sol–gel materials based on non-functional organosilanes [124]. Monomeric silicon chemicals are known as silanes. A silane that contains at least one carbon-silicon bond (Si-C) structure is known as an organosilane [125], Figure 3.2 presents the structure of an organosilane based layer [126].

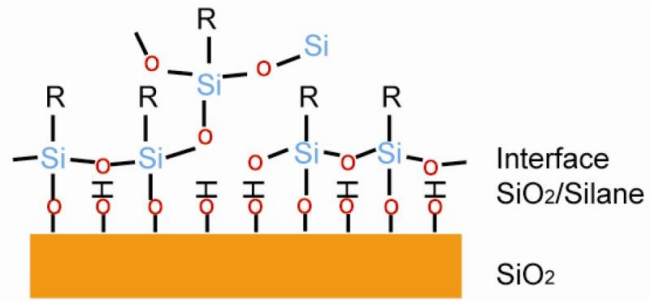

Figure 3.2 Structure of organosilane based layer [126]

Hybrid coatings ormosils (organically modified silicates) are organic-inorganic hybrid solids in which the organic component may be chemically bound to a silica matrix. The structure of the silica network is partially similar to inorganic silicate glasses and it can be modified by the presence of organic groups [127] .

Organic molecules can be added within the silica matrix by incorporating organic molecules with the silicon alkoxide precursors in a common solvent. Hydrolysis and condensation then lead to the formation of a silica network around the organic components that remains physically trapped within the glass [78]. However the reactivity of both organic and inorganic precursors is usually quite different and phase separation tends to occur unless chemical bonds link organic and inorganic species [74] .

When the hydrolysis and polycondensation of an organometallic precursor take place at the same time, a silica gel may be produced by the formation of an interconnected 3-D network or it can be constructed by network growth from several colloidal particles. A gel is defined as dried when the physically adsorbed water is completely evacuated. This occurs between 100 and 180 °C [76]. The condensation reaction continues to take place because of the large concentration of silanol (SiOH) groups in a newly formed gel. As the hydroxyls are lost during aging, new bonds are formed creating more cross-linked structures [75].

An example of the mechanism with silica is shown in Figure 3.3:

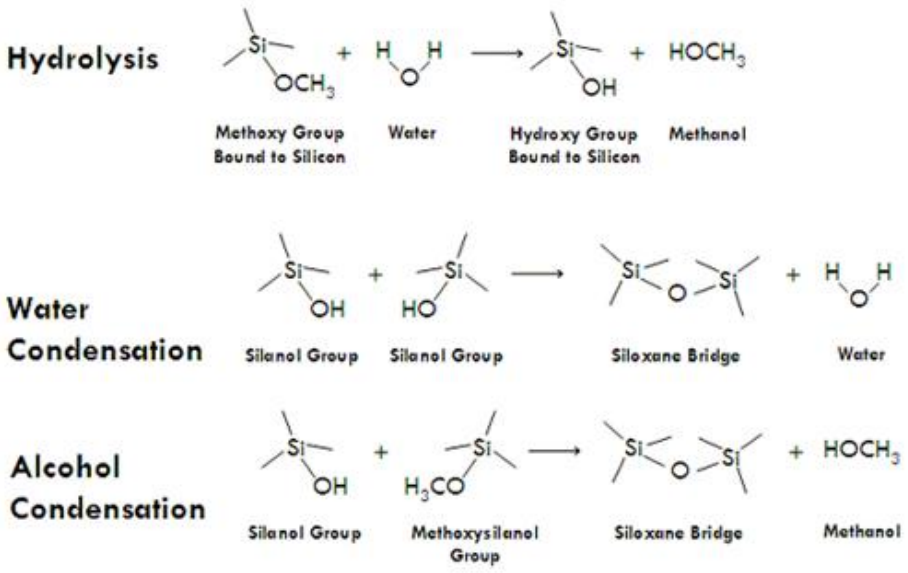

Figure 3.3 Reactions in silica gel formation [128]

3.2.6 Properties

Cracks are easy to form due to this internal stress if the film formation conditions are not carefully controlled [57]. That is why both mechanical and physical properties of the coatings must be studied. The evolution of corrosion and its rate depend on the coating and its properties.

This section presents the main properties which can be studied.

3.2.6.1 Mechanical Properties

The mechanical properties important for the durability of the coatings are [129]:

- Elasticity: ability of a coating material to resist changes in its volume or shape under mechanical stress due to increase in internal energy. It can be calculated with the help of Young modulus (Pa or $N.m^{-2}$)
- Hardness: resistance of a material to local deformation (Pa)
- Bending and tensile strengths (Pa): stresses corresponding to maximum loads that a coating may withstand in tests for bending and tension

- Impact strength: characterizes the resistance of the coating material to dynamic impact [129]

For thick coatings, it is sometimes possible to detach the coating from the substrate and to measure properties such as the elastic modulus and the fracture toughness by carrying out mechanical tests [130]. However, it is usually impossible to dissociate the coating [131]. Consequently, a clear way to measure the mechanical properties of the coating is to deform it on a very small scale. A useful way to accomplish this is by indentation testing on a nanometer scale, commonly referred to as nano-indentation [130, 132, 133]. However large indentation will not solely represent the mechanical properties of the coating but the properties of the coating in addition of the properties of the substrate. Hence, these techniques have become the most widely used techniques for measuring the mechanical properties of thin coatings, although a complete methodology to determine the full set of relevant mechanical properties is still lacking [131].

The indentation is carried out into a coating of thickness t, which is adherent to a substrate. In the case of a thin coating, however, the response will be a combination of both coating and substrate behaviour [131]. This means that the parameters obtained are actually a combination of the properties of the coating and the substrate which means that the coating properties will dominate for shallow indentation depths, and the substrate will dominate for deeper indentations [131].

The hardness is traditionally measured by performing an indentation at a certain indentation load, removing the load and optically examining the surface to determine the area of the plastic residual imprint. The hardness is then defined as the ratio of the maximum indentation load and the measured area [131].

In modern nano-indentation, the definition of hardness is somewhat different. In this case, the area used in the definition of hardness is actually the projected contact area at maximum load, which is not necessarily equal to the area of the final residual imprint.

3.2.6.2 Physical Properties

The physical properties that are known to be important are [129]:

- Density: ratio of the body mass m to the volume of its compact nonporous matrix V_R: $\rho_{true} = m/V_R$ ($kg.m^{-3}$)
- Porosity: ratio of the entire pore volume to the total volume of a porous body
- Permeability of liquids: characterizes the mass of the liquid flowing through the coating in a time unit depending on the pressure differential across the coating (D or μm^2) [129]
- Thermal conductivity: characterized by the amount of heat transferred in unit time through a unit area of a unit of length thick plate with the temperature different of 1 degree between its surfaces ($W.m^{-1}.K^{-1}$)
- Thickness (m)
- Roughness [129]

Use of the passive metal as a substrate should provide higher corrosion resistance to the coating system compared to an active metal. This is due to a passive oxide film formed on the passive metal might act as a barrier layer to retard a contact between an electrolyte and the metal substrate, and therefore, reduce the corrosion rate of the coating system.

The surface can be prepared or pre-treated in order to be corrosion-protected. This is a crucial step in the coating preparation. The coatings have to adhere to the substrate so the surfaces must be free from any soils, corrosion products and lose particulates. The choice of cleaning method depends on the substrate and the size and shape of the object. To improve coating adhesion, pre-treatments are applied after cleaning [14].

A mechanical bond is built when the surface of a substrate has pores, holes and cavities into which the coating spreads and solidifies The removal of the coating is made more difficult if the substrate has undercut areas that are filled with cured coating [14].

Adhesion of coatings to the substrate and the interlayer adhesion between separate coating layers are the main parameters describing the barrier and protective properties of coatings. The loss of adhesion also means the loss of a protective function of a coating. The known adhesion tests are mostly destructive and suffer from the insufficient sensitivity and accuracy according to Piens and De Deurwaerder [134]. The traditional mechanical tests are straightforward but the information they provide can be more considered as qualitative information about

the adhesion of coatings and its changes with the time of exposure [135]. In application, the adhesion of coatings undergoes standing fluctuations, depending on the conditions of the environmental, which can change. One of the main causes of adhesion loss is the water uptake, the water entering into the interface or interlayer region. This causes the lowering of the polymer adhesion. Destructive methods are difficult to quantify such time-dependent adhesion changes. Water diffusion into organic coatings has been studied extensively with electrochemical impedance spectroscopy (EIS) [136, 137].

Scratch testing is a simple and rapid method of characterizing coatings but the results obtained are influenced by various factors such as coating thickness, substrate mechanical properties, interfacial bond strength and test conditions such as scratch speed, load and indenter tip radius [103]. Figure 3.4 presents a schematic of an indenter scratching a sample. The onset load for coating cracking is referred to as the critical load. There are two critical loads. Lc1 known as 'lower critical load' is the load at which the first crack appears and represents the cohesion of the coating. This will be the parameter studied in this project. The second critical load Lc2, 'upper critical load' represents the load at which total peeling-off the coating from the substrate surface occurs [103, 138]. With this method the adhesion strength is not measured directly but by its performance.

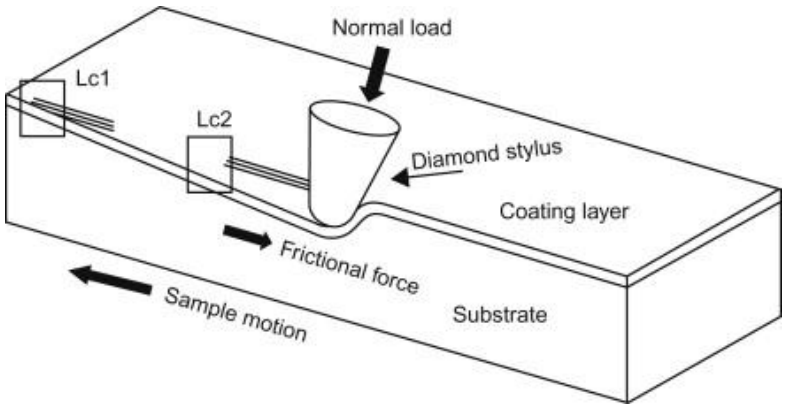

Figure 3.4 Schematic showing an indenter scratching a sample [103]

3.2.7 Methods of Application

A sol-gel coating can be applied to a metal substrate through various techniques, such as dip-coating and spin-coating, spraying and electrodeposition, which are all

methods used by the company sponsor. Depending on the used technique, after the coating deposition, there is a substantial volume contraction and internal stress accumulation due to the large amount of evaporation of solvents and water [57] .

However, the conventional methods for depositing sol–gel films on metals, i.e., dip-coating, spin-coating and spraying are mainly suitable for flat surfaces [139] .

To achieve uniform, defect-free deposition, the substrate must be free of dust and other particles and it must be uniformly wetting to the sol-gel solution. The most common application is to deposit the film on a substrate that is completely wetting to the solution [78] .

- Dip coating

Sol-gel dip coating forms when the substrate is immersed in the liquid solution and then removed at a designated speed under controlled temperature and atmospheric conditions. During this process the initial layer of coating bonds to the surface of the substrate while a boundary layer divides the liquid and the outer layer flows back into the pool of solution. The layer thickness is dependent upon the speed the substrate is withdrawn from the solution. It should be understood that the thicker the coating the longer it will take to age and dry due to increasing porosity levels [99, 140, 141]. Dip coating has major advantages, such as ending in homogeneous coatings with simple thickness control. Some drawbacks of this technique are resultant drain lines and special caution during the drying stage that is needed to obtain homogeneous, crack free materials [141].

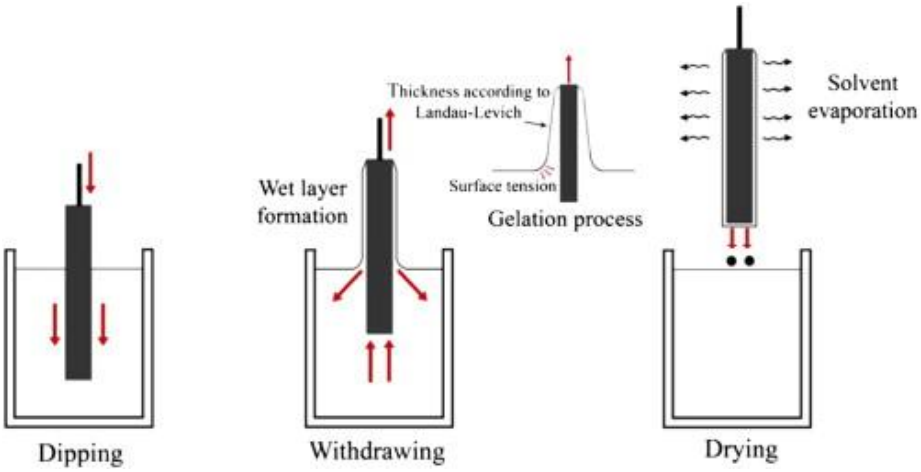

Figure 3.5 Schematic representing the dip-coating process [142, 143]

- Spin coating

Spin coating is characteristically used on flat substrates or small disks since the physics of application limits the coating uniformity but it is not a very economical method. The process is such that the solution is put in one location, typically the center of the substrate and then the substrate is spun at high speeds letting the centrifugal force created spread the coating on the surfaces. This process is mainly used for thin coatings. The higher the rotational speed the thinner the coating becomes [80, 144, 145]. There are four key stages in spin coating:

1. Deposition of the coating fluid onto the substrate
2. Aggressive fluid expulsion from the substrate surface by the rotational motion
3. Gradual fluid thinning
4. Coating thinning by solvent evaporation

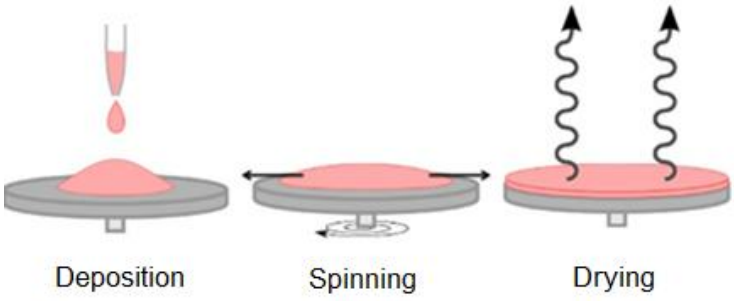

Figure 3.6 Schematic representing the spin-coating process [142]

- Spray coating

A more uniform and smoother surface can be obtained with spray painting rather than with brushing or rolling because the latter methods tend to leave brush or stipple marks and irregular thickness [14]. The most common methods of spray painting are conventional and airless [14]. Spraying is accomplished by atomising a sol with compressed air through a spray gun. Spray coating with sol-gel is much simpler than plasma spray since one can use an air gun at room temperature to deposit layers of the liquid solution. The final microstructure is not dependent on the spray angle.

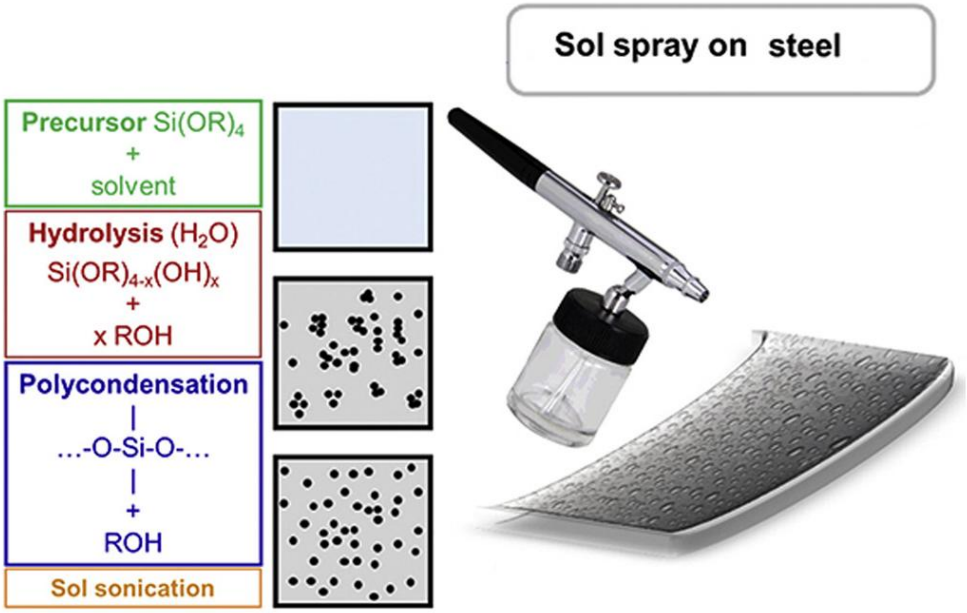

Figure 3.7 Schematic representing the spray-coating process [146]

- Electrodeposition

Electrodeposition technique offers relatively thick homogeneous defect-free hybrid coatings in comparison to dip or spin coating techniques [12]. Electrodeposition is a combination of two processes, electrophoresis and deposition. The electrophoresis involves the motion of charged particles in a stable suspension under an electric field, while the deposition is the result of the impact of these particles against the electrode of opposite sign [147]. This process allows obtaining coatings onto complex shaped substrates of any electrical nature [148].

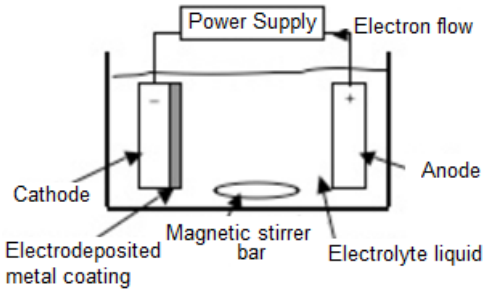

Figure 3.8 Schematic of electrodeposition [149]

3.3 Corrosion of a Coated Sample

In order to protect the metals and enhance their resistance, coatings can be applied. The nature of the coatings depends on the aggressivity and the conditions of the environment.

Most coatings degrade with time, resulting in complex behaviour. Water can permeate all coatings to some extent [14]. Corrosion of coated materials occurs only after the adhesion between the coating and the substrate is broken due to water or oxygen permeation and the electrochemical reactions ensuing within the water thin layer. Hence, corrosion of the coated metals is effectively prevented when these reactions are limited. After a certain amount of time, water penetrates into the coating and forms a new liquid/metal interface under the coating. Corrosion phenomena can occur at this new interface. The analysis of the early stages of corrosion is challenging. The majority of coatings are applied on external surfaces to protect the metal from natural atmospheric corrosion and atmospheric pollution. On some occasions, coatings are applied internally in vessels for corrosion resistance. To be effective, the durability of the coating must be greater than that of the base metal or it must be maintained by some means [14]. For corrosion to take place on a metal surface under a coating, it is necessary for an electrochemical double layer to be established. For this to take place, it is necessary for the adhesion between the substrate and coating to be broken. This permits a separate thin water layer to form as the interface from water that permeated the coating. Water and oxygen permeation are required for corrosion, so transport of water, oxygen and ion through the coatings is also important to better understand the corrosion that occurs under the coatings [150]. Although an improved adhesive property is one of the main functionality of sol-gel coatings, the combination of barrier and active protective effectiveness may lead to an improved anti-corrosion performance of the sol-gel films [151].

Leidheiser [150] reviewed several different types of corrosion underneath organic coatings: wet adhesion, blistering, cathodic delamination, anodic undermining and filiform corrosion, any of which may be related to the others.

First of all, wet adhesion happens when the adhesion between the coating and the substrate is affected after water molecules have reached the substrate/ coating interface.

Blistering means the formation of bubbles under or within the interface coating/interface because of osmotic pressure, considered as the most important mechanism responsible for blister formation and volume expansion due to the swelling caused by water absorption. A schematic is presented in Figure 3.9.

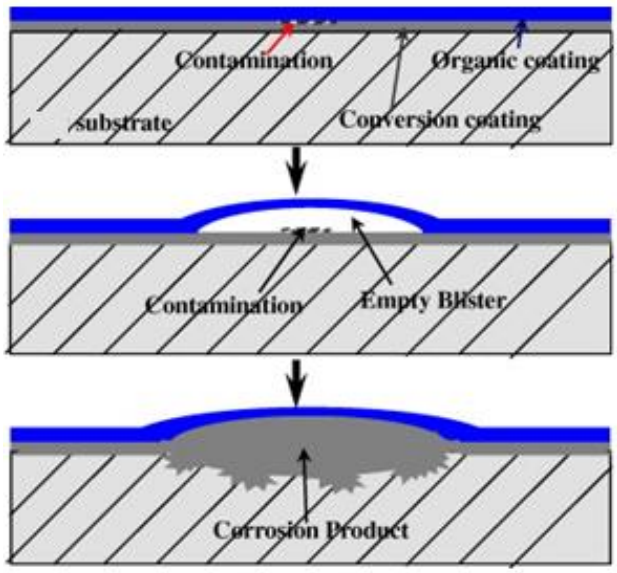

Figure 3.9 Schematic of mechanism and evolution of blistering [152]

Cathodic delamination is a corrosion reaction occurring spontaneously in seawater on cathodically polarized surface thus destroying polymer/metal bonds. When cathodic protection is applied to a coated metal, loss of adhesion between the substrate and the coating takes place. Figure 3.10 presents the situation with an ideal schematic.

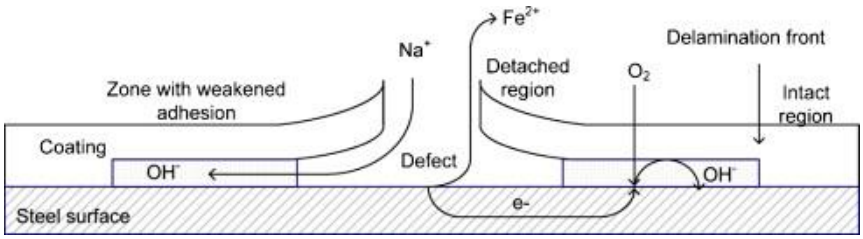

Figure 3.10 Idealized schematic of cathodic delamination [153]

An anodic dissolution of the substrate metal leads to a loss of adhesion resulting in anodic undermining. Coating defects may cause anodic undermining, but in most cases it is associated with a corrosion-sensitive site under the coating, such as a particle from a cleaning or blasting procedure, or a site on the metal surface with potentially increased corrosion activity [14].

Filiform corrosion is a special form of corrosion on coated metals. Metals with water-permeability coatings or films and defects in the coating may undergo a type of corrosion resulting in numerous meandering thread-like filaments of corrosion beneath the coatings or films [14, 150].

Since the corrosion performance of the coating systems depends on both the coating and substrate properties, metal composition becomes a critical aspect to provide a high quality surface for ceramic coatings [154]. As for the substrate, it seems clear that the use of passive metals should provide higher corrosion resistance, such as 316L stainless steel used as one of the substrates in this research. However, the difficulties which might occur in case of using such materials as protective coatings for the steel base result from the fact that in most cases they have high electrochemical potentials in aqueous solutions. They belong to cathodic coatings and may perform their tasks provided that the coating would have no pores, cracks and would physically prevent penetration of the aqueous medium to the steel substrate [145]. The substrate roughness was proven to have a great influence on the corrosion behaviour of the coating system. The rougher the substrate, the more subject to corrosion it will be. It is due to the stress from the heat treatment and the following cooling [155]. When the stainless steel is protected by the conversion layer, no effect on the structure is observed after immersion in pure water and there is no modification of the coating composition either. When it is tested in NaCl, the formation of a rust coloured precipitate on the surface and inside the pores of the conversion layer appears. An important loss of mass equivalent up to 30% can be observed [156]. With the results of impedance measurements, corrosion can be represented by means of resistive and capacitive elements, giving an electrical circuit. Figure 3.11 presents an example of equivalent circuit related to a corroded coating:

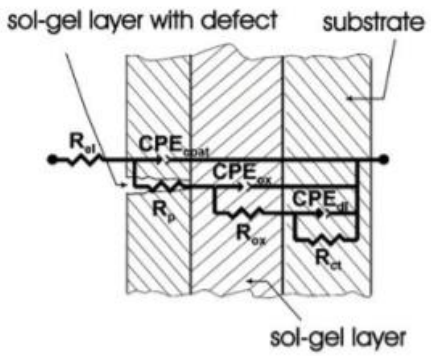

Figure 3.11 Equivalent circuit for a defected coating [114]

3.4 Impedance: Corrosion Studied with Electrochemical Impedance Spectroscopy

EIS allows the measurement of two phenomena: (1) the deterioration of the coating caused by exposure to an electrolyte and (2) the increase in corrosion rate of the underlying substrate due to the deterioration of the coating and subsequent attack by the electrolyte. The particularity of EIS is that an AC voltage of varying frequency is applied to the sample. The capacitance of a metal electrode in contact with an electrolyte is important information for any electrochemical system. As the organic coating deteriorates with time during exposure to an electrolyte, EIS can track changes in the capacitance of the coating. The capacitance will change as the coating swells or absorbs water, for example [51, 157]. In addition, the changes in the porosity of the coating can be measured. EIS is also able to simultaneously track the corrosion rate of the substrate (when metallic). This corrosion rate usually increases as the protective coating fails, allowing a connection between the electrolyte and the substrate [51].

The solution resistance is often an important parameter in the impedance of an electrochemical cell. A three electrode potentiostat compensates for the solution resistance between the counter and reference electrodes.

The impedance of a pure resistor is noted as R and the impedance of an inductor is presented in Equation (3.3):

$$Z_L = j\omega L \tag{3.3}$$

Capacitors in EIS experiments often do not behave ideally. Instead, they act like a Constant Phase Element (CPE) as defined in Equation (3.4). At OCP (η=0) anodic and cathodic current are equal and the external current i=0 A.cm^{-2}, no current flows to or from the electrode [30].
The impedance of a capacitor can be expressed as Equation (3.4) [157]:

$$Z_{CPE} = \frac{1}{j\omega Y_0} \tag{3.4}$$

With Y_0: capacitance (F)

Z: Impedance (Ω)

In the case of the purely capacitive coating or perfect coating system, the metal substrate is covered with an undamaged coating which has generally high impedance. The electrical equivalent circuit model used to analyse the impedance response of this ideal system is presented in Figure 3.12, including a resistor due primarily to an electrolyte (R_s) and the coating capacitance (C_c) in series.

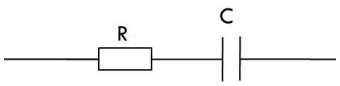

Figure 3.12 Purely Capacitive Coating [157]

The model includes a resistor (mainly due to the electrolyte) and the coating capacitance in series.

There are three different forms of presenting the potential and current values registered during an EIS experiment: one Nyquist plot and two Bode plots. The Nyquist plot shows the imaginary part of the impedance on the Y-axis with regard to the real part of that impedance on the X-axis at each excitation frequency. On the plot presented in Figure 3.13 and for a better understanding of the plot the Y-axis is negative. One Bode plot relates the impedance module to the frequency while the other links the phase shift to the frequency (Figure 3.13).

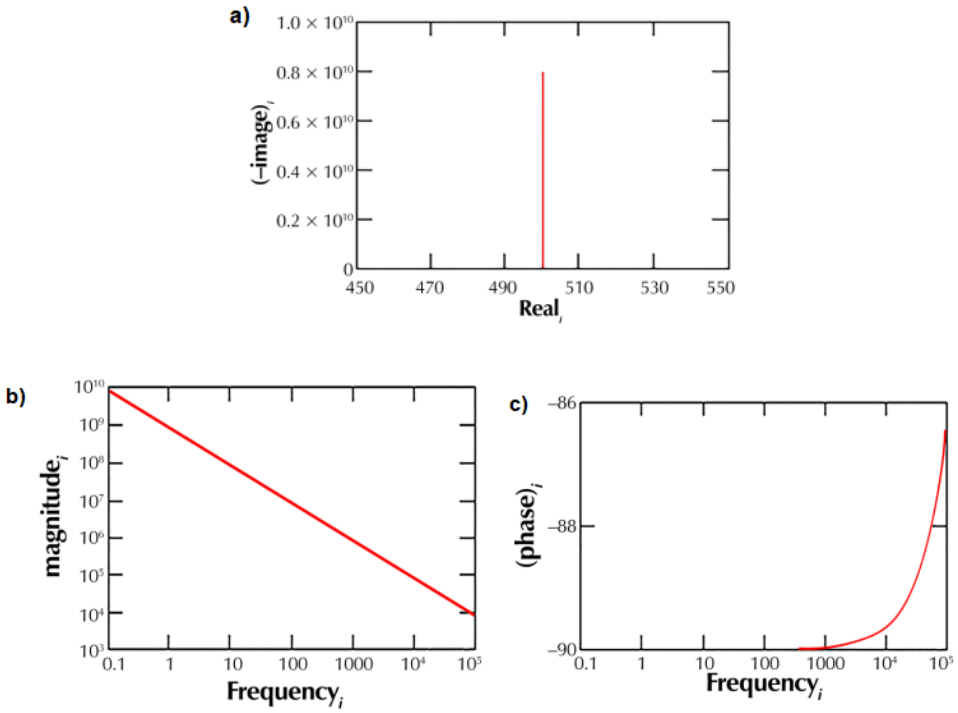

Figure 3.13 Typical Nyquist Plot (a) and Bode plots : Bode magnitude (b) Bode phase (c) for an ideal coating [157]

The value of the capacitance cannot be determined from the Nyquist Plot. It can be determined by a curve fit or from an examination of the data points. The intersection of the curve with the real axis gives an estimate value of the solution resistance.

The example for the Nyquist plot for an ideal coating system is illustrated in Figure 3.13, which is the behaviour of a purely capacitive coating. The intercept of the curve with the real axis gives an estimate of R_s (solution resistance). The Nyquist plot shows no change in the range of frequency, the resistance of the coating is thus unchanged. The same data are shown in a Bode Plot in Figure 3.13b). The capacitance can be estimated from the graph but the solution resistance value does not appear on the chart.

In the case of an actual tested coating, at high frequencies the impedance response is almost entirely created by the Ohmic or the solution resistance R_s as shown in Figure 3.14. The Nyquist plot format makes it easy to see the effects of the Ohmic resistance. At the lowest frequencies, the impedance response approximates a resistance as well but it corresponds to $R_s + R_p$, R_p being the polarization resistance [157, 158](Figure 3.14 (a)). The solution resistance is the potential drop between the reference electrode and the working electrode of an electrochemical cell. The polarization resistance (R_p) is the transition resistance between the electrodes and the electrolyte. An electrode is known as being polarized when its potential is forced away from its value at open circuit or corrosion potential. As a result of the electrochemical reactions that it generates at the electrode surface, the polarization of an electrode causes current to flow. An electrical double layer exists on the interface between a metal surface and its surrounding electrolyte. This double layer is formed as ions from the solution hold on the electrode surface and form a layer balancing the electrode charge [15, 42, 43, 52]. The polarization resistance can also be described as the corrosion rate of the metal substrate beneath the coating is described by the polarization resistance. For a metal in the absence of a coating, the corrosion rate can be determined from the polarization resistance. The polarization resistance is inversely proportional to the corrosion rate. A typical polarization resistance for a bare metal is $5000\Omega.cm^{-2}$. R_p must be normalized because it is electrode area dependent [51].

The second Bode plot Figure 3.14 (c) schematizes the phase angle shift between the applied AC potential and the registered AC current. On the Bode magnitude plot at low frequencies $R_s + R_p$ can also be obtained as $\log(R_s+R_p)$ can be read from the low frequency horizontal plateau. At intermediate frequencies, the impedance

spectrum should be a straight line with a slope of -1, indicating a presence of a capacitor in the equivalent circuit Figure 3.15.

The Bode phase plot (Figure 3.14 (c)) shows that the phase angle is nearly zero at the high and low frequency regions, where the behaviour of the cell is resistor-like. At intermediate frequencies, the inflection is observed due to the existence of the capacitor. In the Bode phase plot, the more the peak of each response is close to -90°, the stronger the capacitive response. An ideal capacitance would be when the peaks reach -90°. In general, the Bode diagrams provide clearer information of the frequency-dependent behaviour of the electrochemical system than the Nyquist plot, in which frequency values are implicit [51, 157].

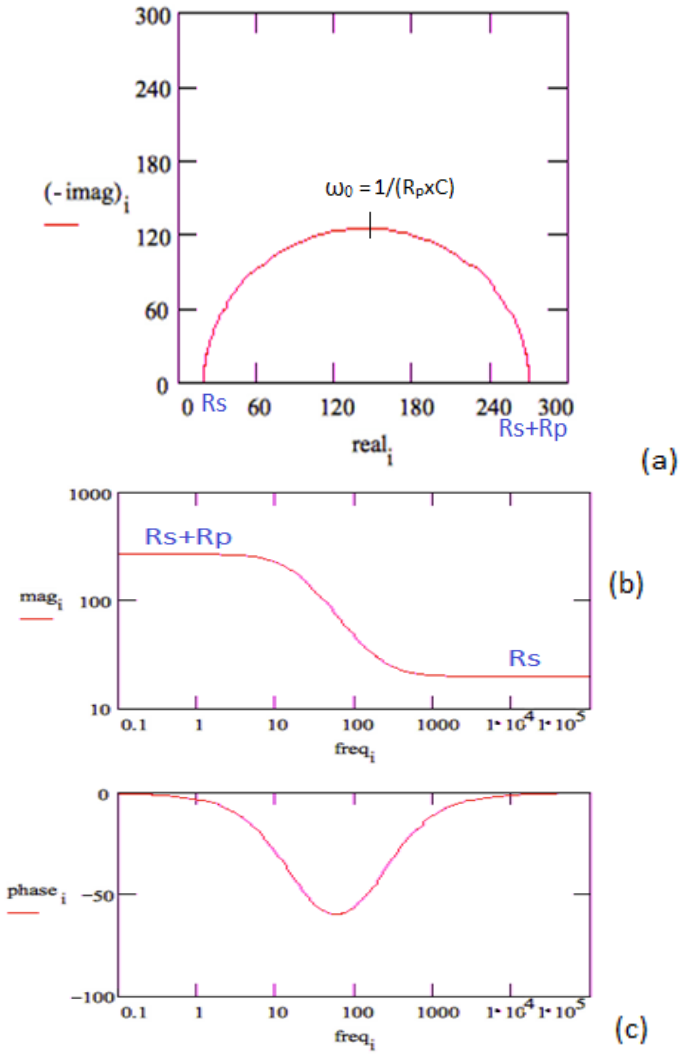

Figure 3.14 Nyquist plot for a real system (a) Bode plot for a real system: Bode magnitude (b) Bode phase (c)[157]

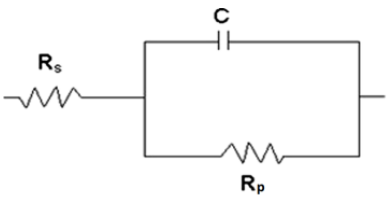

Figure 3.15 Equivalent circuit for a real system (Randles equivalent circuit) [157]

C is parallel to R_p due to the charge transfer reaction.

A constant phase element (CPE) is usually used instead of the ideal capacitor C because the CPE takes into account the non-ideal value of the slopes in the plots.

The AC impedance technique, although having some disadvantages, has become an effective method in the study of corrosion protection and is accepted as a standard technique for the analysis of corrosion and coatings [159] and the study of the relationship between the corrosion behaviour and the coating properties.

The research group of Van Westing [160-163] provided several works about AC test on coatings, especially epoxy coatings. According to their studies, the Nyquist plots of the impedance spectra obtained indicated no change during the exposure to saline water. However, information about the evolution of dielectric properties of the coatings could be obtained with the equivalent circuits and the use of the CPE. It was thus possible to detect localised loss of adhesion and the start of corrosion process at the coating/substrate interface. They also found that water uptake has an influence on the values of CPE.

Studies of AC impedance on ceramic coatings [145, 155] are fewer and can sometimes present different results for a same measurement: there can be inconsistency between the results in Nyquist and Bode plot. Masalski [145] presented Bode diagrams showing no significant change in the impedance spectra throughout the experiment, which was correlated to the visible results that there was no coating decomposition detected. The impedance response for the Nyquist plot showed to vary with the immersion time and flatten due to the frequency dispersion, suggesting the presence of more than one time constant. The changes in the impedance spectra with time indicate that the electrochemical properties of the film vary with the time of exposure.

In the case of corrosion taking place, it is assumed that an area of the coating has been delaminated on the metal side of the pore and that a cavity filled with the electrolyte solution has developed. This electrolyte solution can be very different

than the bulk solution outside of the coating. The interface between this cavity of solution and the bare metal is associated to a double-layer capacitance in parallel with a kinetically controlled charge-transfer reaction [157]. When using EIS to test a coating, the data curve is fit to a certain type of model. The fit returns estimates for the model parameters, such as the pore resistance and the double layer capacitance. Then these parameters are used to evaluate the degree to which the coating has failed [157]. The resistance of the coating changes during exposure due to the penetration of electrolyte into the micropores of the coating. Upon immersion, the pore resistance can be very high (>1010Ω) and usually decreases with time of exposure to the electrolyte. However, it is not unusual for R_{pore} to increase after long exposure times. The increase in its value is usually associated to corrosion products from the metal substrate blocking the pores [51].

The coating resistance R_c represents the ease with which ions can move into and out of the physical channel of the pores of the coating. For a failed coating the allure of the circuit is shown in Figure 3.16 while the curves of this system are shown in Figure 3.17. For the interpretation of the electrochemical behaviour of a system from the EIS data, an appropriate physical model of the electrochemical reactions occurring can be used [52, 164].

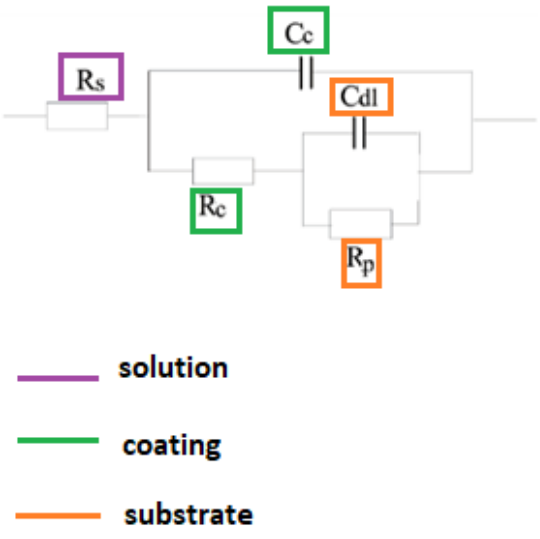

Figure 3.16 Equivalent circuit for a failed system [157]

This equivalent circuit model is the simplest model used to analyze the impedance response of a coating with defects. After some time of the contact between the coated substrate and the electrolyte has been made, water and ions penetrate into the coating and form a new electrolyte/metal substrate interface under the coating

where corrosion can occur. The circuit contains two time constants, indicating two processes take place in the investigated frequency range. The first time constant in the high frequency region is responsible for the response of the coating, consisting of the coating capacitance (C_c) and the coating resistance (R_c). The second time constant at low frequencies is used to model the interfacial process occurred at the interface between pores or delaminated coating areas filled with an electrolyte and the metal substrate. The latter time constant contains of the double layer capacitance (C_{edl}) in parallel with the kinetic controlled polarization resistance (R_p) or charge transfer resistance (R_{ct}) [15, 42, 43, 52].

The coating is not the only feature of the sample that gives rise to a capacitance. There is a charge on the metal electrode and a charge in the electrolyte that are separated by the metal electrolyte interface. Since this interface is commonly known as the “double layer” in electrochemical theory and presented in Figure 2.10 , the capacitance is called the Double Layer Capacitance and abbreviated C_{edl}. This capacitance has a much higher value, so the C_{edl} of even a small element will be apparent in the EIS response.

A coating that is adhering strongly to the metal surface acts as a barrier so that there is no metal-electrolyte contact. C_{edl} can sometimes be related to delamination of the coating. This element must be normalized because it is electrode area dependent.

The value of C_c cannot be determined directly from the Nyquist plot.

Due to coating degradation and diffusion of water and ions from the solution, the equivalent circuit will change from system under activation control (Figure 3.17) to system under diffusion control (Figure 3.19).

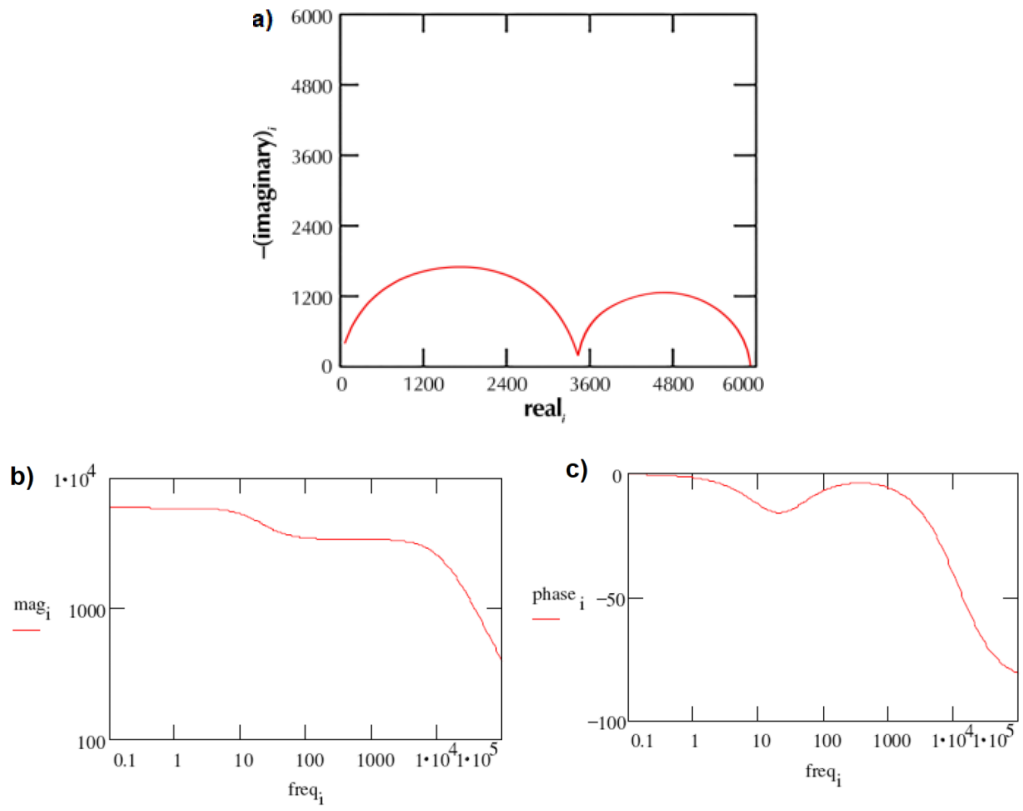

Figure 3.17 Nyquist plot (a) and Bode plots for a failed coating system (b) Bode magnitude and (c) Bode phase [157]

The electrochemical process at the coating/substrate interface is represented by a Warburg (W) element instead of R_pC_{edl}. In this case, the diffusion process is suggested to be a rate-determining step, indicating that the electrical behaviour of the coating/metal interface is dominated by the Warburg element. The Warburg diffusion element is a common diffusion circuit element that can be used to model semi-infinite linear diffusion. It is a CPE with a constant phase of 45° [51, 157, 165].

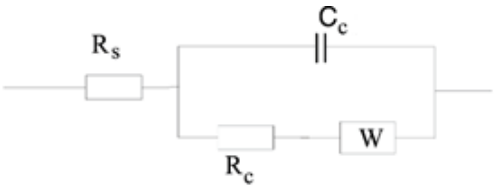

Figure 3.18 Equivalent circuit for a failed coating system [157]

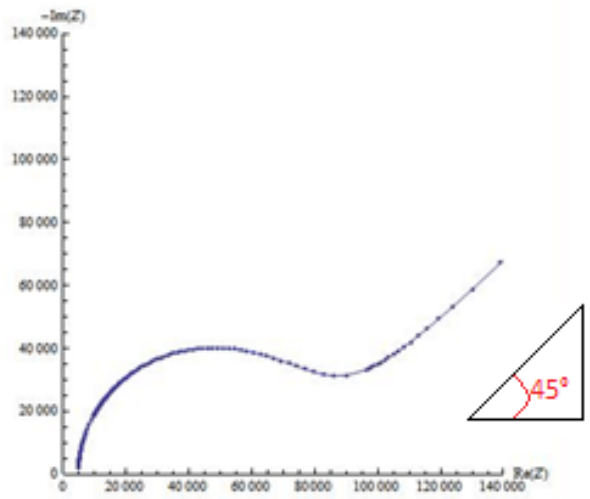

Figure 3.19 Nyquist plot of a failed coating [157]

When the curves are complete semi-circles, the corrosion phenomenon can be explained with the help of a Randles equivalent circuit, which is a capacitor parallel to a resistance.

The capacitor represents the double electrochemical layer while the resistance is the charge transfer resistance (R_{ct}). The value of the resistance R_t is the second intersection of the semi-circle with the real axis of the Nyquist diagram. The first intersection is the value if the solution resistance. When the curves obtained are not semi-circles, the Randles circuit cannot be assimilated and a more complex electrical circuit must be used. Those plots show that the visual results can be compared to the impedance results as the plots have the allure corresponding to their degree of corrosion [51].

Figure 3.20 presents the equivalent circuit which will be used for the fitting of the data obtained. A constant phase element (CPE) is used instead of an ideal capacitor; since the conditions and the results obtained are not as ideal as the theory is (slopes of the curves in the Bode impedance plot are not equal to 1). The equivalent circuit is defined as follow: R_s represents the electrolyte (or solution) resistance, R_{pore} is the pore resistance, CPE_c the coating capacitance, CPE_{dl} considers the presence of a double layer between the metal surface and the electrolyte, and R_{ct} is related to the charge transfer resistance of the metal and can be known as corrosion resistance [166]. The presence of the coating as an added layer is supposed to increase the values of the resistance and impedance measured of the samples in order to protect the substrate from the corrosion.

This equivalent circuit has been used in several research works to model the behaviour of stainless steel in various conditions of the corrosive electrolyte [167-169].

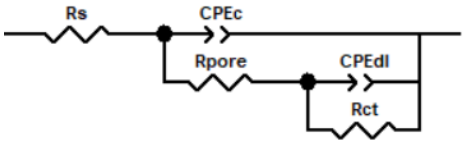

Figure 3.20 Equivalent circuit used to fit EIS data

Figure 3.21 displays an example of the data fitting. The same procedure and equivalent circuit are used for all coating formulations and plots presented.

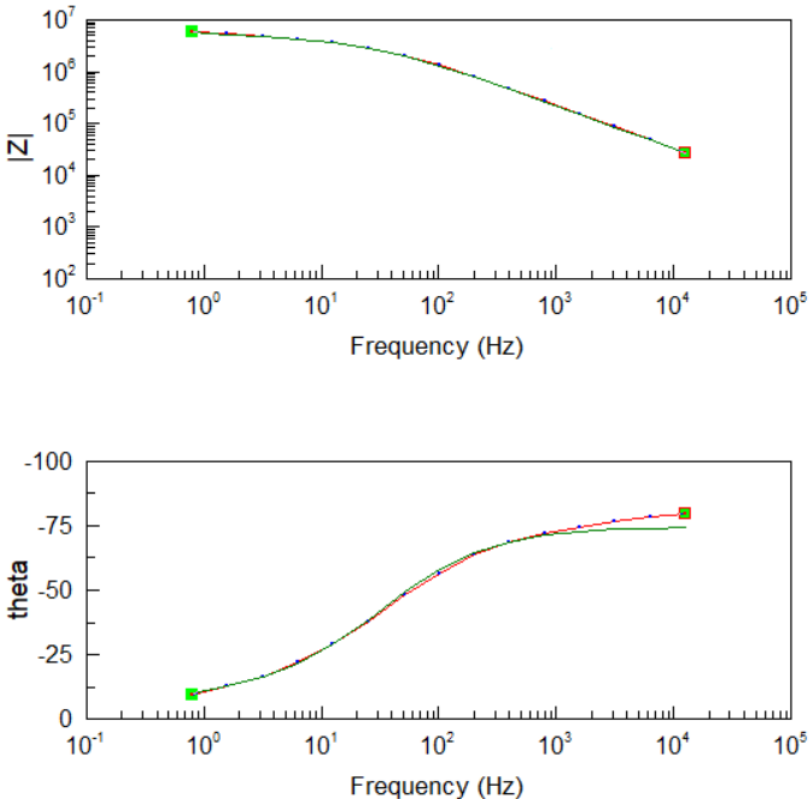

Figure 3.21 Fitting of Bode plots

Errors are coming from the uncertainties of the software. Some constants (such as R_s as the value can be determined with the Nyquist plot) have to be fixed in order to have a decent fitting. If not fixed, the software decides on a more suitable fit but with a R_s value which differs of several orders of magnitude from the actual value.

Some authors have correlated the coating capacitance to the water uptake [170, 171], meaning that an increase in the value of coating capacitance would lead to more water uptake for the sol-gel coatings thus a degradation of the coating. Samples displaying little change in their CPE_c values indicate a significant improvement in the protective performance of their coatings.

R_{ct} is linked to the corrosion. As the substrate comes in contact with the solution (or electrolyte), the electrochemical reactions occur, leading to the start of corrosion and formation of corrosion products.

A decrease in R_{ct} value means an increase of damaged and formation of corrosion product. This can be associated to the addition of titanium precursor, as studies have reported that the doping with titanium enhanced the corrosion protection of coatings.

3.5 Conclusions and Scope of Study

The corrosion of various systems, including coatings particularly relevant to this study, has been described in this chapter. Corrosion is a major problem in sectors using materials in aggressive environments. One major method to ensure its protection is to protect it with a physical barrier known as a coating, especially sol-gel coatings.

This study aims to provide experimental data and a better understanding on the evolution of corrosion on coatings, especially inorganic/hybrid sol-gel coatings, the influence of certain parameters on these coatings performance as well as protective properties.

It also aims to help in the comprehension of the possible processes of corrosion and degradation that can happen:

- Dissolution of coating and if that makes the chemistry of said coating change
- Water uptake during the immersion, does it change the coating and does it increase the internal stress?
- Water penetration, does it affect the substrate?

Firstly the experiments made on the samples will be to develop a definite methodology for the project. Then the focus will be on inorganic/hybrid sol-gel coatings especially the last batch. The inorganic/hybrid sol-gel used will contain

different amounts of titanium butoxide. The hypothesis is that the addition of this element will increase the corrosion resistance properties. One atom of titanium would replace one atom of silicon in the sol-gel network at some positions during the process and thus strengthen the network.

The identification of the behaviour of the coatings in aggressive environment and the methodologies will support the development of knowledge about the selection of materials and manufacture.

This work is to contribute to the development of sol-gel coatings technologies for the protection of steel infrastructure, particularly in oil and gas industry.

Chapter IV. Experimental Procedures and Characterisation Techniques

4.1 Introduction and Chapter Overview

This chapter outlines, presents and discusses the materials and coatings used throughout the study as well as the different experimental procedures and methods of analysis which are used in this research project. The differences between the batches of samples are introduced. Static corrosion tests were performed through Electrochemical Impedance Spectroscopy (EIS). Surface analyses were carried out prior to the experiment then after the immersion studies. Methods comprise Fourier-Transform Infrared Spectroscopy (FTIR), Scanning Electron Microscopy (SEM) and Energy Dispersive X-ray Spectroscopy (EDX) as well as nano-hardness and adhesion test. This includes *mechanical* as well as *chemical* surface analysis techniques and imaging techniques to study surface properties.

4.2 Substrates and Samples Used for this Study

Several materials were used as substrates and were analysed in this study: carbon steel X65, A1008Qpanel steel (cold rolled steel sheet), stainless steel 316L and 304. The compositions are presented in Table 4.1 to Table 4.4. Those metals were coated with different types of coatings throughout the project: organic, inorganic/hybrid and hybrid/composites coatings. In the first batch, the samples for conducting experiments were disks of either X65 or 316L steel with a diameter of 25mm and a thickness of 3mm. For the second and third batch, samples were 100mm by 100mm stainless steel sheets with a thickness of 1mm. They were cut accordingly to the experiment: square samples of 50mm by 50mm for the electrochemical measurement and 15mm by 15mm for the immersion samples which were used for the FTIR, SEM/EDX, and scratch test studies. From the second batch onwards, the substrate was 304 stainless steel due to technical issues. All the inorganic/hybrid and hybrid/composites samples had a coating thickness between 3 and 11µm while the organic samples from the first batch had a thickness between 60 and 80µm. The thickness was measured with the ellipsometry thickness measurement method. A summary of the different experiments done on the samples is presented in Figure 4.1. The purpose of these experiments was to analyse the samples received so they would be improved for oil and gas conditions, then to

study the influence of titanium on the corrosion resistance of the coatings, as well as the influence of the percentage of titanium. Then the influence of the solvent used during sol-gel process and the conditions of curing process itself were investigated.

Table 4.1 Composition of X65 carbon steel [172]

X65 Carbon Steel								
Iron	Carbon	Manganese	Phosphorus	Sulfur	Titanium	Silicon	Nickel	Nitrogen
balance	0.26%	1.40%	0.03%	0.03	0.04%	0.45%	8.00-12.00%	0.10% max

Table 4.2 Composition of 316L stainless steel [173]

316L Stainless Steel								
Iron	Carbon	Manganese	Phosphorus	Sulfur	Silicon	Chromium	Nickel	Molybden
balance	0.030%	1.84%	0.021%	0.0010 % max	0.44%	18.00-20.00%	12.30%	2.470

Table 4.3 Composition of A1008Qpanel [174, 175]

A 1008 Q-PanelSteel					
Iron	Carbon	Manganese	Phosphorus	Copper	Sulfur
balance	0.08%	0.6% max	0.035% max	0.2% min	0.04%

Table 4.4 Composition of 304 stainless steel [176, 177]

304 Stainless Steel								
Iron	Carbon	Manganese	Phosphorus	Sulfur	Silicon	Chromium	Nickel	Nitrogen
balance	0.08%	2.00% max	0.045% max	0.03 % max	0.75%	18.00-20.00%	8.00-12.00%	0.10% max

The samples of the first batch were a combination of either X65 carbon steel or 316L stainless steel substrates, with inorganic/hybrid coatings (5 different systems), organic coatings (2 different systems) or hybrid/composites coatings (2 different systems). They were disc coupons with a diameter of 25mm and a thickness of 3mm. A summary is presented in Table 4.5 to Table 4 7. This first batch included several systems of inorganic/hybrid, organic and hybrid/composites silica sol-gel coatings. No information has been given about the curing process or pre-treatment.

The samples of the first batch were deposited on the substrate with the spray-coating method while the samples from Batch 2 and Batch 3 were deposited through spin coating.

Little information is known about the samples from Batch 1 due to confidential requirement.

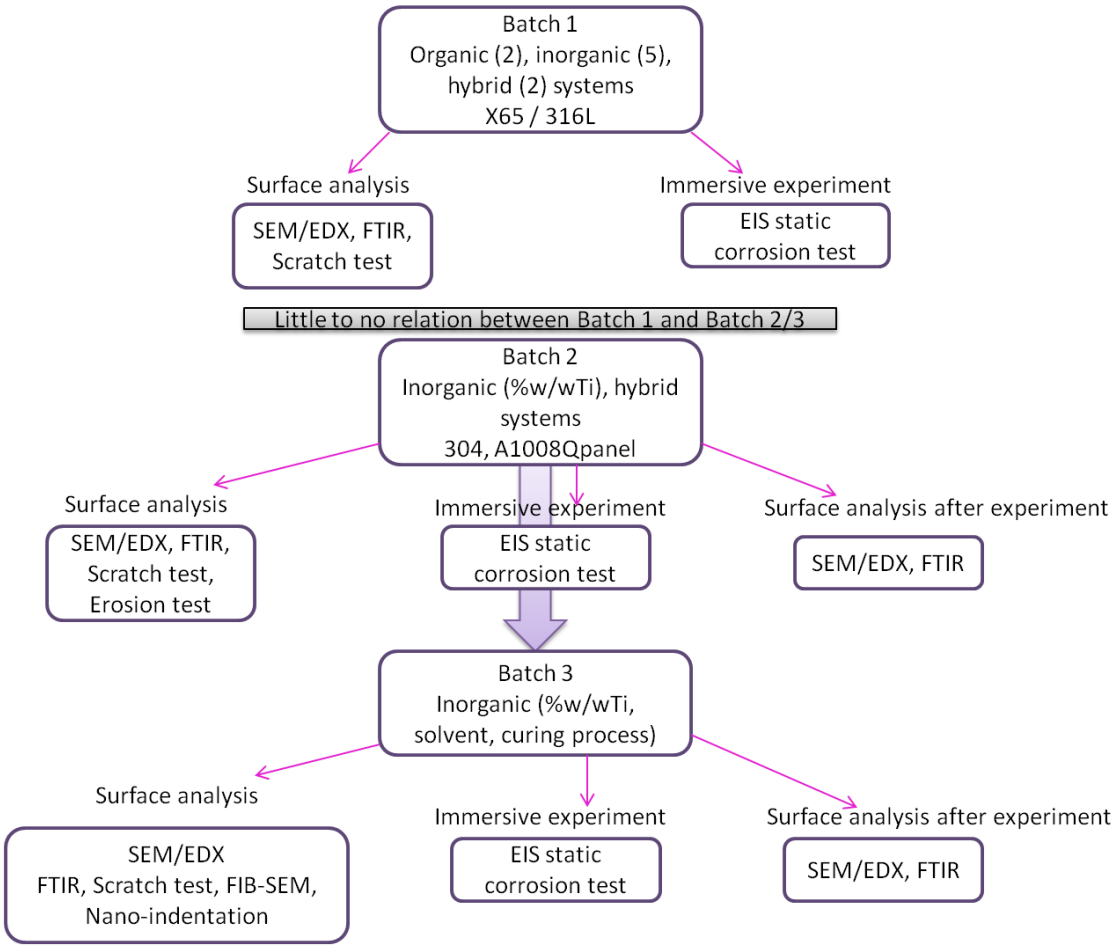

Figure 4.1 Summary of the batches of samples and experiments done (Inorganic: inorganic/hybrid; hybrid: hybrid/composites)

The samples are labelled according to the nature of their coating first (I for inorganic/hybrid, H for Hybrid/composites and O for Organic) then the batch of the sample (B1 for Batch 1, B2 for Batch 2 and B3 for Batch 3) then the changing parameters (from one batch to another). The formulation (1, 2, 3, 4 or 5 depending on the system of sol-gel coating for the first batch, 0%, 1.4%, 2.8%, 5.6% or 11% depending on the amount of titanium precursor for Batch 2 and Batch 3). In last the changing parameter for each batch: substrate (X65 or 316L for Batch 1, 304 or A1008Qp for Batch 2), pre-treatment (No when the samples has not been pre-treated, Yes when the sample has been pre-treated); solvent and curing process for Batch 3 (Mix when a mixture is used as a solvent, Ip when isopropanol is used; N_2 or Air depending on the curing process). 0% to 11.3% for the second batch is the system/percentage of precursor added to the sample; 304/A1008Qp is the

substrate. Batch 2 used two different substrates, A1008Qpanel and 304 stainless steel

Mix/Ip for the third batch depends on the solvent used while N_2/Air depends on the curing process.

Table 4.5 Inorganic/hybrid samples of the first batch

Sample	Material	Pre-treatment	Average thickness (µm)	Nature of coating
$I_{,B1,1,X65,No}$	X65	No	3.9	Inorganic/hybrid system 1
$I_{,B1,1,X65,Yes}$		Yes	3.6	
$I_{,B1,1,316L,No}$	316L	No	3.9	
$I_{,B1,1,316L,Yes}$		Yes	3.7	
$I_{,B1,2,316L,No}$		No	5.9	Inorganic/hybrid system 2
$I_{,B1,2,316L,Yes}$		Yes	6.6	
$I_{,B1,3,316L,No}$		No	4.1	Inorganic/hybrid system 3
$I_{,B1,3,316L,Yes}$		Yes	3.6	
$I_{,B1,4,316L,No}$		No	4.9	Inorganic/hybrid system 4
$I_{,B1,4,316L,Yes}$		Yes	4.8	
$I_{,B1,5,316L,No}$		No	3.9	Inorganic/hybrid system 5
$I_{,B1,5,316L,No}$		Yes	4.6	

Table 4 6 Organic samples of the first batch

Sample	Material	Pre-treatment	Average thickness (µm)	Nature of coating
$O_{,B1,1,X65,No}$	X65	No	10.3	organic system 1
$O_{,B1,1,X65,Yes}$		Yes	12.7	
$O_{,B1,1,316L,No}$	316L	No	8.5	
$O_{,B1,1,316L,Yes}$		Yes	8.4	
$O_{,B1,2,X65,No}$	X65	No	67.2	organic system 2
$O_{,B1,2,X65,Yes}$		Yes	69.2	
$O_{,B1,2,316L,No}$	316L	No	69.0	
$O_{,B1,2,316L,Yes}$		Yes	79.5	

Table 4 7 Hybrid/composites samples of the first batch

Sample	Material	Pre-treatment	Average thickness (μm)	Nature of coating
$H_{,B1,1,X65,No}$	X65	No	7.0	Hybrid/composites system 1
$H_{,B1,1,X65,Yes}$		Yes	5.8	
$H_{,B1,1,316L,No}$	316L	No	5.2	
$H_{,B1,1,316L,Yes}$		Yes	5.5	
$H_{,B1,2,X65,No}$	X65	No	9.3	Hybrid/composites system 2
$H_{,B1,2,X65,Yes}$		Yes	11.0	
$H_{,B1,2,316L,No}$	316L	No	12.4	
$H_{,B1,2,316L,Yes}$		Yes	9.5	

The samples of the second batch were a combination of sol-gel coatings, with an undoped inorganic/hybrid coating, alkaline hydrolysed MTEOS / TEOS. In addition alkaline hydrolysed MTEOS/ TEOS coatings doped with different percentages of titanium butoxide: 0%w/w, 1.4%w/w, 2.8%w/w, 5.6%w/w, and 11.3%w/w and hybrid/composites coatings GPTES/ Epoxy resin were also studied. The substrate was either A1008Qpanel or 304 stainless steel. The summary is presented in Table 4.8. Coatings were deposited on sheet coupons with a dimension of 10x10x0.1cm.

Table 4.8 Summary of the samples of the second batch

Sample	Coating type	Substrate
$I_{,B2,1.4\%,304}$	Inorganic Coating, Alkaline hydrolysed MTEOS/TEOS + Ti(IV)-(1.4%w/w)	304
$I_{,B2,2.8\%,304}$	Inorganic Coating, Alkaline hydrolysed MTEOS/TEOS + Ti(IV)-(2.8%w/w)	304
$I_{,B2,5.6\%,304}$	Inorganic Coating, Alkaline hydrolysed MTEOS/TEOS + Ti(IV)-(5.6%w/w)	304
$I_{,B2,11.3\%,304}$	Inorganic Coating, Alkaline hydrolysed MTEOS/TEOS + Ti(IV)-(11.3%w/w)	304
$I_{,B2,0\%,304}$	Inorganic Coating, Alkaline hydrolysed MTEOS/TEOS	304
$I_{,B2,0\%,A1008Qp}$	Inorganic Coating, Alkaline hydrolysed MTEOS/TEOS	A1008 Q-Panel
$H_{,B2,0\%,\ 304}$	Hybrid Coating, GPTES/Epoxy Resin	304

The samples of the third batch were inorganic coatings, alkaline hydrolysed MTEOS/ TEOS deposited on 304 stainless steel doped with different percentages of titanium butoxide: 0%w/w, 1.4%w/w, 2.8%w/w, 5.6%w/w, and 11.3%w/w. Moreover

there were different solvents used for the sol-gel preparation (mixture EtOH, IpOH and BuOH or isopropanol) and different curing processes (N_2 or Air) as presented in Table 4.9, leading to different final compositions of the coatings. The coatings were deposited on sheet coupons with a dimension of 10x10x0.1cm. This batch was a continuation of the second batch with a change in parameters such as solvent and curing process to see their influence on the evolution of corrosion.

Table 4.9 Summary of the samples of the third batch

Sample	Coating type
$I_{,B3,0\%,Mix,N2}$	Solvent mixture (EtOH,IpOH,BuOH) cured at 500°C - N_2
$I_{,B3,1.4\%,Mix,N2}$	Solvent mixture (EtOH,IpOH,BuOH) with Ti 1.4% w/w precursor cured at 500°C - N_2
$I_{,B3,2.8\%,Mix,N2}$	Solvent mixture (EtOH,IpOH,BuOH) with Ti 2.8% w/w precursor cured at 500°C - N_2
$I_{,B3,5.6\%,Mix,N2}$	Solvent mixture (EtOH,IpOH,BuOH) with Ti 5.6% w/w precursor cured at 500°C - N_2
$I_{,B3,11.3\%,Mix,N2}$	Solvent mixture (EtOH,IpOH,BuOH) with Ti 11.3% w/w precursor cured at 500°C - N_2
$I_{,B3,0\%,Mix,Air}$	Solvent mixture (EtOH,IpOH,BuOH) cured at 500°C – Air
$I_{,B3,1.4\%,Mix,Air}$	Solvent mixture (EtOH,IpOH,BuOH) with Ti 1.4% w/w precursor cured at 500°C - Air
$I_{,B3,2.8\%,Mix,Air}$	Solvent mixture (EtOH,IpOH,BuOH) with Ti 2.8% w/w precursor cured at 500°C - Air
$I_{,B3,5.6\%,Mix,Air}$	Solvent mixture (EtOH,IpOH,BuOH) with Ti 5.6% w/w precursor cured at 500°C - Air
$I_{,B3,11.3\%,Mix,Air}$	Solvent mixture (EtOH,IpOH,BuOH) with Ti 11.3% w/w precursor cured at 500°C - Air
$I_{,B3,0\%,Ip,N2}$	Isopropanol as solvent cured at 500°C - N_2
$I_{,B3,1.4\%,Ip,N2}$	Isopropanol as solvent with Ti 1.4% w/w precursor cured at 500°C - N_2
$I_{,B3,2.8\%,Ip,N2}$	Isopropanol as solvent with Ti 2.8% w/w precursor cured at 500°C - N_2
$I_{,B3,5.6\%,Ip,N2}$	Isopropanol as solvent with Ti 5.6% w/w precursor cured at 500°C - N_2
$I_{,B3,11.3\%,Ip,N2}$	Isopropanol as solvent with Ti 11.3% w/w precursor cured at 500°C - N_2
$I_{,B3,0\%,Ip,Air}$	Isopropanol as solvent cured at 500°C – Air
$I_{,B3,1.4\%,Ip,Air}$	Isopropanol as solvent with Ti 1.4% w/w precursor cured at 500°C - Air
$I_{,B3,2.8\%,Ip,Air}$	Isopropanol as solvent with Ti 2.8% w/w precursor cured at 500°C - Air
$I_{,B3,5.6\%,Ip,Air}$	Isopropanol as solvent with Ti 5.6% w/w precursor cured at 500°C - Air
$I_{,B3,11.3\%,Ip,Air}$	Isopropanol as solvent with Ti 11.3% w/w precursor cured at 500°C - Air

Table 4.10 Average thickness of samples from Batch 2 and Batch 3

Sample	Average thickness (μm)
$I_{,B2,1.4\%,304}$	3.3
$I_{,B2,2.8\%,304}$	3.1
$I_{,B2,5.6\%,304}$	2.9
$I_{,B2,11.3\%,304}$	3.6
$I_{,B2,0\%,304}$	3.8
$I_{,B2,0\%,A1008Qp}$	4.0
$H_{,B2,0\%,\ 304}$	2.5
$I_{,B3,0\%,Mix,N2}$	3.6
$I_{,B3,1.4\%,Mix,N2}$	3.3
$I_{,B3,2.8\%,Mix,N2}$	3.6
$I_{,B3,5.6\%,Mix,N2}$	3.2
$I_{,B3,11.3\%,Mix,N2}$	3.6
$I_{,B3,0\%,Mix,Air}$	3.4
$I_{,B3,1.4\%,Mix,Air}$	3.0
$I_{,B3,2.8\%,Mix,Air}$	3.5
$I_{,B3,5.6\%,Mix,Air}$	3.5
$I_{,B3,11.3\%,Mix,Air}$	3.8
$I_{,B3,0\%,Ip,N2}$	5.3
$I_{,B3,1.4\%,Ip,N2}$	5.0
$I_{,B3,2.8\%,Ip,N2}$	3.6
$I_{,B3,5.6\%,Ip,N2}$	3.6
$I_{,B3,11.3\%,Ip,N2}$	3.2
$I_{,B3,0\%,Ip,Air}$	4.7
$I_{,B3,1.4\%,Ip,Air}$	4.8
$I_{,B3,2.8\%,Ip,Air}$	4.1
$I_{,B3,5.6\%,Ip,Air}$	3.7
$I_{,B3,11.3\%,Ip,Air}$	3.6

4.3 Brine Used for the Research

During the study the samples were immersed in a brine of 3.5%w/w NaCl solution (from sodium chloride obtained from Merck, 99.5% purity) to simulate a corrosive environment. The samples were cleaned with distilled water and acetone before being immersed in the brine. The environment was sealed and saturated with bubbling CO_2 before any electrochemical measurement (for Batches 2 and 3). The temperature for the first batch was 60°C then for the next batches was 25°C.

4.4 Experimental Method for Static Corrosion Tests

The corrosion study of the coated systems can be done by Direct Current DC techniques or Alternating Current AC impedance techniques. The corrosion is measured by electrochemistry mostly because of the sensitivity of the modern electronics equipment which allows the detection of corrosion product on substrates before it is even visible to the eye. Electrochemical corrosion measurements use the electrochemical nature of metallic corrosion. An external power source is used to apply a voltage to a metal specimen submerged in an electrolyte. The electrical current which can be measured is due to the applied voltage which forces the metal-electrolyte interface to go further its steady conditions [30].

The corrosion characteristics of the batch of coatings deposited on X65 carbon steel, on 304 and 316L stainless steel substrates were studied by electrochemical methods. Electrochemical corrosion tests were conducted in order to analyse the rate of corrosion. EIS is a method to examine anti corrosion protective coatings. It is a well-developed branch of AC theory that describes the response of a circuit to an alternating current or voltage as a function of frequency.

One of the main attributes of AC impedance tests in coating evaluation is the ability to translate the data into a physical equivalent circuit or electrical model. This way, passive elements such as resistors, inductors and capacitors are used to represent the electro-chemical process and provide a way of modelling and discussing the corrosion process [157].

Since EIS is best suited for high-impedance interfaces, it is particularly applicable for the elevation of organic coatings on steel. As EIS measurements do not damage nor perturb the system, they are useful in long time tests. Moreover, they allow the monitoring of the gradual change of the coating-metal system over time.

The batches of samples were composed of three kinds of coatings (hybrid/composites, inorganic/hybrid and organic) and of three types of metal substrates (carbon steel X65, stainless steel 304 and stainless steel 316L). Electrochemical measurements were performed on the samples under relatively aggressive environmental conditions, consisting of an aqueous, air exposed, sodium chloride (3.5% NaCl) solution at 60°C for thirty days for the first batch then 25°C for 30 days for Batch 2 and Batch 3. The integrity of the coatings was evaluated visually and through EIS. EIS measurements do not disturb the system while the

measurements are taken. The resistance of the solution is shown as well as the resistance of the coatings. Only the coated surfaces of the samples were in contact with the electrolyte as the other surfaces were in the sample holder and sealed with O-rings in order to prevent premature corrosion along the edge of the substrates; or a PVC tube was sealed on the sample to prevent any leak of the brine as presented in Figure 4.2. The number of samples studied for each type of combination substrate/coating was three.

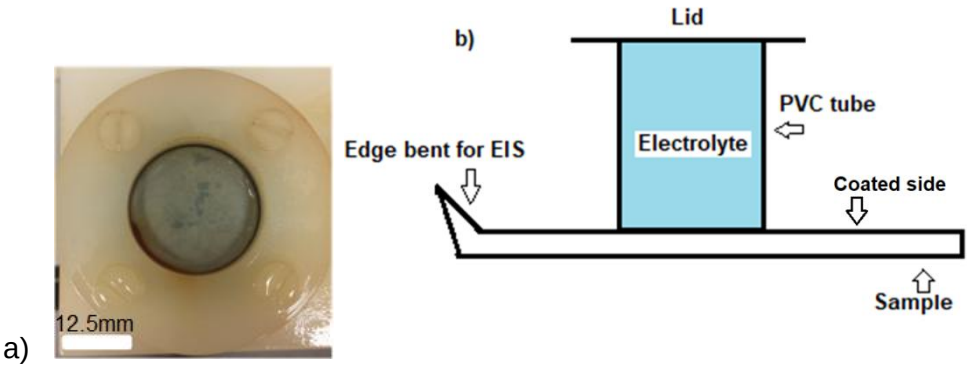

Figure 4.2 Setup for the samples of a) Batch 1 b) Batch 2 and Batch 3

The working electrode is the sample which corrosion rate is being measured. Nowadays, both the reference electrode and the counter-electrode are included in a single oxydo-reduction electrode readily available such as silver-silver chloride or saturated calomel electrode. AC impedance data are obtained using an Ivium-n-stat multi-channel electrochemical analyser connected to a computer for recording the results. A small sinusoidal voltage perturbation (±10mV) is applied to the system over a frequency range from 20 kHz to 0.1Hz. Impedance data were collected at regular intervals from initial immersion up to 30 days of exposure. Impedance data are represented in two types of diagrams, which are the Nyquist plot and the Bode plots including Bode phase and Bode magnitude plots. The graphs of the imaginary values as a function of the real values (Nyquist plot) are plotted (all the units of the axes are $\Omega.cm^2$). The X-axis gives us information about the polarization resistance. All the Bode plots have a logarithmic x-axis [157]. With the aim of comparing corrosion susceptibility of the coated samples in comparison with the uncoated metal, impedance spectra have been recorded and presented in this part and Zview modelling software (version 3.5d by Scribner Associates, Inc) is used to fit the experimental data with electrical equivalent circuits.

The aim of this experiment was to screen the resistance of the coatings regarding the corrosion in a relatively aggressive environment. Firstly to evaluate coatings of

the first batch to reduce the amount of samples studied then for the other batches to have the order of magnitude of the resistance of the coatings and its evolution during the immersion.

4.5 Surface Analysis

The morphology and composition of the coatings and corrosion products were analysed with several methods: Fourier-Transform Infrared Spectroscopy (FTIR), Scanning Electron Microscopy (SEM) and Energy Dispersive X-Ray Spectroscopy (EDX), these non-destructive methods allowed to assess the evolution of the coatings during the experiment. Destructive methods are also used to analyse the coatings: nano-indentation, scratch test, and erosion. The number of samples examined for each type of combination substrate/coating was two for these methods.

4.5.1 Fourier-Transform Infrared Spectroscopy (FTIR)

Infra-red spectroscopy measures the infra-red intensity adsorbed versus the wavelength of the light. Fourier-Transform Infrared Spectroscopy is used to analyse the species and functional groups on the surface of the coatings. Analyses were performed by FTIR with a PerkinElmer Spectrum 100 FTIR with Universal ATR accessory fitted, used to obtain chemical information about the surface of the sample. FTIR spectra were recorded between 600cm^{-1} and 4000 cm^{-1} and collected using 20 scans at 8cm^{-1} resolution. The spectrometer was coupled with an imaging system which permitted optical images of the surface to be collected. Its schematics are presented in Figure 4.3.

Figure 4.3 Schematics of FTIR Spectrometer [178]

There are expected peaks which can be found in Table 4.11 and Table 4.12 [179-182] with the possibilities of the groups which can be attributed to the peaks present in the spectra.

Table 4.11 Assignment of FTIR bands [109, 179-183]

Wavenumber (cm^{-1})	**Group possibility 1**	**Group possibility 2**
3400	-O-H (stretching)	
3056	Aromatic rings (stretching)	
2920-2950	-C-H (stretching)	$-C-H_2$ (stretching)
2400	$-C-O_2$	
1600-1630	C=C (stretching)	
1582	Aromatic rings (stretching)	
1400	-C-H (stretching)	
1200-1240	-C-O- (stretching)	-Si-O-Si (stretching)
1080	C-O-C (stretching)	
1080-1050	-Si-O-Si (stretching)	$-Si-O-C-H_3$ (stretching)
940-850	- Si-OH (stretching)	$Si-C-H_3$ (deformation)
750-780	-Si-O (stretching)	Si-O-C (stretching)

Table 4.12 Assignment of FTIR bands with titanium [184, 185]

Wavenumber (cm^{-1})	**Group possibility 1**	**Group possibility 2**
2400	Ti-O (deformation)	
950-920	Ti-O-Si (stretching)	
800	Ti-O-C (stretching)	Ti-O-Ti (stretching)
600	Ti-O-Ti (stretching)	

4.5.2 Scanning Electron Microscopy (SEM)

While optical microscopy is the simplest and least expensive small-scale materials characterization technique, optical microscopy is limited in its resolution by the wavelength of light [186]. The visible light used in optical microscopes has wavelengths varying between 400 and 700 nm [187]. A scanning electron microscope (SEM) uses electrons rather than light to generate images and the

resolution of an SEM is therefore limited by the wavelength of electrons, which at the standard energy of 5keV is only 0.55 nm [187]. With the presence of other limiting factors, again such as lens aberration, the ultimate resolution power of a 5keV SEM is on the order of a few nanometers [187]. SEM has been used throughout the study to examine and obtain images of the morphology of the surface at different days of immersion of coated samples. The surface of the samples to be examined was scanned with an electron beam; the reflected beam of electrons was collected then displayed at the same scanning rate. The image on the screen represented the surface of the specimen. The surface must be electrically conductive. SEM was carried out on the samples using a Carl Zeiss EVO MA15 SEM to assess coverage and topography of corrosion product. All images were collected at an accelerating voltage of 20kV and at a working distance of about 8mm.

The setup is presented in Figure 4.4.

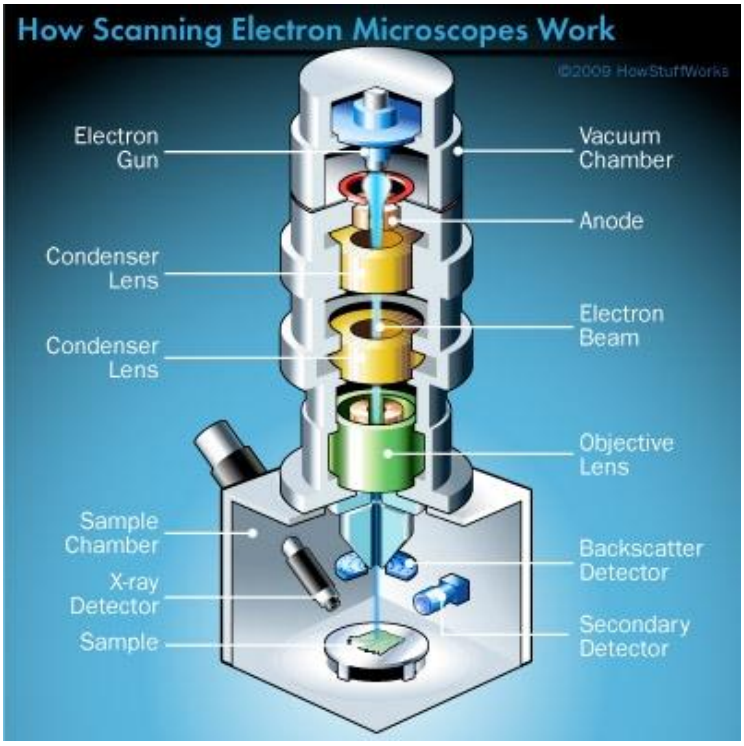

Figure 4.4 SEM setup [188]

4.5.3 Energy Dispersive X-Ray Spectroscopy (EDX)

Energy Dispersive X-Ray Spectroscopy has been used to identify and quantify the elemental composition of the surface of the coatings. EDX spectra were obtained using AZTEC software with the “mapping” mode. This mode was used to verify the composition of the coating and the interlayer structure as well as calculating the percentage of titanium for the different types of doped samples. The EDX gives sigma values with the quantification, but only for the wt%. The errors are normally larger than this, because of the sample not being perfect (flat and perfectly horizontal, homogeneous throughout the interaction volume, not charging, no overlapping peaks etc.). It has a limit of detection of around 0.1%, depending on element, and a limit of quantification of about 0.5%. Unfortunately, quantification and errors on the EDX is very complicated when done properly, which is why we say it is a semi-quantitative technique.

The schematic of this method is presented in Figure 4.5.

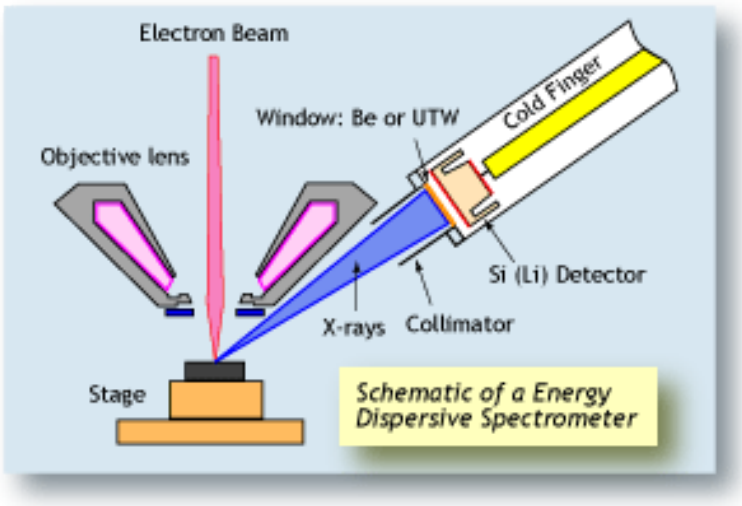

Figure 4.5 Schematic of EDX [189]

4.5.4 Nano-Hardness Measurements

The nano indentation of the coatings was also studied to assess the hardness of the coatings. Surface hardness values were obtained using a Nanotest™ Nano Indenter produced by Micro Materials Ltd Wrexham, UK. The extremely small force and

displacement resolutions possible with the machine, which are as low as 3 nN and 0.001 nm, respectively, are combined with very large ranges of applied forces (0 – 500 mN) and displacements (0-50 µm or more) [190]. The experiments were performed at a constant loading and unloading rate equal to 0.01mN/s.The test apparatus was in an enclosed, temperature regulated box to ensure no fluctuations due to heating or cooling processes. The Nanotest platform software suite and micro capture camera were used to obtain, analyse the data and measure the penetration depth of the calibrated diamond indenter as a function of the applied load during a cycle. Following the experimental Oliver and Pharr method [191] a diamond tipped probe with a Berkovich indenter of 130° was employed for testing. All samples were mounted to the holder using a high strength adhesive. A schematic of this method is presented in Figure 4.6.

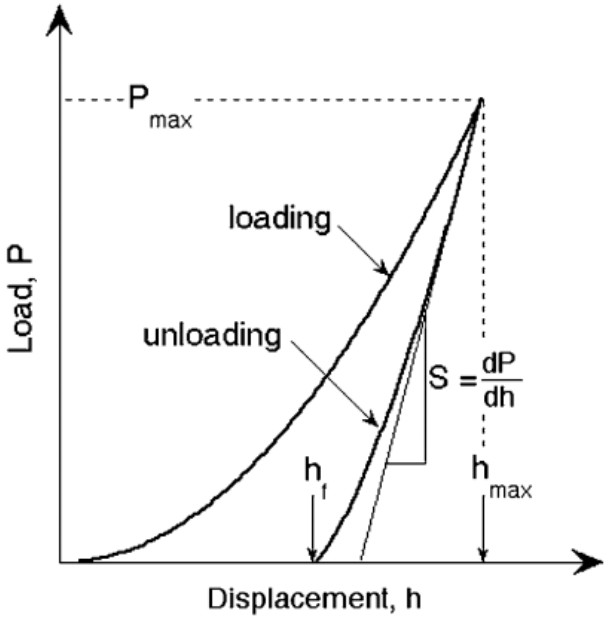

Figure 4.6 Schematic of the indentation data as typically obtained from the experiment. Adapted from [192]. P represents load, h represents displacement and S represents the elastic unloading stiffness.

4.5.5 Adhesion Test (Scratch Test)

In order for two or more materials to perform as one material, as a composite, there needs to be an adhesive bond between these materials that allows them to deform as one. The adhesive, the adhesive bond, and the materials must be able to withstand external stresses and strains to perform as a composite.

Adhesion is an important property of thin coatings, but is also difficult to assess. Scratch testing can be used to assess coating adhesion which leads to information given on adhesive failure. In the scratch testing of thin coatings, the usual procedure is to move the scratch tip to which is applied an increasing load across the coated surface until, at a defined load called the critical load, a clear and distinct failure appears or the film is detached from the substrate [193]. The critical loads of the coatings depend on several parameters such as the material properties of the coating and the substrate, the adhesive strength of the coating to the substrate, the coating thickness, the loading rate and the indenter geometry [194]. It is usually determined by visual examination of the scratch track, using a microscope [193]. The position of the crack is found and the corresponding load is obtained by direct observation. Interfacial adhesion plays a crucial role in the structural stability, performance and the reliability of coating-substrate systems. High adhesion strength can avoid delamination and cracking of the coating when exposed to stresses [195]. From determining a critical load at which the coating delaminates from the substrate, an assessment of the coating adhesion can be made [196]. The critical loads can be compared for various coatings as a measure of the adhesion and different stages of adhesion can be identified in the scratch track [197]. If the critical load leads to a defined failure, this represents the loss of coating-substrate adhesion and the critical load can be used as a qualitative measure of the adhesion of the system [198]. However, it is well known that a range of possible failure modes can occur and only some of these are dependent on adhesion [198]. Scratch testing can give useful information about the adhesion of coatings, provided that careful identification of the failure mode is carried out [199].

The scratch tests in this project are mainly used for testing the adhesion strength of coatings. These critical loads can be used to compare the scratch resistance of various materials; a material with a higher critical load would be considered to have a higher scratch resistance.

The adhesion was the first property to be studied as a surface mechanical property with scratch resistance of the coating by the mean of a Scratch Tester Millenium 200 as presented in Figure 4.7 and Figure 4.8. A Rockwell diamond indenter with a tip radius of 200µm was used to scratch the samples.

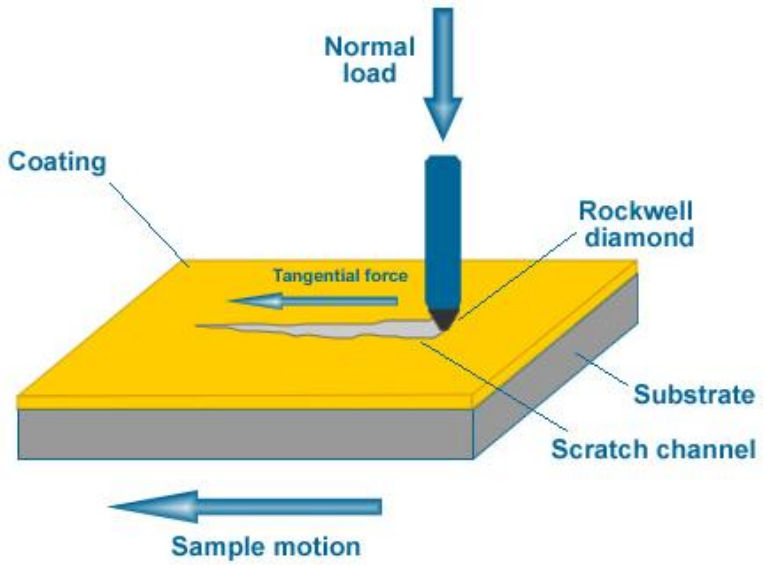

Figure 4.7 Representation of scratch test [200]

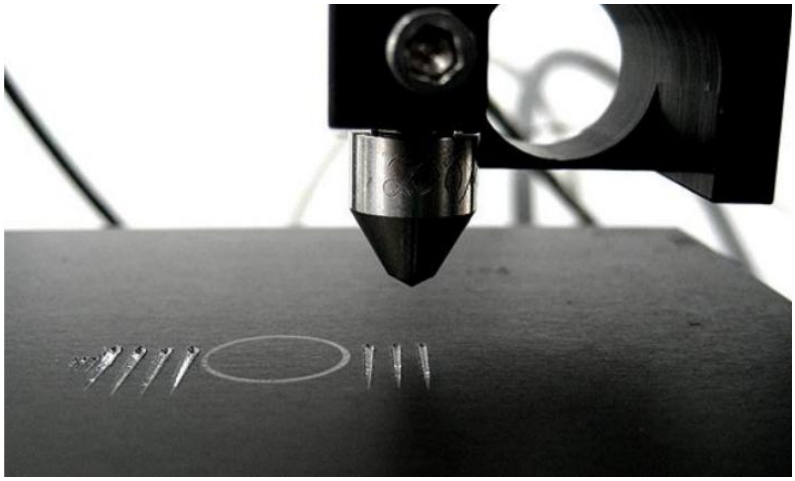

Figure 4.8 Image of the tip over the scratches of a tested sample [201]

This is an automatic instrument which enables the measurement of mechanical strength adhesion and intrinsic cohesion of coatings. The scratch test method consists of scratching the surface with a diamond tip while applying on it a constant or progressive load. To ensure proper alignment in the system, the sample is moved under the stationary indenter (diamond tip). When the scratch is finished, the sample moves under the video system to examine the different kind of damage done by the tip and to correlate it with the load applied [202]. With the help of two magnified lenses, the critical load (as defined in theory and in Figure 3.4) is determined visually, which means that the value is approximate, not accurate.

This method allows the comparison of different coatings, substrates, coating thicknesses and preparation of surfaces before coating and scratching resistance of

bulk materials. The tip must be wiped after each test with ethanol or methanol (any alcohol), not with acetone. During the scratch test the indenter and the specimen surface are involved and interact with each other, the result depending also on the environmental conditions. Therefore, scratch tests should be carried out under similar environmental conditions when comparing the results for different specimen. The scratch segments of the tests were done with a progressive load scratch in which the load increased with scratch distance. The range of the value which was applied on the sample is for standard tests from 0 to 20N then 10N (decided after some results showing the highest critical load around 5N). It was adapted from the international standard values from ASTM C1624-05 (2015) with 10 mm/min for the speed and 100N/min for the loading speed. The scratch length was 5.0 mm. The average value of the critical load for the adhesion of a coating was about 10N. The critical load is the maximum value reached before the failure or delamination of the coating which means the limit of the adhesion [198, 203, 204].

Figure 4.9 presents the principle of this test:

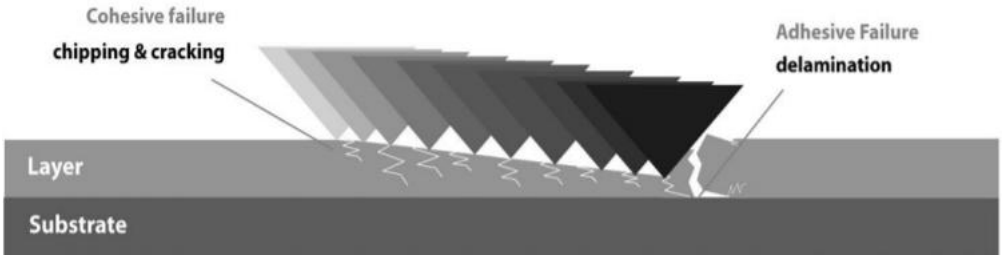

Figure 4.9 Principle of scratch-test [203]

Once the scratch is done and once the sample was wiped with a dry tissue to avoid the presence of powders, magnified lenses were used (x50 and/or x200) which allow the examination of the scratch and the deformation made on the coating.

4.5.6 Erosion Test

Erosion and erosion-corrosion properties of the coatings were investigated. Measurement of the resistance of the coatings to sand erosion was undertaken using a submerged impinging jet. The submerged impinging jet reservoir was filled with 50-litres of tap water and 1000mg/L of sand that was re-circulated through a dual nozzle arrangement onto the flat specimens at an angle of 90°, positioned 5mm from the exit of the nozzle. Spherical sand particles were used with an average

particle diameter of 250μm. The solution was sparged with nitrogen (N_2) during the test and for a minimum of 12 hours prior to starting the test, to reduce the dissolved oxygen concentration in the solution to below 50ppb. Tests were conducted at a flow velocity of 15m/s and a temperature of 25°C. The mass of the samples was measured before and after the test using a mass balance accurate to 1μg. A representation of the set up can be found in Figure 4.10.

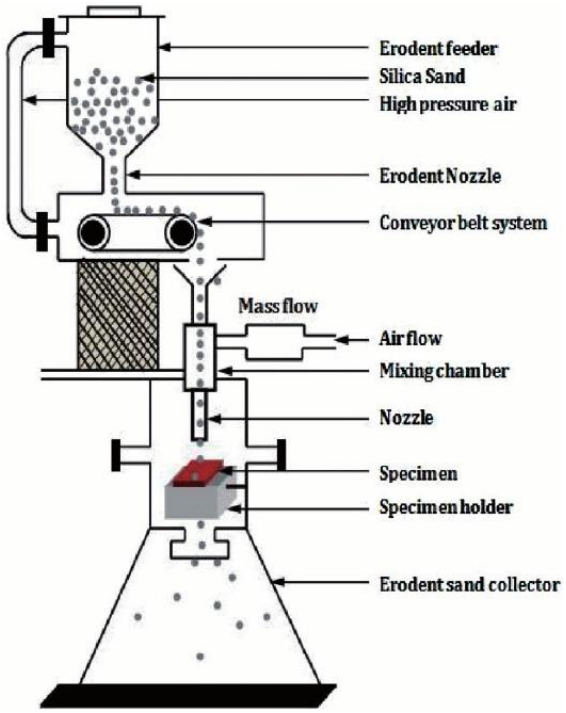

Figure 4.10 Representation of the erosion test setup [205]

4.5.7 Salt Spray Test

The salt spray test, as defined by ASTM B117, is one of the most used widely tests to evaluate corrosion protection of coatings on metals. It is an accelerated corrosion test trying to duplicate in laboratory the corrosion performance that a product would endure. The test offers many advantages, including standardized protocols for conducting the exposure and evaluating the results and procedural simplicity [206]. However it is criticized for its lack of reproducibility from one test chamber to another, failure to predict service performance and its inability to provide a quantitative measure of corrosion damage easily [206]. The schematic of a set up of a salt spray chamber is presented in Figure 4.11.

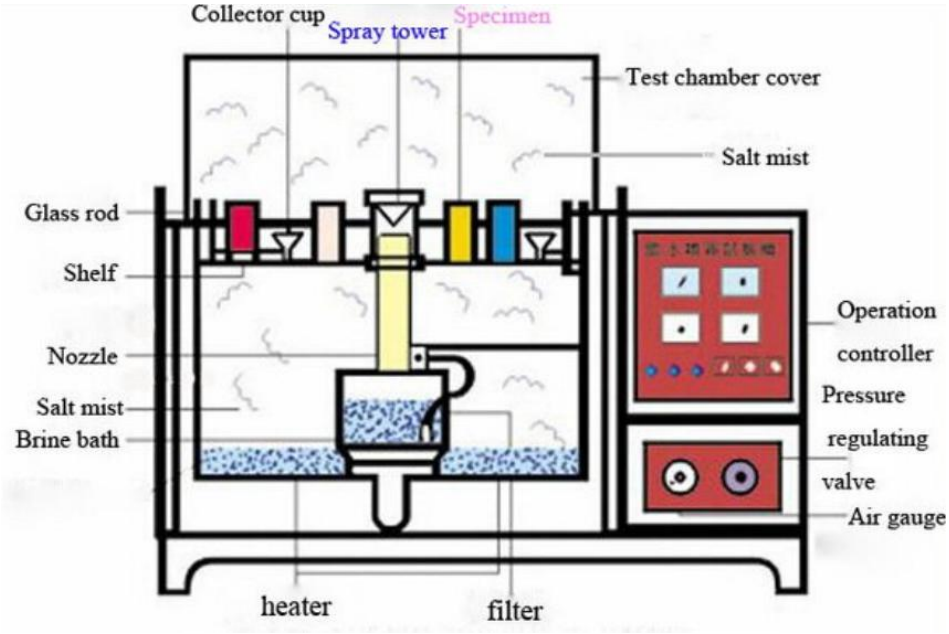

Figure 4.11 Representation of a salt spray chamber [207]

Chapter V. Characterisation and Properties of the Coatings Prior to Corrosion Tests

5.1 Introduction and Chapter Overview

Coatings technology is fundamentally dependent upon good adhesion between the coating and the substrate, and in many cases adhesion is the limiting factor for the wider application of the technology [208, 209]. The mechanical properties of the coatings play a crucial role in the reliability of the products to which they are applied. If a coating fails, or experiences substantial deformation, its function may be deteriorated.

This chapter first presents the results of different analyses made on the surface of the samples from the first batch: Energy Dispersive X-ray Spectroscopy (EDX), Fourier-Transform Infrared Spectroscopy (FTIR), as well as results from analyses of mechanical properties of the samples such as adhesion. The first batch was composed of several systems (inorganic/hybrid, organic and hybrid/composites) deposited on either carbon steel X65 or 316L stainless steel. The purpose of the experiments was to screen those samples. The second part focuses on the samples from the second batch (alkaline hydrolysed MTEOS (methyltriethoxysilane) / TEOS (tetraethoxysilane), inorganic/hybrid coating on different substrates (A1008Qpanel or 304 stainless steel), alkaline hydrolysed MTEOS/ TEOS. In addition, coatings doped with different percentages of titanium butoxide: 0%, 1.4%w/w, 2.8%w/w, 5.6%w/w, and 11.3%w/w or hybrid coatings GPTES/ Epoxy resin) are studied. Results from analyses made on the surface of the samples as well with FTIR are presented while the adhesion was evaluated through scratch tests. The third part presents the third batch (inorganic coatings, alkaline hydrolysed MTEOS/ TEOS deposited on 304 stainless steel doped with different percentages of titanium butoxide: 0%w/w, 1.4%w/w, 2.8%w/w, 5.6%w/w, and 11.3%w/w as well as different use of solvent for the sol-gel preparation (mixture of ethanol, isopropanol, butanol; or isopropanol). Also, different curing processes (in N_2 or in air) are evaluated. These changes were made in order to increase the protective properties of the coatings. The results presented are from Scanning Electron Microscopy (SEM), EDX, adhesion and hardness in order to define the influence of the addition of different types of precursor in the coatings.

5.2 Surface Analyses of the First Batch: Series of Coatings with Different Formulations

5.2.1 Energy Dispersive X-ray Spectroscopy (EDX) on Inorganic/Hybrid, Organic and Hybrid/Composites Systems from the First Batch

EDX was used as an analytical technique for the elemental quantification of samples. It was used on the samples of the study to obtain information on their elemental composition. Batch 1 included 5 inorganic/hybrid systems, 2 organic systems and 2 hybrid/composites systems on either carbon steel X65 or 316L stainless steel. All these systems were alkaline hydrolysed MTEOS / TEOS with addition of polymers for the organic systems. Figure 5.1 presents the graph obtained from the results calculated through EDX, which was used on the different systems all deposited on stainless steel 316L in order to have only the parameter of the nature of the coating changing. It was supposed that since the coatings systems are the same regardless of the substrate and that it was before any experiment, the composition of the coatings would be the same and thus only one type of substrate was chosen. Three different points on two different samples were measured and analysed.

The graph shows that for all the coating systems but one (organic system 2 with an average value of 0.065%), silicon is the most or second most present element on the surface of the samples. Carbon is present at a high percentage for both organic and hybrid/composites systems while oxygen has a constant presence for all systems.

Due to the penetration range of X-rays and backscattered electrons the iron and chromium detected for inorganic/hybrid and hybrid/composites coatings originate from the substrate when coatings are a few µm thick [210] which means that the coatings where iron is detected before any experiment are thinner.

As presented in Figure 5.1 and as expected, the percentages of carbon for the inorganic/hybrid systems are low compared to the organic systems. Considering that the hybrid/composites systems contain both compositions of organic and inorganic/hybrid coatings, their percentage of carbon and oxygen is relatively high.

It would be expected that the amount of silicon detected would be low for the organic samples since they are not supposed to contain as it is what makes the

inorganic/hybrid sol-gel coating. Organic system 1 presents a 60% amount of silicon while it is close to 0% for organic system 2.

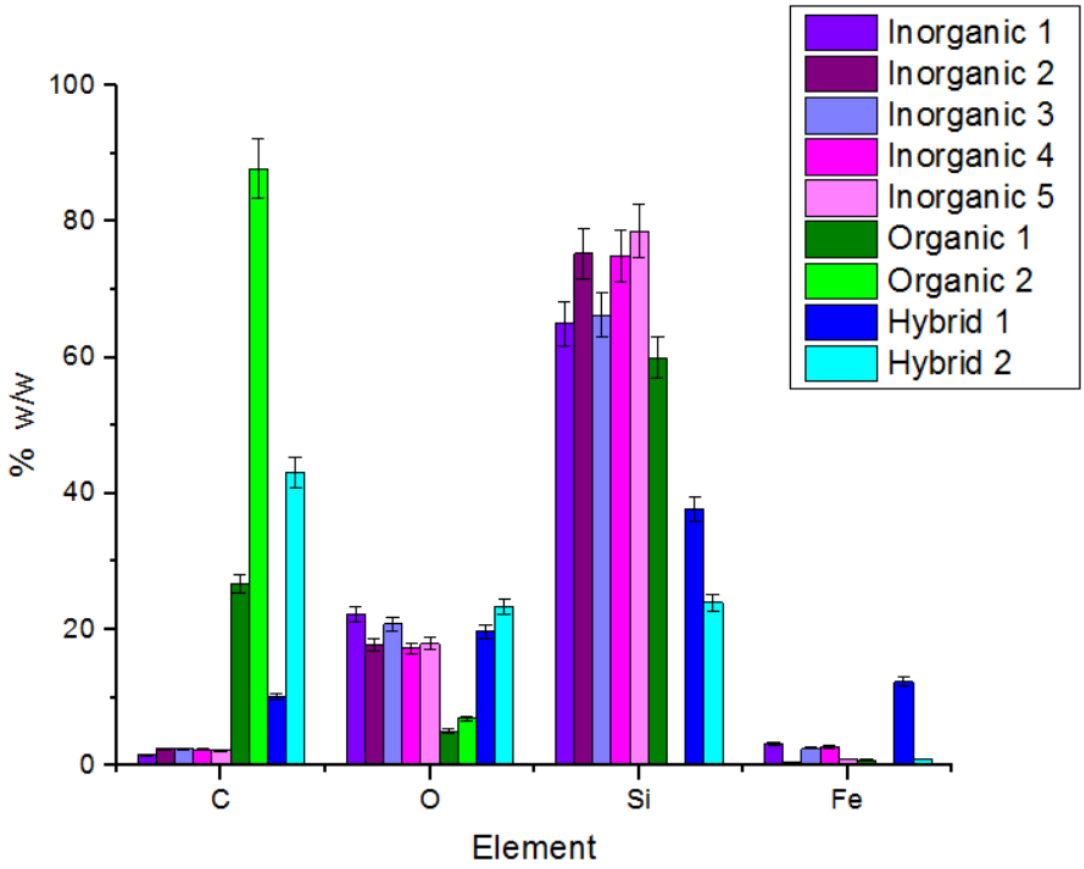

Figure 5.1 Weight percentage of C, O, Si and Fe elements for the different coating systems of Batch 1

The amount of iron as a function of the thickness is presented in Figure 5.2. Since these measurements were made before any experiment, there should be a really low amount of iron detected. The hybrid/composites system 1 presents an amount of about 12% which is high since the sample was not tested yet.

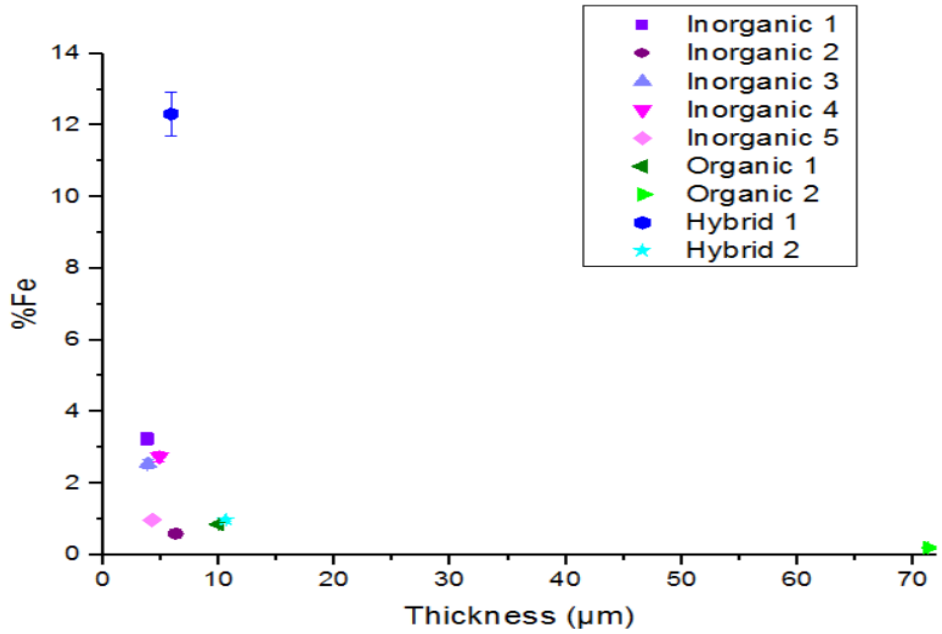

Figure 5.2 Percentage of iron as a function of thickness for the coatings of Batch 1

5.2.2 Fourier-Transform Infrared Spectroscopy on Inorganic/Hybrid, Organic and Hybrid/Composites Systems from the First Batch

The results obtained from FTIR analyses on non-tested samples are presented in Figure 5.3 to Figure 5.5 . The FTIR spectra were all taken in the wavenumber range of 600-4000 cm^{-1}. The spectra of inorganic/hybrid systems are similar to one another and are close to the spectra of hybrid/composites systems. Some differences can be due to the differences in the sol-gel process.

Figure 5.3 presents the FTIR spectra of all 5 different inorganic/hybrid systems. It appears that the coatings have the main functional groups in common (Si-C and Si-O-Si). However C-O bond and C-H stretching vibrations are also detected for most of them and Si-OH for only two of them [181] correspond to residual Si-OH due to incomplete condensation. It seems that the inorganic/hybrid systems 2 to 5 contain little silanol groups which could be due to incomplete reaction during the sol-gel process.

Figure 5.4 presents the FTIR spectra of the organic systems. They both present functional groups from pure epoxy coatings such as aromatic rings at 1582 and 3056cm^{-1}. Some of their peaks are at the same position than the silicon peaks from inorganic/hybrid coatings and this cannot be excluded since silicon was detected through SEM.

Figure 5.5 presents the FTIR spectra for the hybrid/composites systems, it shows group Si-O-Si from the inorganic/hybrid system but these peaks (1070-1080cm^{-1}) are close in value to the aromatic peaks value and thus can be superimposed or shifted. The hybrid/composites samples have a more complex structure as it can be seen in Figure 5.5.

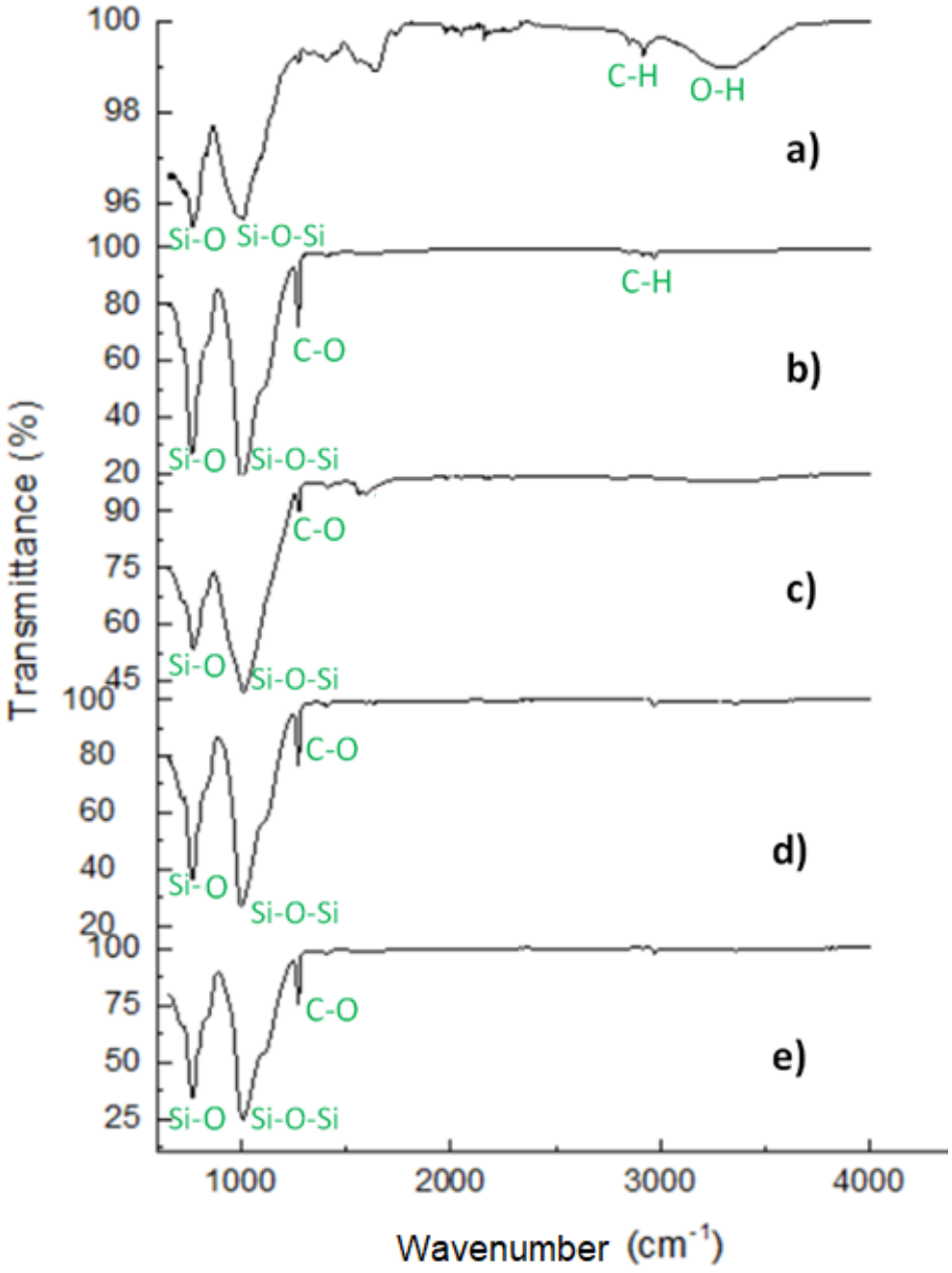

Figure 5.3 FTIR analysis of a) inorganic/hybrid system 1; b) inorganic/hybrid system 2; c) inorganic/hybrid system 3; d) inorganic/hybrid system 4; e) inorganic/hybrid system 5

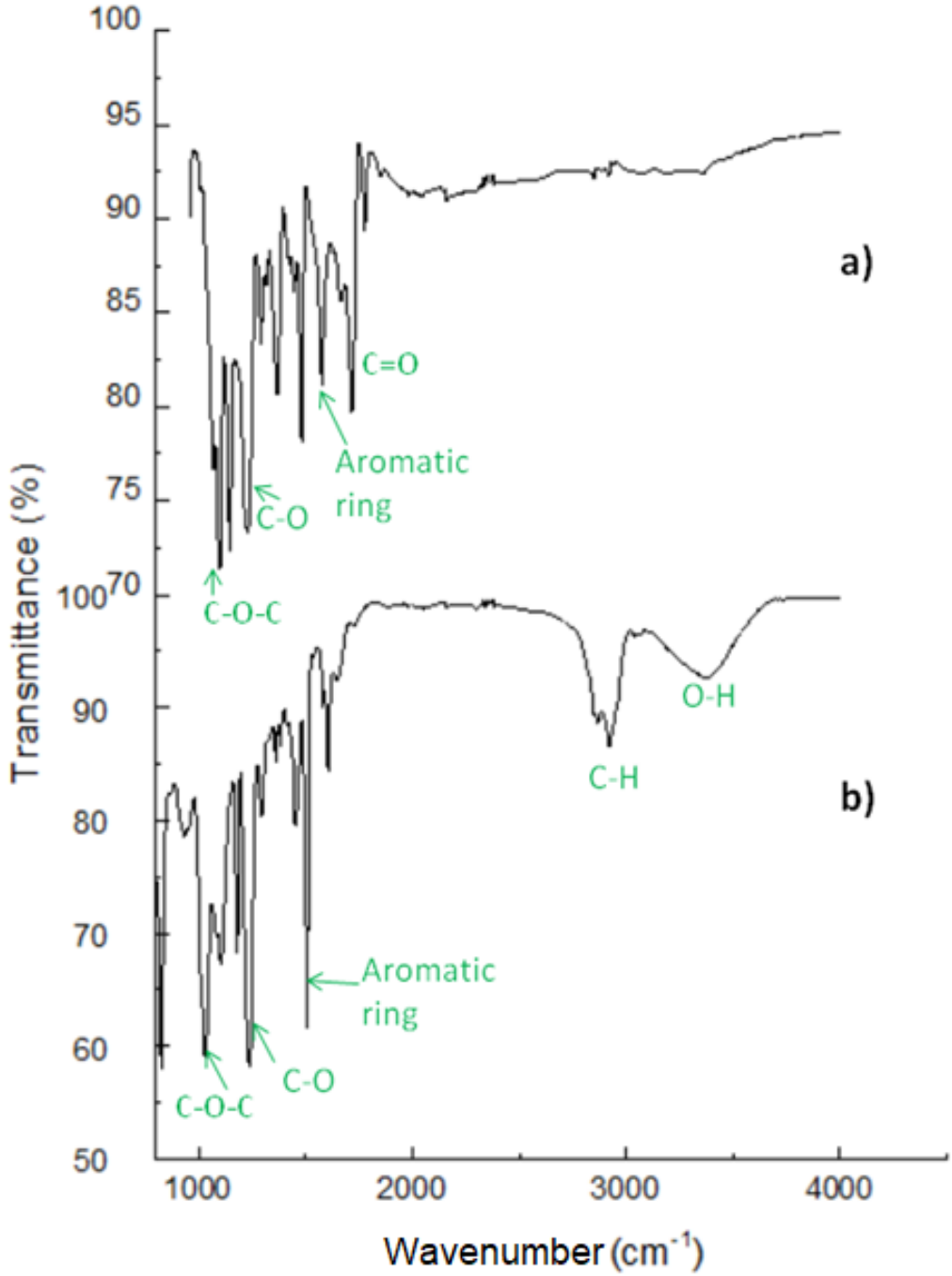

Figure 5.4 FTIR analysis of a) organic system 1; b) organic system 2

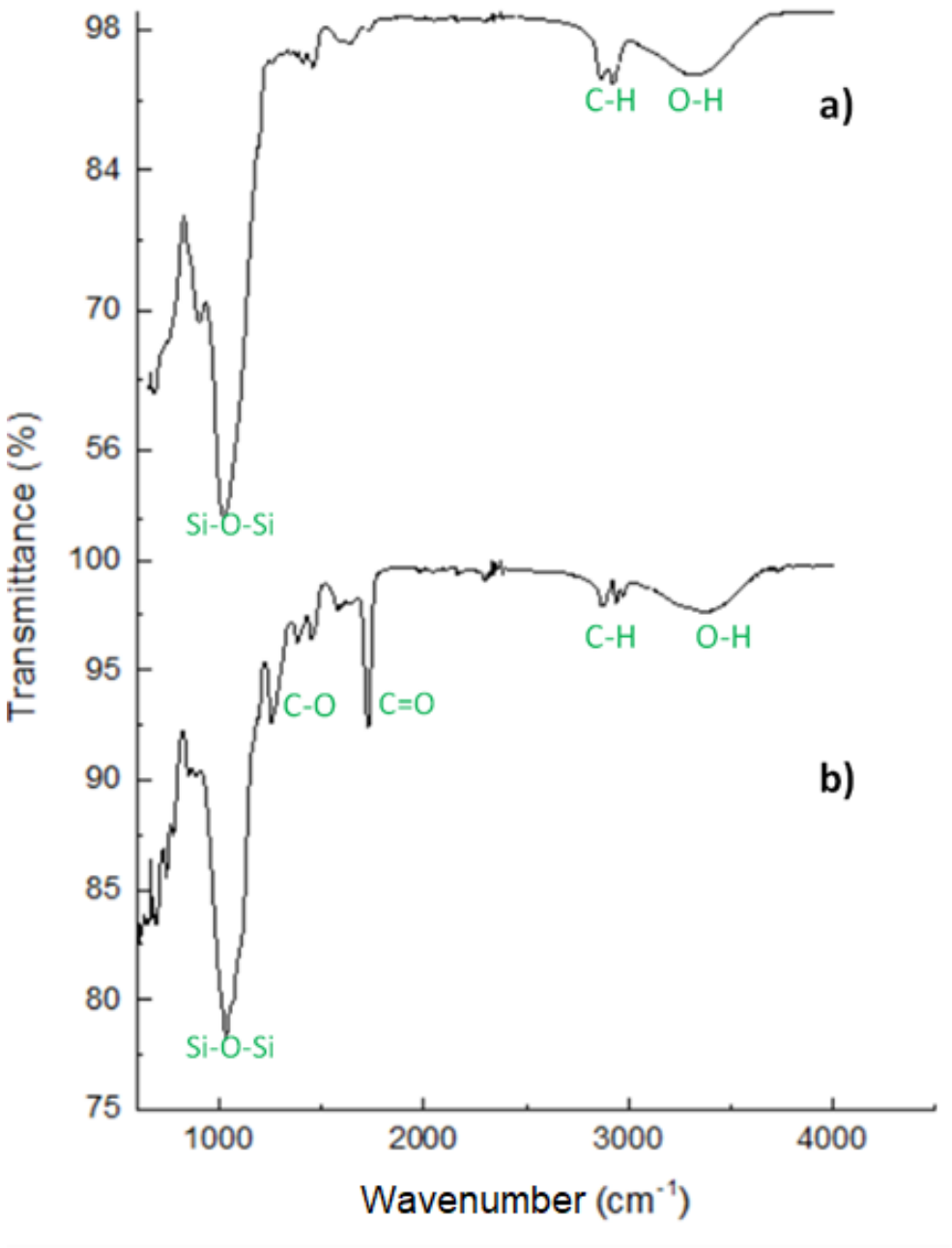

Figure 5.5 FTIR analysis of a) hybrid/composites system 1 b) hybrid/composites system 2

Some samples, for example inorganic /hybrid system 1, organic system 2 and both hybrid/composites systems present the –OH stretching bond from water. This could come from the curing process.

When the samples presented close to no –OH bonds it means that the condensation process was close to completion with the available silanol groups. Further hydrolysis and condensation could occur if there are residual alkoxy groups..

5.2.3 Critical Load on Inorganic/Hybrid, Organic and Hybrid/Composites Systems from the First Batch

This part presents the results of the scratch tests, thus giving information about the adhesion of the coatings on the substrates. Depending on the nature of the coating, the samples presented different types of failure and different critical loads. This load, also labelled as L_c, has been proposed as a quantitative value to evaluate the adhesion of the coating [211]. The results can be divided in three types of failure: cracking, ductile and ripping as presented in Figure 5.6. Table 5.1 presents the different type of failures obtained while Table 5.2 presents the values of the critical loads obtained for the samples of Batch 1. Figure 5.7 to Figure 5.9 present the appearance of all the systems.

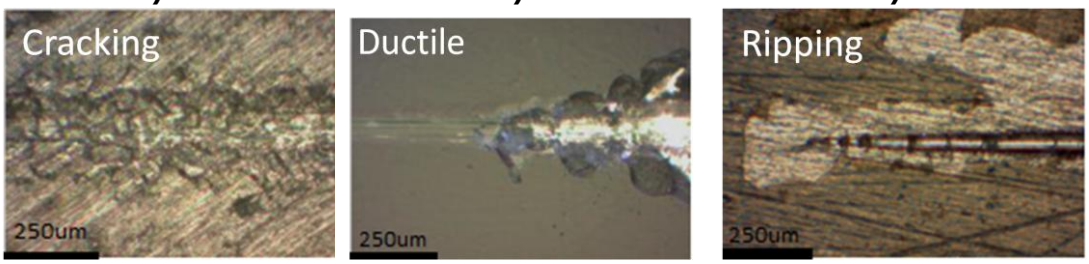

Figure 5.6 Different types of failure observed a) cracking b) ductile c) ripping

Table 5.1 Summary of the types of failure for Batch 1

Cracking	Ductile	Ripping
$I_{,B1,1,316L,No}$	$I_{,B1,1,X65,Yes}$	$I_{,B1,1,X65,No}$
$I_{,B1,1,316L,Yes}$	$I_{,B1,2,316L,No}$	
$I_{,B1,3,316L,No}$	$I_{,B1,2,316L,Yes}$	
$I_{,B1,3,316L,Yes}$	$I_{,B1,5,316L,No}$	
$I_{,B1,4,316L,No}$	$I_{,B1,5,316L,Yes}$	
$I_{,B1,4,316L,Yes}$	$O_{,B1,1,X65,No}$	
$H_{,B1,1,X65,No}$	$O_{,B1,1,X65,Yes}$	
$H_{,B1,1,316L,No}$	$O_{,B1,1,316L,No}$	
$H_{,B1,1,316L,Yes}$	$O_{,B1,1,316L,Yes}$	
$H_{,B1,2,X65,No}$	$O_{,B1,2,X65,No}$	
$H_{,B1,2,X65,Yes}$	$O_{,B1,2,X65,Yes}$	
$H_{,B1,2,316L,No}$	$O_{,B1,2,316L,No}$	
$H_{,B1,2,316L,Yes}$	$O_{,B1,2,316L,Yes}$	

Only one sample had a ripping type of failure (and was from an inorganic/hybrid system) while all the samples from the organic systems had a ductile type of failure and the hybrid/composites systems presented a cracking type of failure. The

inorganic/hybrid systems (except for $I_{,B1,1,X65,No}$) had either a cracking or ductile failure. The pre-treatment had little effect on the type of failure as compared in this table.

The hybrid/composites systems exhibit performance closer to the inorganic/hybrid systems than organic in this experiment, even though it contains high quantity of carbon material.

Table 5.2 Critical loads obtained for the samples of Batch 1

Sample	Critical load (N)
$I_{,B1,1,X65,No}$	1.42
$I_{,B1,1,X65,Yes}$	1.91
$I_{,B1,1,316L,No}$	3.32
$I_{,B1,1,316L,Yes}$	5.49
$I_{,B1,2,316L,No}$	1.92
$I_{,B1,2,316L,Yes}$	4.83
$I_{,B1,3,316L,No}$	2.01
$I_{,B1,3,316L,Yes}$	1.76
$I_{,B1,4,316L,No}$	3.87
$I_{,B1,4,316L,Yes}$	4.59
$I_{,B1,5,316L,No}$	4.59
$I_{,B1,5,316L,No}$	2.8
$O_{,B1,1,X65,No}$	0.39
$O_{,B1,1,X65,Yes}$	0.33
$O_{,B1,1,316L,No}$	0.89
$O_{,B1,1,316L,Yes}$	0.38
$O_{,B1,2,X65,No}$	5.1
$O_{,B1,2,X65,Yes}$	4.5
$O_{,B1,2,316L,No}$	4.5
$O_{,B1,2,316L,Yes}$	4.0
$H_{,B1,1,X65,No}$	5.39
$H_{,B1,1,316L,No}$	5.34
$H_{,B1,1,316L,Yes}$	5.13
$H_{,B1,2,X65,No}$	5.46
$H_{,B1,2,X65,Yes}$	8.03
$H_{,B1,2,316L,No}$	8.61
$H_{,B1,2,316L,Yes}$	7.81

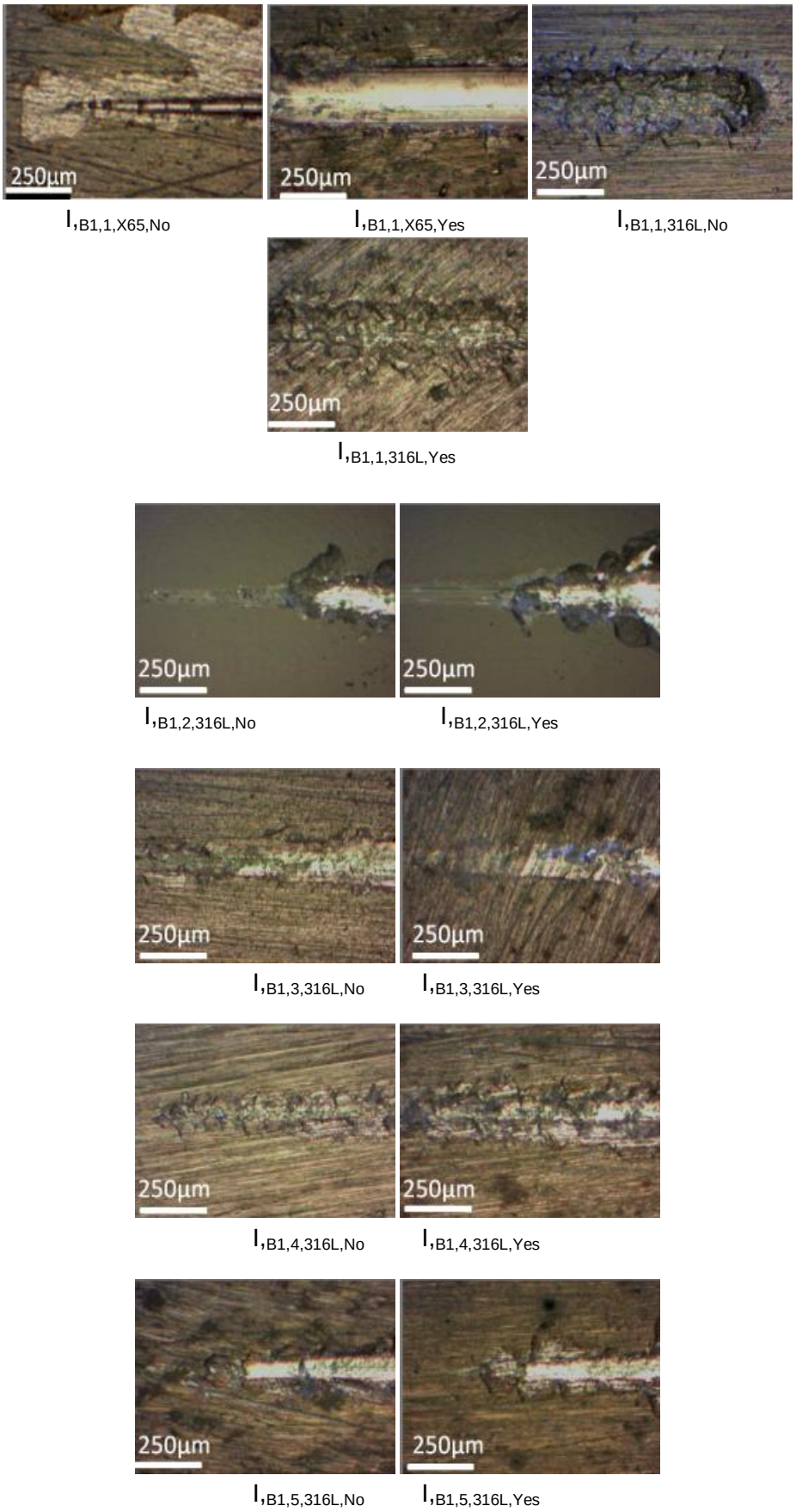

$I_{B1,1,X65,No}$ $I_{B1,1,X65,Yes}$ $I_{B1,1,316L,No}$

$I_{B1,1,316L,Yes}$

$I_{B1,2,316L,No}$ $I_{B1,2,316L,Yes}$

$I_{B1,3,316L,No}$ $I_{B1,3,316L,Yes}$

$I_{B1,4,316L,No}$ $I_{B1,4,316L,Yes}$

$I_{B1,5,316L,No}$ $I_{B1,5,316L,Yes}$

Figure 5.7 Appearance of the scratch tracks for the inorganic coating systems of Batch 1

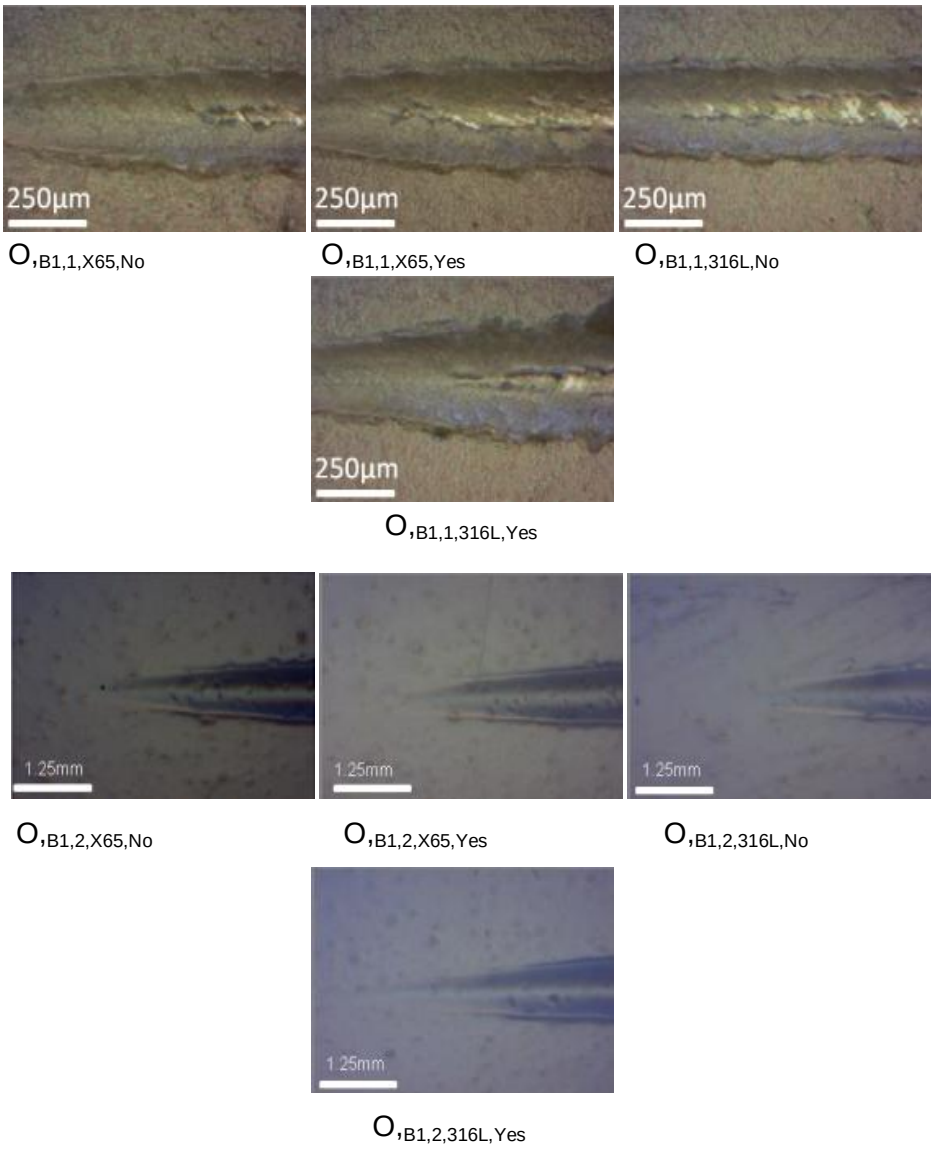

Figure 5.8 Appearance of the scratch tracks for the organic coating systems of Batch 1

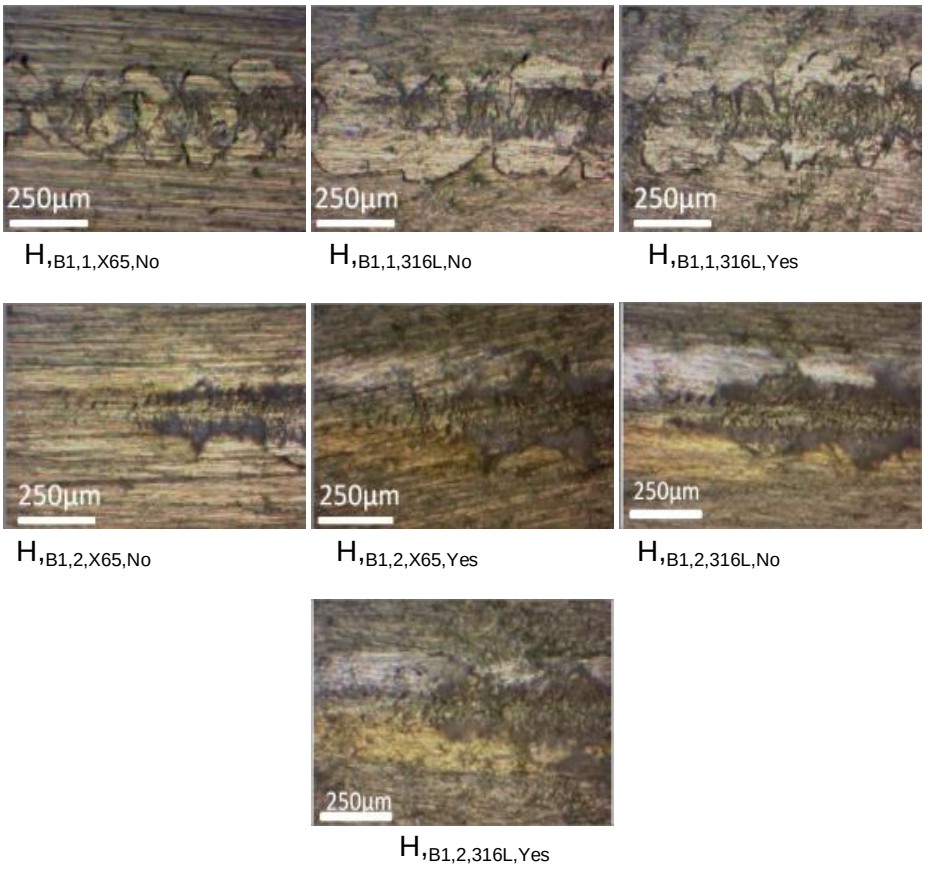

Figure 5.9 Appearance of the scratch tracks for the hybrid/composites coating systems of Batch1

Figure 5.10 to Figure 5.13 summarise the values obtained for the critical loads of the samples of the first batch. For the inorganic/hybrid coatings (except system 1), the coatings did not adhere on the X65 carbon steel (with or without pre-treatment); the samples were not sent by the company so there can only be a presentation of the results on 316L stainless steel. This means that the inorganic/hybrid coatings of this batch had a low, even non-existent adhesion on carbon steel X65. The adhesion appeared to be low for the inorganic/hybrid coating systems as the critical load values are below 5N. The substrate could be seen almost as soon as the scratch begins. As for the organic coatings, it seems like the samples from the same systems have a similar value of critical load and that the scratch had the same effect and ended in the same failure for both systems, regardless of the substrate. The critical load of the organic system 1 is extremely low (less than 1N) while the critical load for organic system 2 is higher (between 3N and 5N).

Hybrid/composites systems have the highest value of critical load (between 5N and 9N) compared to the other types of coatings studied. Unlike the inorganic/hybrid and organic coatings, the substrate cannot be seen on the surface of the sample after

the scratch. It is expected since they have advantages of both types as presented in Chapter III.

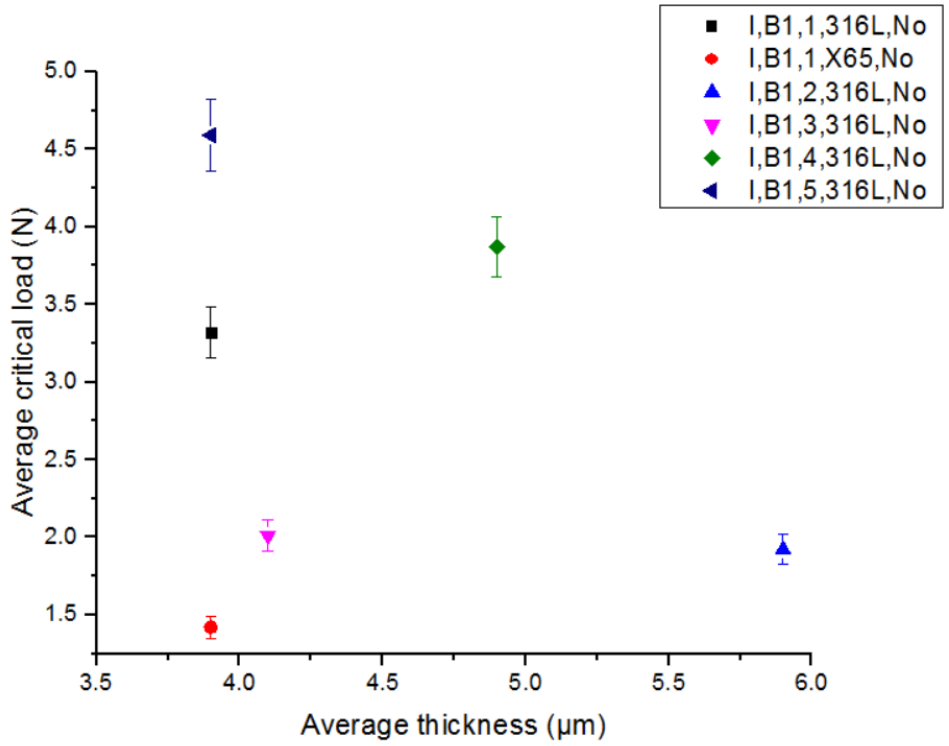

Figure 5.10 Critical loads as a function of the average thickness of the inorganic/hybrid samples of Batch 1 without pre-treatment

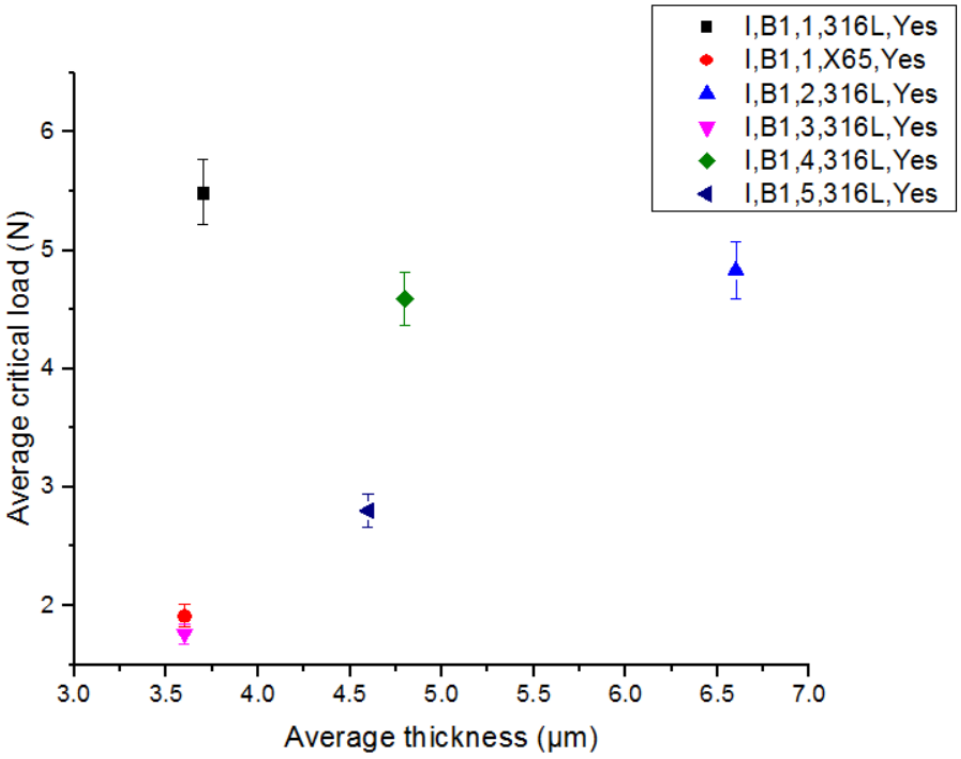

Figure 5.11 Critical loads as a function of the average thickness of the inorganic/hybrid samples of Batch 1 with pre-treatment

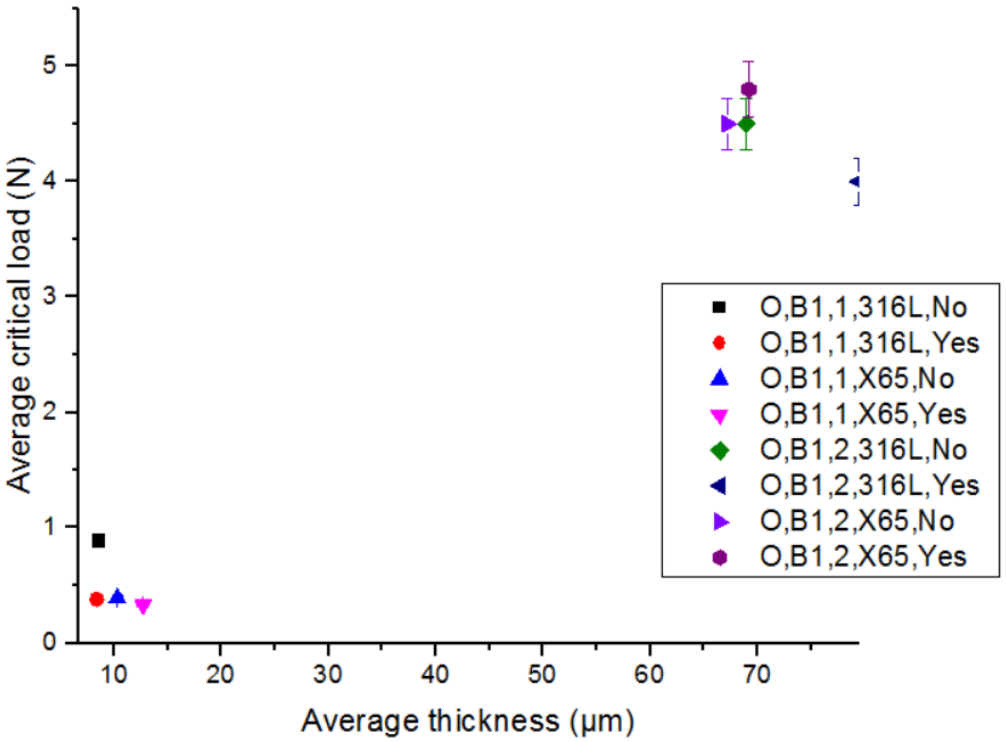

Figure 5.12 Critical loads as a function of the average thickness of the organic samples of Batch 1

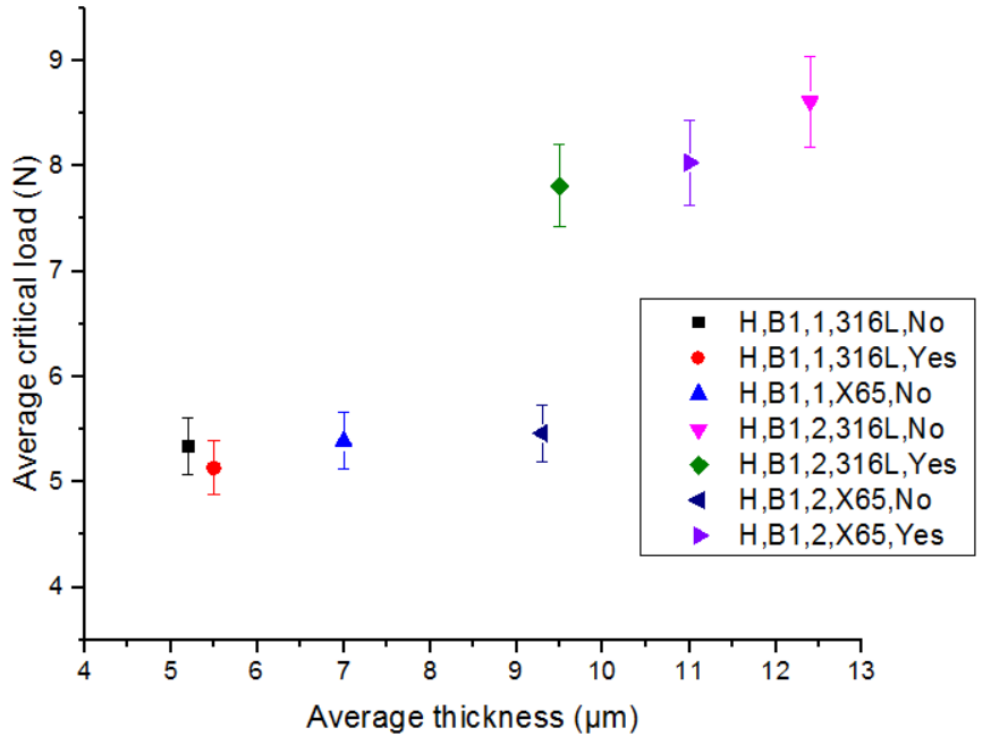

Figure 5.13 Critical loads as a function of the average thickness of the hybrid/composites samples of Batch 1

5.2.3.1 Inorganic/Hybrid Samples

As presented in Figure 5.7, Figure 5.10 and Figure 5.11, the samples $I_{,B1,1,X65,No}$, $I_{,B1,1,X65,Yes}$, $I_{,B1,1,316L,No}$ and $I_{,B1,1,316L,Yes}$ are all coated with an inorganic/hybrid sol-gel system 1 but it is clear that the results of scratch-tests are all different.

While comparing both samples of the inorganic/hybrid system 1, the result of the scratch test seems different; as on X65 the coating looks like it is ripped off the substrate while on the 316L stainless steel it is more like a crack. The critical load for $I_{,B1,1,X65,No}$ is 1.4N while for $I_{,B1,1,316L,No}$ it is 3.3N. In this case of both coated samples without pre-treatment it is a value which can be characterized as low but the value of the 316L-inorganic 1 combination is greater compared to the value of X65-inorganic 1. The combination 316L-inorganic/hybrid system 1 with pre-treatment has also a higher critical load value compared to the combination of X65-inorganic/hybrid system 1 with pre-treatment. Moreover, the results with the stainless steel as a substrate have a higher value of the critical load compared to the coatings on carbon steel.

In Figure 5.7 the adhesion of the sample $I_{,B1,1,X65,No}$ seems poor and the coating could be torn off from the substrate. Its critical load value is really low (1.4N), as well as for the sample $I_{,B1,1,X65,Yes}$ (1.9N). Scratch marks make the coating look really soft and with poor adhesion. For this one, the substrate can be seen. The results on X65 show that the adhesion of the coating on the substrate is not very strong and that it can easily be removed while it can be seen in the results for 316L that even if it is the same coating, it does not have the same effect on the substrate. From Figure 5.7 it can be seen that cracks are formed on $I_{,B1,1,316L,No}$ (critical load of 3.3N) and $I_{,B1,1,316L,Yes}$ (critical load value of 5.5N) and the substrate is not easily seen under the coating.

The sample $I_{,B1,1,316L,Yes}$ has a stronger adhesion. Its critical load value is the highest of the samples and more than 5N, which for this first batch, is considered in the top half of the critical load values.

For inorganic/hybrid systems 2 to 5 there are only results of coatings on 316L stainless steel as there was no adhesion at all on the samples on carbon steel so no measurements could be made.

In this case (Figure 5.7), the samples $I_{,B1,2,316L,No}$ and $I_{,B1,2,316L,Yes}$ which are both from the inorganic/hybrid system 2 have the same visual result (ductile failure) but the

values of their critical load are different: 1.9N for $I_{,B1,2,316L,No}$ and 4.5N for $I_{,B1,2,316L,Yes}$. $I_{,B1,2,316L,Yes}$ seems to strongly adhere to the substrate. The substrate can also be seen once the coating has been removed for both samples.

Figure 5.7 presents both samples $I_{,B1,3,316L,No}$ (critical load value of 2.0N) and $I_{,B1,3,316L,Yes}$ (critical load value of 1.8) from the inorganic/hybrid system 3 but having approximately the same result (cracking failure) and critical load. The failure in both cases is more of a delamination.

Both samples $I_{,B1,4,316L,No}$ and $I_{,B1,4,316L,Yes}$ are from the inorganic/hybrid system 4 and also have approximately the same results, visually as well as for the critical load: 3.9N for $I_{,B1,4,316L,No}$ and 4.6N for $I_{,B1,4,316L,Yes}$ and both having cracking as failure. The failure here shows that the coatings are harder and that the critical load values are higher than the precedent samples.

Both samples, $I_{,B1,5,316L,No}$ and $I_{,B1,5,316L,Yes}$ are from the inorganic/hybrid system 5. The sample $I_{,B1,5,316L,No}$ has a higher value of critical load (4.59N compared to 2.80N for $I_{,B1,5,316L,Yes}$) while both samples look like having a soft coating and a ductile failure. The substrate can be seen for both samples shortly after the start of the failure. In this case, the sample on X65 carbon steel substrate has a higher value of critical load compared to the sample on 316L stainless steel.
For the critical loads of inorganic/hybrid systems, the pre-treatment seems to have an impact on the scratch resistance as the values can have up to 2N of difference.

5.2.3.2 Organic Samples

The four samples, $O_{,B1,1,X65,No}$, $O_{,B1,1,X65,Yes}$, $O_{,B1,1,316L,No}$ and $O_{,B1,1,316L,Yes}$ from the organic system 1 have the lowest values of the critical load according to Figure 5.12, which means a really poor adhesion and Figure 5.8 also shows the presence of the substrate. $O_{,B1,1,X65,No}$ has a critical load value of 0.4N, $O_{,B1,1,X65,Yes}$ has a value of 0.3N, $O_{,B1,1,316L,No}$ has a value of 0.9N and $O_{,B1,1,316L,Yes}$ has a value of 0.4N. The four samples have the same type of failure: ductile failure.

As shown in Figure 5.8, the substrate has no influence on the adhesion as the coating is too soft to be properly scratched.

The samples $O_{,B1,2,X65,No}$, $O_{,B1,2,X65,Yes}$, $O_{,B1,2,316L,No}$, $O_{,B1,2,316L,Yes}$, are from the same organic system 2 and have a higher critical load value compared to the other

organic system. The critical load values are respectively 5.1N, 4.5N, 4.8N and 4.5N. There is a clear distinction between the two organic systems. Organic system 1 presents a low critical load for a low thickness while organic system 2 has a higher critical load (about 5 times compared to system 1) for a thickness about 7 times greater. The substrate is not being shown in any of the pictures. The results from Figure 5.8 are similar and appear as a ductile failure while their critical load values are comparable regardless of the substrate. For applications requiring greater scratch resistance, thicker coatings of this type would be more appropriate.

5.2.3.3 Hybrid/Composites Samples

The samples $H,_{B1,1,X65,No}$ (critical load value of 5.4N), $H,_{B1,1,316L,No}$ (critical load value of 5.3N) and $H,_{B1,1,316L,Yes}$ (critical load value of 5.1N) are from the hybrid/composites system 1 have a high value of critical load as shown in Figure 5.13, but the failures seem to be both delamination and crack of the coating. All of those samples have a cracking-like failure (Figure 5.9). The results presented are visually comparable.

The samples $H,_{B1,2,X65,No}$ (critical load value of 5.5N), $H,_{B1,2,X65,Yes}$ (critical load value of 8.0N), $H,_{B1,2,316L,No}$ (8.6N) and $H,_{B1,2,316L,Yes}$ (7.8N) are from the hybrid/composites system 2. These samples have a high critical load value (Figure 5.13), especially $H,_{B1,2,316L,No}$ which present the highest value of all. In these cases, the failure seems like a crack of the coating (Figure 5.9).

The pre-treatment seems to have little effect on the hybrid/composites systems.

5.3 Surface Analyses of the Second Batch

The second batch consisted of three types of coatings, hybrid/composites sol-gel coatings, undoped inorganic/hybrid sol-gel coating and inorganic/hybrid coating with titanium precursor doping deposited on either stainless steel 304 or A1008Qpanel.

5.3.1 FTIR on Sample Coated with Undoped Sol-Gel Inorganic/Hybrid Coating and on Sample Coated with Inorganic/Hybrid Sol-Gel Coating Doped with Titanium Precursor

This part presents the results obtained from FTIR analyses, on intact samples before any experiment is performed. The FTIR spectra were all taken in the range wavenumber of 4000 to 600cm^{-1}. All the inorganic/hybrid sol-gel coatings were prepared with the same bases and have similar functional groups detected through FTIR to form a general structure, with addition of different peaks according to the type of doping or additives.

Figure 5.14 presents the spectrum for the inorganic/hybrid sol-gel coatings without any doping (0%) and the different percentages of doping before any immersion.

The most important bands appear at 1070-1080cm^{-1}, which corresponds to the Si–O–Si asymmetric stretching vibration [180]. The absorption bands observed at around 2950cm^{-1} and 1400cm^{-1} stem from stretching and bending vibrations of C–H bonds respectively [179, 212]. The absorption bands observed at around 750cm^{-1} could be ascribed to Si-O groups [213]. The sample is at Day 0 and has not been tested yet, thus the O-H bonds detected such as the peak at 1600cm^{-1} [181] can correspond to residual Si-OH due to incomplete condensation or from water from the curing step of process.

The presence of Si-O-Si groups in the FTIR results confirms that the condensation reactions have been properly produced [214].

The results for the spectra of doped samples are not totally conclusive and additional characterisation is needed as it analyses only the surface. The samples present a shifting of peak at about 1000 cm^{-1} or as a peak it can be assigned to Ti-O-Si and another peak at 800 cm^{-1} for Ti-O-Ti [212]. No peak can be clearly associated to the Ti-OH group, suggesting that the condensation occurred immediately after the hydrolysis after the titanium precursor [212].

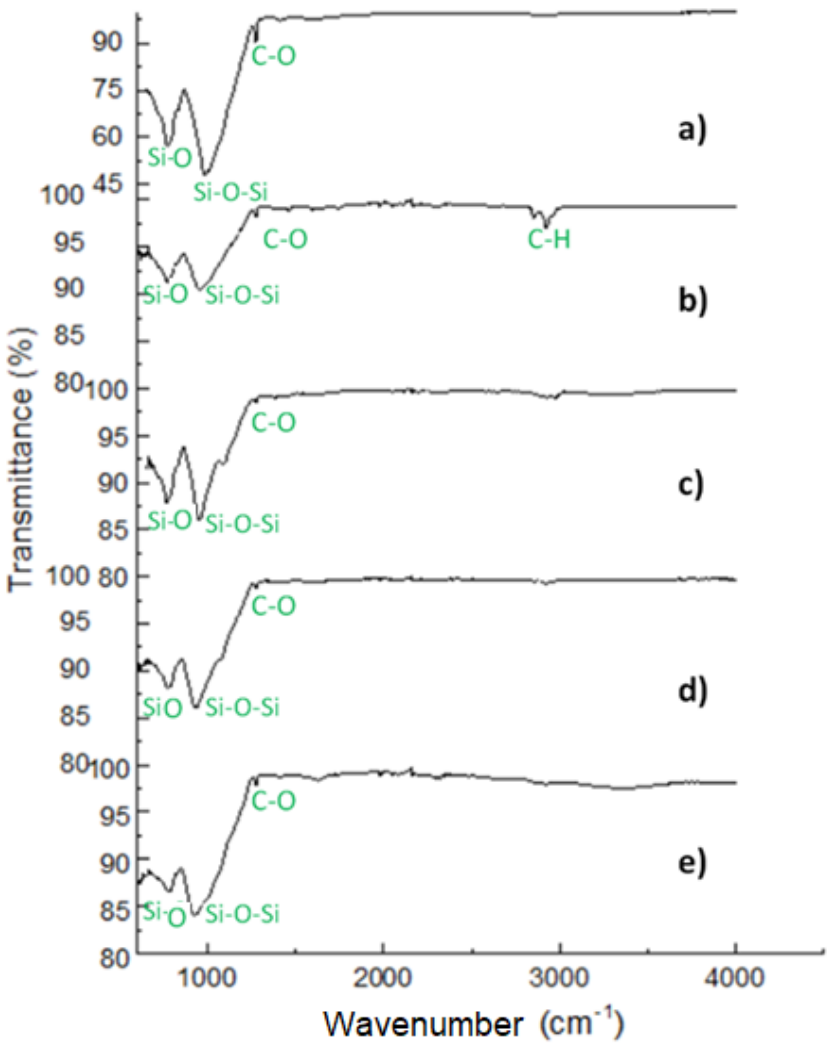

Figure 5.14 FTIR spectra of inorganic/hybrid sol-gel coating samples of Batch 2 with different percentages of titanium precursor before the experiment: a) 0%w/w; b) 1.4%w/w; c) 2.8%w/w; d) 5.6%w/w; e) 11.3%w/w

The structure of the undoped inorganic/hybrid sol-gel coating (0%w/w of titanium precursor) is the base of the other coatings such as the doped coatings as well as the samples from the third batch which includes samples whose solvent used during the process are isopropanol or the mixture, samples cured in N_2 or in air. Before any experiment, there are no additional peaks for those samples compared to the undoped inorganic/hybrid sol-gel coating used as a reference and presented in Figure 5.14.

Besides the high number of peaks, the spectra showed different intensities, sharpness and some shifts in peaks, highlighting an admitted limitation encountered during FTIR analysis: the more molecules there are, the more difficult it is to assess which peaks correspond to a certain molecule. This is due to the fact that there can

be interferences between the different components [215]. In addition, broad peaks can be due to the presence of specific bonds such as the O-H bond, or the presence of two component presenting stiff bonds vibrating in the same region [216]. Therefore, the results from FTIR analysis have to be considered with caution.

5.3.2 Adhesion of Second Batch

Samples from Batch 2 deposited on 304 stainless steel were analysed. The samples were too reflective for the pictures to be shown but all presented a cracking failure. Table 5.3 presents the results of these samples and the critical loads obtained. One sample of each category was chosen.

Table 5.3 Critical loads for Batch 2

Sample	Critical load (N)
Hybrid/composites coating	0.9 ± 0.5
Undoped inorganic/hybrid coating	3.1 ± 0.5
Inorganic/hybrid coating with 2.8%w/w Ti precursor	4.5 ± 0.5

In this batch, the hybrid/composites coating has a really low value of critical load compared to the first batch with a value of less than 1N whereas hybrid/composites coatings are supposed to have a higher critical load compared to the other coatings. The addition of titanium to this coating seems to have an influence on the adhesion or strength of the sol-gel coating since the value of the critical load for the undoped coating is about 3N and there is a slight increase with the addition of precursor to about 4.5N. Visually, the substrate cannot be seen on the surface of the samples and the failures look like cracks.

5.4 Surface Analyses of the Third Batch

The third batch consisted of undoped inorganic/hybrid sol-gel coatings and inorganic/hybrid coatings with titanium precursor doping deposited on stainless steel 304.

5.4.1 Scanning Electron Microscopy / Energy Dispersive X-Ray Spectroscopy (SEM and EDX)

This part focuses on the third batch of coating (see Chapter IV) and the differences between the samples with different formulations and solvents used and curing process. All coatings were inorganic/hybrid sol-gel coatings with 0%w/w, 1.4%w/w, 2.8%w/w, 5.6%w/w or 11.3%w/w of doping with titanium precursor with either isopropanol or solvent mixture as solvent and air or N_2 used in the curing process.

For the sol-gel coatings which were cured in air, there was presence of cracks on their surface, with the main cracked samples being the ones with 11.3%w/w of titanium butoxide in the system. These samples, even before immersion, were weakened. Some examples are shown in Figure 5.15.

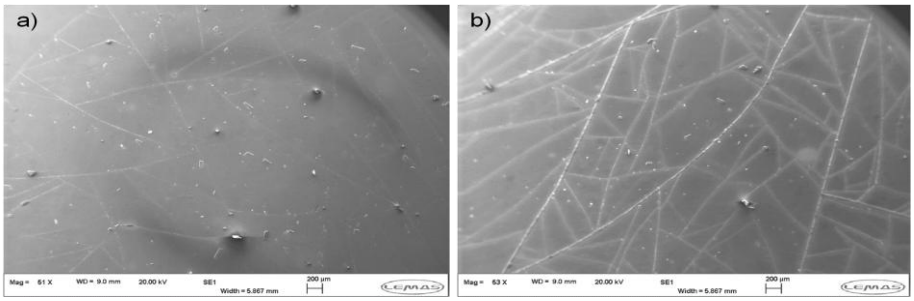

Figure 5.15 SEM image before immersion a) sample with isopropanol as solvent cured in air ($I_{B3,11.3\%,Ip,Air}$) b) sample with mixture as solvent cured in N_2 ($I_{B3,11.3\%,Mix,N2}$)

Cracks can be seen through these SEM images and prove that the substrates are not properly covered. Those samples contain 11.3%w/w of titanium butoxide.

Both undoped inorganic/hybrid coatings with the mixture as solvent ($I_{B3,0\%,Mix,N2}$ and $I_{B3,0\%,Mix,Air}$) show asperities on their surface before immersion. This is presented in Figure 5.16. Cracks can be seen before the experiment, which can lead the sample to be more inclined to corrosion.

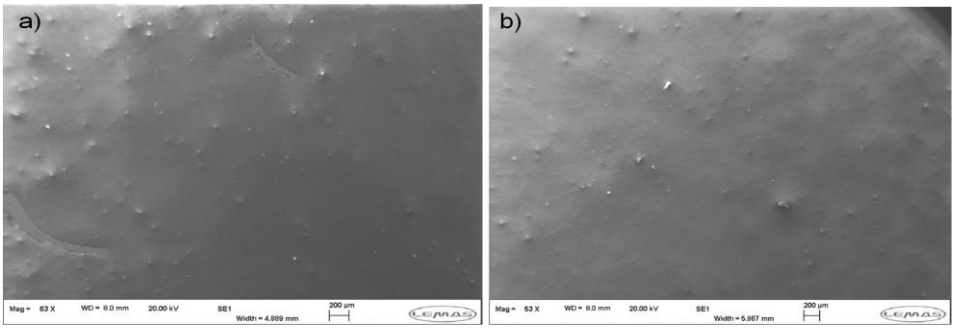

Figure 5.16 SEM image before immersion a) sample cured in air ($I_{B3,0\%,Mix,N2}$) b) sample cured in N_2 ($I_{B3,0\%,Mix,Air}$)

5.4.2 Composition of the Samples Determined with EDX

Figure 5.17 to Figure 5.21 present the average value of silicon, iron and titanium measured through EDX for the samples of the third batch. Measurements were taken before any experiments to have a more accurate value of the percentage of the chemical elements. The focus is to show the differences in the measured values depending on the curing process or solvent used.

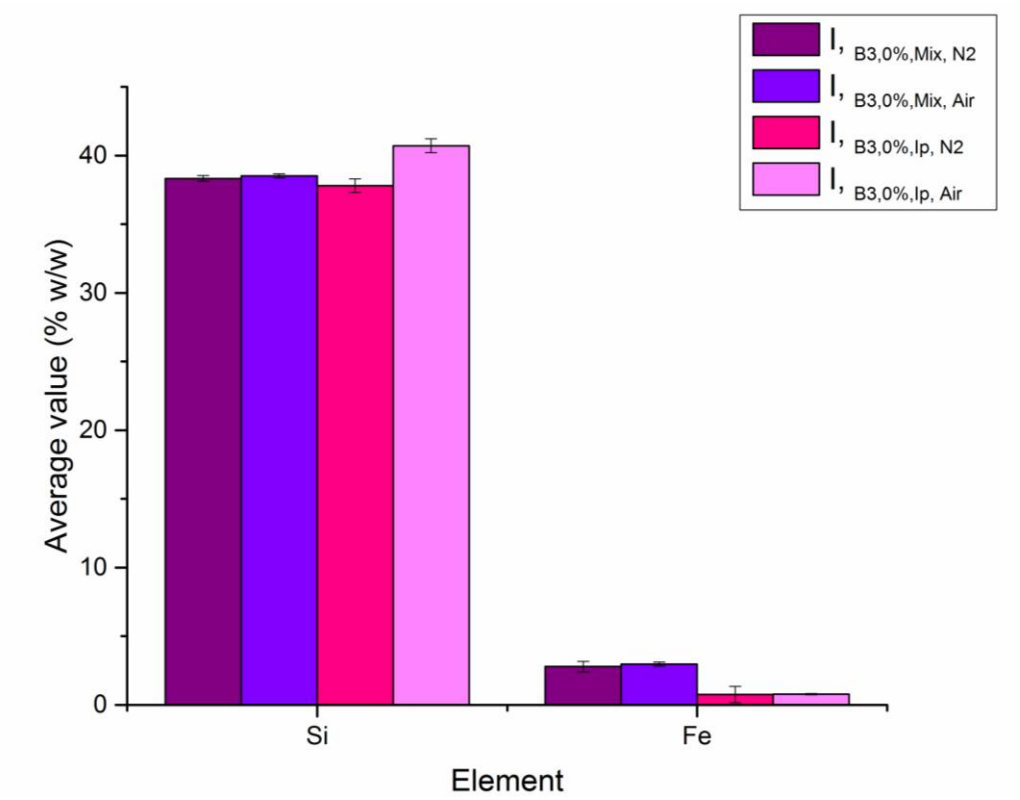

Figure 5.17 Average amount of silicon and iron according to EDX for non-doped samples of Batch 3

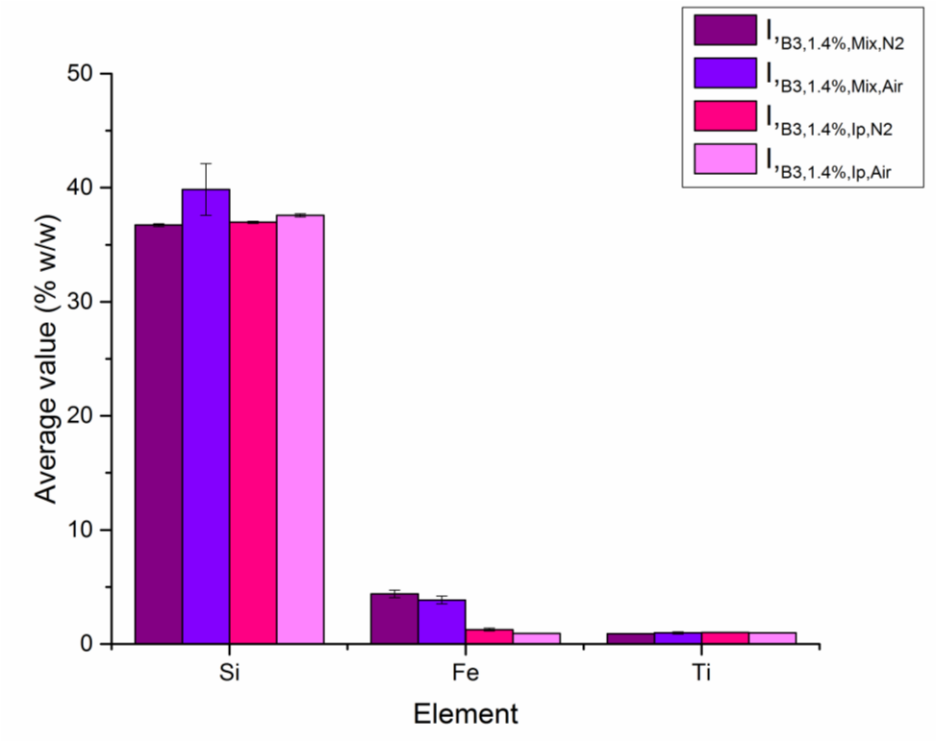

Figure 5.18 Average amount of silicon, titanium and iron according to EDX for 1.4%w/w titanium butoxide samples from Batch 3

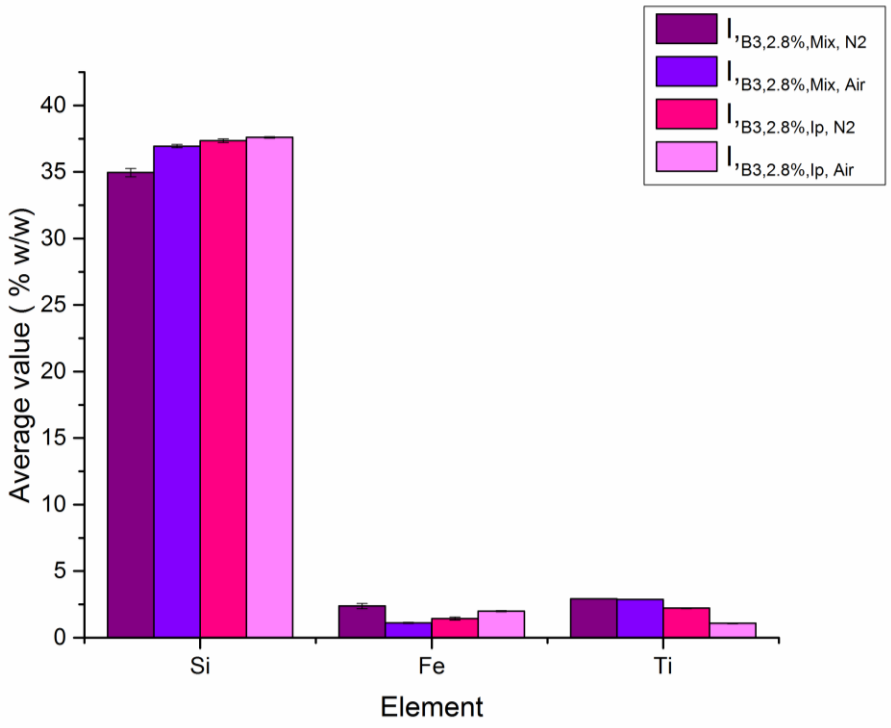

Figure 5.19 Average amount of silicon, titanium and iron according to EDX for 2.8%w/w titanium butoxide samples from Batch 3

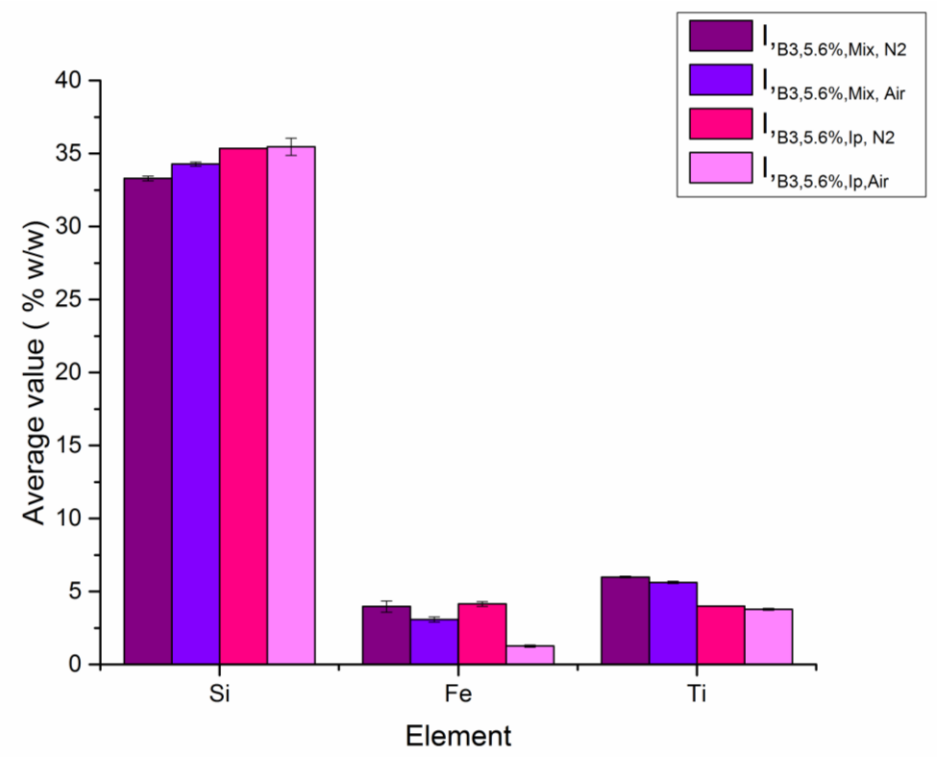

Figure 5.20 Average amount of silicon, titanium and iron according to EDX for 5.6%w/w titanium butoxide samples from Batch 3

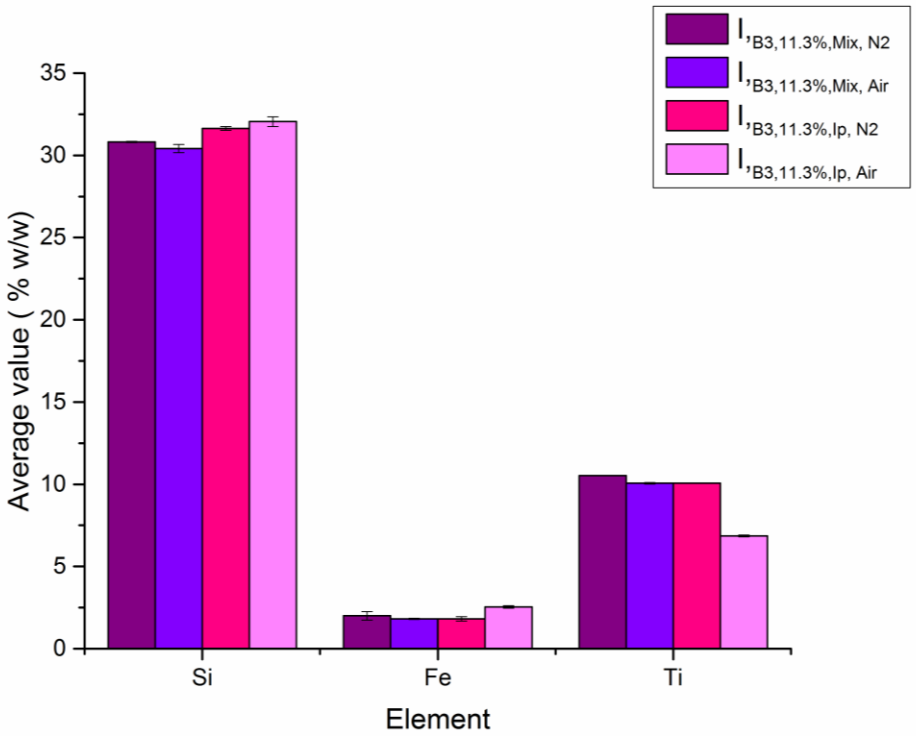

Figure 5.21 Average amount of silicon, titanium and iron according to EDX for 11.3%w/w titanium butoxide samples from Batch 3

Depending on the curing process and the solvent used during the sol-gel method, the concentration of the silicon and titanium elements are different for samples which are supposed to have the same concentration of titanium precursor. Especially for samples with a doped value from 2.8%w/w to 11.3%w/w the percentage of titanium present and measured is lower for the samples with isopropanol as a solvent and the gap between the systems with different solvents increase with the amount of titanium.

Figure 5.22 presents a summary of the ratio Ti/Si for the samples of the third batch.

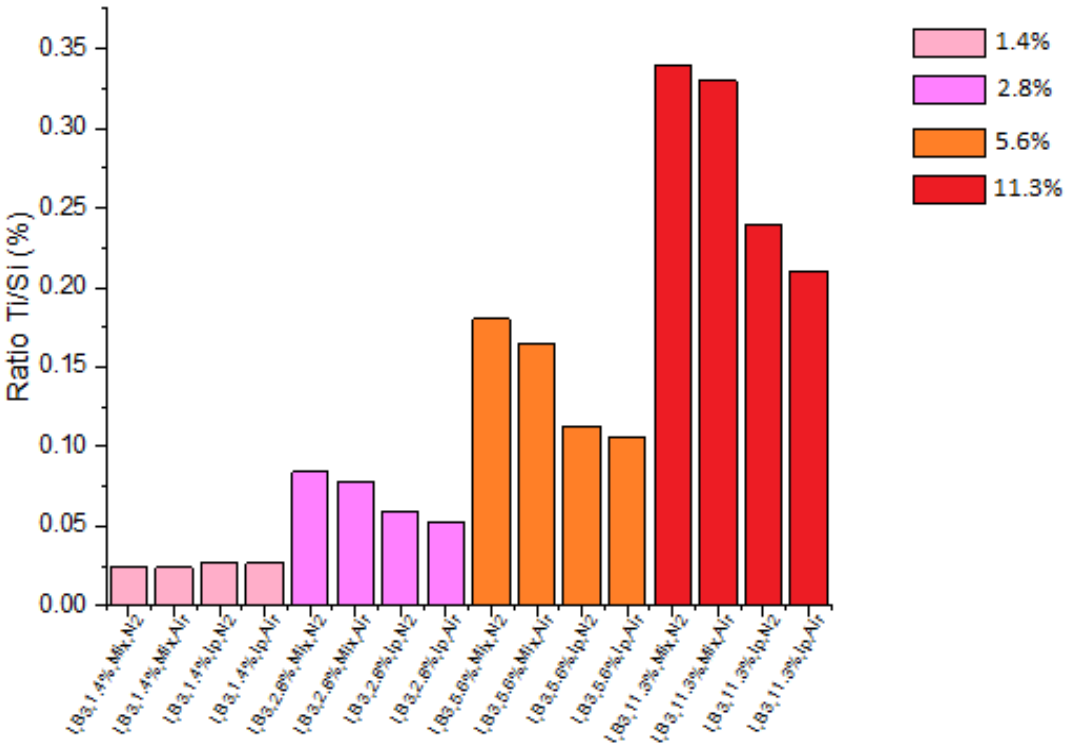

Figure 5.22 Ratio Ti/Si for the samples with different formulations of Batch 3

Thus, there is considerable potential between the input (target) formulation and the final coating composition. It was not possible to accurately determine this difference. For the nomenclature the percentage of precursor added was therefore kept although this does not correspond exactly to what the sample contains. The higher the concentration of titanium added, the bigger the difference is for the percentage of titanium measured between the samples with different solvents. Less titanium is present for samples with isopropanol as a solvent compared to samples with the mixture as solvent.

Figure 5.23 and Figure 5.24 present the amount of iron detected as a function of thickness. The thicknesses are similar to the thickness of the inorganic/hybrid

coatings from the other batches: close to 5µm. The amount of iron detected is below 5% for all samples, even for the samples with 11.3%w/w of precursor which showed cracks on their surface as presented in Figure 5.15.

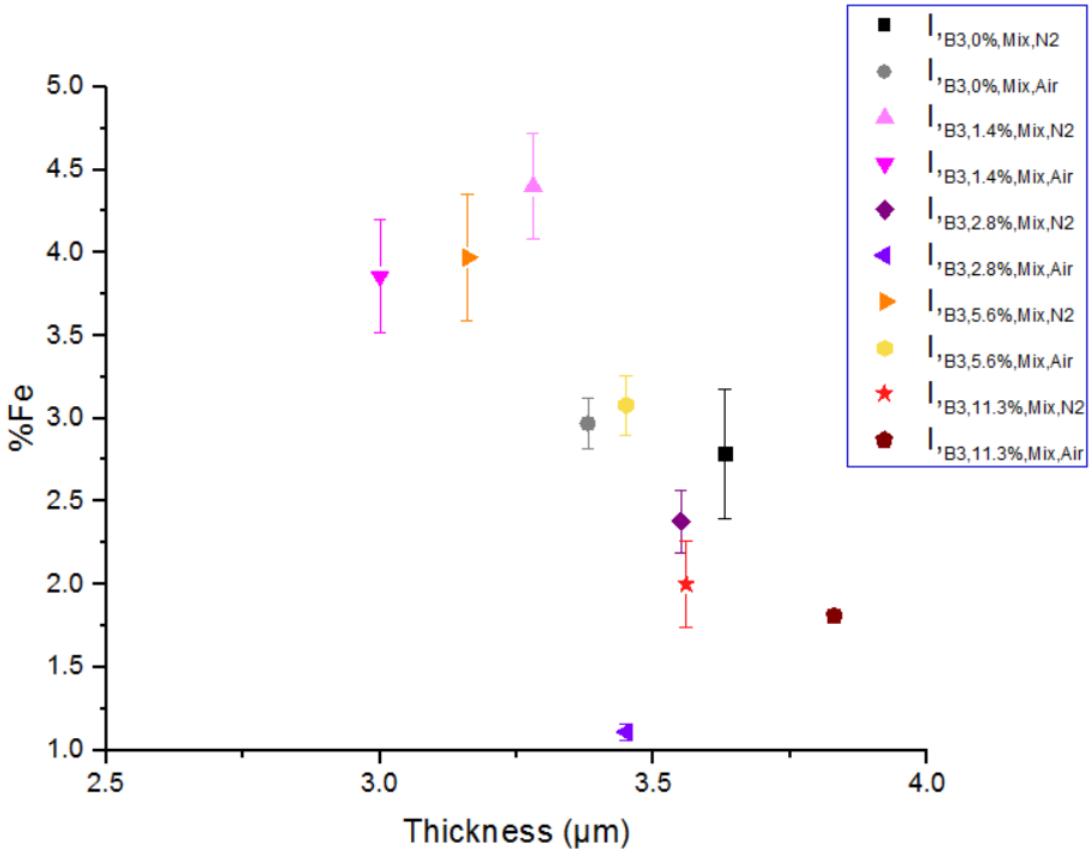

Figure 5.23 Weight percentage of iron detected for Batch 3 as a function of thickness for the samples with the mixture as solvant

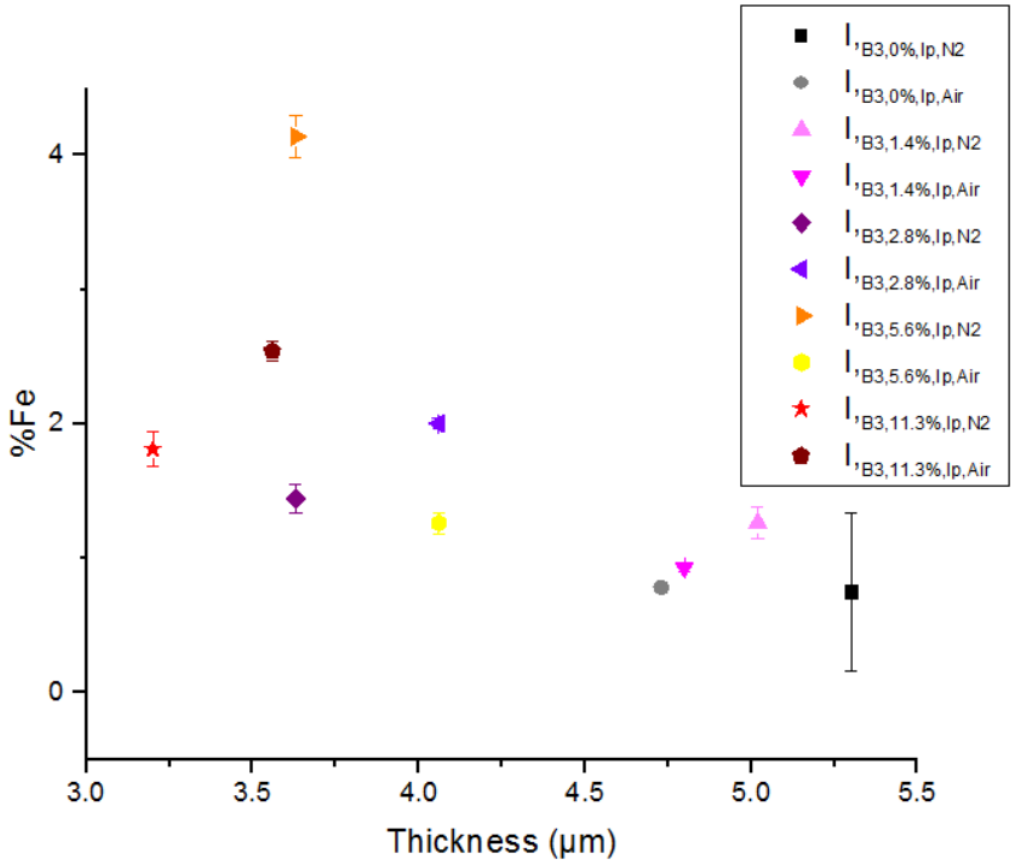

Figure 5.24 Weight percentage of iron detected for Batch 3 as a function of thickness for the samples with isopropanol as solvent

5.4.3 Cross-Section of Sample Doped with 11.3%w/w of Titanium Precursor and Analysis with EDX

A cross section of one of the samples doped with 11.3w/w% of titanium precursor with the mixture as solvent and cured in N_2 ($I_{,B3,11.3\%,Mix,N2}$) was studied through SEM and EDX in order to have information about the dispersion of silicon and titanium elements in the coating as shown in Figure 5.25 (which also shows the thickness of the coating) and Figure 5.26. The sample with the highest percentage of titanium was chosen in order to have more information about the dispersion of this element throughout the coating.

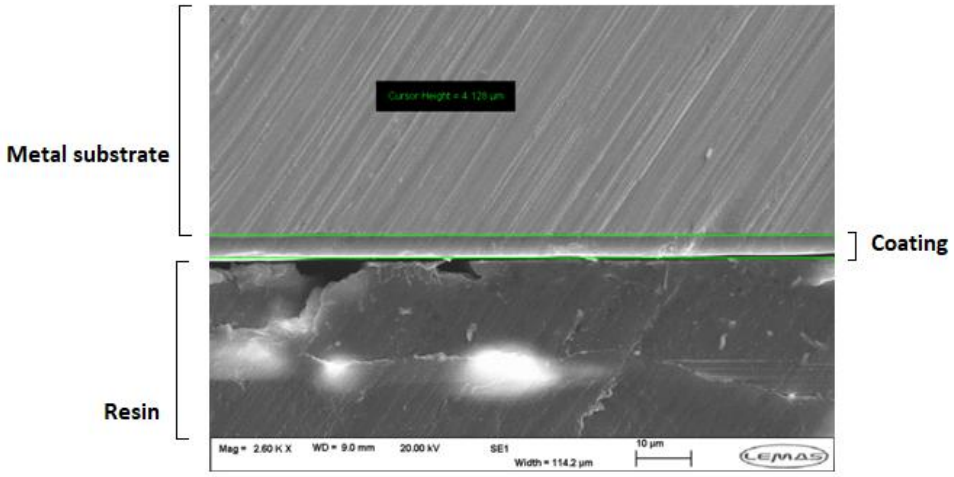

Figure 5.25 SEM image of the cross section of the doped sample with 11.3w/w% of titanium precursor, mixture as solvent and cured in N_2 ($I_{,B3,11.3\%,Mix,N2}$)

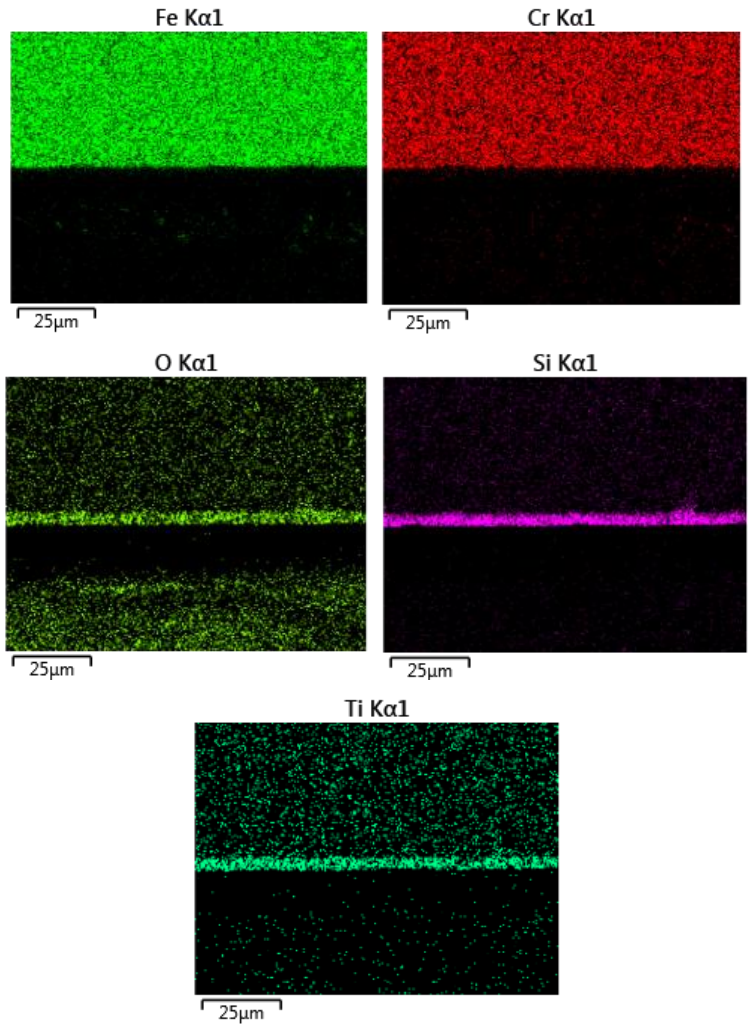

Figure 5.26 EDX mapping of the cross section of $I_{,B3,11.3\%,Mix,N2}$

These EDX results show that the titanium and silicon elements are homogeneously distributed throughout the whole coating, from the surface to the interface.

- Coating thickness

Focused Ion Beam (FIB) was used to study the surface morphology of samples doped with titanium in order to investigate the thickness of the coatings. The images were obtained with the SEM mode. The analyses were made on samples before any immersion or contact with an aggressive environment. FIB etching was used to allow cross-sectional images of the film to be taken.
Viewing the films in this manner enabled measurements of their thickness to be taken. The results of the samples analysed are presented in Figure 5.27.

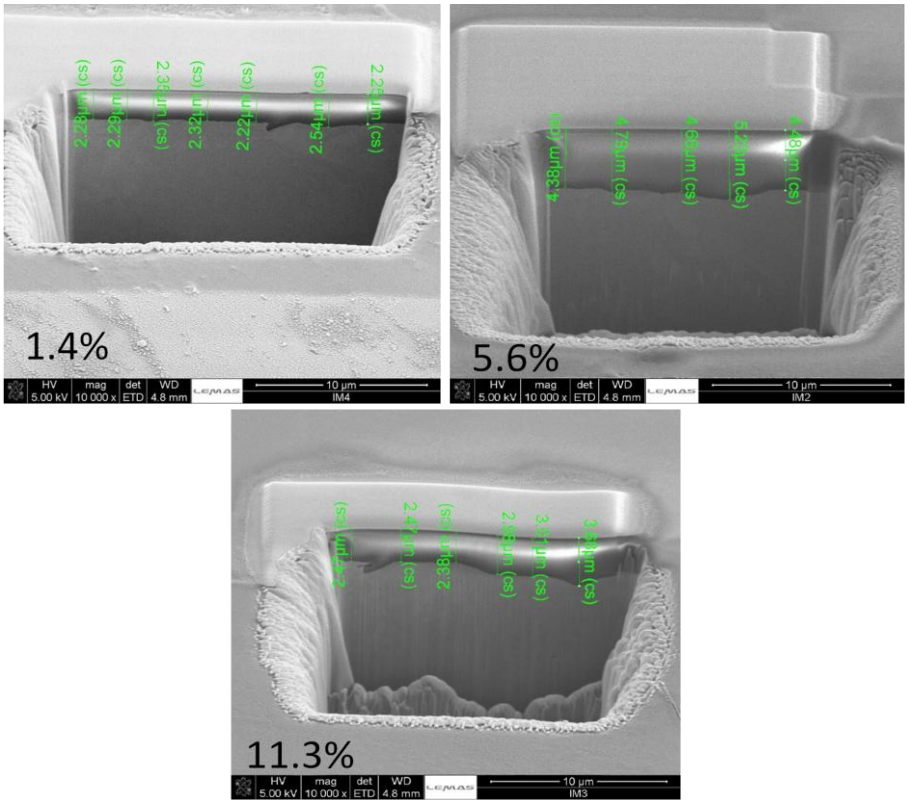

Figure 5.27 FIB images of samples $I_{,B3,1.4\%,Mix,N2}$ $I_{,B3,5.6\%,Mix,N2}$ $I_{,B3,11.3\%,Mix,N2}$ from Batch 3

Thicknesses displayed:
- 1.4%w/w: 2.28µm, 2.29µm, 2.35µm, 2.32µm, 2.22µm, 2.54µm, 2.26µm
- 5.6%w/w: 4.38µm, 4.79µm, 4.66µm, 5.23µm, 4.48µm
-11.3%w/w: 2.47µm, 2.47µm, 2.38µm, 2.98µm, 3.01µm, 3.68µm

These pictures show that the coatings containing 1.4%w/w and 5.6%w/w seem homogeneous but not very rough as the surface of the coatings appears really smooth. For the sample with 1.4%w/w precursor, the coating appears to measure between 2.22µm and 2.54µm. The sample with 5.6%w/w precursor has a coating measuring between 4.38µm and 5.23µm. The interface of the 11.3%w/w sample shows part of a really thin coating which could be a link to corrosion and it is not homogeneous compared to the other coatings. The thickness of this layer appeared to vary across the surface between 2.38µm and 3.68µm but one part on the right end seems to be barely coated and the thickness would be lower than 1µm.

5.4.4 Adhesion of Third Batch

The third batch consisted of inorganic/hybrid sol-gel coatings and inorganic/hybrid coatings with titanium precursor doping on stainless steel.

The scratch results of the samples with no doping are presented in Figure 5.28. Figure 5.31 presents the values of the critical loads for this batch. All values are low and between 1N and 6N. The values are similar than the results obtained for the first batch for similar thicknesses of coating.

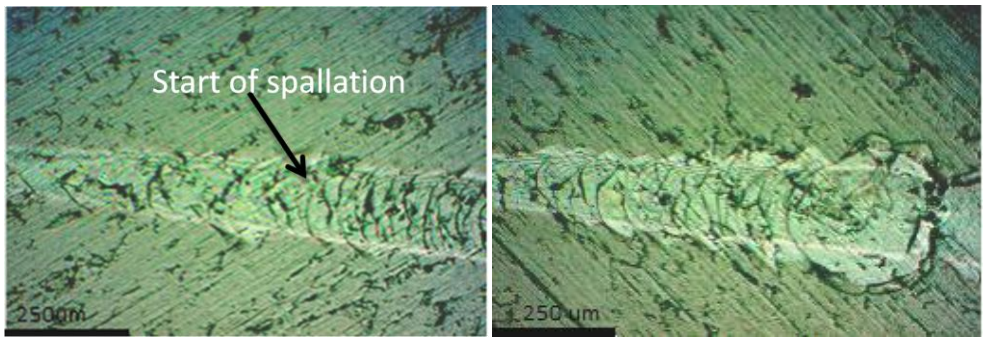

Figure 5.28 Scratch test result on a) sample cured in N_2 ($I_{,B3,0\%,Mix,N2}$) b) sample cured in air ($I_{,B3,0\%,Mix,Air}$) from Batch 3.

Both samples have an undoped inorganic/hybrid sol-gel coating. The difference between those two samples is the curing process: in N_2 for $I_{,B3,0\%,Mix,N2}$ and in air for $I_{,B3,0\%,Mix,Air}$. This does not seem to have an impact on the hardness of the coating as both critical load values are close to each other: about 2N and the failures look similar as well in the form of cracking. The critical load is determined with the beginning of the visible cracks.

Figure 5.29 presents the result for the sample doped with 2.8%w/w of titanium butoxide.

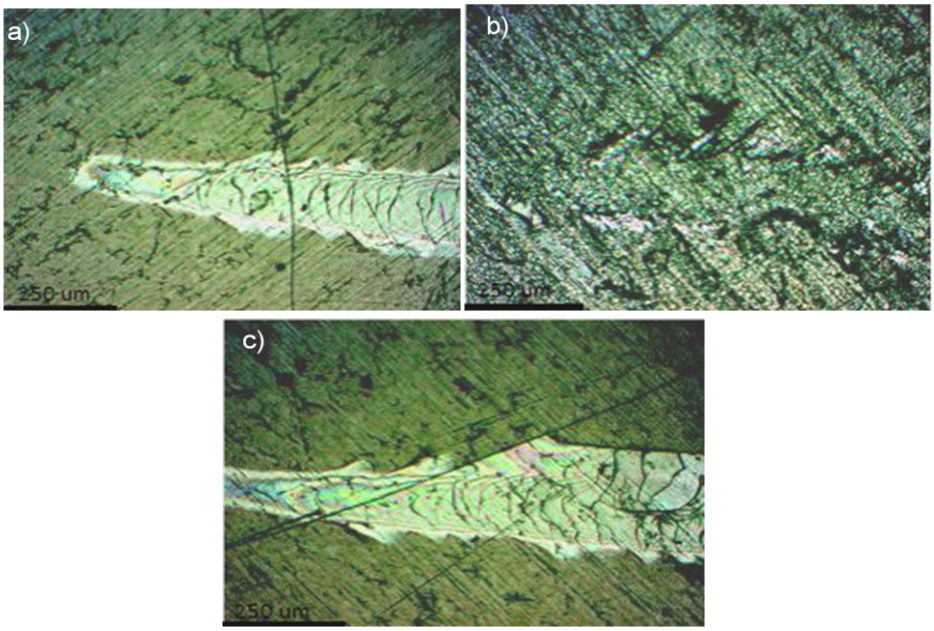

Figure 5.29 Scratch test result on a) sample with isopropanol as solvent, cured in air ($I_{,B3,2.8\%,Ip,Air}$) b) sample with mixture as solvent cured in N_2 ($I_{,B3,2.8\%,Mix,N2}$) c) sample with mixture as solvent cured in air ($I_{,B3,2.8\%,Mix,Air}$) from Batch 3.

The differences between those samples are the curing process for two of them: in N_2 for $I_{,B3,2.8\%,Mix,N2}$ and in air for $I_{,B3,2.8\%,Mix,Air}$, while $I_{,B3,2.8\%,Ip,Air}$ was cured in air but has isopropanol as a solvent and $I_{,B3,2.8\%,Mix,N2}$ and $I_{,B3,2.8\%,Mix,Air}$ have a mixture of ethanol, isopropanol and butanol as a solvent. All three of these samples have a titanium precursor concentration of 2.8%w/w.

Here the samples cured with air have a lower value of critical load, close to 2N while the sample cured in N_2 has a value of 5N. Visually, the scratch marks are different: the surface of $I_{,B3,2.8\%,Mix,N2}$ looks like a crack while the surfaces of $I_{,B3,2.8\%,Ip,Air}$ and $I_{,B3,2.8\%,Mix,Air}$ look more like delamination and crack at the same time. Except for $I_{,B3,2.8\%,Mix,N2}$, the values of critical load are lower than for the sample without any doping. The failure of the three samples seems to be craking.

The results for the samples doped with 5.6%w/w of titanium precursor can be seen in Figure 5.30.

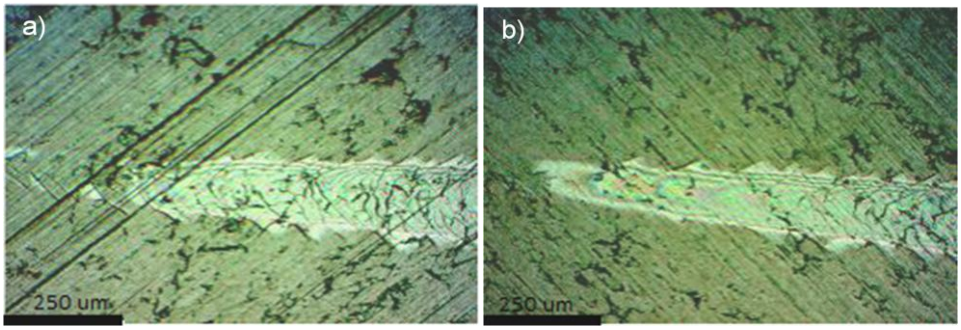

Figure 5.30 Scratch test result on a) sample with isopropanol as solvent ($I_{,B3,5.6\%,Ip,N2}$) b) sample with mixture as solvent ($I_{,B3,5.6\%,Mix,N2}$) from Batch 3.

The difference between those two samples is the composition of the solvent used: isopropanol for $I_{,B3,5.6\%,Ip,N2}$ and a mixture of ethanol, isopropanol and butanol for $I_{,B3,5.6\%,Mix,N2}$. Both samples have been doped with a titanium precursor and a concentration of 5.6%w/w. Here the samples have a similar scratch mark on the surface with a low critical load value: less than 2N for both samples which are lower values than for the samples without doping. As we can see from the pictures, all the samples (despite the reflectivity) are subjected to cracking failure and the critical load value is determined as the starting point of the visible cracks.

Table 5.4 Critical loads for Batch 3

Sample	Critical load (N)
$I_{,B3,0\%,Mix,N2}$	2.0 ± 0.5
$I_{,B3,0\%,Mix,Air}$	2.1 ± 0.5
$I_{,B3,2.8\%,Ip,Air}$	1.8 ± 0.5
$I_{,B3,2.8\%,Mix,N2}$	5.0 ± 0.5
$I_{,B3,2.8\%,Mix,Air}$	2.0 ± 0.5
$I_{,B3,5.6\%,Ip,N2}$	1.6 ± 0.5
$I_{,B3,5.6\%,Mix,N2}$	1.2 ± 0.5

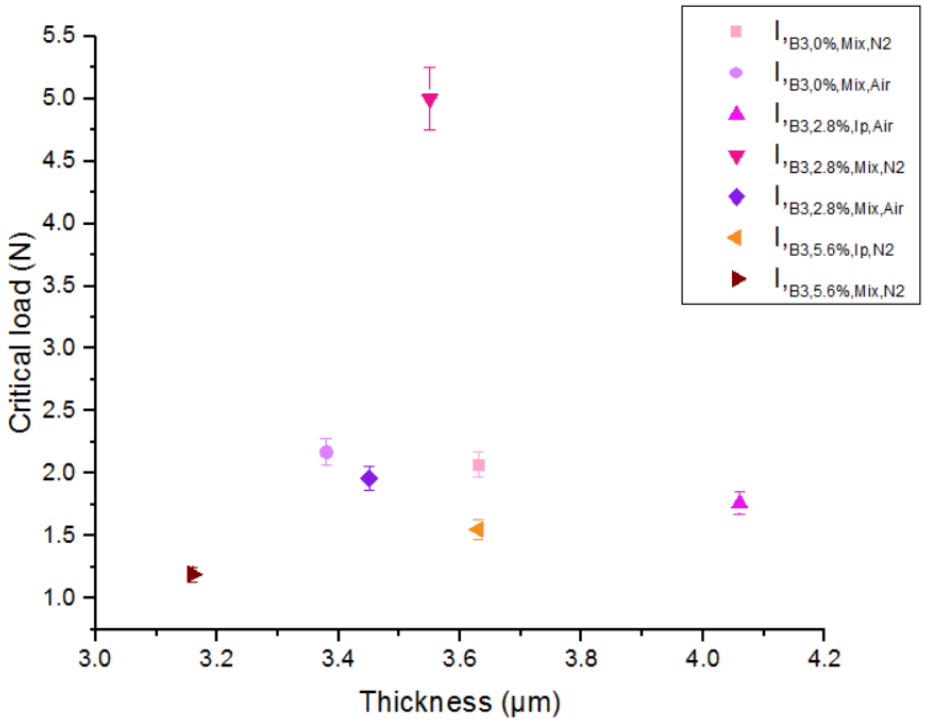

Figure 5.31 Critical loads as a function of the average thickness of samples from Batch 3

5.5 Hardness of Coatings from Batch 3 Containing Different Amounts of Titanium Precursor

The nano-indentation was used to assess the hardness of the coatings and the influence of the addition of titanium precursor on its value for the samples from Batch 3 with 0%w/w (undoped), 2.8%w/w, 5.6%w/w and 11.3%w/w..

The focus was put on the coatings doped with titanium butoxide and the undoped coating as they seem to have better properties and suggest being more appropriate for the optimization.

The indentation depth should be less than one tenth of the coating thickness in order to measure the properties of the coating without significant interference of the substrate [131]. Other effects that can influence the results are cracking and delamination of the coating, occurring in response to the indentation stress [131], [217]

The results for the samples are presented in Figure 5.32 .

The reduced elastic modulus (Young modulus) can be deduced from indentation experiments. It is a combination of the moduli of the coating and substrate, with the

substrate having an increasing influence for larger loads, since the elastically deformed volume underneath the indenter will then increasingly penetrate into the substrate [131]. As in the case of the modulus, the combined responses of the coating and the substrate are actually measured when determining the hardness of thin coatings using indentation. This is caused by the fact that plastically deformed volume under the indenter extends into the substrate when the load (and hence the displacement) reaches a certain level.

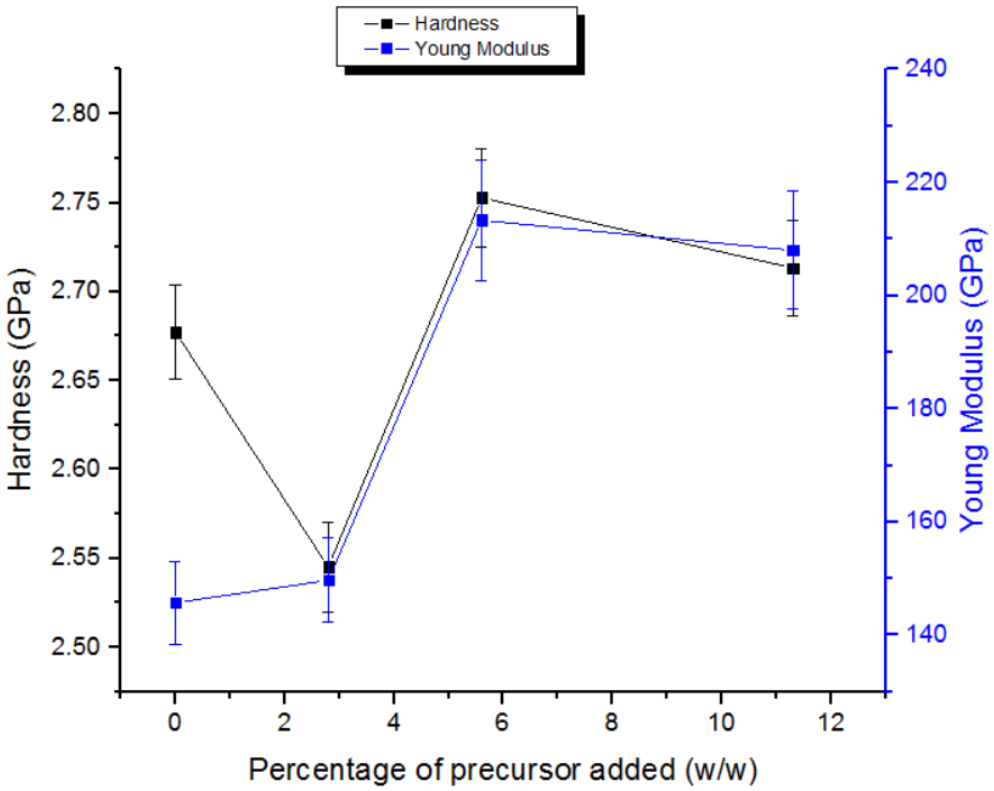

Figure 5.32 Young's modulus and hardness values for different percentages of added precursor of Batch 3: $I_{B3,0\%,Mix,N2,}$ $I_{B3,2.8\%,Mix,N2,}$ $I_{B3,5.6\%,Mix,N2}$ $I_{B3,11.3\%,Mix,N2}$

The values of the hardness seem to barely change with the percentage of precursor added, the values being between 2.50GPa and 2.75GPa. The values of the Young's modulus are increasing with the percentage of titanium butoxide added but there is a limit to this evolution as the values for both samples with less than 5%w/w are similar, as well as for both samples with more than 5%w/w have values close to each other. However the gap between the samples with less than 5%w/w and the samples with more than 5%w/w is important. The values of the Young's modulus obtained are comparable to the value for silicon which are 130-185GPa [218-220]. The trend for the samples with presence of precursor is similar for both properties

where the addition of titanium butoxide leads to an increase in the value of the modulus.

The ratio of hardness to Young's modulus, H/E, also termed brittleness index is presented in Figure 5.33 . A material with a low brittleness is more inclined to deform than fracture.

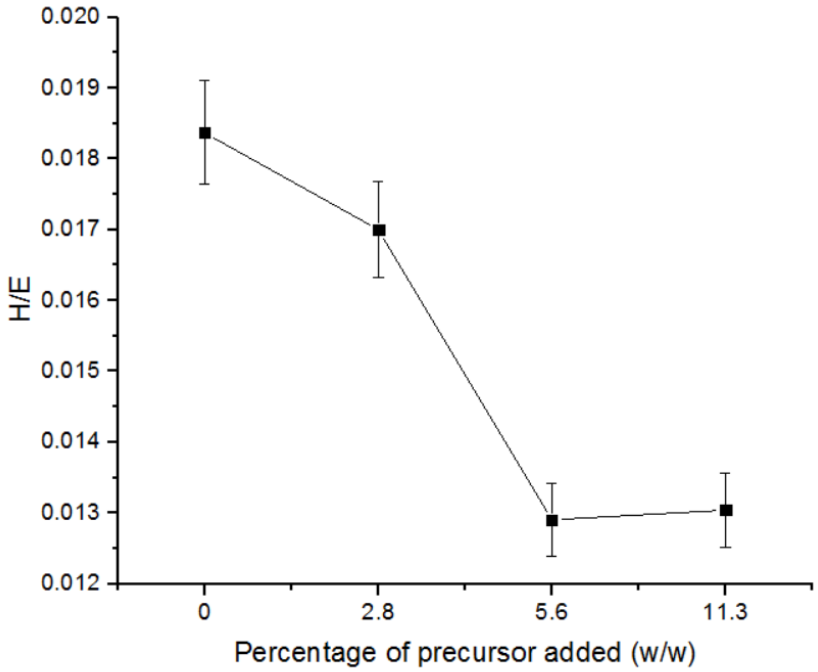

Figure 5.33 Brittleness index H/E for samples of Batch 3 ($I_{,B3,0\%,Mix,N2,}$ $I_{,B3,2.8\%,Mix,N2,}$ $I_{,B3,5.6\%,Mix,N2}$ $I_{,B3,11.3\%,Mix,N2)}$

The addition of precursor seems to contribute to decreasing values of brittleness index, with the sample with no precursor added (0%) having the highest value.

The addition of titanium butoxide as precursor leads to coatings which are less brittle until a threshold is reached when the percentage is more than 5%w/w but there does not seem to be an influence on the hardness.

The addition of titanium precursor makes the coating stiffer while having little or no influence on the hardness.

5.7 Summary of Chapter V

In this chapter, the coatings are characterised through different methods and mechanical properties are studied.

The FTIR spectra show that the nature of the coating (inorganic/hybrid, hybrid/composites or organic) change the spectra obtained, the hybrid/composites samples presenting a relation between the two spectra of organic and inorganic/hybrid as it is composed of those two coatings. The inorganic/hybrid systems 2 to 5 contain very little silanols, which would mean that they are either highly condensed or incompletely reacted.

However the addition of doping element and/or change in solvent or curing process barely affects the structure of the functional groups detected on the surface of the samples.

The scratch test results showed that depending on the substrate, the presence of pre-treatment in some cases and the nature of the coating, the value of critical load could be influenced. The types of failure observed in the test depend critically on the properties of both the substrate and coatings. If the coating is softer than the substrate, considerable plastic deformation occurs within it and the scratch test critical load may be defined as the load at which the coating is scraped off exposing the substrate [211]. However it was not easy to determine when this occurs and quantification of the failure mode is difficult [199]. For a hard coating on a softer substrate, spallation and buckling failure modes result from interfacial detachment but a range of other cracks and deformed regions can be observed [198]. Depending on the nature of the coating, pre-treatment may have an influence. Systems on 316L stainless steel generally perform better than the same systems deposited on X65 carbon steel.

The addition of doping precursor also has an influence on the adhesion of the coating. For a same coating, different types of failures could be obtained as well as depending on the curing process. For Batch 1 the critical load of hybrid/composites samples was higher than for inorganic/hybrid and organic coatings which is in agreement with their properties but that was not the case for the hybrid/composites sample of Batch 2 which had a really low value of critical load (the hybrid/composites coatings as stated in Chapter IV, are different).

Through the SEM and EDX fluctuations on the surface of samples could be seen, as one hybrid/composites sample from Batch 1 presented a high percentage of iron before any experiment and the SEM showed that its surface was very variable. This is correlated to the results with the FIB-SEM presenting an inconstancy in the coating's thickness deposited on a metal substrate. SEM results also showed that the addition of precursor doped with Titanium butoxide has an effect such as a high quantity creates cracks in the coating, rendering it not suitable for industrial application. The solvent or the curing process used has an influence on the percentage of titanium or silicon actually present in the coating, making its value decreasing depending on these conditions.

The nanoindentation tests of the coatings showed that the hardness of the coating is barely influenced by the concentration of the doping precursor but that it is a parameter to be considered regarding the Young's modulus and the stiffness of the sample.

Chapter VI. Resistance to Corrosion and Erosion-Corrosion

6.1 Introduction and Chapter Overview

This chapter presents corrosion results from experiments to assess the behaviour and corrosion resistance of the samples from Batch 1, 2 and 3.

For the first batch several parameters are highlighted: effect of the nature of the coating (inorganic/hybrid, organic or hybrid/composites), effect of the substrate (carbon steel X65 or 316L stainless steel) and the effect of time while comparing the visual and Open Circuit Potential (OCP) results obtained throughout the experiment. Electrochemical Impedance Spectroscopy (EIS) results for one sample of each type from this batch are presented. The main aim was to understand, in broad terms, the nature of the coatings, to assess what techniques are best to understand their characteristics (mechanical and chemical) and the links between these and the corrosion behaviour.

The results of the second batch present the effect of the substrate (stainless steel 304 or A1008Qpanel), the effect of percentage of precursor added and the effect of time. EIS data for all coatings from Day 0 to Day 30 of experiment are presented then comparison is made between the samples with the help of the corrosion resistance R_{ct} and the capacitance phase element from the coating CPE_c which is linked to the water uptake.

For the third batch, EIS results of samples deposited on 304 stainless steel from Day 0 to Day 30 for the effect of percentage of precursor added (0%w/w, 2.8%w/w and 5.6%w/w), solvent, curing process are presented with comparison of R_{ct} and CPE_c. Then are presented surface morphologies of samples from this batch tested through salt spray.

The last part of this chapter presents erosion results and total weight loss for bare stainless steel and samples from Batch 3 with 0%w/w, 1.4%w/w, 5.6%w/w and 11.3%w/w of titanium precursor: $I_{,B3,0\%,Mix,N2}$ $I_{,B3,1.4\%,Mix,N2}$ $I_{,B3,5.6\%,Mix,N2}$ and $I_{,B3,11.3\%,Mix,N2}$.

For the first batch, relatively aggressive environmental conditions were applied in order to do a screening of the performance in arduous environments. The objective

was to assess the penetration of liquid through the coating and to focus on the samples which would present the least damage:

- aqueous, air exposed solution
- sodium chloride (3.5% NaCl) solution
- 60°C
- time of immersion of 30 days

For the second and third batches:

- CO_2 saturated environment
- sodium chloride (3.5% NaCl) solution
- 25°C
- time of immersion of 30 days

The focus of this chapter is about understanding the extent of corrosion, the time for water to penetrate through the coatings and the changes that can be observed during 30 days of immersion for the different types of samples. The EIS measurements help to provide an insight into the corrosion mechanism occurring at the interface of the sample. An equivalent circuit can be developed with these results, representing the coating through different elements. The last part presents the results of erosion test on the coatings doped with titanium precursor to evaluate the influence of its percentage.

6.2 EIS Results of the First Batch: Inorganic/Hybrid, Organic and Hybrid/Composites Coatings

6.2.1 Surface Morphology of the Samples After Immersion

Several samples coated with different systems were studied: inorganic/hybrid, organic and hybrid/composites.

Figure 6.1 to Figure 6.3 present the appearances of the inorganic/hybrid, organic and hybrid/composites samples of the first batch after 30 days of immersion in 3.5%w/w NaCl brine. Next to the name is also written the day of failure, stated as the measured impedance being lower than the impedance of the substrate or could not be measured at all, of the samples studied. Some samples display evident signs of a damaged coating or a corroded substrate.

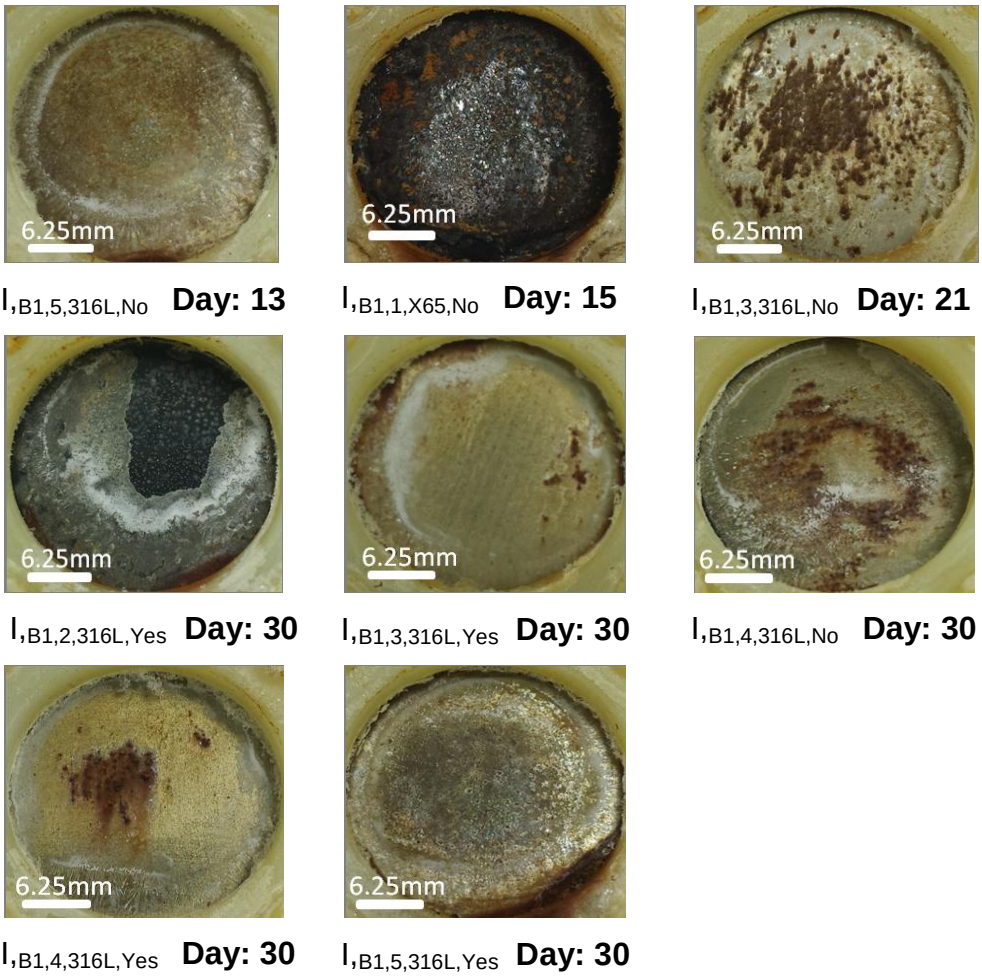

Figure 6.1 Appearance of the inorganic/hybrid samples from Batch1 after 30 days of immersion. The Day indicates the day of failure for each sample.

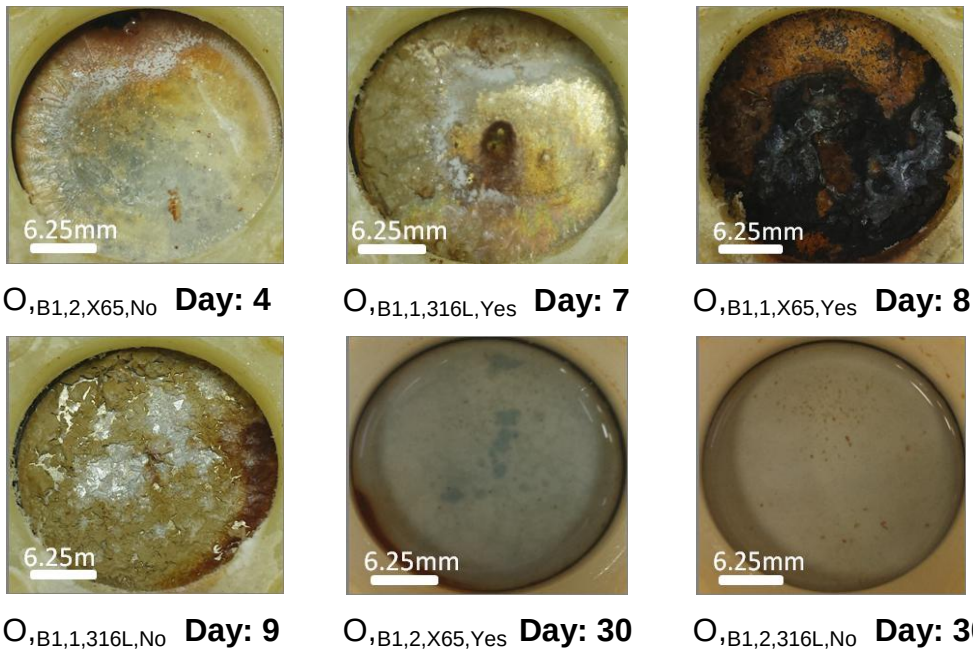

Figure 6.2 Appearance of the organic samples from Batch 1 after 30 days of immersion. The Day indicates the day of failure for each sample.

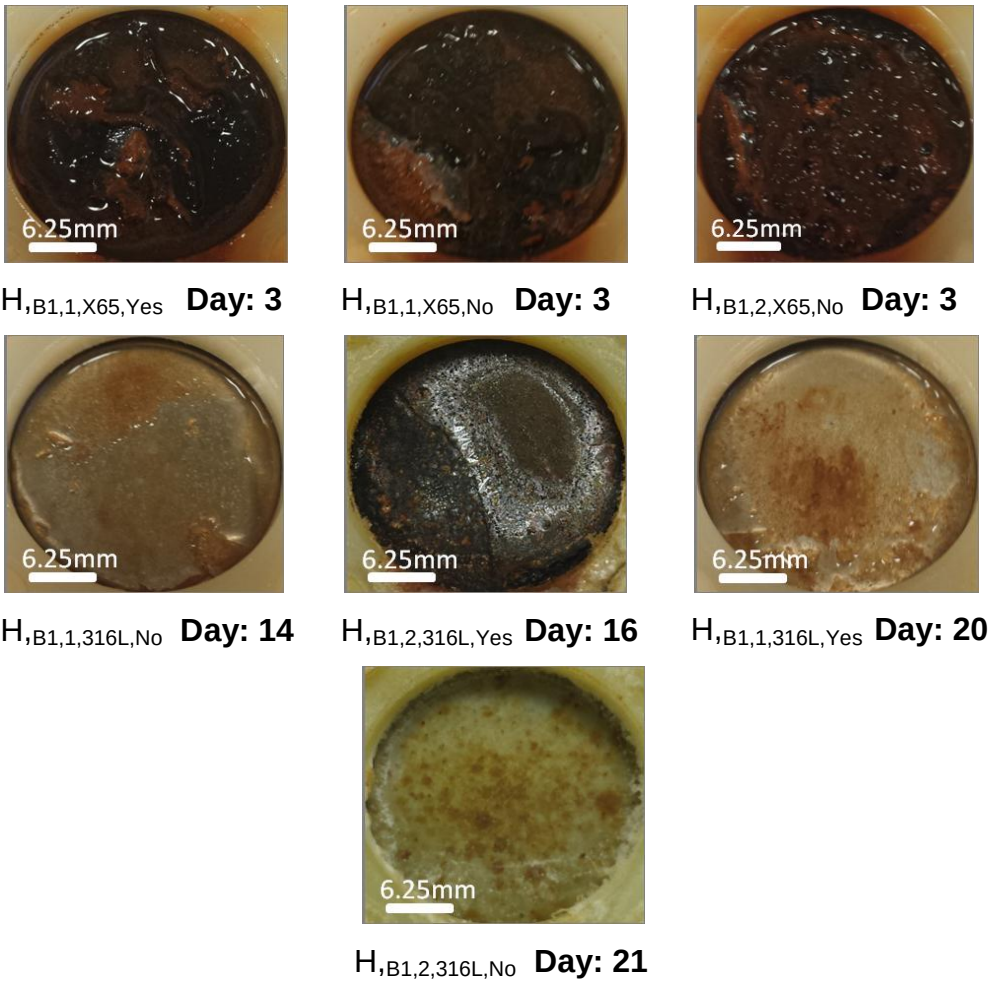

Figure 6.3 Appearance of the hybrid/composites samples from Batch 1 after 30 days of immersion. The Day indicates the day of failure for each sample.

6.2.2 Impedance Results for the First Batch

The Open Circuit Potential (OCP) values measured are shown as a function of time in Figure 6.4 which presents the evolution for each type of coating system.

The values of OCP measured for the bare substrate in the conditions of this experiment are: -0.204V ± 0.050 for 316L stainless steel and -0.500V ± 0.050 for X65 carbon steel.

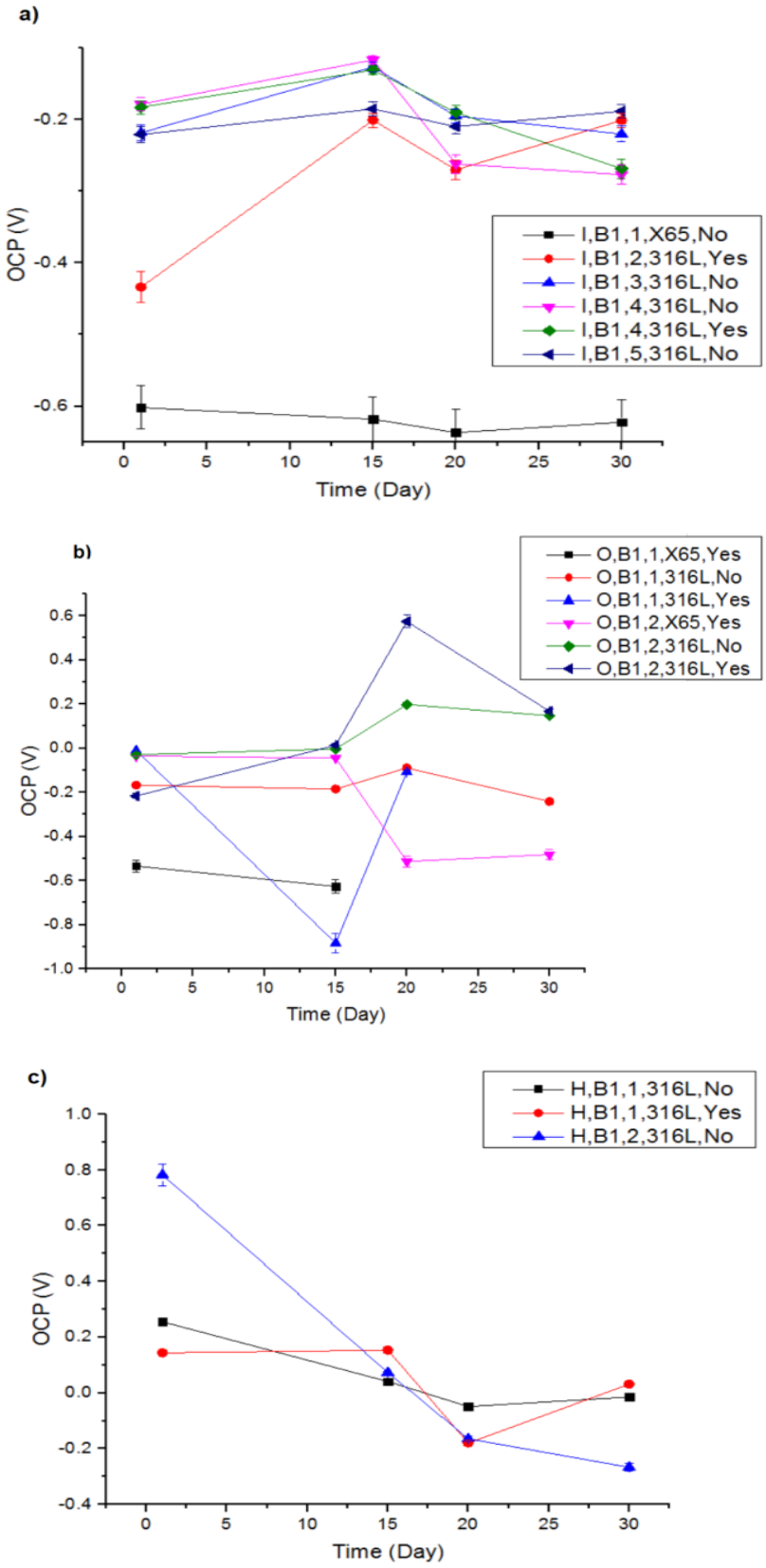

Figure 6.4 OCP as a function of time for the samples of the first batch a) inorganic/hybrid systems b) organic c) hybrid/composites

Except for $I_{,B1,1,X65,No}$, the other samples from the inorganic/hybrid systems have an evolution of OCP leading to the value of the OCP of their bare substrates. For the organic systems, except for the samples $O_{,B1,1,316L,Yes}$ and $O_{,B1,2,316L,Yes}$ the organic coated samples have their OCP values tending to the values of the bare substrates as well. Regarding the hybrid/composites systems, $H_{,B1,1,316L,No}$ and $H_{,B1,2,316L,No}$ have this evolution but that is not the case for $H_{,B1,1,316L,Yes}$ whose value is closer to 0V. When comparing the detected day of failure, the samples with Day 30 (last day of experiment) are among the samples with the OCP value being close to their substrate's value, except for $O_{,B1,2,316L}$.

The inorganic/hybrid systems change slightly with time while for the hybrid/composites systems the decrease is important.

The EIS results for one sample, $O_{,B1,2,316L,No}$ are presented in the following part. The sample barely showed signs of corrosion after the immersion. Figure 6.5 presents the surface topography of the sample after immersion. Figure 6.6 present the Nyquist plot, Figure 6.7 shows an enlargement of the plots to see the performance of the coating after the first day (from Day 5 to Day 30) then Figure 6.8 presents the Bode plots.

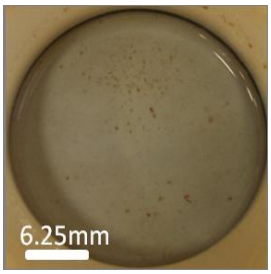

Figure 6.5 Appearance of sample $O_{,B1,2,316L,No}$ after the immersion test.

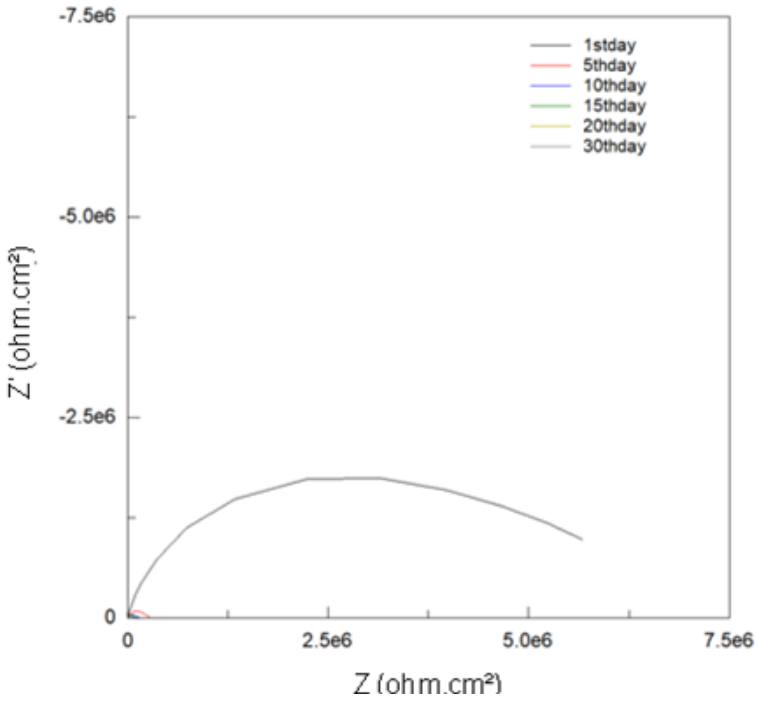

Figure 6.6 Nyquist plot for the sample $O_{,B1,2,316L,No}$ over the 30 days of immersion

This sample visually showed little corrosion after the experiment and managed to maintain a high value of impedance throughout the duration of the experiment as well as defined semi-circle shaped curves.

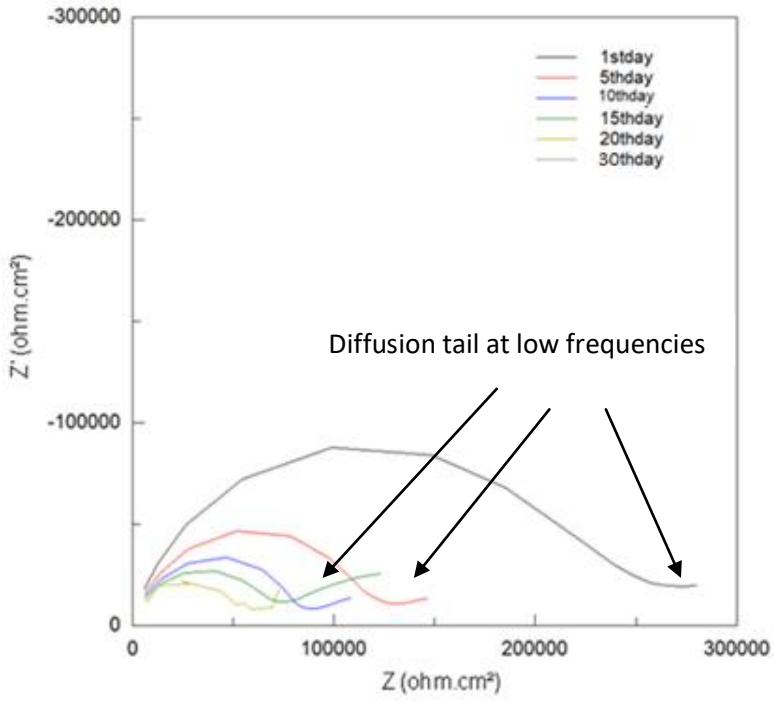

Figure 6.7 Nyquist plot of sample $O_{,B1,2,316L,No}$ from Day 5 to Day 30 of immersion

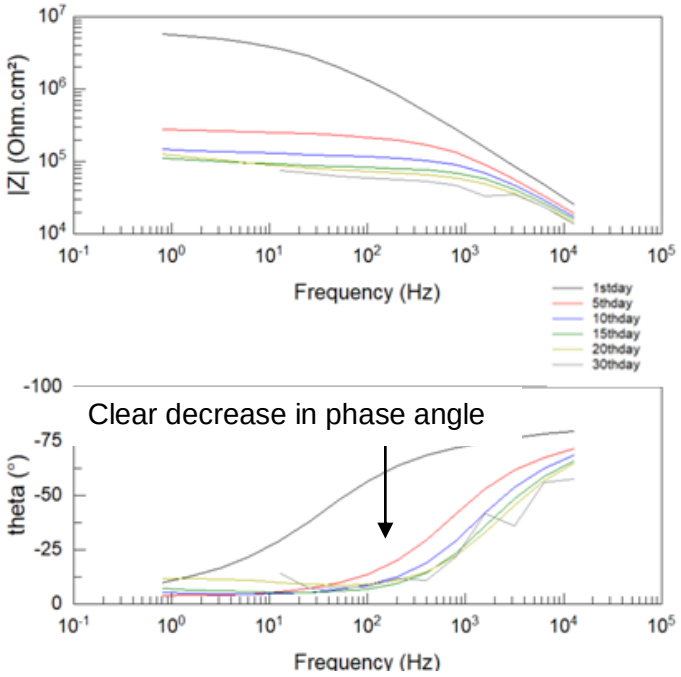

Figure 6.8 Bode plots a) impedance b) phase shift for the sample $O_{,B1,2,316L,No}$ over 30 days of immersion

The values are decreasing with time but the appearance of the curves is still the same with the shape of semi-circles. A capacitive behaviour is present on all Nyquist plots from the start up to the end of immersion. This can be defined from the shape of semicircle displayed in all impedance spectra. However the Bode phase shift plot presents a clear decrease in its phase angle. The values seem to decrease with time. The overall appearance of the curves has not changed much. Depressed semi-circles are obtained which indicate only one time constant occurring in the system. The bigger the diameter of the circle, the bigger the coating resistance. The capacitive behaviour possibly relates to a high corrosion-resistant film formed on the surface of the uncoated stainless steel [169]. The capacitive response of the film tends to decrease at longer immersion time (> Day 5), suggesting a passive film dissolution, as seen from a declining slope of the response after Day 5 in the Nyquist diagram. However, the response seems to reach a stable condition after Day 10, indicated by an unchanged behaviour from Day 10 to 30.

The diffusion tail at low frequencies represents the diffusion controlled corrosion process taking place at the substrate. Compared to the curve of the first day, the following ones tend to rise slightly at the end of the measurement.

Generally, coatings with resistance over $10^8 \Omega.cm^2$ are considered as providing good corrosion protection, while those with resistance under $10^6 \Omega.cm^2$ provide poor corrosion protection [221].

6.2.3 Summary of the First Batch

After the immersion some samples showed little corrosion (Figure 6.1) such as the sample $O_{,B1,2,316L,No}$ and $O_{,B1,2,X65,Yes}$ while the other samples presented different degrees of damage: slight corrosion on $I_{,B1,5,316L,Yes}$, $I_{,B1,2,316L,Yes}$, $I_{,B1,4,316L,Yes}$, $I_{,B1,4,316L,No}$, $I_{,B1,3,316L,Yes}$, more corrosion on $I_{,B1,5,316L,No}$ or appearing as pitting corrosion on $I_{,B1,3,316L,No}$ and $H_{,B1,2,316L,No}$. Some samples appear to have no coating left on their surface and a deeply corroded substrate such as $H_{,B1,2,316L,Yes}$, $I_{,B1,1,X65,No}$, $O_{,B1,1,X65,Yes}$, $H_{,B1,1,X65,No}$, $H_{,B1,1,X65,Yes}$ and $H_{,B1,2,X65L,No}$. $H_{,B1,1,316L,Yes}$, $H_{,B1,1,316L,No}$, $O_{,B1,1,316L,No}$ appear to have their coating delaminated while $O_{,B1,1,316L,Yes}$ and $O_{,B1,1,X65,No}$ both have a delaminated coating and a corroded substrate.

During this experiment some samples start early to present signs of corrosion after a few days. All the hybrid/composites sol-gel coatings belong to the category of damaged samples. They present poor results both visually and electrochemically. The coating is damaged before the end of the immersion (Day 3 for $H_{,B1,1,X65,Yes}$, $H_{,B1,1,X65L,No}$ and $H_{,B1,2,X65,No}$, Day 14 for $H_{,B1,1,316L,No}$, Day 16 for $H_{,B1,2,316L,Yes}$, Day 20 for $H_{,B1,2,316L,Yes}$ and Day 21 for $H_{,B1,2,316L,No}$.

Overall, the samples which are the most corroded and damaged are the ones with a carbon steel X65 substrate which has significantly less resistance to corrosion than stainless steel. For the same coating, the X65 sample is more damaged than the 316L sample: as an example shown in Figure 6.1, the sample $O_{,B1,1,316L,No}$ is shown with a totally delaminated coating but the sample $O_{,B1,1,X65,Yes}$ has no coating at all and the metal is deeply corroded. This experiment is needed to compare the diverse levels of corrosion on the different samples coated with systems of coatings. The coatings, apart from $I_{,B1,1,X65,No}$, $O_{,B1,1,316L,Yes}$, $O_{,B1,2,316L,Yes}$ and $H_{,B1,1,316L,Yes}$ see their OCP value tending to the one of their substrate throughout the experiment. This is also the case for samples with a high day of failure which means that the OCP measured is closer to the value of the substrate than the coating's.

It is thus sensible to use EIS to understand the evolution of corrosion.

6.3 EIS Results of the Second Batch: Inorganic/Hybrid Sol-Gel Coatings, Undoped or Doped With Titanium Precursor

This batch contained samples on metal sheets (100mm x 100mm x 1mm) as opposed to the coupons received for Batch 1. The samples here have all been through the same pre-treatment process.

6.3.1 EIS on Uncoated Stainless Steel

Figure 6.9 to Figure 6.11 present the Nyquist and Bode plots for 304 stainless steel (uncoated sample):

These results will be used as a reference for coated samples in the discussion part in order to assess the ability of the coating to prevent the penetration of corrosive species.

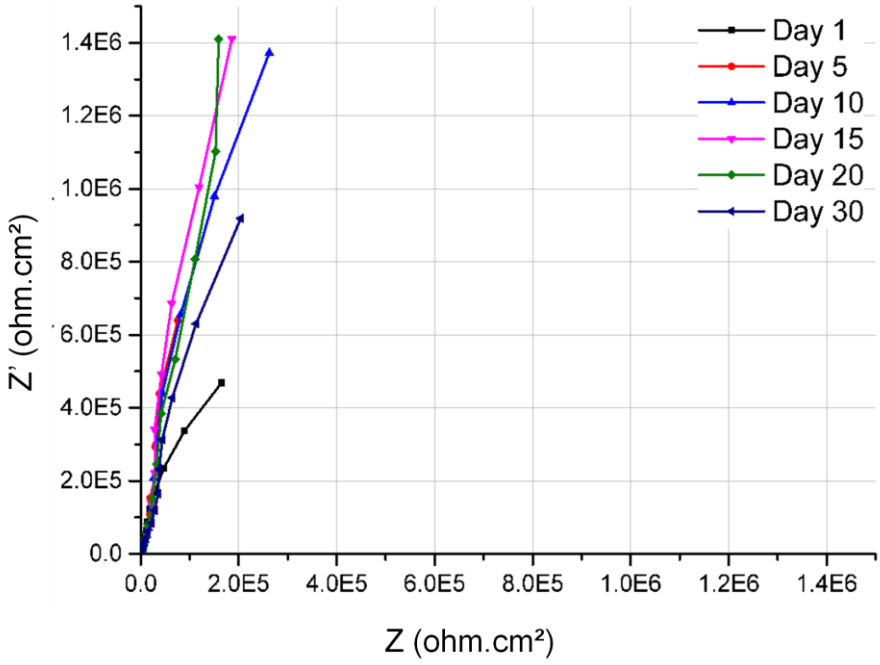

Figure 6.9 Nyquist plot for bare 304 stainless steel over 30 days of immersion

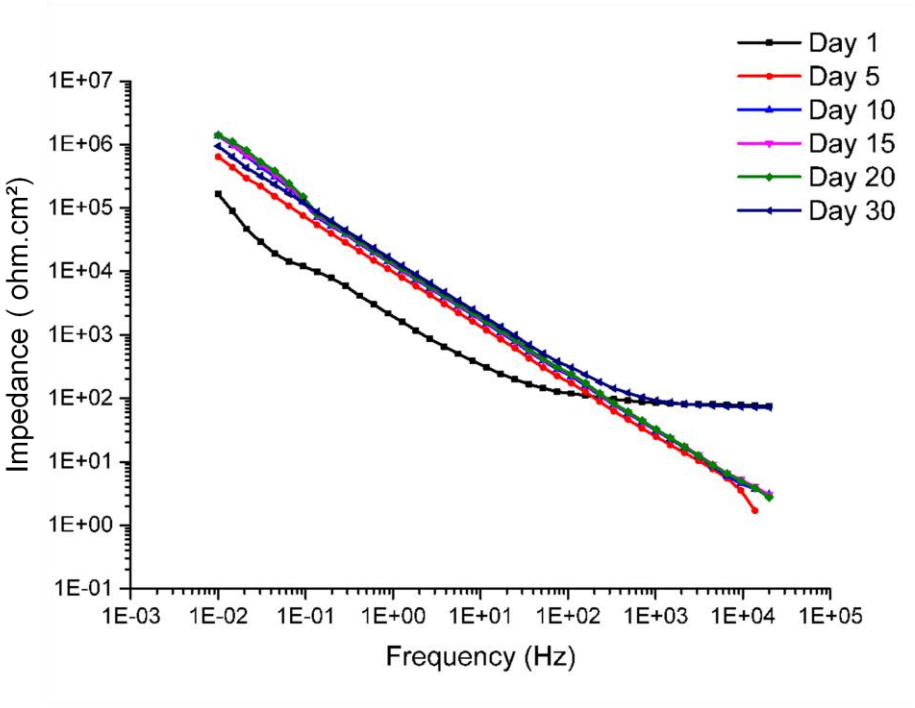

Figure 6.10 Bode impedance plot for bare 304 stainless steel over 30 days of immersion

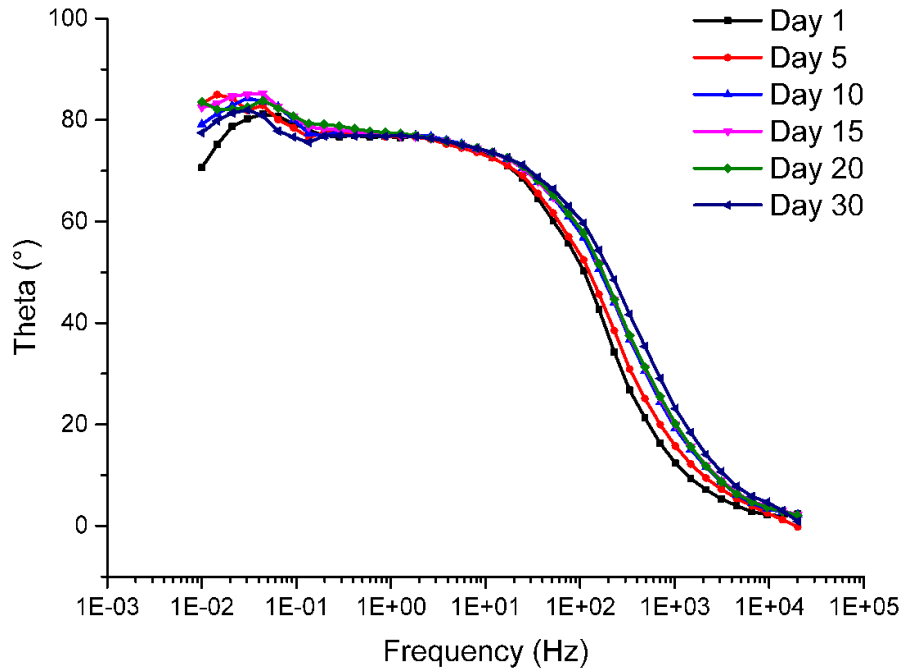

Figure 6.11 Bode phase shift plot for bare 304 stainless steel over 30 days of immersion

The Nyquist plot presents the spectra from Day 1 to Day 30 (end of immersion) of the bare substrate. The Bode plots show that even during the immersion period, the shape of the impedance response remains almost the same with time, which

suggests a stable structure of the passive film [169]. In the Bode phase shift plot it can be seen that the plots reach a value close to 80-85°, which means a capacitive response of the passive film from the substrate. The fact that it is not exactly equal to 90° implies that this film does not behave like an ideal capacitor and thus its value changing during the experiment means that the coating is affected by the environment.

Figure 6.12 shows the equivalent circuit used to model and to fit the bare substrate and its data. This equivalent circuit has been used in several research works to model the behaviour of stainless steel in various conditions of the corrosive electrolyte [167-169].

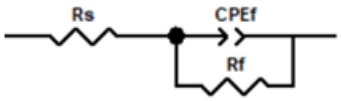

Figure 6.12 Equivalent circuit corresponding to the EIS spectra of uncoated stainless steel after exposure to 3.5%NaCl

Evolution of R_f and CPE_f as a function of time is presented in Figure 6.13 and Figure 6.14.

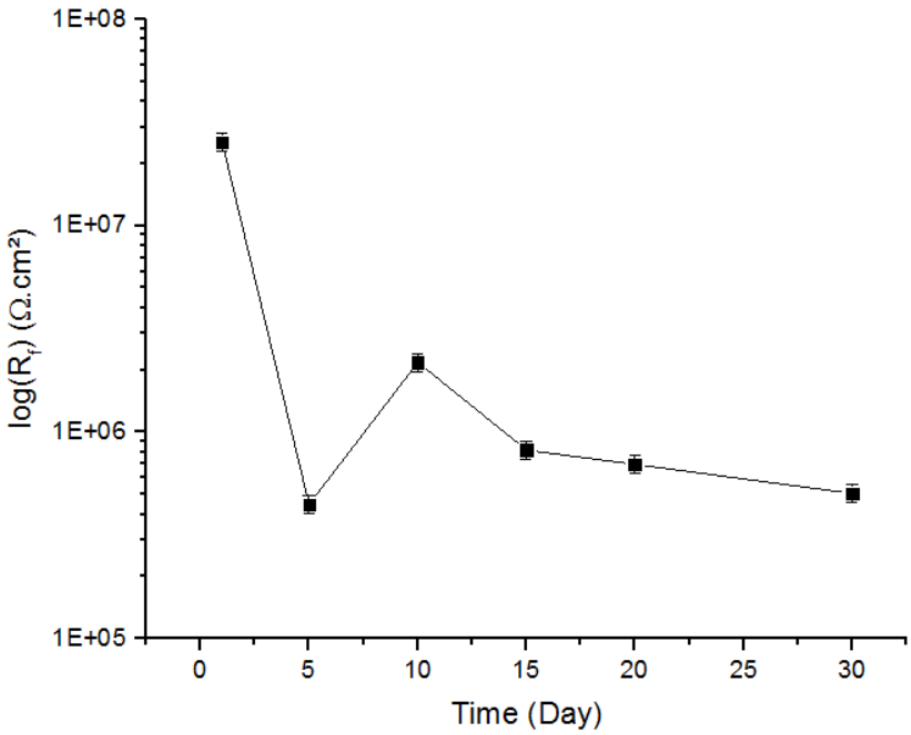

Figure 6.13 R_f as a function of time during the experiment for bare 304 stainless steel over 30 days of immersion

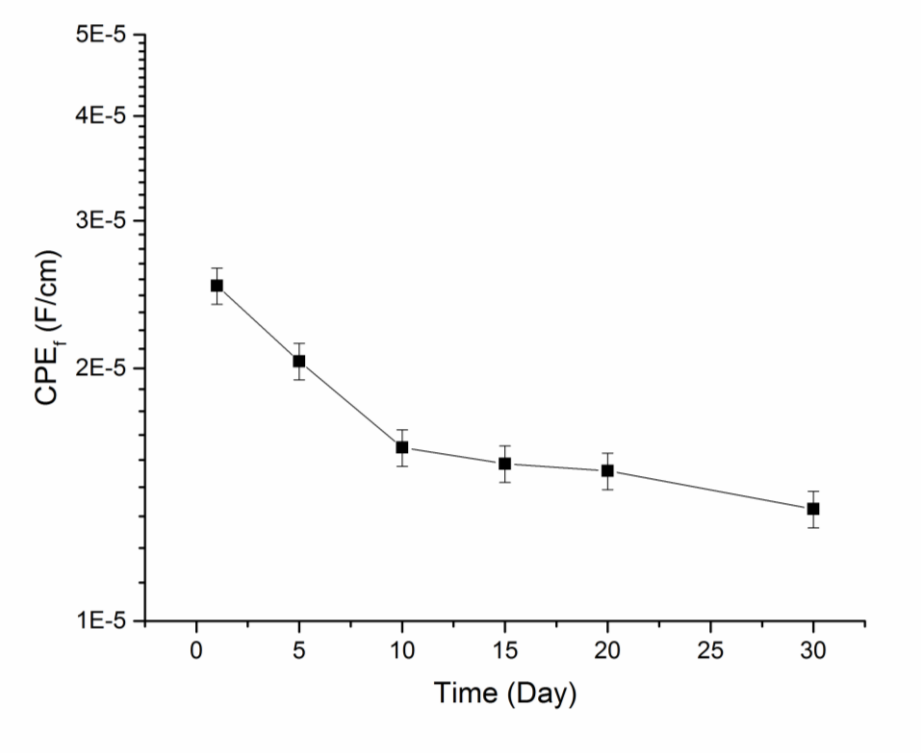

Figure 6.14 CPE_f as a function of time during the experiment for bare 304 stainless steel over 30 days of immersion

As it can be seen in Figure 6.13 and Figure 6.14, R_f decreases with time while CPE_f also decreases with time but slightly and could be considered as constant as its values stay between 1.10^{-5}F/cm and 3.10^{-5}F/cm throughout the immersion. A decrease in resistance implies the presence of damage with time on the surface of the sample.

6.3.2 EIS on Silica Inorganic/Hybrid Sol-Gel Coated Samples

For the second batch the same silica inorganic/hybrid sol-gel coating was deposited on two different substrates: A1008 steel Qpanel and 304 stainless steel. Figure 6.15 to Figure 6.17 present the Nyquist and Bode plots for a sample coated with an undoped inorganic/hybrid sol-gel coating on A1008Qpanel substrate. Their values are being compared in Figure 6.23 and Figure 6.24.

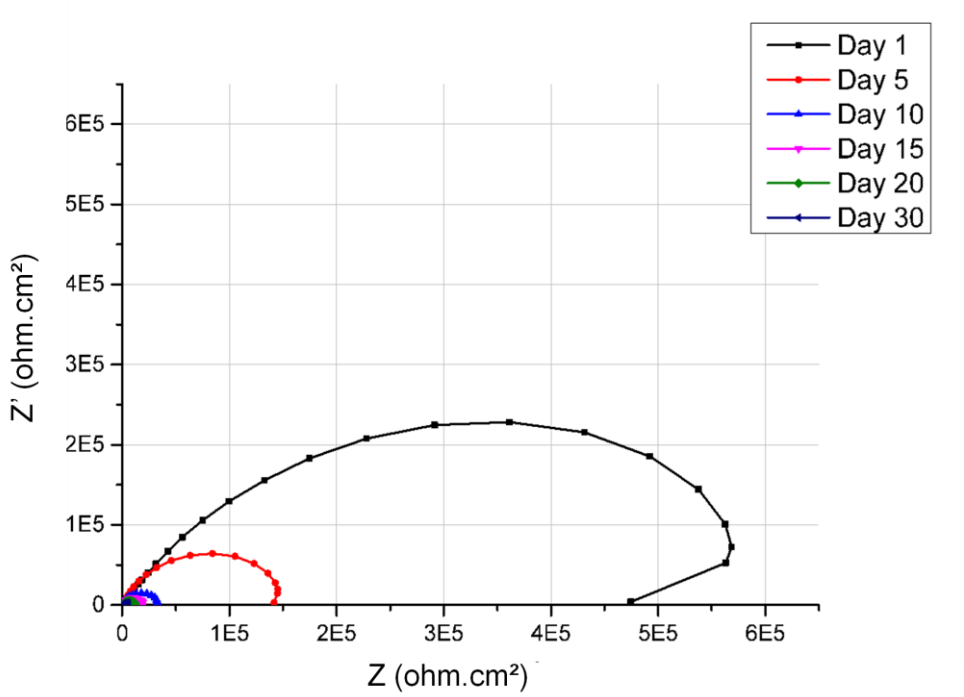

Figure 6.15 Nyquist plot of inorganic/hybrid sol-gel coating on A1008Qpanel over 30 days of immersion ($I_{,B2,0\%,A1008Qp}$)

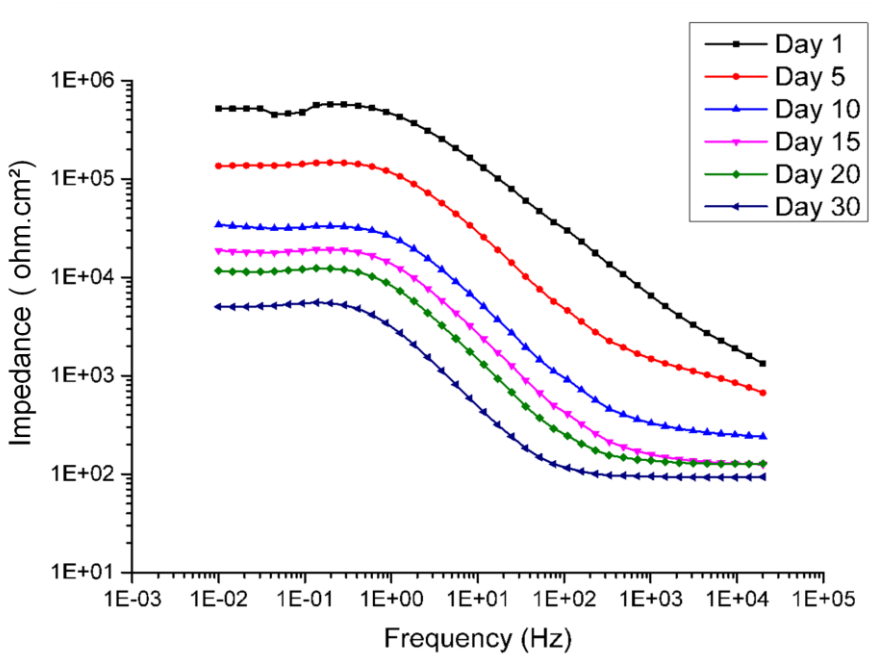

Figure 6.16 Bode impedance plot of inorganic/hybrid sol-gel coating on A1008Qpanel over 30 days of immersion ($I_{,B2,0\%,A1008Qp}$)

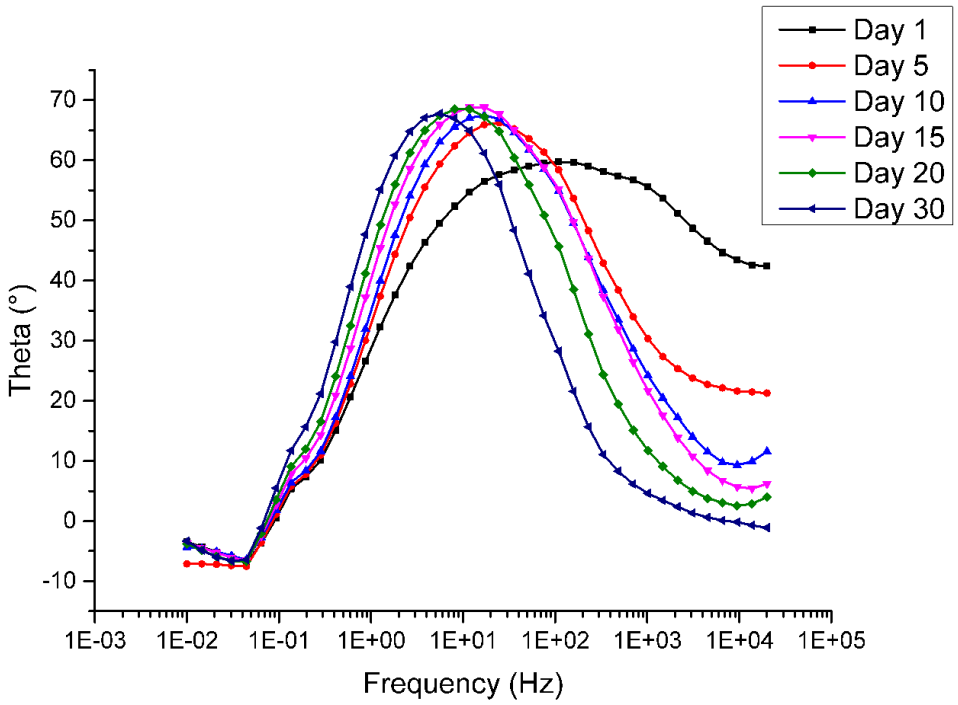

Figure 6.17 Bode phase shift plot of inorganic/hybrid sol-gel coating on A1008Qpanel over 30 days of immersion ($I_{,B2,0\%,A1008Qp}$)

An important decrease of the impedance response in the Bode impedance plot for the whole frequency range can be witnessed for the curve of Day 1. This can be due to a fast diffusion or penetration of electrolytes in the coating. This is also supported with the Nyquist plots, showing a dropping in the values after the first day. The response from the Bode phase diagram in Figure 6.17 shows a decrease of peak height as increasing exposure, indicating an increase of corrosion rate of the metal (or metal dissolution) as a function of immersion time. Moreover, a shift of the peak toward higher frequency (about 15 Hz) is also detected from Day 5 to 10, suggesting a more dominant effect of the corrosion products formation on the carbon steel surface [169]. The effect of corrosion products formation is less pronounced at prolonged immersion as it can be seen that the peak of the response at Day 15 and 20 moves back towards the same frequency region as Day 1 (~1 Hz) as shown in Figure 6.17. The phase angle drastically decreased from -60° at the initial exposure to 20° within the first days of immersion and remained in the same region during the rest of the experiment. This can be due to the loss in dielectric properties of the coating as water and electrochemically active species diffuse through the coating.

Figure 6.18 to Figure 6.20 present the Nyquist and Bode plots for a sample coated with an undoped inorganic/hybrid sol-gel coating on 304 stainless steel substrate.

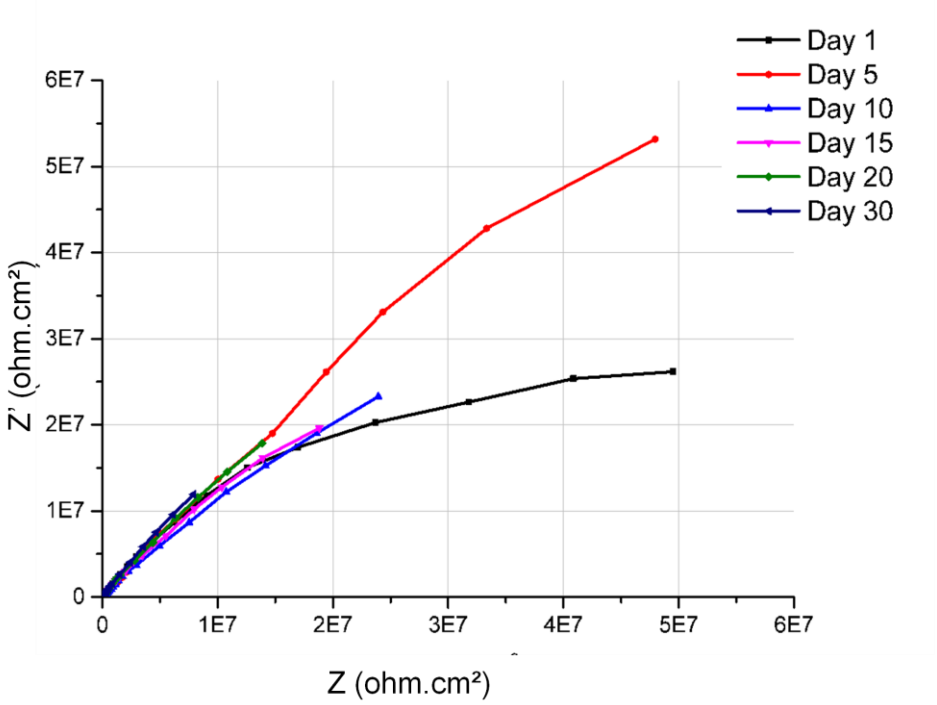

Figure 6.18 Nyquist plot of inorganic/hybrid sol-gel coating on 304 stainless steel over 30 days of immersion ($I_{,B2,0\%,304}$)

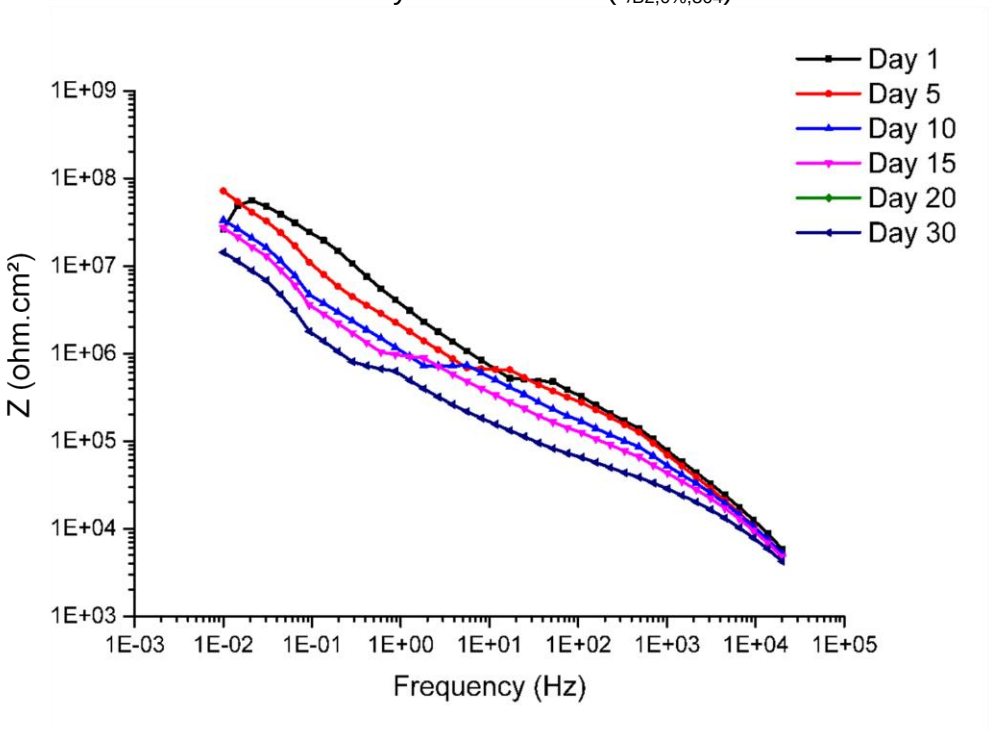

Figure 6.19 Bode impedance plot of inorganic/hybrid sol-gel coating on 304 stainless steel over 30 days of immersion ($I_{,B2,0\%,304}$)

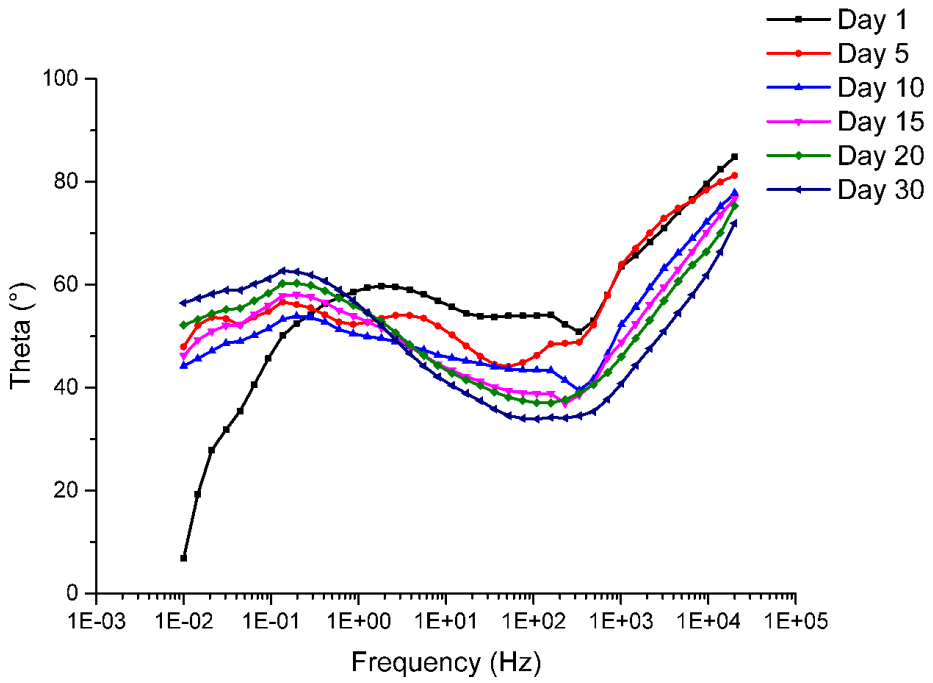

Figure 6.20 Bode phase shift plot of inorganic/hybrid sol-gel coating on 304 stainless steel over 30 days of immersion ($I_{,B2,0\%,304}$)

The results obtained for the coating deposited on stainless steel show a higher resistance to corrosion, as the value of the impedance for the first day is about $10^7 \Omega$ cm² and stays in this order of magnitude throughout the immersion. From Day 5 onwards, the shape of the Nyquist and Bode plots are similar which can be associated to a similar behaviour [61]. The presence of broad semicircles indicates that more than one time constant is taking place in the system, which is also shown in the Bode phase plot. The impedance responses obtained for Day 1 to Day 15 can be considered as higher than the other responses and hint to a strong capacitive behaviour, also present in the values of the angles close to 90° as shown in the Bode phase plot.

The two samples had the same inorganic/hybrid sol-gel coating but deposited on different substrates. From these results it can be seen that the sample deposited on 304 stainless steel has a higher value for the impedance results and showed almost no sign of corrosion while the same coating but on A1008Qpanel is more corroded. Those results being poorer, the focus was made on the coatings on 304 steel as the system as a whole (coating + substrate) was evaluated in order to be optimized. As the coatings deposited were the same and only the substrate differed, the difference in resistance values between the two systems seemed to display a contrast in their properties, even permeation or porosity of the coating.

Figure 6.21 presents the equivalent circuit for coated stainless steel before exposure.

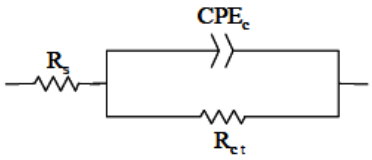

Figure 6.21 Equivalent circuit for coated steel before exposure

Figure 6.22 presents the equivalent circuit for the coated steel once the exposure to the saline solution has begun.

.

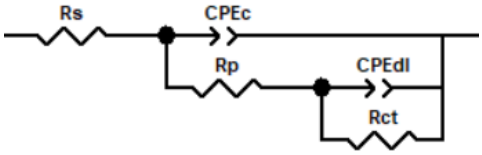

Figure 6.22 Equivalent circuit for coated steel after exposure to 3.5% NaCl solution Day 1 to Day 30

This agrees with data published in literature [222] that R_s values are generally higher for a coated metal compared to an uncoated metal, tested in the same electrolyte (Order of magnitude 10^1 – $10^2\Omega$ for bare substrate, 10^2-$10^3\Omega$ for coated sample). Its variation can be correlated to the coating degradation level. A decrease in R_s value with time of immersion indicates a deterioration in the ability of the coating to protect the substrate.

Comparisons of both the evolution of R_{ct} and CPE_c as a function of time for the same coating on different substrates are presented in Figure 6.23 and Figure 6.24 .

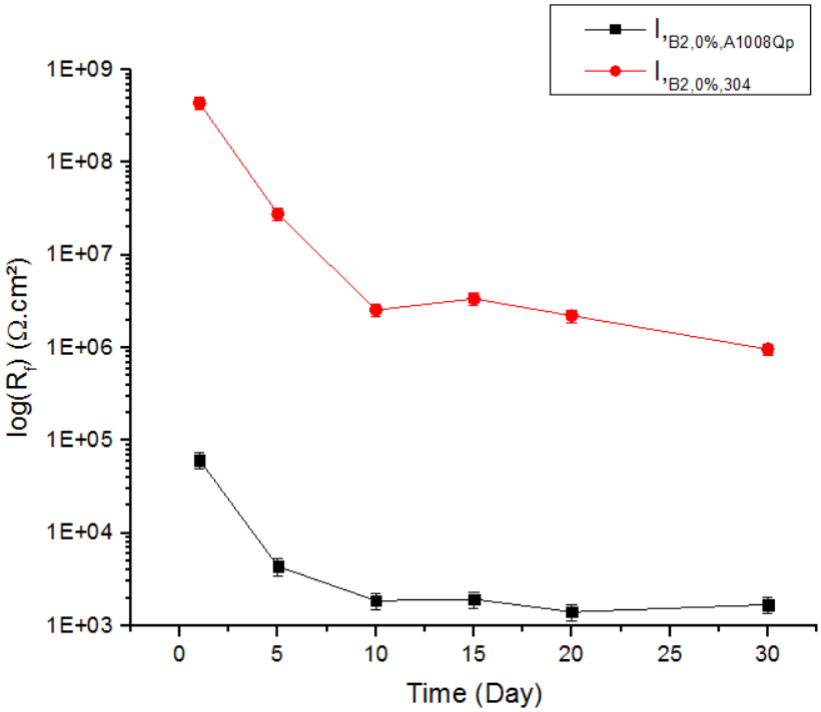

Figure 6.23 Comparison of R_{ct} as a function of time for $I_{,B2,0\%,\ A1008Qp}$ and $I_{,B2,0\%,304}$ over 30 days of immersion

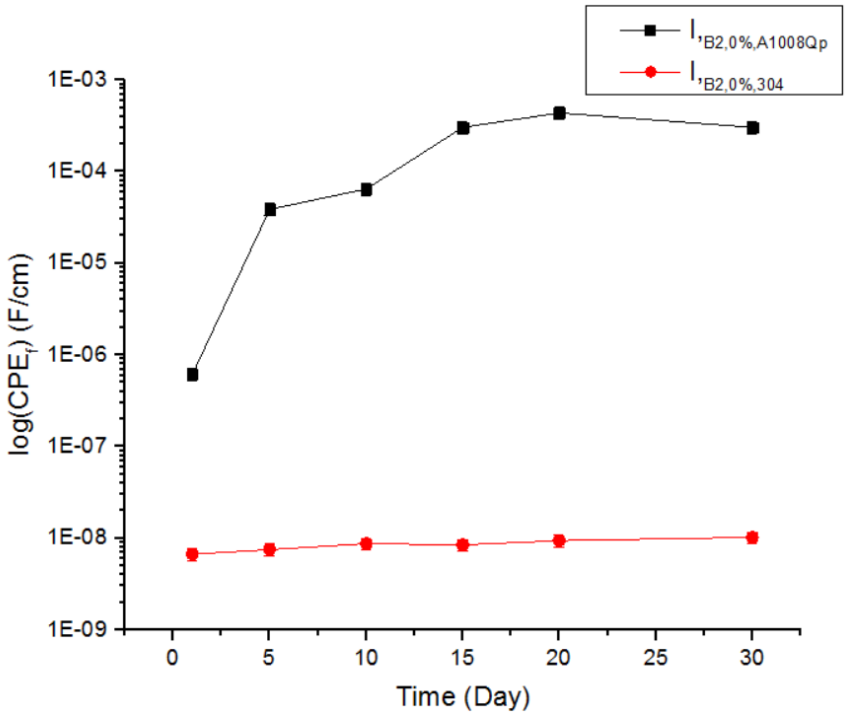

Figure 6.24 Comparison of CPE_c as a function of time for $I_{,B2,0\%,\ A1008Qp}$ and $I_{,B2,0\%,304}$ over 30 days of immersion

The resistances of both samples decrease with time which indicate a damage in the coating or corrosion of the substrate. Both resistances follow the same pattern but

for $I_{,B2,0\%,\ A1008Qp}$ the values are lower which hint to a lower corrosion resistance. The values of this resistance are higher for $I_{,B2,0\%,304}$ than for $I_{,B2,0\%,\ A1008Qp}$.

An increase of the capacitance means an increase of the water uptake, as both parameters can be associated [170, 171]. This leads to an increase in coating degradation. It is the case for $I_{,B2,0\%,A1008Qp}$ whose value of capacitance increases within several orders of magnitude (with a rapid increase during the first days). All samples show an increase in the values of capacitance with immersion time and thus in coating degradation. However the values for $I_{,B2,0\%,304}$ are several orders of magnitude lower than for $I_{,B2,0\%,\ A1008Qp}$, indicating an improvement in the protective performance of the coating.

6.3.3 EIS on Silica Inorganic/Hybrid Sol-Gel Coated Samples Doped With Titanium Butoxide for the Second Batch

The EIS spectra obtained for a same sample through different days of immersion may have a different shape but a same equivalent circuit can be applied. The Bode plots are more indicated for monitoring the evolution of the electrochemical behaviour in the system with time [164]. Thus the equivalent circuit in Figure 6.22 can be used for the tests recorded until Day 30 of immersion. The tests showed a capacitive behaviour in order to extract passive elements values that are representative of the physical environment. It can be compared to circuits obtained in literature for similar coatings [22, 223-226]. Sometimes a better fit would be possible but that would include too many components, which would not be able to properly reproduce a physical circuit and thus be not representative of the reality. The equivalent circuit Figure 6.22 gives an acceptable fit with a minimum of elements.

The samples coated with the silica inorganic/hybrid sol-gel coating presented good resistance to corrosion but it was decided to dope the coating with a titanium precursor (titanium butoxide) in order to improve the anti-corrosion properties of these samples. All the samples doped with titanium precursor (2.8%w/w, 5.6%w/w and 11.3%w/w) are deposited on 304 stainless steel.

The samples doped with titanium from the second batch, while showing different values of impedance results show the same pattern and shape of spectra. In their cases, the same equivalent circuit Figure 6.22 can be used as well.

For example for the sample doped with 2.8%w/w of titanium precursor the spectra in Figure 6.25 to Figure 6.27 are obtained.

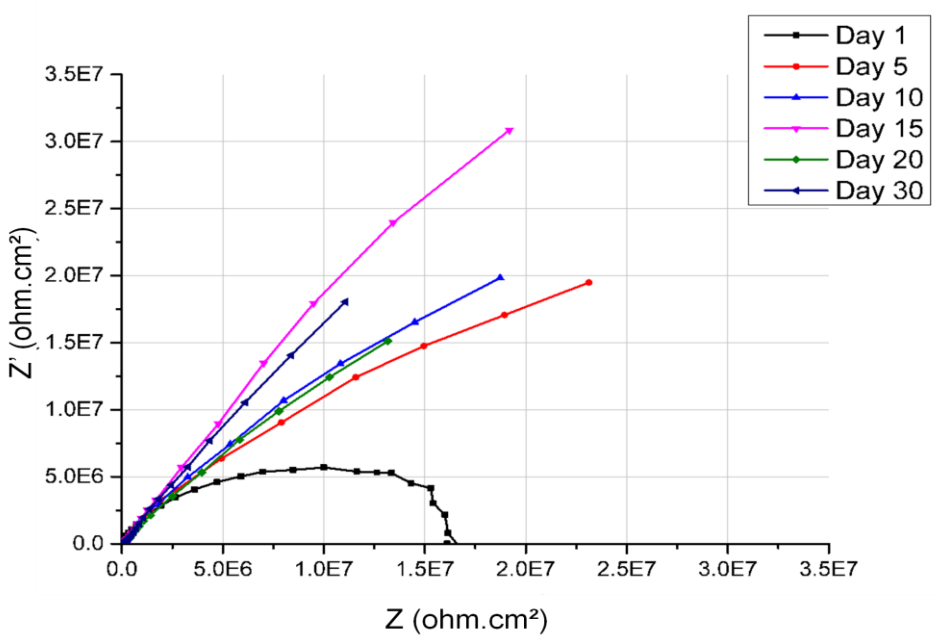

Figure 6.25 Nyquist plot of $I_{,B2,2.8\%,304}$ over 30 days of immersion

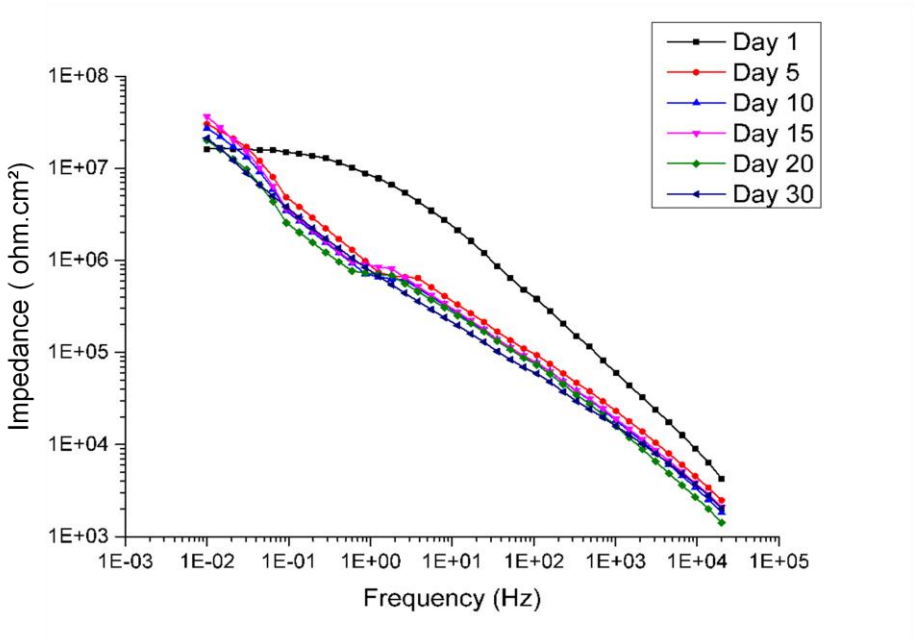

Figure 6.26 Bode impedance plot of $I_{,B2,2.8\%,304}$ over 30 days of immersion

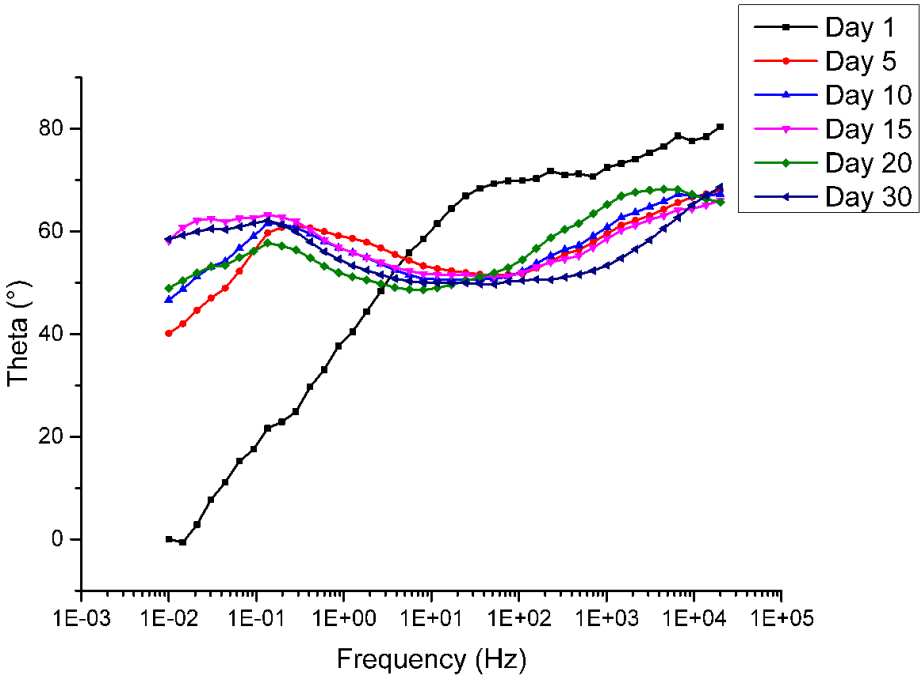

Figure 6.27 Bode phase shift plot of $I_{,B2,2.8\%,304}$ over 30 days of immersion

This sample was doped with 2.8%w/w of titanium precursor. The impedance responses are about $10^7 \Omega.cm^2$ which stays in the same order of magnitude of the samples doped with titanium. The Nyquist plot obtained for the first day has a semi-circle shape, indicating only one time constant. The diameter of the semicircle can be related to the value of R_{ct}. The source of this time constant can be identified by the spectra in the Bode phase plot: for the first day, the impedance response appears as a single peak at high frequencies. This can be correlated to the response of the dielectric properties of the coating [144]. As seen in the plots, for the other days two time constants can be noticed. The Bode phase plot presents the responses with stable values at high frequencies, expressing a stable behaviour of the coating. The decrease of these peaks with time indicates that the response becomes less capacitive as water and ions penetrate through the coating [227].

For the sample doped with 5.6%w/w of titanium precursor (Appendix A) the values of the impedance are in the same order of magnitude. The plots show that the sample has been keeping the same behaviour throughout the period of exposure. The Nyquist and Bode phase plots present the curves with most of them having at least two time constants occurring in the system. Here as well, the response for the whole range of experiment has a high value and indicates a strong capacitive behaviour. The height of the peaks in the Bode plot decreases as time increases which can be due to water and electrolyte penetration. The decrease of the

impedance response with time throughout the frequency range studied is probably due to increased porosity of the coating and the corroding area [159]. The decrease of the impedance for the whole frequency range as a function of immersion time suggests that water penetration is uniform throughout the coating [228].

Another sample has been doped with 11.3%w/w of titanium precursor (Appendix B), the highest amount, and has the lowest value of impedance among all the titanium doped samples. The early impedance response for most of the days presents two indistinct semi circles in the Nyquist plot. This can indicate a low barrier effect of the coating. The impedance response at high frequencies is related with the dielectric properties of the coating while the semi circle at low frequencies corresponds to the corrosion products formed at the interface between the coating and the metal interface [169].

The hybrid/composites sample (Appendix C) presents a value of about $3.10^5 \Omega$ cm² the first day which drops by one order of magnitude by the end of the experiment. The diameter of the semi circle plots decreases with time, which indicates a decrease in the resistance of the coating and suggests a high permeability of the coating. Starting from Day 5, the Bode phase diagram shows that the intermediate-frequency peak (10 to 10^3 Hz) corresponding to the processes occurring at the passive film/coating interface [169] is affected by the experimental environment as seen by a shift towards low frequency. This indicates an active charge transfer process at the passive film/solution interface. This shift occurs simultaneously with a slight decrease of peak height as exposure time increases from Day 5, suggesting that the dielectric properties of the passive film decrease with time at this prolonged exposure period and that the capacitive behaviour of the coating decreases as well. The values obtained for the Nyquist plot, being lower than $10^6 \Omega.cm^2$, suggest a coating with defects, causing the corrosion of the substrate.

The equivalent circuits can sometimes be difficult to obtain as there are more parameters to consider. The values can sometimes be changed without having an effect on the fit and thus an order of magnitude can be given instead of an accurate value, particularly R_{ct}.

The values of R_{ct} and CPE_c as a function of time for the samples of the second batch with different percentages of titanium added are presented in Figure 6.28 and Figure 6.29.

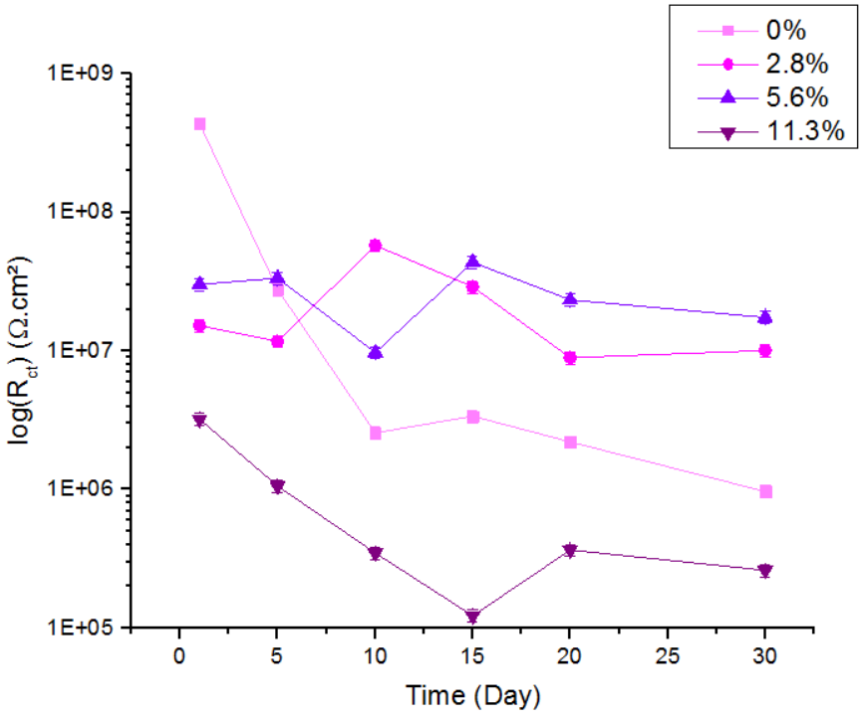

Figure 6.28 Comparison of R_{ct} as a function of time for the different percentages of precursor over 30 days of immersion for Batch 2

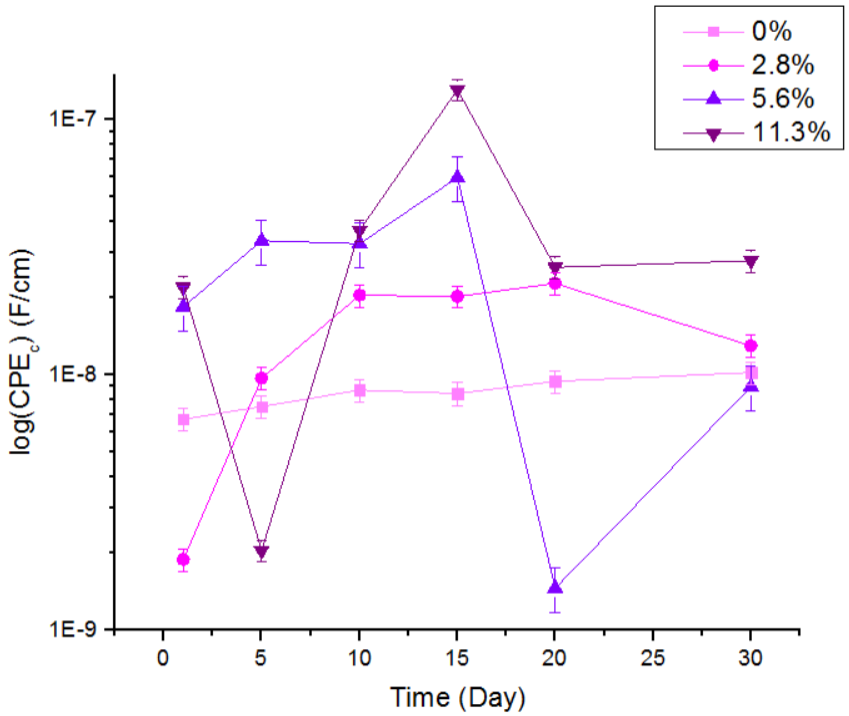

Figure 6.29 Comparison of CPE_c as a function of time for the different percentages of precursor over 30 days of immersion for Batch 2

From Figure 6.28 and Figure 6.29 it can be seen that the samples doped with 2.8%w/w and 5.6%w/w precursor present stable values of resistance while for 0%w

and 11.3%w/w the values decrease more than one order of magnitude. R_{ct} is linked to the corrosion. As the substrate comes in contact with the solution (or electrolyte), the electrochemical reactions occur, leading to the start of corrosion and formation of corrosion products. A decrease in R_{ct} value means an increase of damage and formation of corrosion product. This can be associated to the addition of precursor, as studies have reported that the doping with titanium enhanced the corrosion protection of coatings.

Some authors have correlated the coating capacitance to the water uptake [170, 171], meaning that an increase in the value of coating capacitance would lead to more water uptake for the sol-gel coatings. The samples display an increase in CPE_c as a function of time thus meaning a degradation of the coating even though the values for $I_{,B2,5.6\%,304}$ and $I_{,B2,11.3\%,304}$ seem variable. $I_{,B2,0\%,304}$ and $I_{,B2,2.8\%,304}$ have their values stabilized throughout the immersion or only changing from one order of magnitude whereas some presents an important change of value meaning a critical degradation of the coating.
The values of CPE_c give information for the samples with 0%w/w and 2.8%w/w as their values increase with time and thus indicate a rise in the water uptake. The values obtained for the samples with 5.6%w/w and 11.3%w/w are not stable and show more fluctuation which could come from the amount of titanium.

6.4 EIS Results of Third Batch

The samples had an inorganic/hybrid coating, alkaline hydrolysed MTEOS/ TEOS deposited on 304 stainless steel doped with different percentages of titanium butoxide and in this part 0%w/w, 2.8%w/w and 5.6%w/w are studied. The samples doped with 11.3%w/w were not studied anymore due to the poor results obtained in Batch 2.

Moreover, each percentage has been divided in four parts: mixture as a solvent for the sol-gel process then curing temperature 500°C in N_2, solvent mixture for sample cured at 500°C in air, isopropanol as a solvent for a curing temperature of 500°C in N_2 or isopropanol for a curing process at 500°C in air. A summary of the names of the samples can be found again in Table 4.9.

If the sample $I_{,B3,0\%,Mix,N2}$ (inorganic/hybrid sol-gel coating without doping, solvent mixture, cured at 500°C in N_2) can also be fitted with the same equivalent circuit as presented in Figure 6.22, other samples present a different behaviour such as $I_{,B3,2.8\%,Mix,N2}$ (inorganic/hybrid sol-gel coating doped with 2.8%w/w titanium precursor, solvent mixture, cured at 500°C in N_2) which leads to the introduction of a new component: the Warburg element. The precedent circuit can still be of use but the Warburg element allows more accuracy for the diffusion part as it is usually added to represent the diffusion of ions through the conductive paths within the coating.

Figure 6.30 to Figure 6.32 present the Nyquist and Bode plots of the sample $I_{,B3,2.8\%,Mix,N2}$.

This sample has been doped with 2.8%w/w of titanium butoxide, was cured at 500°C in N_2 and the solvent used for the sol-gel process was the solvent mixture. The values of the Nyquist plots start well at $10^7 \Omega.cm^2$ but drop regularly after the first day. The Nyquist diagram shows broadened semi circles between intermediate and high frequencies, indicating the presence of more than one time constant. This diameter decreases as time increases which can be associated with a decreasing of resistance. The patterns of the curves are similar in both of the Bode plots.

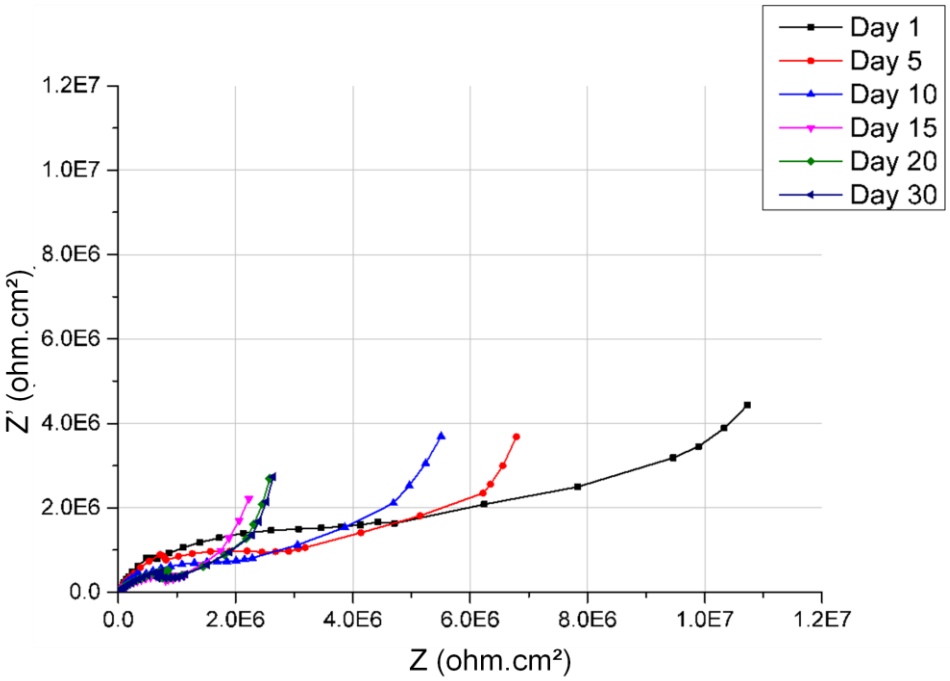

Figure 6.30 Nyquist plot of the sample $I_{,B3,2.8\%,Mix,N2}$ over 30 days of immersion

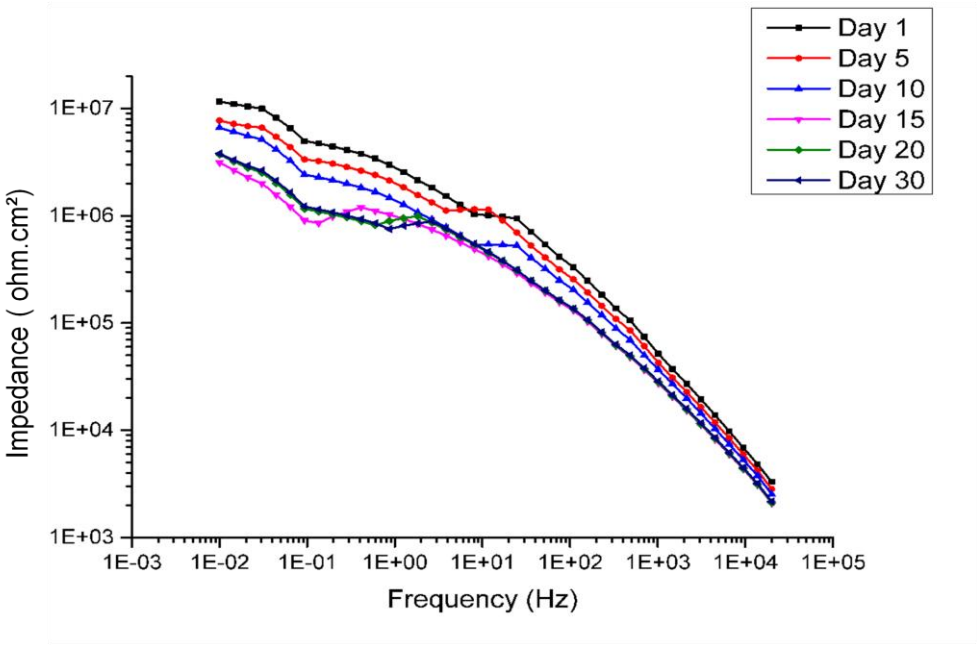

Figure 6.31 Bode impedance plot of the sample $I_{,B3,2.8\%,Mix,N2}$ over 30 days of immersion

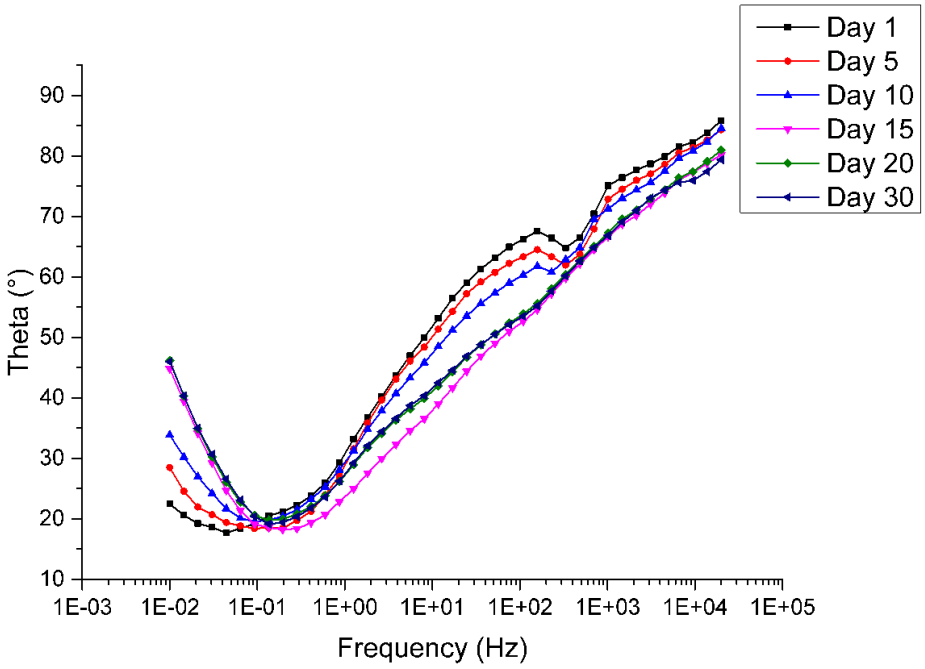

Figure 6.32 Bode phase shift plot of the sample $I_{,B3,2.8\%,Mix,N2}$ over 30 days of immersion

The low frequency arcs of the curves in the Nyquist plots indicate that the response seems to account for the diffusion-controlled process. The low frequency arc behaves like the Warburg diffusion element as indicated by a straight line tail with a slope of 45°. This behaviour is found for all days of exposure. The low-frequency

peak appearing at 10^{-1} to 10^{2} Hz in the Bode phase plot is more likely to come from a combined response of the electrochemical processes occurring at the passive film/coating interface and the slow diffusion of oxygen through a passive film [229]. Another peak can be found at intermediate to low frequencies (10^{1} to 10^{3} Hz) which can be correlated to a diffusion of corrosive species through the corrosion products at the passive film/coating interface. The height of this peak decreases as the time of exposure increases. This suggests that the dielectric properties of the passive film decrease with time in the conditions of the experiment.

In the Bode magnitude plot, it is shown that the total resistance value at low frequencies (total resistance being the sum of all resistances in the system) is higher than 10^{6} Ω.cm^{2}, which is enough for the coating system to provide a corrosion protection to the metal substrate [164]. Here the overall impedance of the coating system stays between 10^{6} and 10^{7} Ω.cm^{2} suggesting that the corrosion protection of the coating holds a stable rate.

Figure 6.33 presents the equivalent circuit which could be used for $I_{,B3,2.8\%,Mix,N2}$

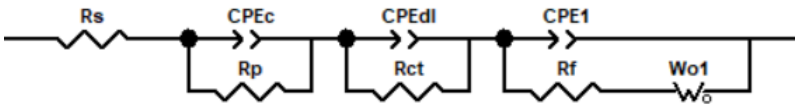

Figure 6.33 Possibility of equivalent circuit

R_fCPE_1Wo represents the presence of the underlying passive film on the stainless steel surface. The Warburg element is used to model the diffusion of the electrolyte through this film but it can give high percentage of error compared to the experimental data.

After testing a number of different electrical circuit models in the analysis of the impedance spectra obtained, it is found that the set of data with a total resistance higher than 10^{6} Ω.cm^{2} could be satisfactorily fitted with the two equivalent circuits presented in Figure 6.34 [159, 164, 230]. Adding too many components in the circuits may give more mathematical accuracy to the fitting but there is loss of physical meaning and so this needs to be optimised.

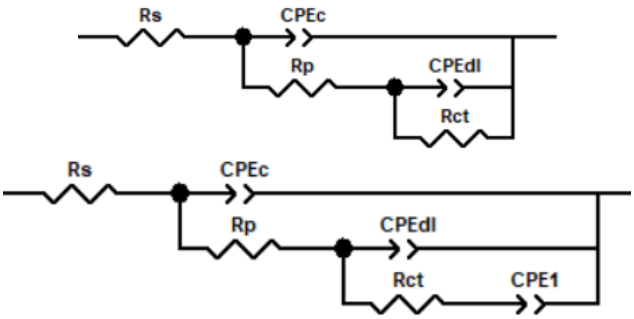

Figure 6.34 Equivalent circuits used for the interpretation of the data

- Effect of the solvent and curing process

In the third and last batch the samples were either prepared with isopropanol as a solvent or a mixture (ethanol, isopropanol and butanol). The curing process was either in N_2 or air. The purpose of these changes in parameters is to find the combination improving the corrosion resistance of coatings the most.

Figure 6.35 presents the Nyquist plots of the samples $I_{,B3,0\%,Mix,N2}$, $I_{,B3,0\%,Ip,N2}$, $I_{,B3,0\%,Mix,Air}$ and $I_{,B3,0\%,Ip,Air}$ (0% w/w titanium precursor) at Day 1 while Figure 6.36 presents the Nyquist plots at Day 30. The detailed Nyquist and Bode plots for each sample are in Appendix D.

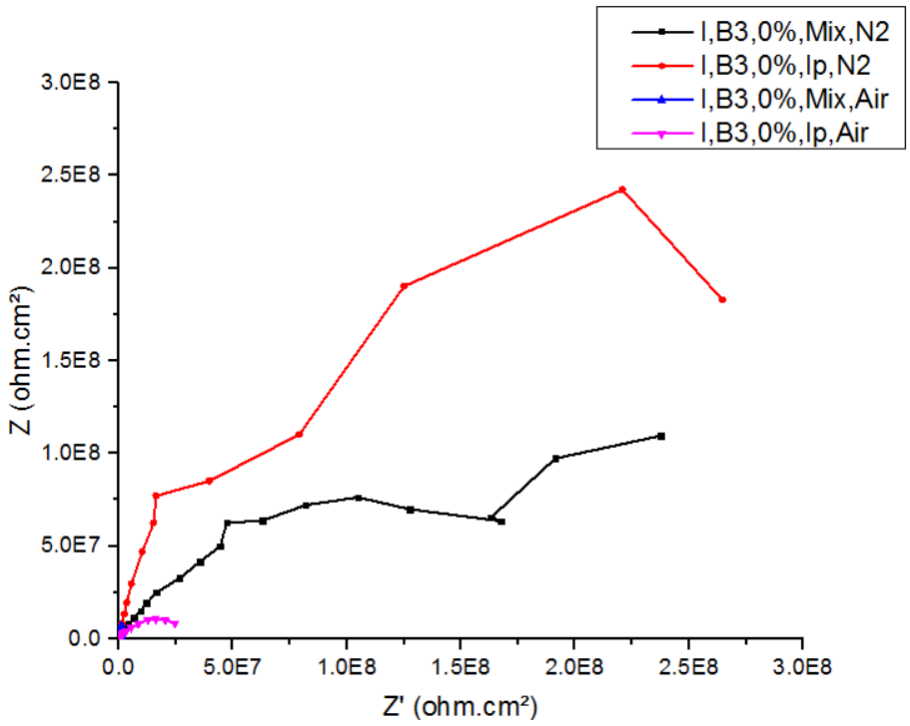

Figure 6.35 Nyquist plot of the sample a) $I_{,B3,0\%,Mix,N2}$ b) $I_{,B3,0\%,Ip,N2}$ c) $I_{,B3,0\%,Mix,Air}$ d) $I_{,B3,0\%,Ip,Air}$ at Day 1 of immersion

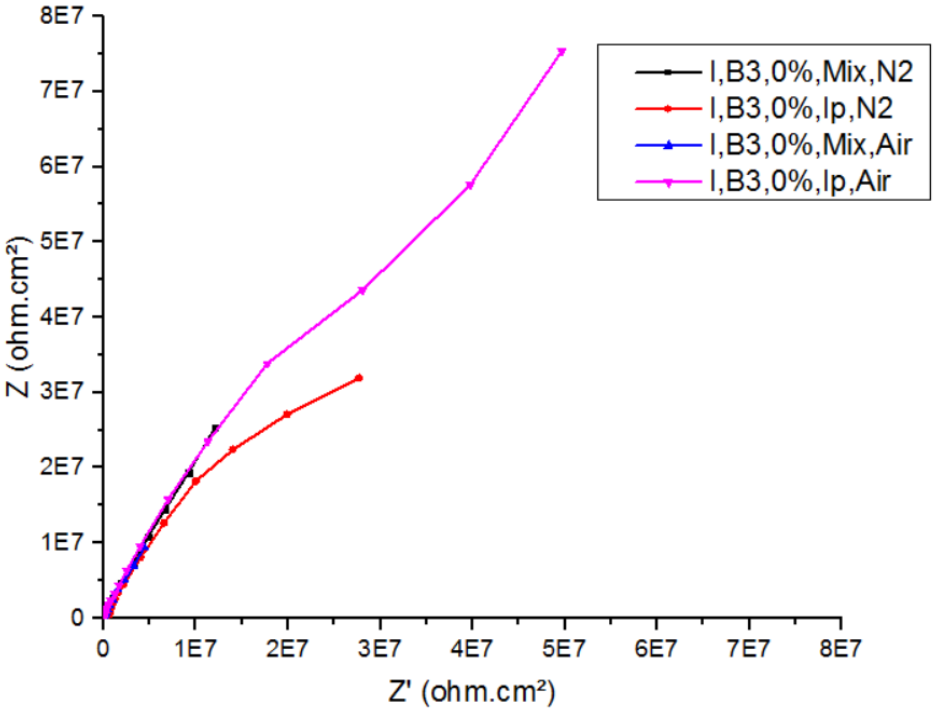

Figure 6.36 Nyquist plot of the sample a) $I_{,B3,0\%,Mix,N2}$ b) $I_{,B3,0\%,Ip,N2}$ c) $I_{,B3,0\%,Mix,Air}$ d) $I_{,B3,0\%,Ip,Air}$ at Day 30 of immersion

The values of the impedance for $I_{,B3,0\%,Mix,N2}$ seem to stay in the same order of magnitude ($10^7 \Omega.cm^2$) during the period of immersion. It can be seen on the Nyquist plot of Day 1 that there are already variations in the impedance spectra occurring at the beginning of the immersion. The shape being a segment of semi circle, it suggests that the coating is performing as an efficient barrier against the penetration of the electrolyte. This is confirmed with the value of the phase angle close to 90° in the Bode phase plot.

The impedance of $I_{,B3,0\%,Ip,N2}$ starts with a high value, around $10^8 \Omega.cm^2$ and stays high, more than 10^7 $\Omega.cm^2$ at the end of the experiment. The peak heights of the curves in the Bode phase plot decrease while the time of exposure increases, meaning that the dielectric properties of the interface decrease. The magnitude of the impedance response decreases as well during the time of the immersion but the values of impedance stay high throughout the experiment, indicating good protective properties.

$I_{,B3,0\%,Mix,Air}$ presents low values of impedance at Day 1 which stay in the order of magnitude of $10^6 \Omega.cm^2$ during the experiment. The results here are really similar to $I_{,B3,0\%,Ip,Air}$. $I_{,B3,0\%,Ip,Air}$ has values of the impedance in the order of magnitude of $10^7 \Omega.cm^2$ from the start and stay in this order until Day 30. The Nyquist plot obtained

for Day 1 shows a clear semi-circle, indicating only one time constant, the diameter being close to the value of R_{ct}. At longer time of exposure the responses are segments of semi-circle which differs from the behaviour of the first day. Their values in the Nyquist plot are broadened

Two patterns, especially for the Bode plots, can be noted: the samples cured in N_2 on one side and the samples cured in air in the other. The samples cured in N_2 present a higher impedance throughout the experiment. The curing process seems to influence the impedance more than the solvent.

The values of total resistance are different as well but all values are higher than 10^7 $\Omega.cm^2$ within 30days of exposure. The values of total resistance for $I_{,B3,0\%,Mix,N2}$ and $I_{,B3,0\%,Ip,N2}$ are higher (close to $10^9\Omega.cm^2$) and have a higher decrease of impedance during the immersion.

The values of R_{ct} and CPE_c as a function of time for the samples of the third batch with no doping but with different solvents and curing processes are presented in Figure 6.37 and Figure 6.38. The values of R_{ct} for the samples $I_{,B3,0\%,Ip,N2}$, $I_{,B3,0\%,Mix,Air}$ and $I_{,B3,0\%,Ip,Air}$ decrease with time which means that the protective properties of the coatings lessen as well. The values of the capacitance for $I_{,B3,0\%,Mix,N2}$, $I_{,B3,0\%,Mix,Air}$ and $I_{,B3,0\%,Ip,Air}$ seem to stay stable while for $I_{,B3,0\%,Ip,N2}$ changes more.

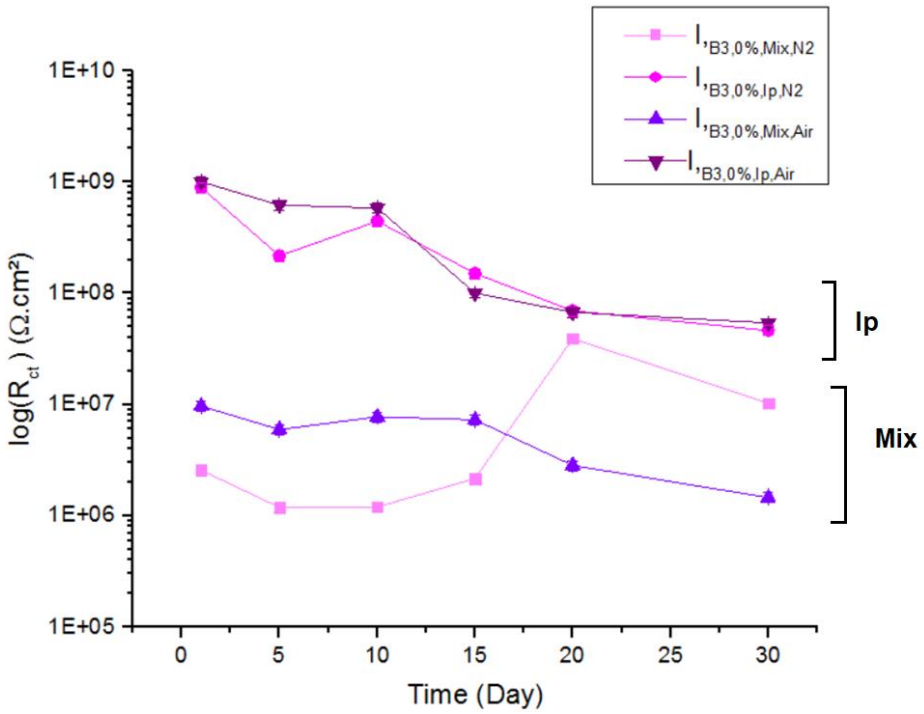

Figure 6.37 Comparison of R_{ct} as a function of time for the different solvents and curing processes from Batch 3 over 30 days of immersion

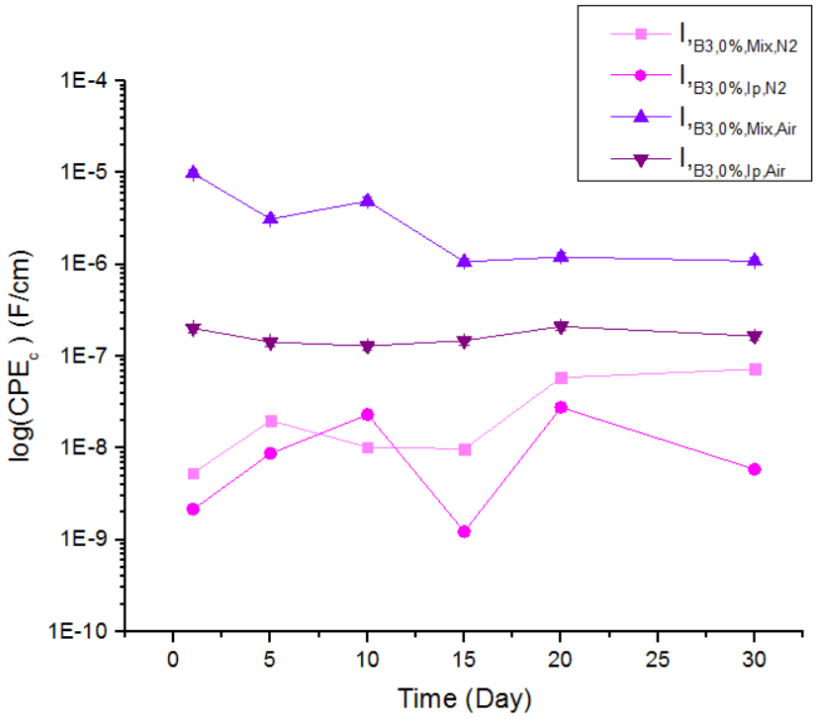

Figure 6.38 Comparison of CPE_c as a function of time for the different solvents and curing processes from Batch 3 over 30 days of immersion

Figure 6.37 shows that the samples with the mixture as a solvent have a lower resistance than the samples with isopropanol as a solvent while Figure 6.38 show that the curing process influence the values of capacitance.

Figure 6.39 presents the Nyquist plots at Day 1 for the samples $I_{,B3,2.8\%,Mix,N2}$, $I_{,B3,2.8\%,Ip,N2}$, $I_{,B3,2.8\%,Mix,Air}$ and $I_{,B3,2.8\%,Ip,Air}$ (2.8%w/w titanium butoxide) while Figure 6.40 presents the plots at Day 30. The detailed Nyquist and Bode plots for each sample are in Appendix D.

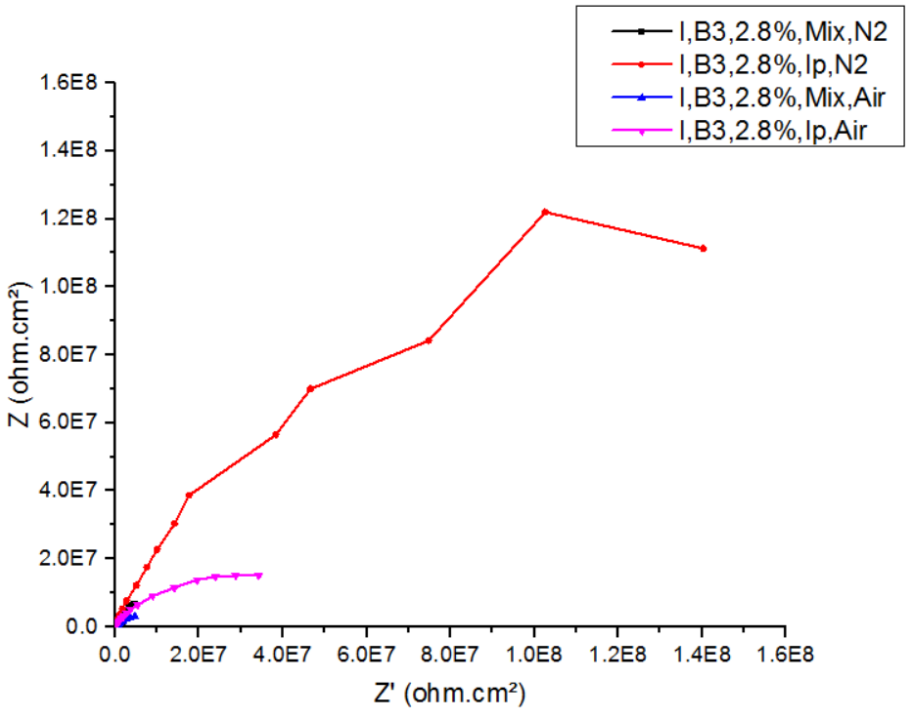

Figure 6.39 Nyquist plot of the sample a) $I_{,B3,2.8\%,Mix,N2}$ b) $I_{,B3,2.8\%,Ip,N2}$ c) $I_{,B3,2.8\%,Mix,Air}$ d) $I_{,B3,2.8\%,Ip,Air}$ at Day 1 of immersion

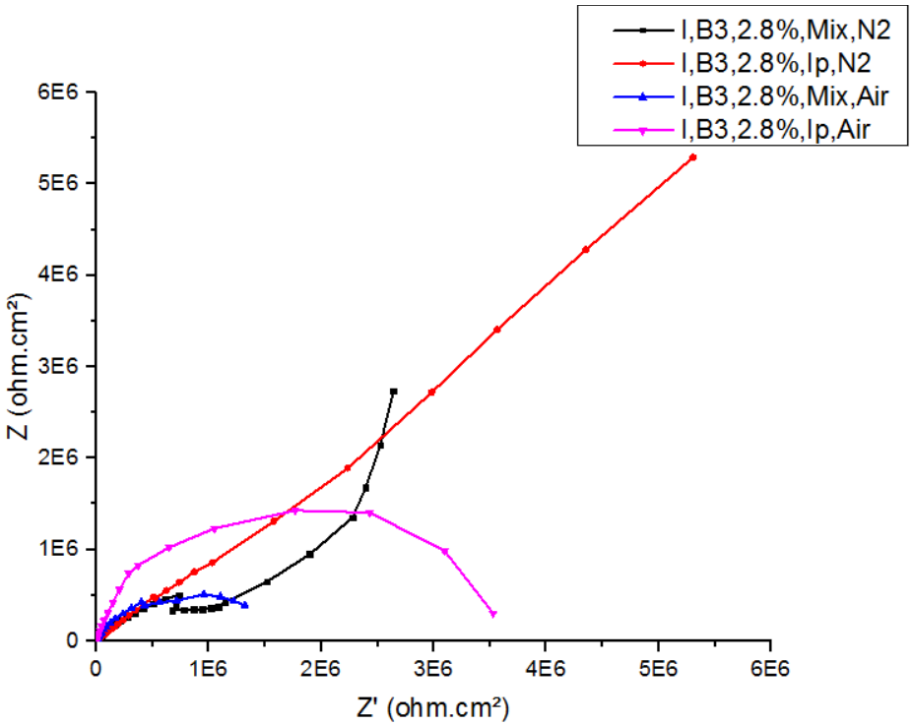

Figure 6.40 Nyquist plot of the sample a) $I_{,B3,2.8\%,Mix,N2}$ b) $I_{,B3,2.8\%,Ip,N2}$ c) $I_{,B3,2.8\%,Mix,Air}$ d) $I_{,B3,2.8\%,Ip,Air}$ at Day 30 of immersion

$I_{,B3,2.8\%,Mix,N2}$ behaviour has been described earlier in the equivalent circuit part.

The Nyquist plot of $I_{,B3,2.8\%,Ip,N2}$ for the 1st Day shows a strong response with a high value which drops after a few days, going from $10^8\Omega.cm^2$ to $10^7\Omega.cm^2$. The same results are obtained here as for the sample $I_{,B3,0\%,Ip,N2}$, with the 3 different plots having the same pattern and the same order of magnitude.

The values of $I_{,B3,2.8\%,Mix,Air}$ decrease during the experiment and according to the Nyquist plots the system started with one time constant but ended having two.

There is an obvious decrease and change in the shapes of the Nyquist plots for $I_{,B3,2.8\%,Ip,Air}$, as the plot for Day 30 is a defined semi-circle unlike the others. The values also decrease in magnitude. The Bode phase plot shows a clear distinction between the first day and the rest of the experiment. At high frequencies (higher than 10^4Hz), which is linked to the coating properties, the plots of the first days present a clear decrease of value within the first day and then remain similar for the rest of the experiment. This can be due to the loss in dielectric properties of the coating, as water and electrochemical species diffuse through the coating [169].

For these samples the Bode impedance plots are more similar between the four of them but they can still be divided in two types: curing in N_2 as opposition to curing in air. There is a greater decrease of impedance for $I_{,B3,2.8\%,Ip,Air}$ compared to the other samples.

On another point, the Bode phase shift presents more differences between $I_{,B3,2.8\%,Mix,N2}$/ $I_{,B3,2.8\%,Ip,N2}$ and $I_{,B3,2.8\%,Mix,Air}$ / $I_{,B3,2.8\%,Ip,Air}$. The Nyquist plots are more similar for $I_{,B3,2.8\%,Ip,N2}$, $I_{,B3,2.8\%,Mix,Air}$ and $I_{,B3,2.8\%,Ip,Air}$, except for Day 30 of $I_{,B3,2.8\%,Ip,Air}$.

The values of R_{ct} and CPE_c as a function of time for the samples of the third batch with 2.8%w/w doping with different solvents and curing processes are presented in Figure 6.41 and Figure 6.42. The resistances can be seen as decreasing for all the samples except for $I_{,B3,2.8\%,Mix,Air}$ which is stable compared to the others.

The values of the capacitor usually increase (meaning a rise in the water uptake) except for $I_{,B3,2.8\%,Mix,N2}$ in this case, which is stable and the values stay within the same order of magnitude.

There is less evidence of influence of solvent or curing process here. However the samples cured in air have similar values of R_{ct} and CPE_c at the end of the immersion.

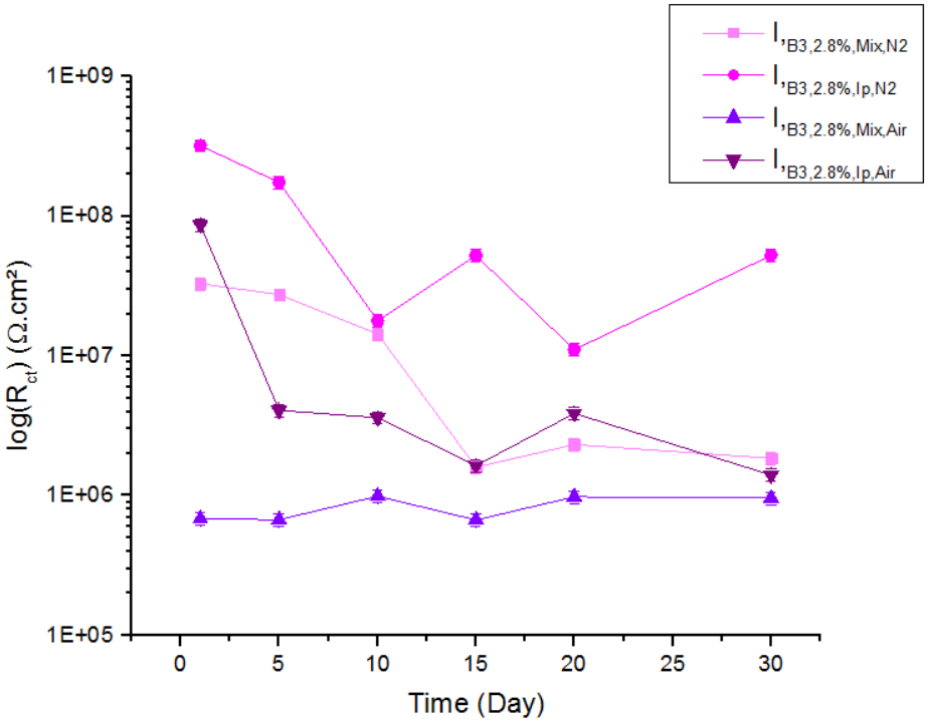

Figure 6.41 Comparison of R_{ct} as a function of time for the different solvents and curing processes for 2.8%w/w doping from Batch 3 over 30 days of immersion

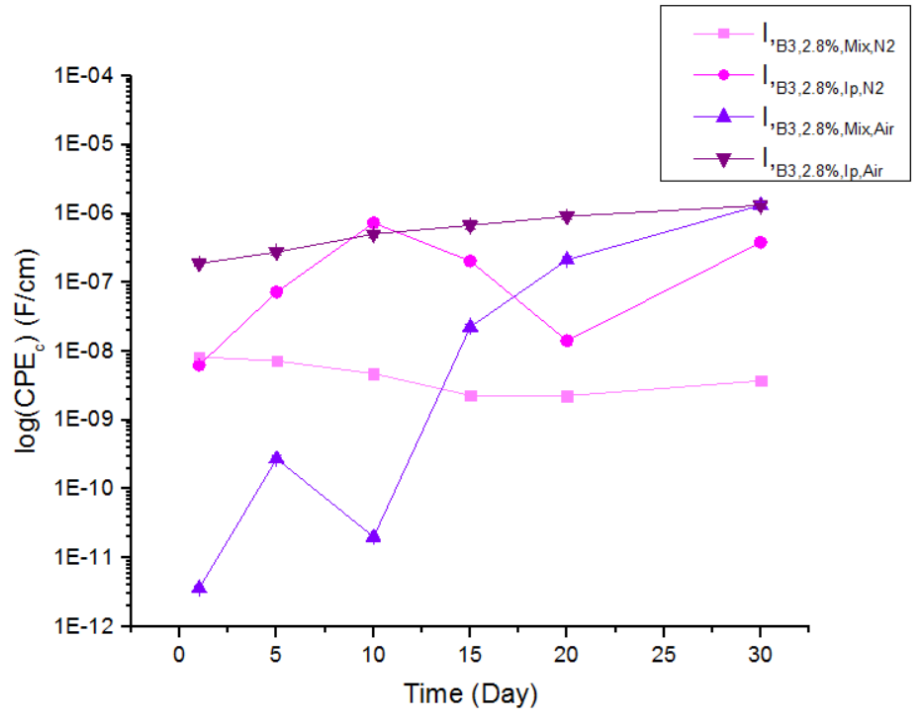

Figure 6.42 Comparison of CPE_c as a function of time for the different solvents and curing processes for 2.8%w/w doping from Batch 3 over 30 days of immersion

Figure 6.43 presents the Nyquist plots of the samples $I_{,B3,5.6\%,Mix,N2}$, $I_{,B3,5.6\%,Ip,N2}$, $I_{,B3,5.6\%,Mix,Air}$ and $I_{,B3,5.6\%,Ip,Air}$ (5.6%w/wTi) at Day 1 of experiment while Figure 6.44

presents the plots at Day 30. The detailed Nyquist and Bode plots for each sample are in Appendix D.

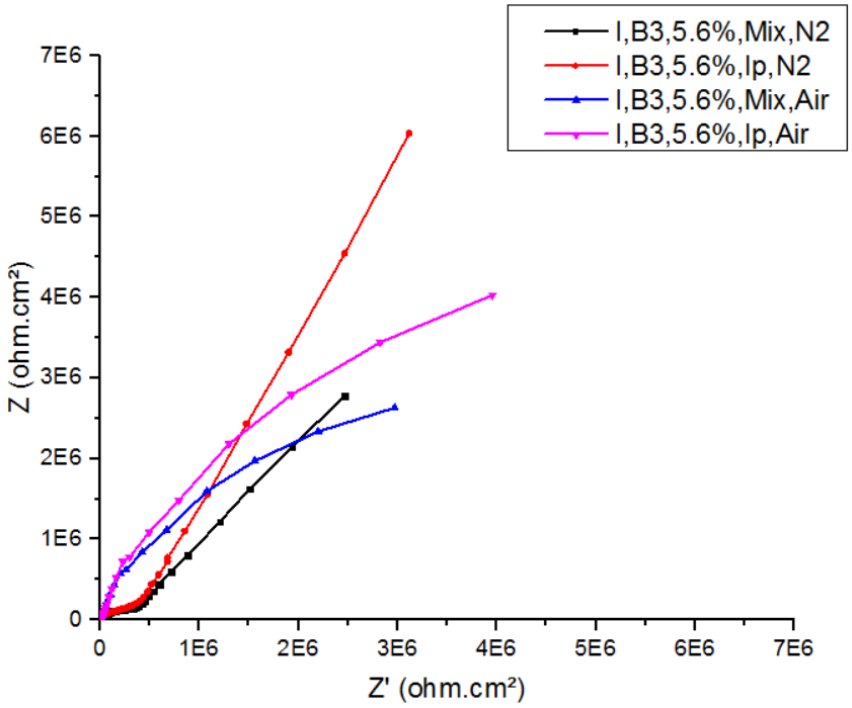

Figure 6.43 Nyquist plot of the sample a) $I_{,B3,5.6\%,Mix,N2}$ b) $I_{,B3,5.6\%,Ip,N2}$ c) $I_{,B3,5.6\%,Mix,Air}$ d) $I_{,B3,5.6\%,Ip,Air}$ at Day 1 of immersion

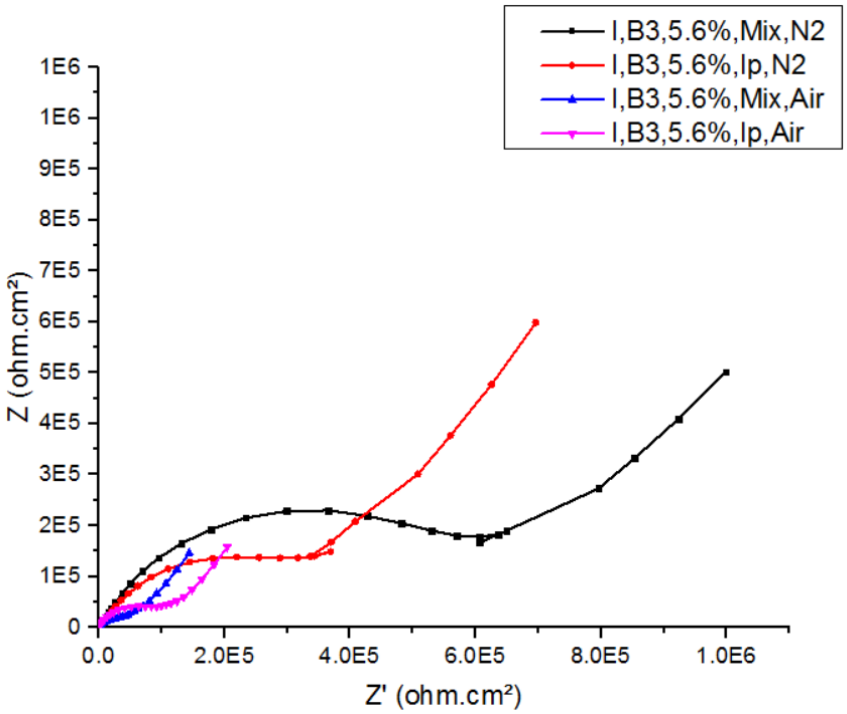

Figure 6.44 Nyquist plot of the sample a) $I_{,B3,5.6\%,Mix,N2}$ b) $I_{,B3,5.6\%,Ip,N2}$ c) $I_{,B3,5.6\%,Mix,Air}$ d) $I_{,B3,5.6\%,Ip,Air}$ at Day 30 of immersion

The impedance values for $I_{,B3,5.6\%,Mix,N2}$ are low as the order of magnitude is about $10^6\Omega.cm^2$ from the start but two constants can be observed. The results obtained for this sample are quite similar to the results obtained for $I_{,B3,2.8\%,Mix,N2}$.

The same can be said about $I_{,B3,5.6\%,Ip,N2}$, its Nyquist plots mainly show two time constants and start at $10^6\Omega.cm^2$ to finish near $10^5\Omega.cm^2$. The curves in the Nyquist plot present a similar shape. The depressed semicircle at high frequencies is associated with the dielectric properties of the ceramic coating, while the diffusion tail at low frequencies is related to a diffusion-controlled process [169].

The impedance of $I_{,B3,5.6\%,Mix,Air}$ drops after a few days as the values of total resistance has a decrease of about one order of magnitude within 5 days of immersion.

There is a strong response for $I_{,B3,5.6\%,Ip,Air}$ from the first day but which drops after a few days to one order of magnitude compared to its original value, meaning that the resistance of the coating decreases as well, the barrier properties of the coating being lowered.

Here again the samples with the same curing process but different solvents have a similar pattern for the Bode plots but also for the Nyquist plots which really show a design for $I_{,B3,5.6\%,Mix,N2}$/ $I_{,B3,5.6\%,Ip,N2}$ and another one for $I_{,B3,5.6\%,Mix,Air}$ / $I_{,B3,5.6\%,Ip,Air}$.

The values of total resistance have a drop in value for $I_{,B3,5.6\%,Mix,Air}$ and $I_{,B3,5.6\%,Ip,Air}$ especially after the first day of immersion.

The values of R_{ct} and CPE_c as a function of time for the samples of the third batch with 5.6%w/w doping with different solvents and curing processes are presented in Figure 6.45 and Figure 6.46. The values of R_{ct} for $I_{,B3,5.6\%,Mix,Air}$ and $I_{,B3,5.6\%,Ip,Air}$ quickly decrease the first week then stay midly stable while for $I_{,B3,5.6\%,Mix,N2}$ and $I_{,B3,5.6\%,Ip,N2}$ keep the same order of magnitude throughout the experiment.

$I_{,B3,5.6\%,Mix,Air}$ has the lowest values in R_{ct} and highest for CPE_c which mean that this sample is the one with the lowest protective properties and highest damage rate.

Among the samples of Batch 3, it seems like the samples cured in air present a performance compared to the samples cured in N_2 for a same percentage of titanium precursor. An increase in the amount of titanium has an influence as well; however it decreases the values as soon as its amount is over 5% while it was expected to improve the protective properties. The solvent does not seem to have a strong influence.

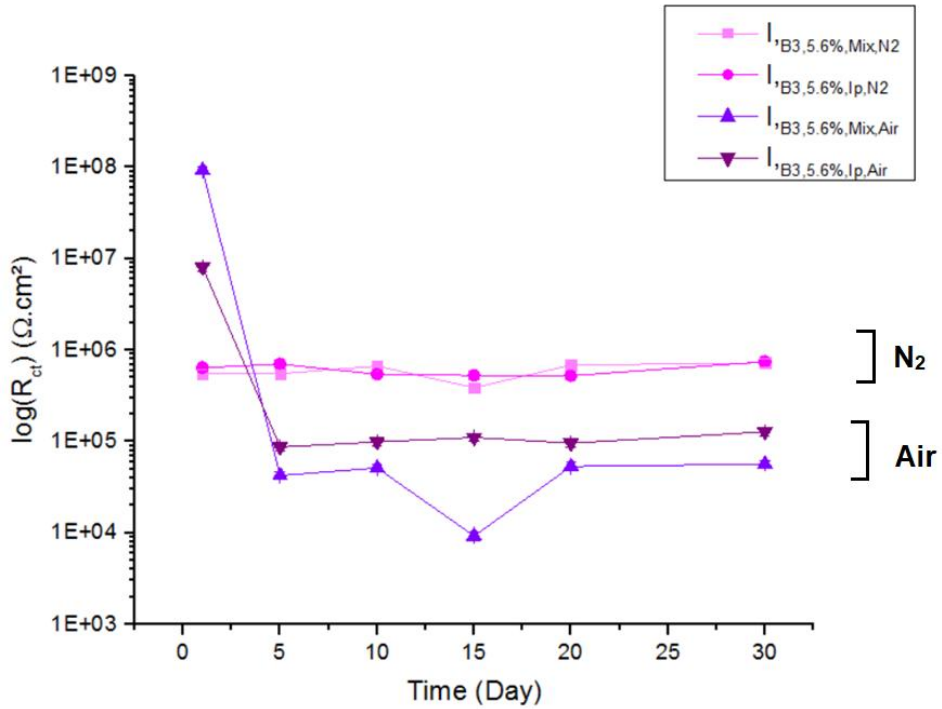

Figure 6.45 Comparison of R_{ct} as a function of time for the different solvents and curing processes for 5.6%w/w doping from Batch 3 over 30 days of immersion

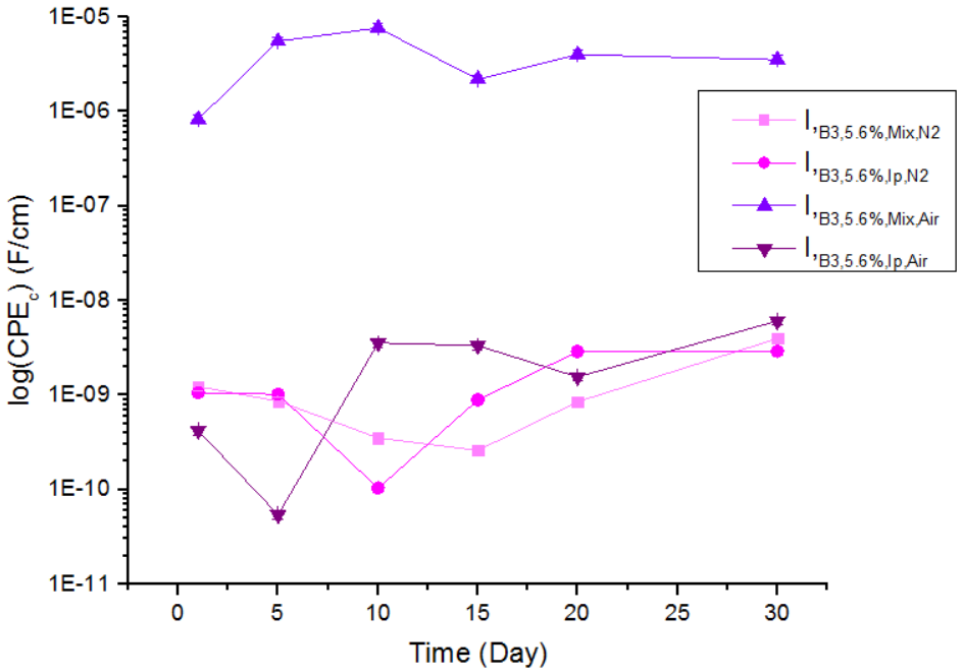

Figure 6.46 Comparison of CPE_c as a function of time for the different solvents and curing processes for 5.6%w/w doping from Batch 3 over 30 days of immersion

6.5 Salt Spray Test Results on Inorganic/Hybrid Sol-Gel Coatings Doped with Titanium Precursor from Batch 3

The salt spray test was used by the industry sponsor to assess the corrosion performance of the coatings over 5 weeks. Inspection of the samples were carried out with images of the specimens taken at specific times. Week 3 and week 5 are presented in this part.

Figure 6.47 to Figure 6.52 show surface morphologies of the coating formulations after exposure at the different interval times. It can be observed that the addition of precursor does little to improve the coating performance for the samples a) and d) in each figure as they are the ones presenting less corrosion. For the other samples there is no improvement in corrosion performance.

There is a notable increase of corrosion product for b) and c) from week 3 to week 5 regardless of the amount of precursor added.

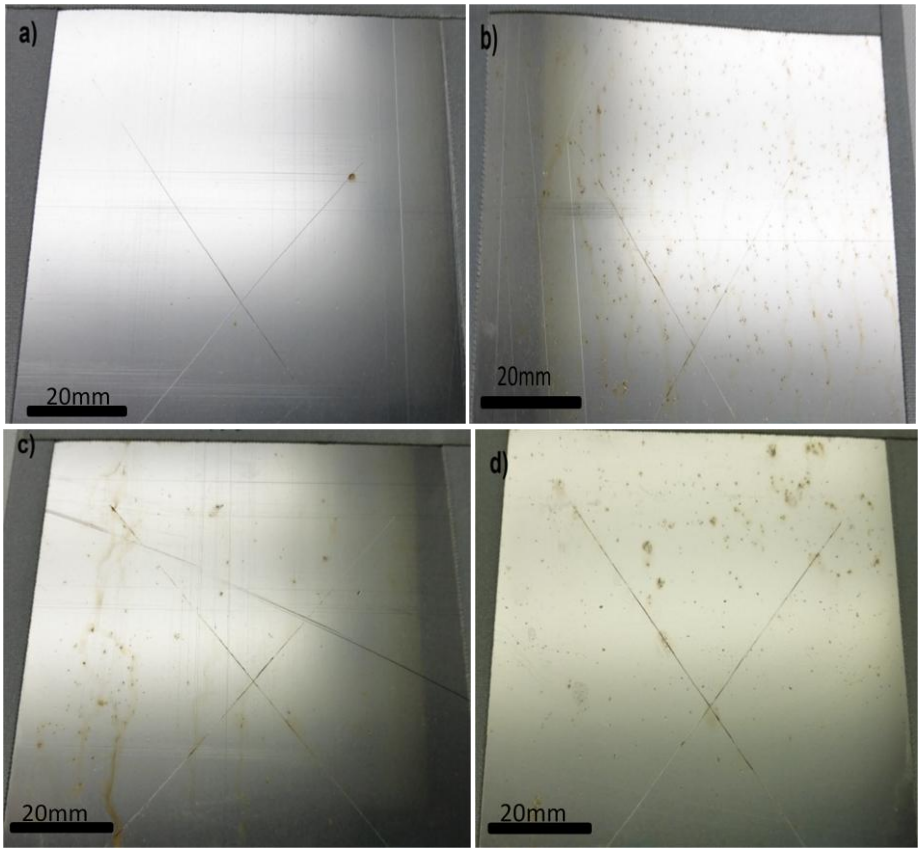

Figure 6.47 Salt spray results at week 3 a) $I_{,B3,0\%,Mix,N2}$ b) $I_{,B3,0\%,Mix,Air}$ c) $I_{,B3,0\%,Ip,N2}$ d) $I_{,B3,0\%,Ip,Air}$

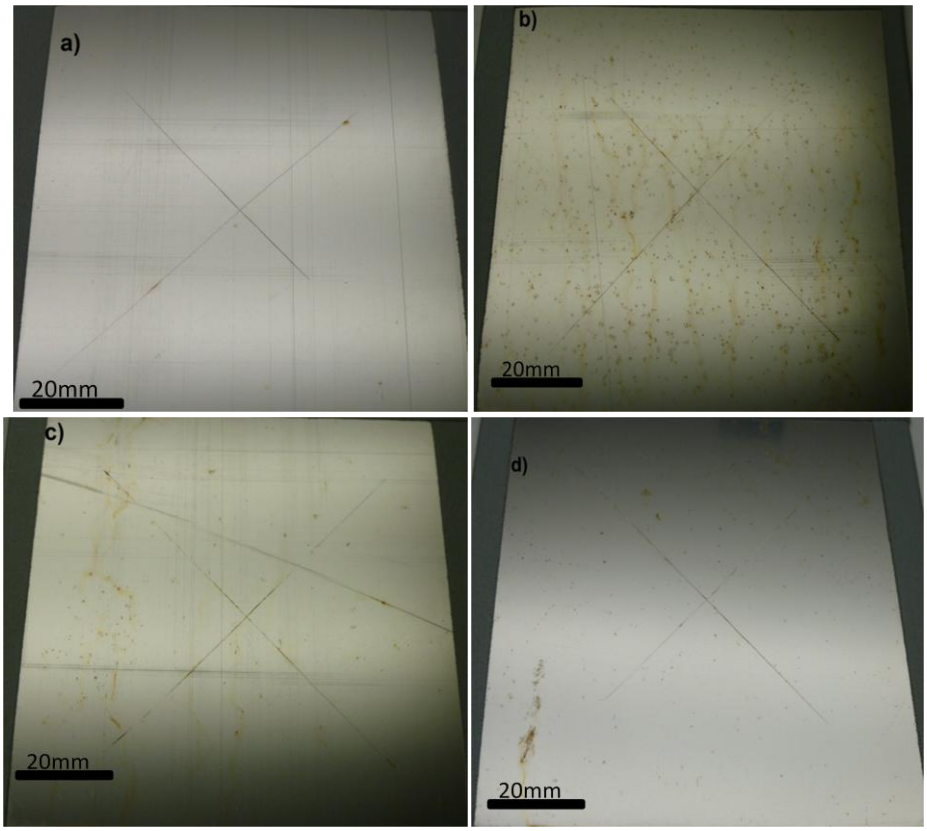

Figure 6.48 Salt spray results at week 5 a) $I_{,B3,0\%,Mix,N2}$ b) $I_{,B3,0\%,Mix,Air}$ c) $I_{,B3,0\%,Ip,N2}$ d) $I_{,B3,0\%,Ip,Air}$

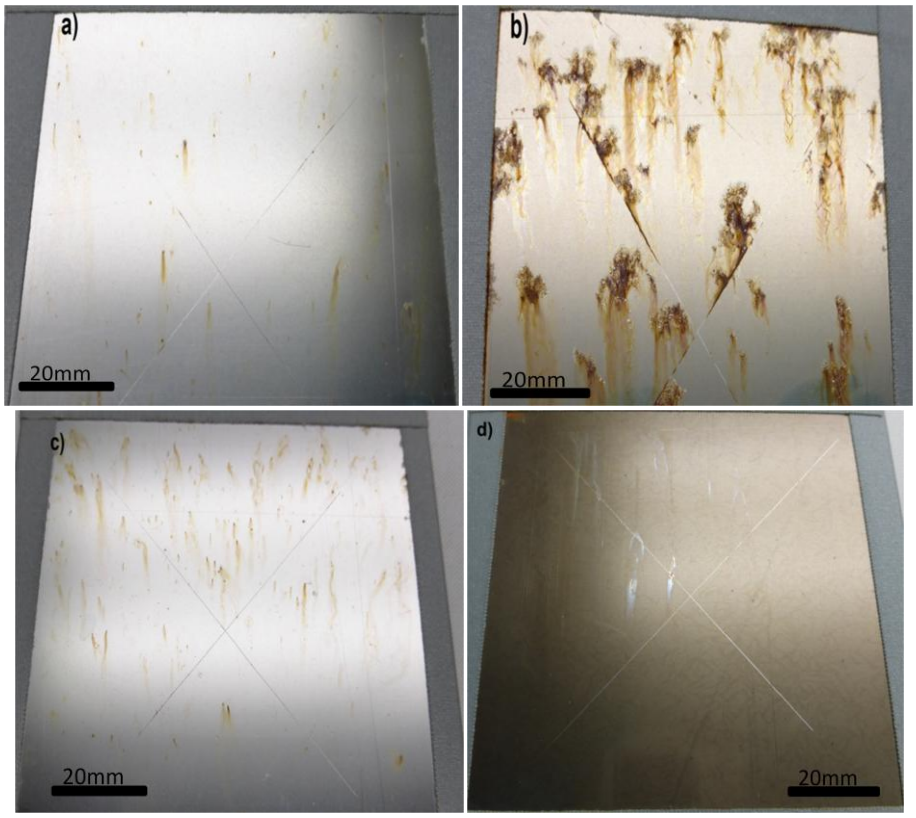

Figure 6.49 Salt spray results at week 3 a) $I_{,B3,2.8\%,Mix,N2}$ b) $I_{,B3,2.8\%,Mix,Air}$ c) $I_{,B3,2.8\%,Ip,N2}$ d) $I_{,B3,2.8\%,Ip,Air}$

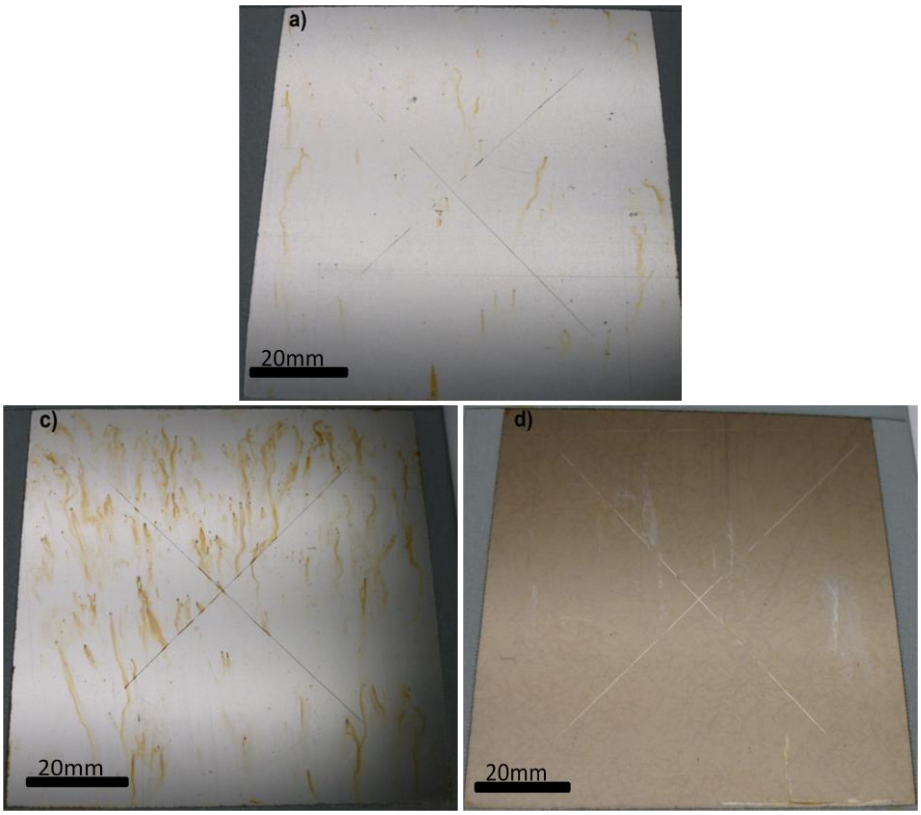

Figure 6.50 Salt spray results at week 5 a) $I_{B3,2.8\%,Mix,N2}$ b) $I_{B3,2.8\%,Mix,Air}$ [Not supplied by the company] c) $I_{B3,2.8\%,Ip,N2}$ d) $I_{B3,2.8\%,Ip,Air}$

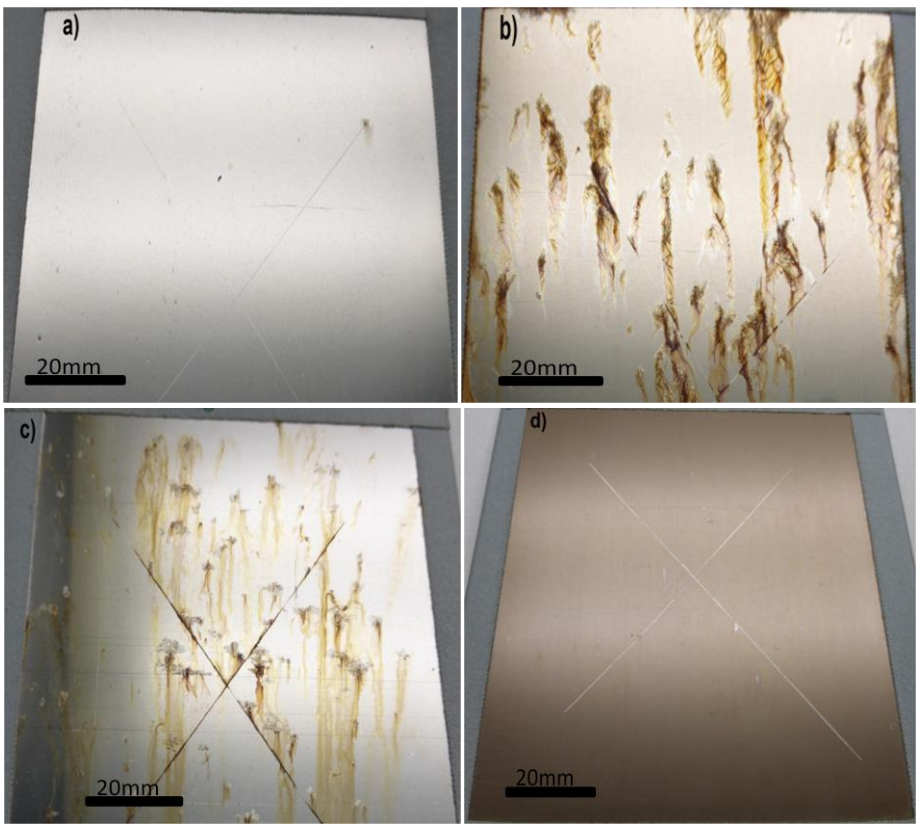

Figure 6.51 Salt spray results at week 3 a) $I_{B3,5.6\%,Mix,N2}$ b) $I_{B3,5.6\%,Mix,Air}$ c) $I_{B3,5.6\%,Ip,N2}$ d) $I_{B3,5.6\%,Ip,Air}$

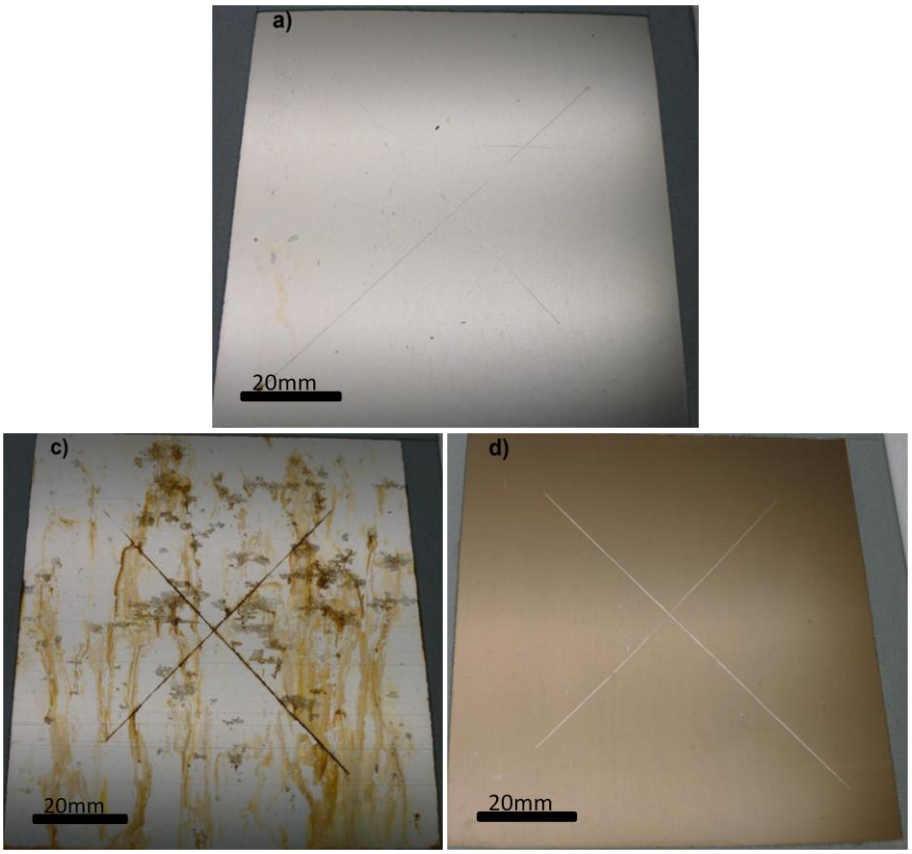

Figure 6.52 Salt spray results at week 5 a) $I_{,B3,5.6\%,Mix,N2}$ b) $I_{,B3,5.6\%,Mix,Air}$ [Not supplied] c) $I_{,B3,5.6\%,Ip,N2}$ d) $I_{,B3,5.6\%,Ip,Air}$

It can be observed that the samples with no doping show good corrosion protection compared to the other samples.

6.6 Erosion Test on Bare Substrate and Coated Sample with Inorganic/Hybrid Sol-Gel Coatings Doped with Titanium Precursor from Batch 2

The durability of the coatings can also be affected depending on the environment. Sand and rain for example can cause erosion which reduces the durability of the coatings. Wear resistance of the coatings has thus been studied through erosion tests.

The following samples were submitted to an erosion test: $I_{,B2,0\%,304}$, $I_{,B2,1.4\%,304}$, $I_{,B2,5.6\%,304}$ and $I_{,B2,11.3\%,304}$. Table 6.1 presents the conditions of the experiment, Figure 6.53 and Figure 6.54 the results.

Table 6.1 Conditions of the erosion experiment

Speed	$15m.s^{-1}$
Temperature	25°C
Acidity	Unbuffered
Sand loading	$1000mg.L^{-1}$
Salinity	No salt
Impinging angle	90°
Test duration	4h
Atmosphere	N_2

The addition of titanium precursor did not improve erosion or impact resistance as Figure 6.53 shows that the mass loss is increasing with the percentage of precursor added. The undoped sample with no doping (0%w/w of precursor) presents a good protection of the coating, the sample being resistant to the erosion test in the condition by having a low value of total weight loss (TWL).

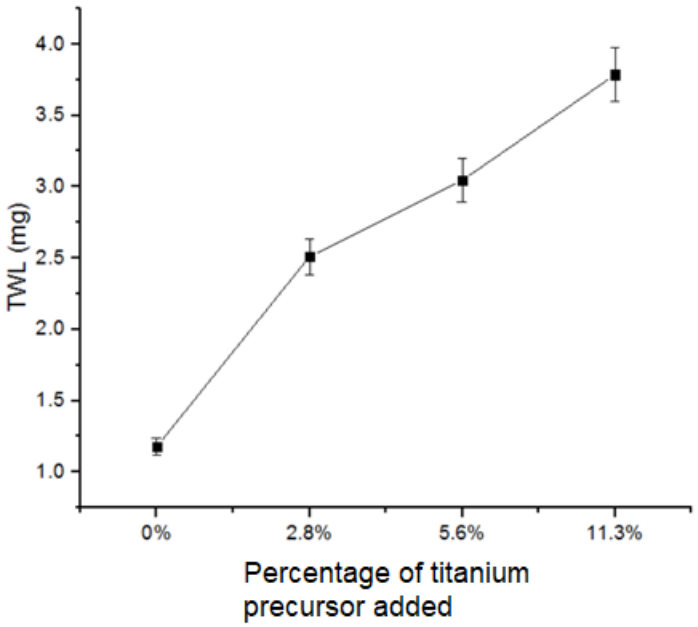

Figure 6.53 Erosion resistance of four different amounts of doping precursor from Batch 2 after 4h erosion tests (sand concentration of 1000mg/L, speed of 15m/s)

The addition of titanium precursor seems to have an influence on this parameter as the average weight loss increases with the percentage of precursor added.

Surface morphology images of the samples after erosion test can be seen in Figure 6.54.

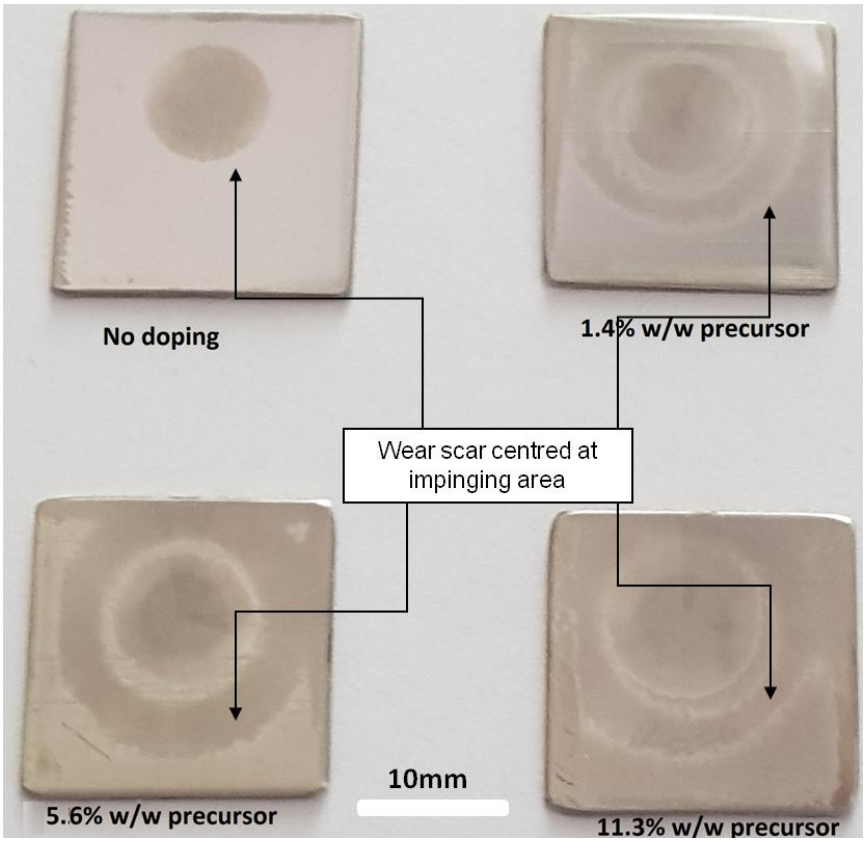

Figure 6.54 Appearance of samples from Batch 2 after the 4h erosion test.

As seen in Figure 6.54, a minor change is observed: after erosion, a slight ring is visible where the sample is in contact with the erosive environment. The sand impact is visible. Some of the coating is slightly removed on the edges of the samples where very few impacts from sand particles occurred. However the main removal is concentrated at the impinging area. Most of the direct impingement was on the undoped sample compared to the other samples were it seems like there was less direct impingement due to the presence of the rings. The coated sample containing no doping presented the lowest mass loss after the test and less noticeable change in its appearance.

6.6 Summary of Chapter VI

The first batch is made of inorganic/hybrid, organic and hybrid/composites samples and tested in aggressive conditions. There are different levels of damage such as little corrosion to coating delaminated and substrate deeply corroded. The most damaged samples had carbon steel as a substrate. The least damaged coatings are from the organic system 2 and from the inorganic/hybrid systems 2, 3, 4 and 5. The

OCP measured showed that with time their values tend to the OCP value of the substrate.

For the second batch, a same silica inorganic/hybrid sol-gel coating is studied on two different substrates: 304 stainless steel and A1008Qpanel. In this case as well the coating on stainless steel showed little to no corrosion while the sample on Qpanel is proven deficient and damaged after the experiment. An experiment has been done on bare substrate and while comparing the values of impedance obtained for both uncoated/coated samples on stainless steel, these values are higher for the coated sample. Then a dopant was added to the coating (titanium butoxide with different amounts). The addition of titanium with the amounts of 2.8%w/w and 5.6%w/w gave results with about the same order of magnitude than without any doping but a higher amount (11.3%w/w) seems to weaken the coating as the values obtained are lower. A hybrid/composites sample of this batch was tested but values lower by 2 orders of magnitude were obtained.

The third batch confirms the presence of titanium and corrosion resistance but different levels of elements expected compared to the added elements. Then were presented the results for different curing environment and different solvents used during the sol-gel process. The samples with same curing process but different solvents usually have the same evolution with equivalent shape for the curves plotted. The samples without doping and with 2.8%w/w present a higher value of resistance compared to higher dopant levels. The highest values would be the samples having the isopropanol as a solvent. The samples cured in air present the lowest resistance. When comparing EIS results and salt-spray test, the combination mixture as a solvent/cured in air have low resistance, high capacitance and the most damaged surface after the salt spray test.

Chapter VII. Characterisation and Properties of the Coatings After Experiment

7.1 Introduction and Chapter Overview

This chapter presents the results of different analyses made on the surface of the samples (SEM, EDX and FTIR) after the immersion of 30 days. It is focused towards the understanding of the mechanisms of corrosion and is in parallel with Chapter V as some of the same methods are used here. It also focuses on Batch 2 and Batch 3. There is no post-test analysis of Batch 1 samples.

Samples were taken during the immersion and others are kept after the immersion in order to obtain more information about the evolution of corrosion. The immersion conditions were the same than for the static corrosion test: CO_2 saturated environment, 3.5% NaCl at 25°C.

7.2 Scanning Electron Microscopy / Energy Dispersive X-Ray Spectroscopy (SEM and EDX) on Samples From Second Batch Before and After Experiment

The SEM is used to visually determine the formation of general corrosion, localised corrosion and deposition of corrosion product on the surface and analyse the surface of the samples. EDX gives information about the surface constituents of samples. This part presents the corrosion product morphology and the observed changes on the surface of the samples when corrosion or damage cannot be visually seen without a microscope.

The top surface of the samples was analysed through the SEM while the chemical composition of the materials was assessed along with their chemical homogeneity through EDX. This method helps to determine the physical degradation of the samples after the immersion of 30 days and to compare the surface of the samples before and after the experiment. The samples presented here are from the second batch.

Figure 7.1 to Figure 7.5 present the percentages of C, Si, Ti and Fe obtained for Day 0 (before immersion), Day 15 and Day 30 of experiment for the samples $I_{,B2,0\%,304}$, $I_{,B2,1.4\%,304}$, $I_{,B2,2.8\%,304}$, $I_{,B2,5.6\%,304}$, $I_{,B2,0\%,304}$ and $H_{,B2,0\%,304}$.

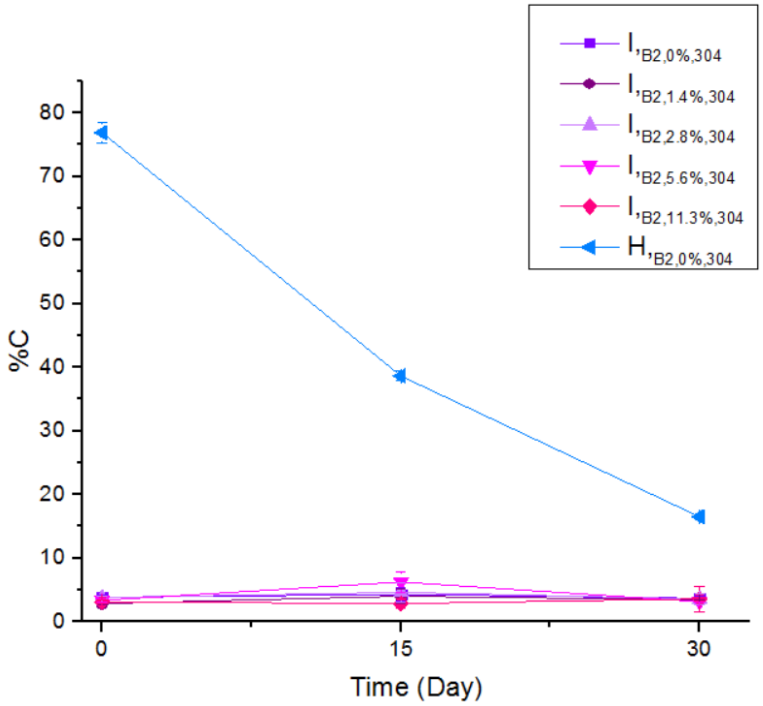

Figure 7.1 Percentage of carbon for the different samples of Batch 2 throughout the experiment

Figure 7.2 presents only the amount of carbon detected for the inorganic/hybrid coatings in order to see if the addition of titanium has an effect on its value.

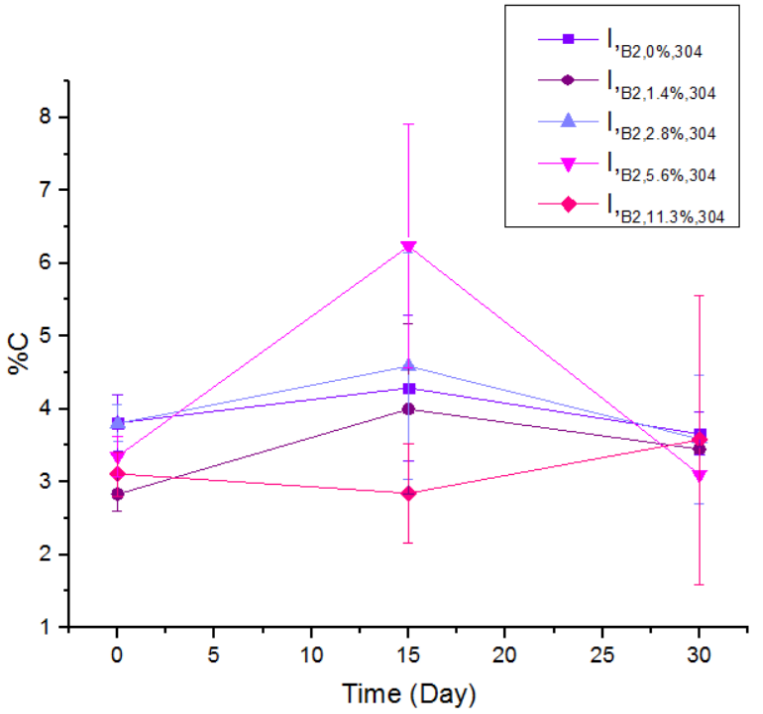

Figure 7.2 Percentage of carbon for the different inorganic/hybrid samples of Batch 2 throughout the experiment

The percentages of carbon is similar throughout the experiment for the inorganic/hybrid sample independent of the percentage of precursor as inorganic/hybrid coating have a low proportion of carbon. The values are lower than 6% for all samples at all times of the experiment. The similarities are clear at the start and end of the experiment but even if the behaviour changes in the middle of the experiment, the difference can come from the error of the measurement since it is only 3%. It is not conclusive enough to say that the titanium precursor has an influence on the carbon percentage. The percentage decreases greatly with time for the hybrid/composites coating. This can be linked to the behaviour of this coating during the experiment which presented poor corrosion resistance. Thus the carbon detected before the experiment, coming from the coating decreases to only be the carbon from the substrate.

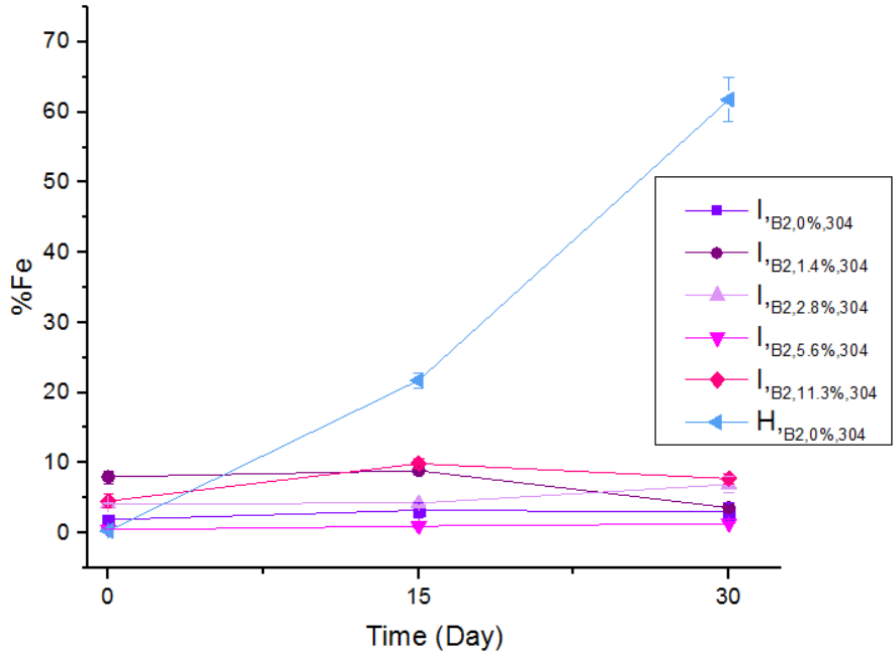

Figure 7.3 Percentage of iron for the different samples of Batch 2 throughout the experiment

The presence of an increasing percentage of iron means the delamination of coating and the apparition of the substrate. The hybrid/composites coating shows a high percentage of iron after immersion meaning that there is barely any coating left as it does not protect the substrate anymore.

The samples coated with an inorganic/hybrid sol-gel coating (from 0%w/w to 11.3%w/w of precursor) presented an amount of iron less than 10% throughout the experiment, with constant amounts. The detection of iron, given the thickness of

coatings and the penetration range of the EDX method does not mean the detection of failure.

The percentage of silicon is presented in Figure 7.4. It is higher than 40% for all different types of inorganic/hybrid sol-gel coatings while presenting a lower value for the hybrid/composites sample.

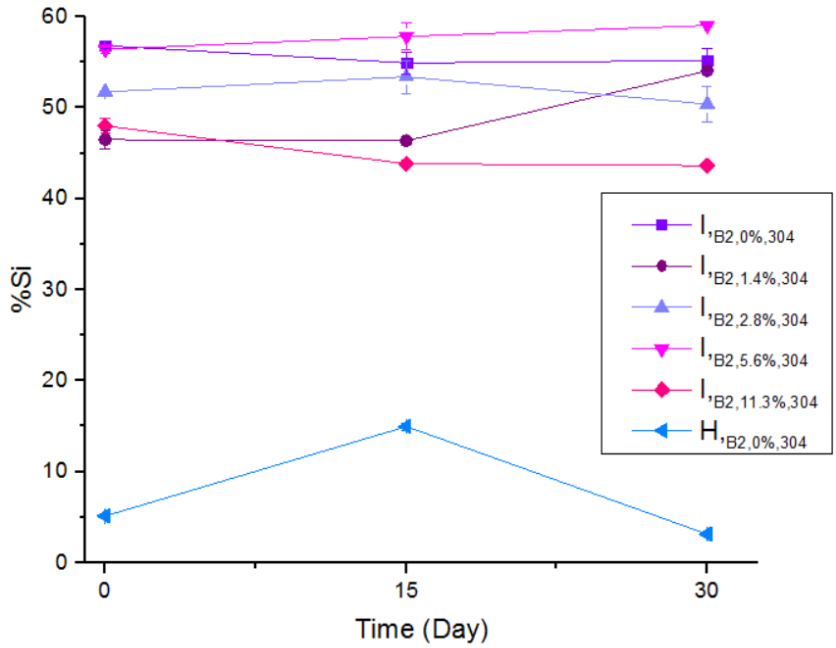

Figure 7.4 Percentage of silicon for the different samples of Batch 2 throughout the experiment

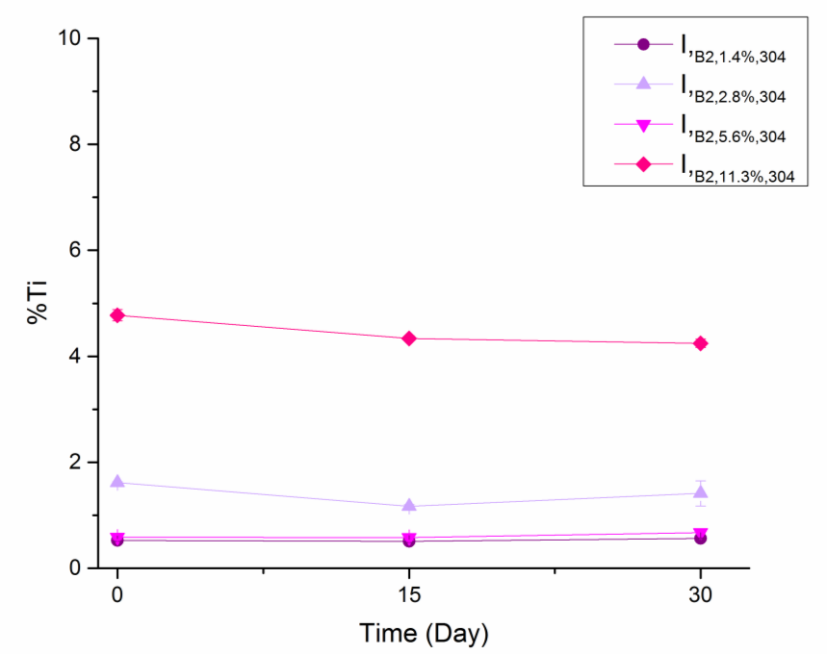

Figure 7.5 Percentage of titanium for the different samples of Batch 2 throughout the experiment

Figure 7.3 gives information about corrosion as the percentage of iron increases with time which means that the substrate becomes apparent, the coating either being damaged or delaminated. In Figure 7.1 the percentage of carbon, in the case of the hybrid/composites sol-gel coating sample, decreases with time which also mean that the coating has been damaged and the substrate is detected. The percentages of titanium for the different doped samples keep a regular value throughout the experiment.

Figure 7.6 presents an example of the scanned EDX image of the hybrid/composites sample $H_{,B2,0\%,304}$ after immersion and presents iron on the main part of the scanned part. This sample had the more degradation and corrosion. The image shows that the coating does not protect the whole surface of the substrate as iron can be detected.

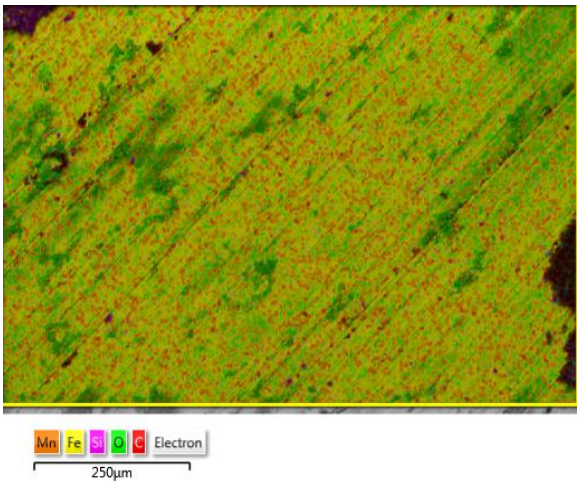

Figure 7.6 EDX image of $H_{,B2,0\%,304}$ after immersion

After 30 days of immersion in the aggressive environment, the surface of the coating has been totally delaminated and the chemical composition confirms this with the amount of iron present on the surface.

In Figure 7.7 are presented the SEM images according to evolution of time in order to compare the different samples and the evolution of their surfaces such as levels of degradation. Some asperities can be seen on the surface of the samples before any immersion, which means that it can be more inclined to corrosion.

The observation of the images for the non-doped sample $I_{,B2,0\%,304}$ showed general corrosion and clusters of shallow pits/localised corrosion on the surface of this sample after being in contact with the corrosive environment for 30 days.

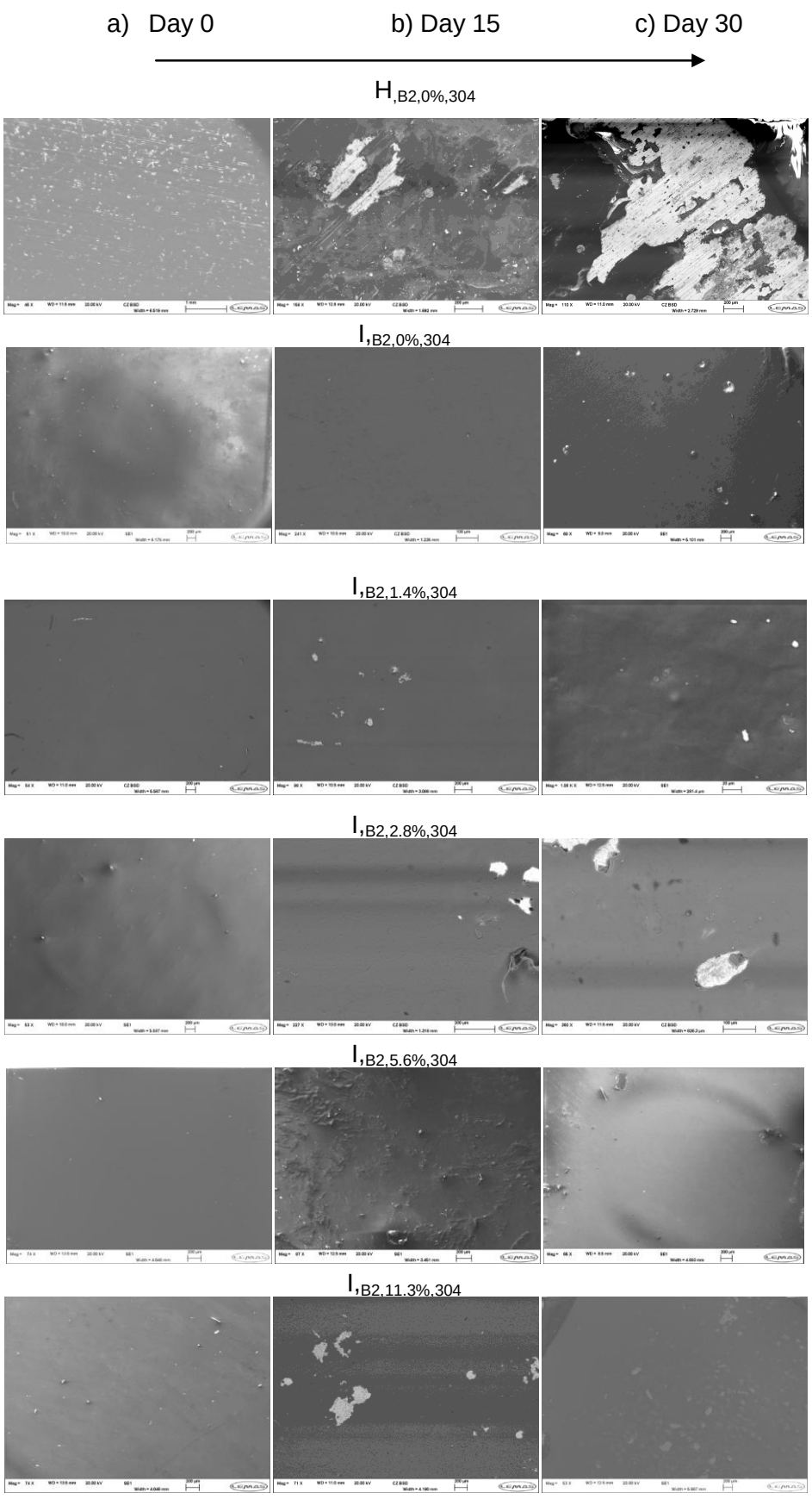

Figure 7.7 SEM images of the samples of Batch 2 throughout the immersion

For the sample with 1.4%w/w precursor $I_{,B2,1.4\%,304}$, before any immersion, the surface does not show many asperities and the surface of the coating seem homogeneous. After immersion the sample shows some signs of corrosion on some definite spots of the surface but only on a small portion. The remaining surface of the sample does not appear to be damaged.

The majority of the surface of the sample doped with 2.8%w/w precursor $I_{,B2,2.8\%,304}$ appears smooth while some asperities are showing on some points before any experiment but despite this only a small part of the sample presents corrosion and the iron of the substrate after immersion.

The surface of the sample doped with 5.6%w/w $I_{,B2,5.6\%,304}$ appears to be rather smooth; then after the experiment the coating shows corrosion products on some areas of the coating.

For the sample with 11.3%w/w titanium precursor $I_{,B2,11.3\%,304}$, the surface of the coating does not appear as smooth as some products and cracks can been seen before the immersion. This sample presents signs of corrosion spread everywhere on the coating and iron from the substrate is detected on some damaged areas.

7.3 Fourier-Transform Infrared Spectroscopy (FTIR) on Undoped Inorganic/Hybrid Coated Sample and Sample with Inorganic/Hybrid Coating Doped with Titanium Precursor

FTIR can be used to identify any chemical bond that may exist on the surface of the tested samples. In this part are presented the results obtained from FTIR analyses. The main results show data in the middle of the immersion and after the experiment to see the evolution of the functional groups and water uptake if present. The data obtained for Day 0, Day 15 and Day 30 are all displayed in a same graph to see the evolution of the composition of the surface in appendices E and F. The FTIR spectra collected at initial and after certain time intervals of 15 and 30 days are plotted. Day 0 means that the sample has not been immersed and has not been in contact with the synthetic sea-water. The FTIR spectra are all taken in the range wavenumber of 600-4000 cm^{-1}.

All the inorganic/hybrid sol-gel coatings were prepared with the same bases and had similar functional groups detected through FTIR to form a general structure, with

appearance of different peaks according to the type of doping or additives. Then, after immersion and according to their different anti-corrosion properties, there was presence of peaks linked to groups for water uptake and/or presence of corrosion in the case of corroded sample or presence of water adsorbed.

The FTIR spectrum of the undoped inorganic/hybrid sol-gel coating $I_{,B2,0\%,304}$ at Day 0 has been detailed in Chapter V and is used as a reference sample for its structure.

Figure 7.8 presents the spectrum for $I_{,B2,0\%,304}$ after 30 days of immersion in the salt water.

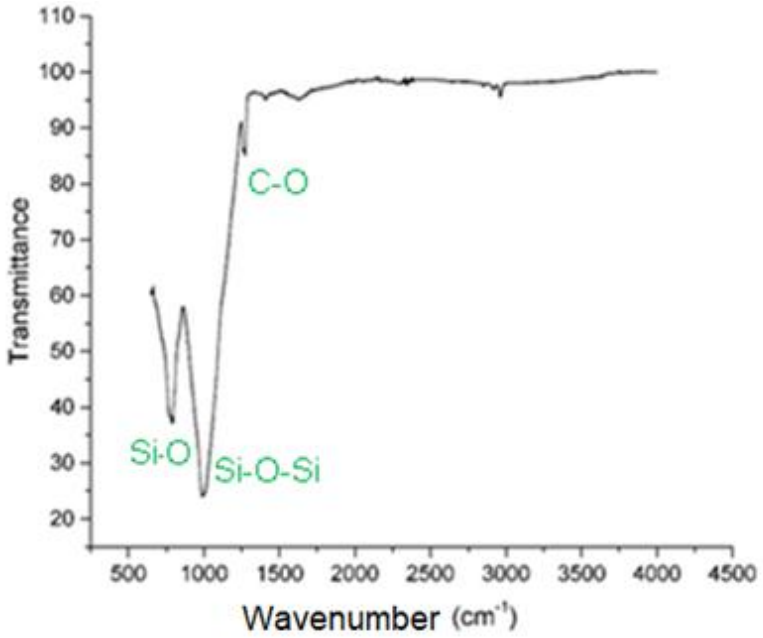

Figure 7.8 FTIR spectrum of $I_{,B2,0\%,304}$ Day 30

No additional peak at 3400cm^{-1}, which assigned to O-H stretch band in water, is detected after exposure of the coating to sea water in the case of this sample. This implies that water does not contribute to the chemical structure of the coating following the immersion in synthetic sea-water as there is no adsorption of water. The functional groups which are detailed as present on Day 0 are still present at Day 30.

Figure 7.9 presents the FTIR spectra of the sample doped with 2.8%w/w titanium precursor, $I_{,B2,2.8\%,304}$.

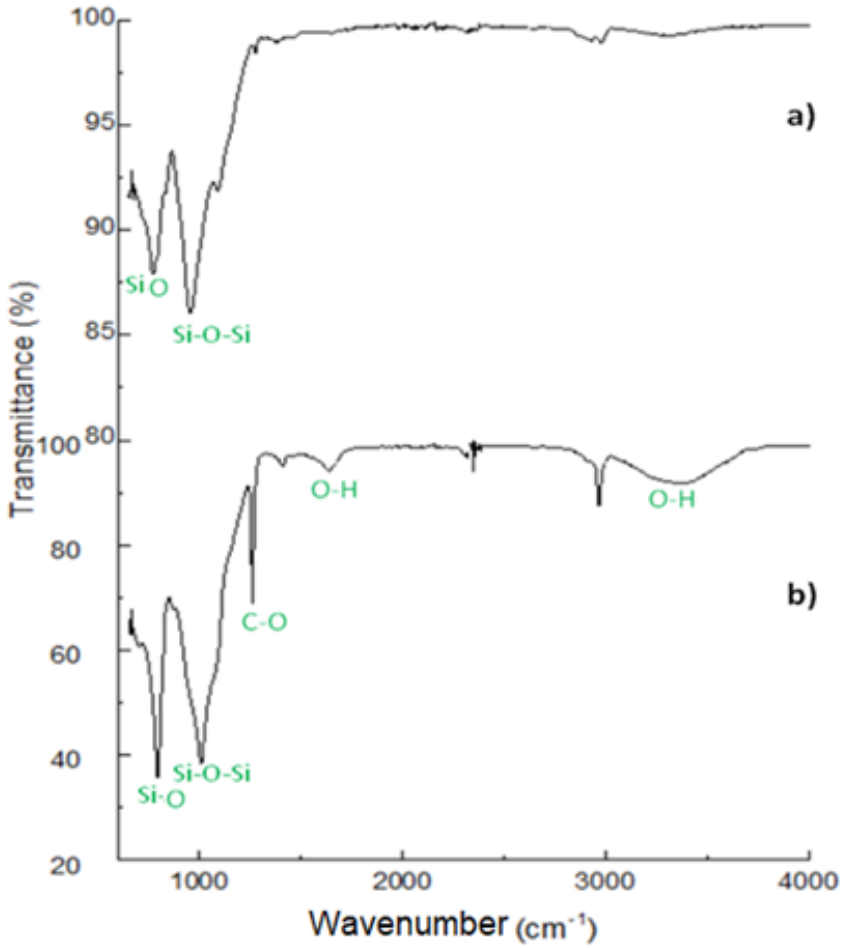

Figure 7.9 FTIR spectra of $I_{,B2,2.8\%,304}$ a) Day 0 b) Day 30

There are additional peaks linked to the doping with titanium in the system:

This sample, as opposition to $I_{,B2,0\%,304}$, shows peaks related to a damaged coating after immersion. There is a peak at 3400cm^{-1}, assigned to O-H stretch band in water which is detected after exposure of the coating in the experimental environment, meaning that there is presence of water, as well as an additional peak at about 1600cm^{-1} after immersion linked to the –OH group of water.

There is a slight peak at 2400cm^{-1} which can be attributed to Ti-O groups before immersion, but also to presence of CO_2 after immersion.

The presence of corrosion can also shift the peaks slightly in the spectra.

The rest of the samples of Batch 2 and Batch are presented in Figure 7.10 to Figure 7.14.

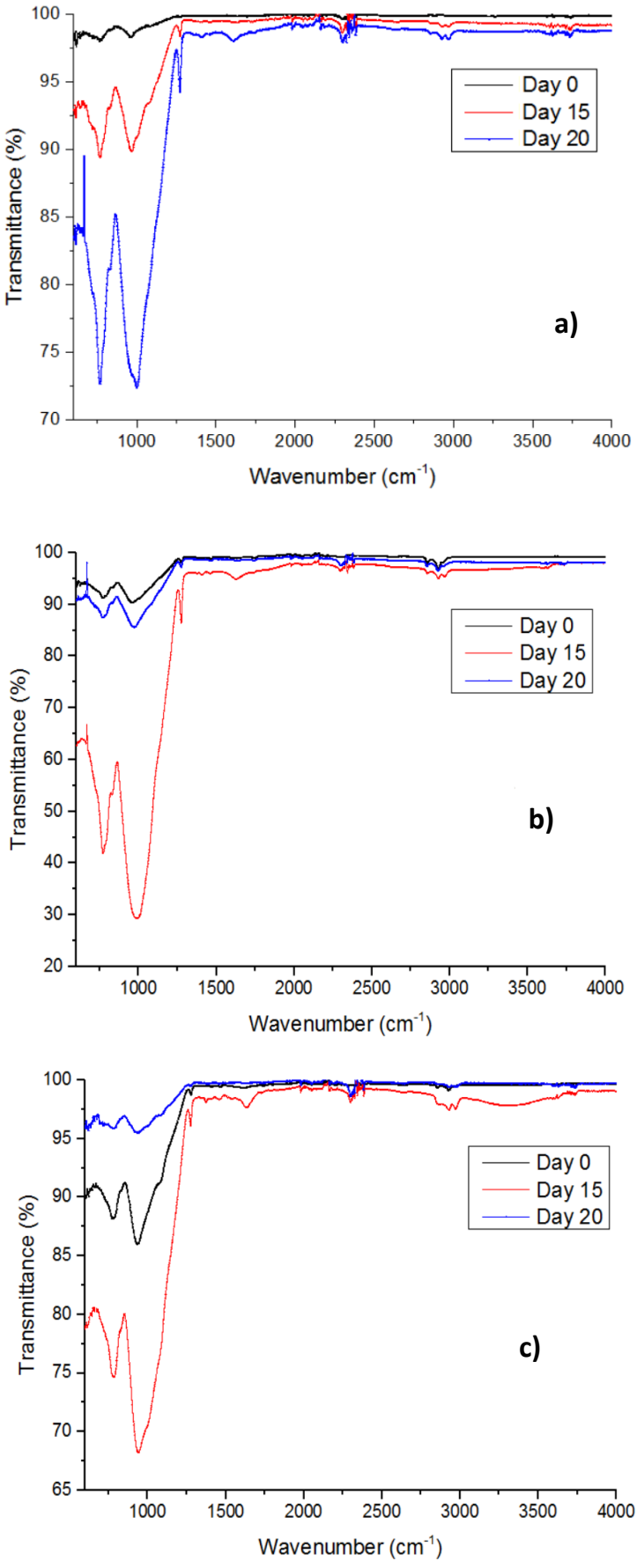

Figure 7.10 FTIR spectra of a) $I_{,B2,0\%,304}$ b) $I_{,B2,1.4\%,304}$ c) $I_{,B2,5.6\%,304}$

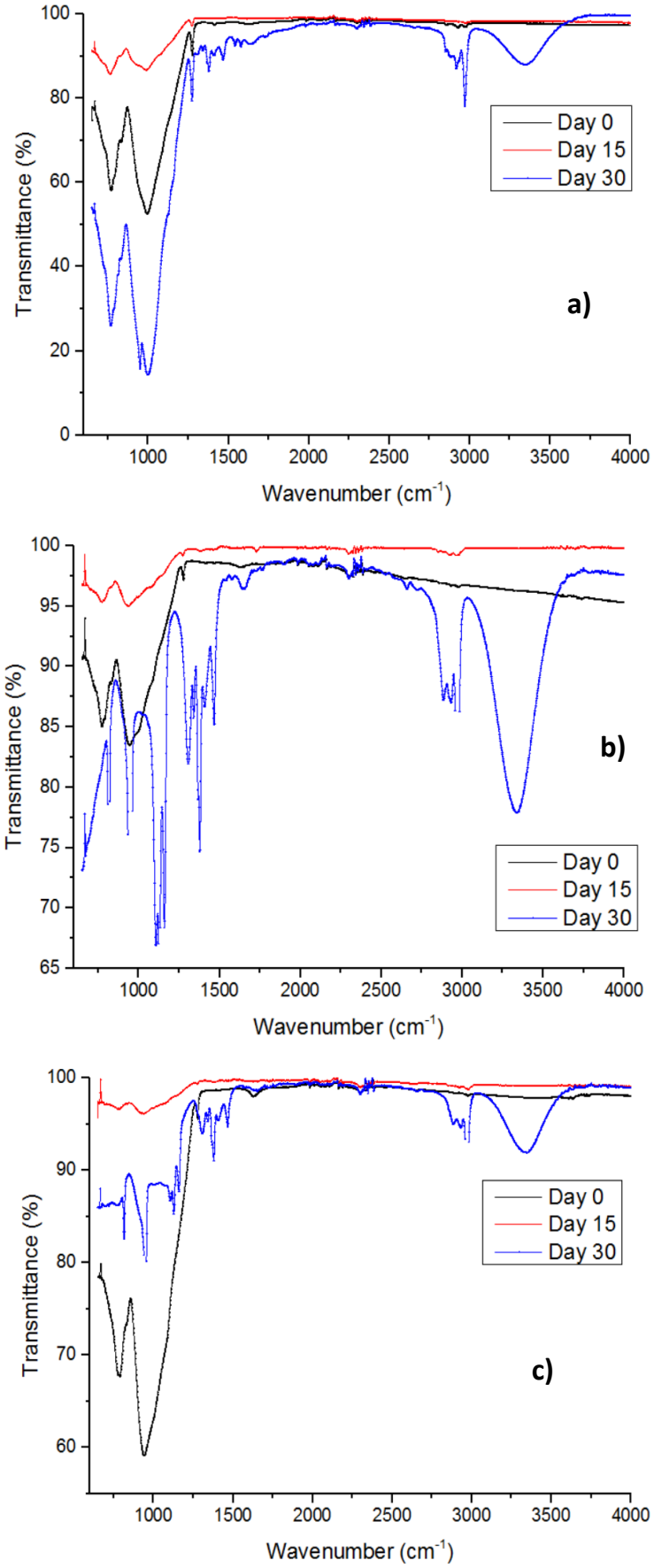

Figure 7.11 FTIR spectra of a) $I_{,B3,0\%,Ip,N2}$ b) $I_{,B3,2.8\%,Ip,N2}$ c) $I_{,B2,5.6\%,ip,N2}$

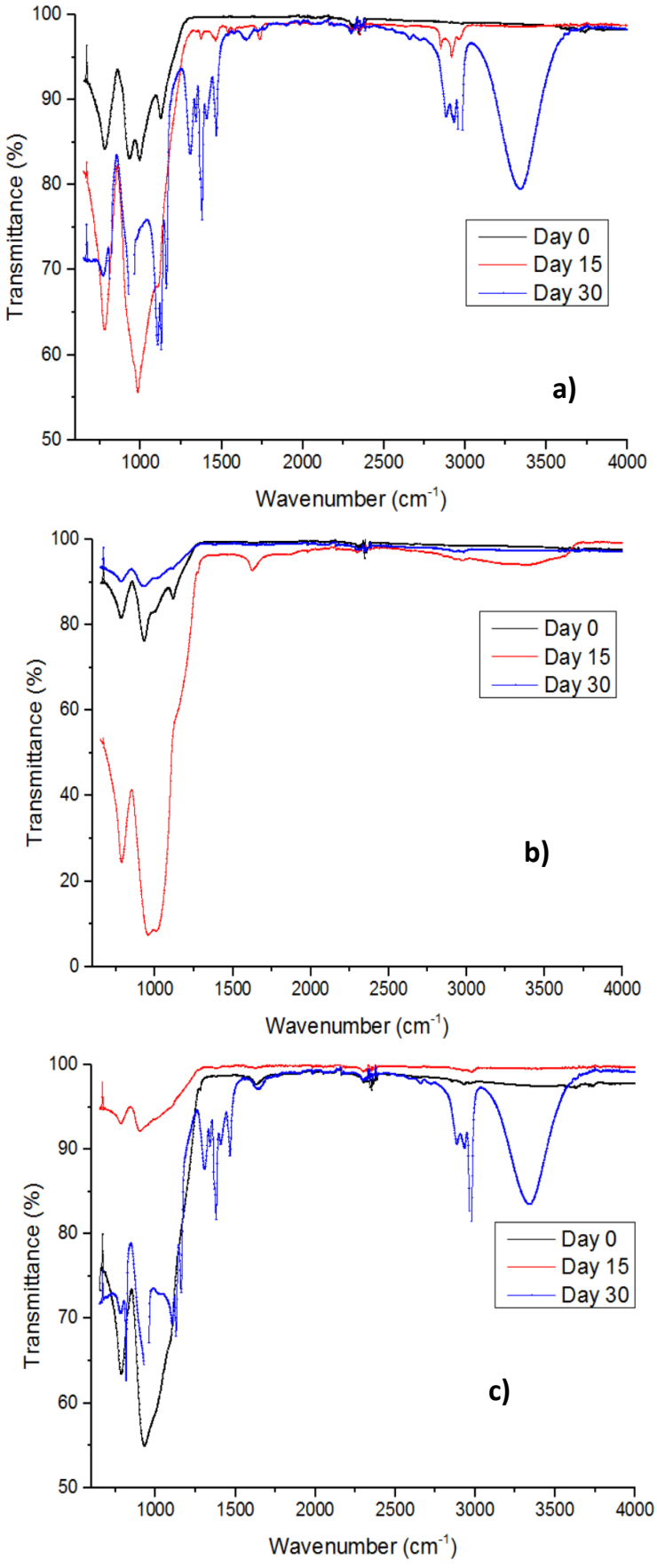

Figure 7.12 FTIR spectra of a) $I_{,B3,0\%,Ip,Air}$ b) $I_{,B3,2.8\%,Ip,Air}$ c) $I_{,B2,5.6\%,Ip,Air}$

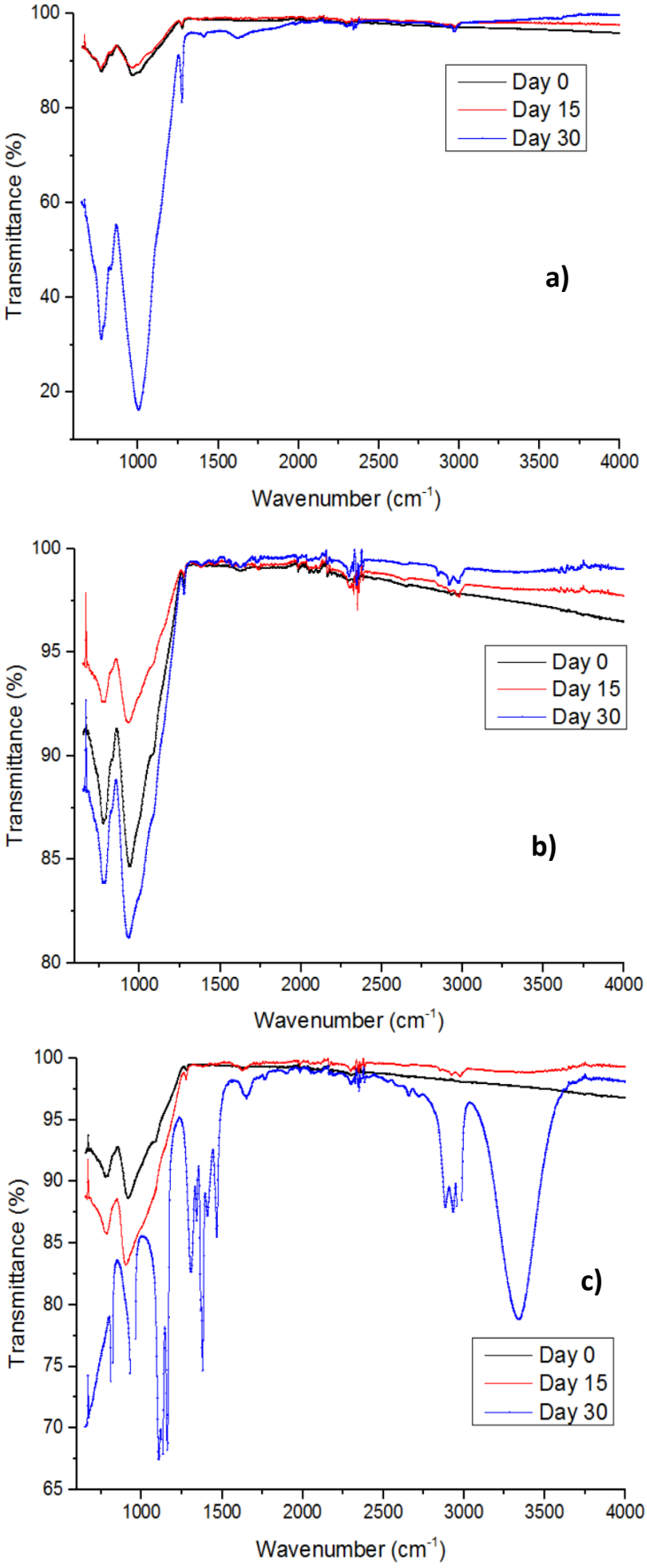

Figure 7.13 FTIR spectra of a) $I_{,B3,0\%,Mix,N2}$ b) $I_{,B3,2.8\%,Mix,N2}$ c) $I_{,B2,5.6\%Mixp,N2}$

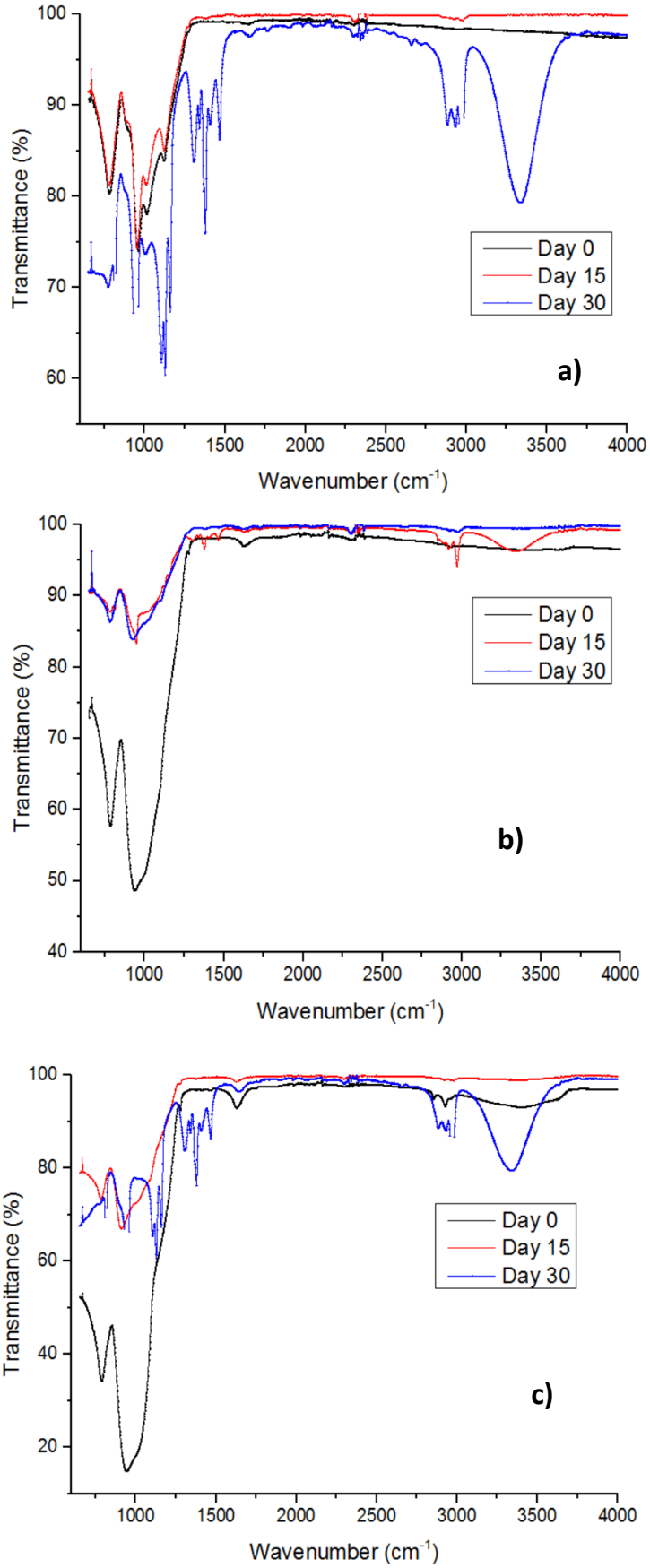

Figure 7.14 FTIR spectra of a) $I_{,B3,0\%,Mix,Air}$ b) $I_{,B3,2.8\%,Mix,Air}$ c) $I_{,B2,5.6\%,Mix,Air}$

Most of the samples present signs of water uptake during or after the experiment: $I_{,B2,2.8\%,304}$, $I_{,B2,11.3\%,304}$, $I_{,B3,0\%,Ip,N2,}$ $I_{,B3,0\%,Ip,Air}$, $I_{,B3,0\%,Mix,Air}$, $I_{,B3,2.8\%,Ip,N2}$, $I_{,B3,2.8\%,Ip,Air}$, $I_{,B3,2.8\%,Mix,Air}$, $I_{,B3,5.6\%,Ip,N2}$, $I_{,B3,5.6\%,Ip,Air}$, $I_{,B3,5.6\%,Mix,N2}$ and $I_{,B3,5.6\%,Mix,Air}$. The water can be significant and growing as a function of time which could also indicate a swelling of the coating.

$I_{,B2,0\%,304}$, $I_{,B2,1.4\%,304}$, $I_{,B2,5.6\%,304}$, $I_{,B3,0\%,Mix,N2}$ and$I_{,B3,2.8\%,Mix,N2}$ do not seem to change in peak appearance throughout the immersion.

$I_{,B3,5.6\%,Mix,N2}$ and $I_{,B3,5.6\%,Mix,Air}$ present peaks which can be ascribed as –OH at 3300-3500cm^{-1} and –C-O at 1200-1300cm^{-1}. $I_{,B3,0\%,Ip,Air}$, $I_{,B3,2.8\%,Ip,N2}$, $I_{,B3,5.6\%,Ip,N2}$, $I_{,B3,5.6\%,Ip,Air}$, $I_{,B3,5.6\%,Mix,N2}$ and $I_{,B3,5.6\%,Mix,Air}$ show these peaks too and in addition C-O-C (stretch) at 750-850cm^{-1} ([180, 231, 232]).

The two samples cured in N_2 did not present any peaks of water uptake unlike the two samples processed with the same system but cured in air.

The samples with 0%w/w, 2.8%w/w and 5.6%w/w of titanium precursor are chosen to be focused on in the new batch because of the favourable results obtained in the precedent batch.

7.4 Summary of Chapter VII

In this chapter, the coatings are analysed through different methods both before and after the immersive experiment of 30 days.

The EDX is used in order to have information about the evolution of certain elements (Si, Ti, Fe and C) on the surface of the samples from Batch 2 to follow the degradation of the coating. A decrease in carbon for the hybrid/composites sample means the degradation of the coating while an increase in iron means a damaged coating and the apparition of the substrate for all sol-gel coatings. The inorganic/hybrid sol-gel coatings display a stable value of iron throughout the experiment, which means that the coating has not been damaged, or barely. The hybrid/composites sample on another hand, presented a high percentage of iron leading to presence of corrosion.

The SEM is also used to follow the evolution of corrosion on the surface of the samples after the immersion of the samples in a mildly corrosive environment. Some

samples presented a damaged coating and a corroded substrate while others appeared partially damaged.

The FTIR spectra present the evolution of the functional groups of the surface of the coating with additional peaks being added in case of damage. Some similarities can be found depending on the percentage of titanium precursor, curing process or solvent being used during the sol-gel formation.

Chapter VIII. Summary of Overall Results and Discussion

8.1 Introduction

When the integrity of a material is affected by the external action of the environment, it may become necessary to protect it. Application of coatings is the most suitable route to protect the metallic surfaces. Coatings designed for corrosion protection must offer an effective physical barrier [108]. Application of functional coatings is one of the most promising routes to develop high-performance anti-corrosion systems for diverse sectors.

The objectives of the work presented in this thesis were to provide an understanding of the evolution of corrosion of metal substrates coated with specific coatings by combining *in-situ* and *ex-situ* methodologies. In order to be able to use these coatings in specific environments for an optimum result, it is important to understand the mechanisms of corrosion and degradation. The use of different methodologies allows the examination of different perspectives and aspects of these mechanisms.

The samples of this project are divided in three batches. The first batch of samples contains different systems of coatings: 2 hybrid/composites, 5 inorganic/hybrid and 2 organic systems of coatings deposited on either carbon steel X65 or 316L stainless steel. Batch 2 is formed of 6 silica inorganic/hybrid sol-gel coatings and one hybrid/composites sol-gel coating with different natures of doped precursors: aluminium pigments, titanium butoxide (4 different percentages) or no doping. The substrate of the majority of the samples was changed to 304 stainless steel by EPG (sponsor company). Batch 3 is made of 20 silica inorganic/hybrid sol-gel coatings with different percentages of titanium butoxide as the doping precursors. Two parameters were changed then: the solvent used for the formulation of the sol-gel and the curing process. The substrate of the majority of the samples remained 304 stainless steel. The samples are either prepared with a solvent mixture (Ethanol EtOH, Isopropanol IpOH and Butanol BuOH) or prepared with isopropanol only as solvent. The samples were either cured in N_2 or in air. There is no chemical link between Batch 1 and batches 2 and 3.

The characterisation of the coatings has been introduced in Chapter V while the performance of these coatings has been evaluated and presented in Chapter VI. The characterisation related to post-experiment has been presented in Chapter VII.

This chapter discusses the key findings of the study in relation to the literature review. The focus will firstly be on the mechanical durability and the influence of the composition of the samples. Then the study will continue by presenting a time evolution of the Electrochemical Impedance Spectroscopy (EIS) trends from the experiment across the different batches to determine the time of failure and understand the degradation of the coatings. A comparison of results introduced in Chapter V to Chapter VII is then presented, which could establish factors relating the performance of the coatings to their morphologies.

8.2 Composition of Samples and Influence on Mechanical Properties

In the first batch, 4 of 5 inorganic/hybrid coating systems (systems 2 to 5) displayed extremely low adhesion between the coating and the carbon steel X65 substrate so the samples could not be tested at all (samples were not sent to be experimented).

Values for the organic system 1 are low regardless of the substrate (less than 1N) while for the organic system 2 it is the opposite but the values are close to 5N so the adhesion is better for these systems. The hybrid/composites system 2 has the highest values with an average of 7.5N. The higher the value, the better the adhesion. Thus the hybrid/composites system 2 has the best adhesion compared to the other tested systems which can be correlated to. This is in accordance with the literature [66, 72] since organic-inorganic hybrid coatings are supposed to have their scratch resistance improved as well as their adhesion to the metal substrate due to the inorganic part. Inorganic coatings have excellent mechanical properties but generally do not support impacts without breaking [233]. For the inorganic/hybrid samples it seems that the substrate has an influence on the adhesion as there was no adhesion for 4 of the systems on carbon steel X65 and inorganic/hybrid system 1 on X65 has a value which is less than half of the value obtained for the same system on 316L stainless steel. The inorganic/hybrid systems on carbon steel were then abandoned for the next batches as it is known that silica sol-gel coatings rarely provide durable bonds on carbon steel. Moreover the pre-treatment seems to have an impact on the inorganic/hybrid systems and their critical load which can present up to 2N of difference between a same coating system on a same substrate. There seem to be little to no effect for the hybrid/composites and organic systems.

The values in literature are not consistent as sol-gel coatings such as ZrO_2-CeO_2 coating have displayed a value of about 15N [234]; values from hybrid sol-gel coating containing between 30% and 60% of TEOS go from 5N to 8N while a derived coating with silica nanoparticles reduced this value to 0.2N [235]. Sol-gel SiO_2-TiO_2 mixed films have similar values (between 6N and 9N) [236]. However some works on sol-gel derived hybrid coatings have presented critical loads with values as low as 0.2N to 0.5N [193, 237]. Epoxy coatings can present low loads such as 0.630N [233].

The samples tested for Batch 2 are: hybrid/composites coating on 304 stainless steel, inorganic/hybrid coating with no doping on both substrates, A1008Qpanel and 304 stainless steel; and one sample from the inorganic/hybrid coating with doping in order to compare the values and influence of nature of coating and substrate. The values of critical loads are below 5N. The hybrid/composites sample of this batch has a critical load value of less than 1N which is really low for an hybrid/composites coating. There seems to be an improvement from A1008Qpanel steel as a substrate (3N) to 304 stainless steel (4.5N). The inorganic/hybrid samples with or without any doping have a similar value of critical load, both about 4.5N. Contrary to Batch 1 where the hybrid/composites coatings had the highest values of critical load, in Batch 2 the value for the hybrid/composites sample is barely 1N.

For Batch 3, all the results present a low critical load, close to 5N for only one sample, $I_{,B3,2.8\%,Mix,N2}$ while the others are closer to 2N. While these samples have shown to be resistant to corrosion through the electrochemical experiment, the adhesion of the coatings are low.

The samples $I_{,B3,0\%,Mix,N2}$ and $I_{,B3,0\%,Mix,Air}$ have a similar value of about 2N while $I_{,B3,2.8\%,Mix,N2}$ displays a value of about 5N which is more than twice as much as $I_{,B3,2.8\%,Mix,Air}$ (2N). Except for $I_{,B3,2.8\%,Mix,N2}$ the values presented do not differ much from one another. Works with similar coatings and same solvents presented different results as well so the solvent does not seem to have an important effect on the adhesion [193, 236].

The substrate has an influence on the adhesion of the coatings tested as well as the formulation of the coating but not the amount of precursor added.

Adhesive failure is often a two-stage process. When a coating/substrate system is under sufficient tensile stress it becomes energetically favourable for through-thickness cracks to develop in the coating [238]. This could be witnessed for

samples containing 11.3%w.w of titanium precursor as presented in Figure 5.15. Since the cracks appear only for this amount, it can mean that there is an optimum concentration of precursor to be added and would lead to more stress in the coating if exceeded. Cracks preferentially initiate at coating defects. A through-thickness crack will result in a stress concentration at the corner of the coating adhering to the interface. The crack may therefore propagate along the coating-substrate interface, relieving this stress concentration, propelled by the elastic energy released by the through-thickness cracking event [131, 239].

Organic system 2 from Batch 1 had an important thickness and a higher critical load compared to the inorganic/hybrid samples but not compared to the hybrid/composites samples. The thickness of the inorganic/hybrid coatings was between 3µm and 12µm. The thickness of the coating influences its cracking. However it is not related to its toughness alone but by a combined action of the coating (when considered as thin) and the substrate [240]. The wedge crack firstly forms at the weak coating/substrate interface ahead of the moving indenter due to compressive shear stress. The continued forward motion of the stylus increases the stress and leads to the growth of the interfacial cracks. Eventually the built-up high compressive stress lifts and bends the coating and results in spallation. Such spallation behaviour during the scratch test is often observed on brittle coatings with weak interfacial adhesion to the substrates. Spallation/cracking was observed on inorganic/hybrid systems 1, 3 and 4, both hybrid/composites systems of Batch 1 as well as inorganic/hybrid coatings from batches 2 and 3.

In general, for ductile failure the area of uncovered substrate is small and confined within the track, whereas brittle failure is associated with harder coatings substrate materials. However, some materials such as stainless steel can present both brittle and ductile behaviour, depending on sample preparation [198]. For ductile substrates, interfacial failure can occur for both tensile and compressive stresses if the interfacial adhesion is poor, but failure tends to occur within the coating if the adhesion is good. For brittle substrates, interfacial decohesion can be observed for both tensile and compressive stresses as well if the adhesion is poor. However there is a probability for interfacial cracking to happen for tensile stresses even if the adhesion is acceptable [198].

Large area of spallation occurs if the adhesion is poor or if the residual stress level in the coating is high. In this case, when the tip is in contact with the coating at the start of the track or at some point along the scratch, a crack is formed at the coating-

substrate interface which propagates a considerable distance either side of the track before coming to a halt [198].

Chapter V displayed that the brittleness decreased while the percentage of precursor is increased but stayed low after 5% (Figure 5.33) but the values are still close to one another (between 0.018 and 0.013). Erosion resistance is tested as well and the comparison of both parameters is presented in Figure 8.1.

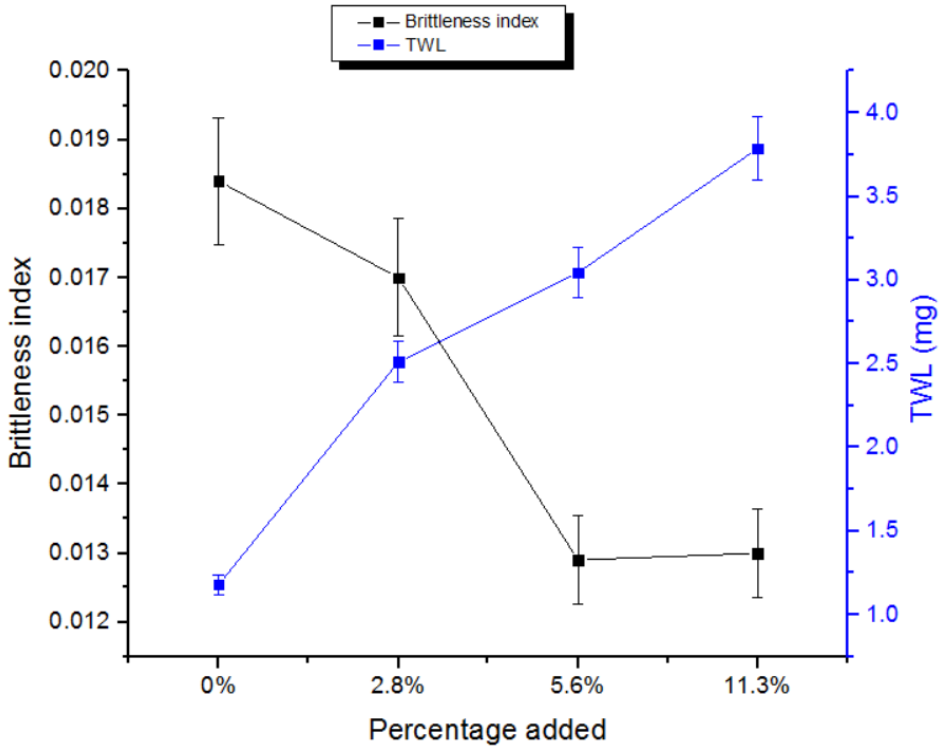

Figure 8.1 Comparison of brittleness and erosion resistance for different amounts of precursor in Batch 3

The increase in precursor percentage did not improve the erosion resistance as the total weight loss increases with its percentage from 1.25mg for 0% (no doping) to 3.75mg for 11.3%w/w but it seems to have a slight improvement on the brittleness index. These results do not correlate as it would be expected that an increase in doping precursor would lead to enhanced hardness [131] and wear resistance but only an enhanced elasticity is witnessed until a threshold is reached. Other works [241-243] showed that cracking is connected to the hardness measurements, including for ceramics and glasses. Takadoum and Bennani [244] explain that the scatter of values for a same coating in the literature is due to authors not taking into account the influence of the substrate in the hardness measurements so this is also a factor important for brittleness.

8.3 Time Evolution of the EIS Trends

The equivalent circuits which can be used for the fitting of data of coated steel are presented in Figure 8.2.

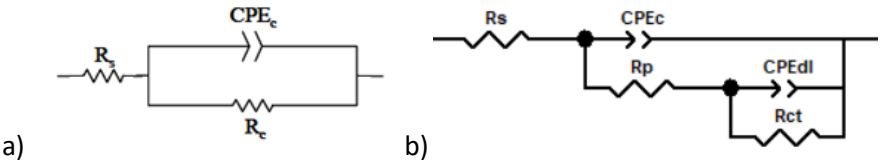

Figure 8.2 Equivalent circuit for coated stainless steel a) before exposure b) after immersion

R_s solution resistance, is the Ohmic resistance of the electrolyte between the working and reference electrode [169] while R_c is the coating resistance, resistance of the ion conducting paths developed in the coating. As mentioned earlier, a constant phase element of the coating, CPE_c, is used instead of the ideal capacitance C, to take into account the irregularity and inhomogeneity of the surface and varying of thickness of the coating. It is used for the fitting if the data presenting a clear and defined semi-circle as their Nyquist plot.

CPE are still used instead of ideal capacitance as Bode plots can present responses with behaviour of non-ideal capacitance.

R_pCPE_c represents the response of the outer coating while $R_{ct}CPE_{dl}$ represents the electrochemical reactions at the passive film/coating interface.

This can be correlated to Figure 8.3 to represent the different elements with the electrolyte and its permeation through the coating to the substrate.

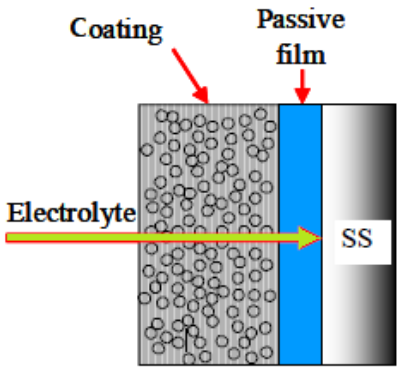

Figure 8.3 Schematic of the equivalent circuit [169]

The behaviour of the basic inorganic/hybrid sol-gel coating and samples with the same configuration of plots and values of total resistance higher than $10^6 \Omega.cm^2$ is presented as capacitive in the Nyquist plot which indicates a protective and intact coating. Although some water can be detected, it is expected to be on the top coating surface and not penetrated since the arc of the plot does not display the characteristic semi-circle [136] but segments of semi-circles, possibly relating to corrosion-resistant film formed on the surface of the bare substrate [169]. The impedance inversely changes as a function of frequency with a slope value close to -1 in the Bode plot. This indicates the capacitive characteristics of the coating. The relatively high Z values at low frequencies are maintained approximately similar within 30 days which highlights the durability of the coating for this period.

The total resistance, R_{tot}, sum of all resistances existing in the system, can be estimated from the impedance at the lowest frequency in the Bode magnitude (impedance) plot.

When the electrolyte comes in contact with the steel surface, electrochemical reactions arise potentially resulting in the formation of corrosion products at the interface. The associated processes are represented by the interfacial resistance, R_{ct}, and the double layer capacitance, C_{dl}.

The water uptake can be calculated (Equation (8.1)) using the empirical formula derived by Brasher and Kingsbury [245] where X_v denotes the volume fraction of water adsorbed by the coating, C_0 and C_c are the coating capacitance at the beginning of the exposure (Day 1) and after the certain time intervals respectively while 80 is the dielectric constant of water in standard conditions.

$$X_V = 100 \times \left[\frac{\log\left(\frac{C_c}{C_0}\right)}{\log 80} \right] \tag{8.1}$$

Figure 8.4 presents the water uptake for the sample $I_{,B2,0\%,304}$ over 30 days of immersion. It correlates to the results of impedance obtained earlier and shows that there is up to 10% of water uptake at Day 30, which is low.

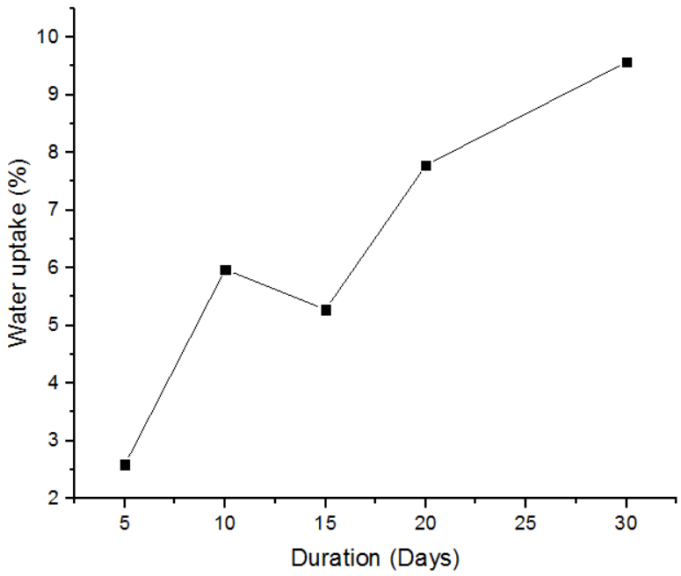

Figure 8.4 Water uptake for $I_{,B2,0\%,304}$ over 30 days of immersion

To avoid mistakes due to the constant values and initial coating capacitance (C_0) which can be determined with more or less accuracy and since the water uptake is linked to the evolution of coating capacitance, the next plots and figures will feature C_c (and thus CPE_{ct} as the values are calculated in chapter VI) instead of the exact values of water uptake. This will give the same evolution since an increase of the coating capacitance value means an increase in the water uptake and thus a decrease in corrosion resistance.

In Chapter VI Figure 6.24 presents the evolution of the water uptake as a function of time for the silica inorganic/hybrid sol-gel coating from Batch 2, $I_{,B2,0\%,304}$. As it can be seen, the coating capacitance (C_c) appears to barely increase with time which suggests a higher water uptake. The coating capacitance depends on the deterioration on a microscopic scale along numerous points of the coating. It is therefore regarded as a parameter of coating behaviour that can be determined throughout the entire exposure period and shows the best reproducibility of all passive elements. The contribution of coating delamination or degradation to impact the coating capacitance at the end of the experiment is significantly higher than the influence of water adsorption.

The most promising coatings from the first batch are from the organic system 1, coating having the greatest thickness (between 60µm and 80µm). However as it is presented in the literature review part [3, 83, 93], organic coatings are thicker, however in certain fields they cannot be used due to their thermal weakness and mechanical properties. The other systems (inorganic/hybrid systems 1 to 5, organic

system 2 and hybrid/composites systems 1 to 2) had a range from 3µm to 15µm. According to Santagata D.M. et al. [246] the electrolyte penetration can increase the ionic conductivity of coatings, and consequently decrease the protective capacity of coatings, since the mass transport process takes place easier. It is found that the loss of barrier protective properties of coatings indicated by decreasing or very low coating resistance occurs a lot faster in thinner polymer coatings compared to thicker coatings.

Then for the second and third batches the thickness of the samples are all below 12µm and FIB images Figure 5.27 showed that the coating, even if spread homogeneously on the surface of the substrate, does not present the same thickness on every part of the substrate, which can lead to faster corrosion.

The post-test investigations using electron microscopy showed little signs of corrosion except for the hybrid/composites sample were the substrate could be seen on most of its surface. The degradation processes are occurring on a very small scale such that no macroscopic damage could be seen. Thus the decline of the coating impedance values during the tests is most likely due to the infiltration of ions in the coatings, which in turn increased the conductance [247]. A coating breakdown can be characterized by a marked decrease in the value of R_{ct}.

Figure 8.5 and Figure 8.6 present a comparison of the samples tested and the values of the capacitance and resistance respectively at Day 30 of immersion. A comparison giving information on the failure is presented in Figure 8.7.

It is displayed that the lowest values of capacitance, about 2.10^{-9} F/cm, and thus of water uptake after the experiment are for $I_{,B3,2.8\%,Mix,N2}$, $I_{,B3,5.6\%,Mix,N2}$ and $I_{,B3,5.6\%,Ip,N2}$. These low values should mean a reduced corrosion [248-250] on these samples and thus a high value of R_{ct}. However, even if those values are close to 10^6 Ω.cm^2, other samples present a more important value and thus resistance to corrosion. The only sample with a resistance lower than 10^4Ω.cm^2 is $I_{,B3,5.6\%;Mix,Air}$ and is also the sample with the highest capacitance. It is the sample with the less efficient coating. The most efficient sample is $I_{,B3,0\%,Ip,N2}$. Most of the samples without doping are efficient according to the figures while the ones doped with 11.3%w/w first presented low protective properties and then are too cracked to be tested.

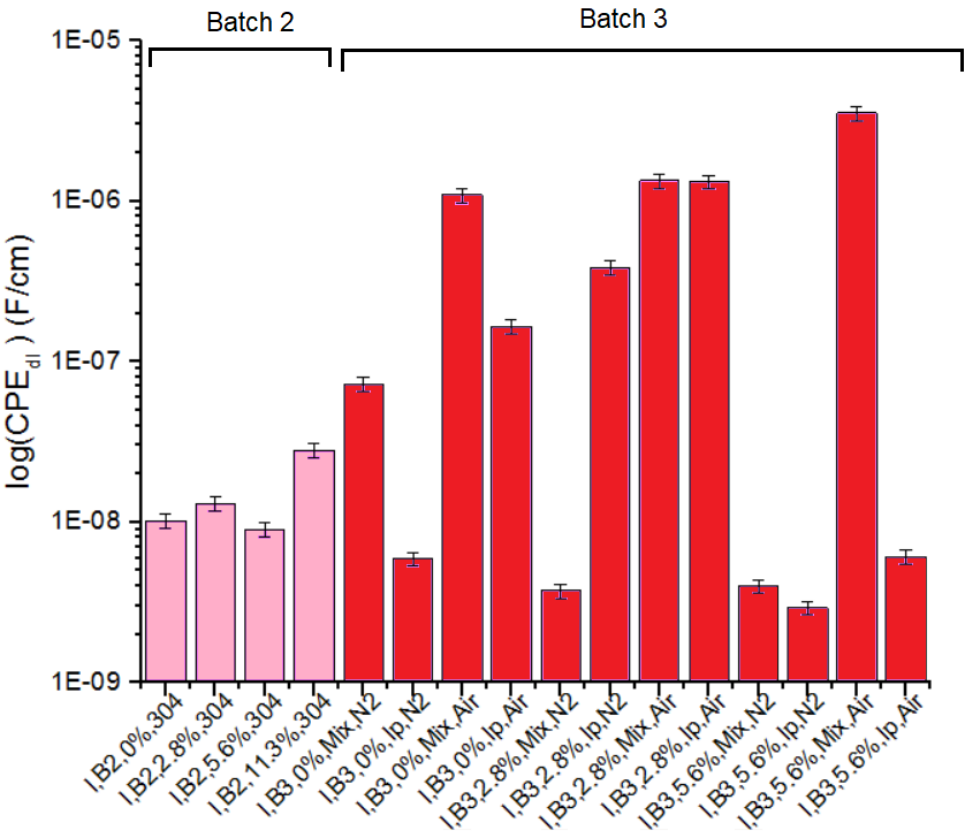

Figure 8.5 Comparison of CPE_{dl} at Day 30 of immersion for Batch 2 and 3

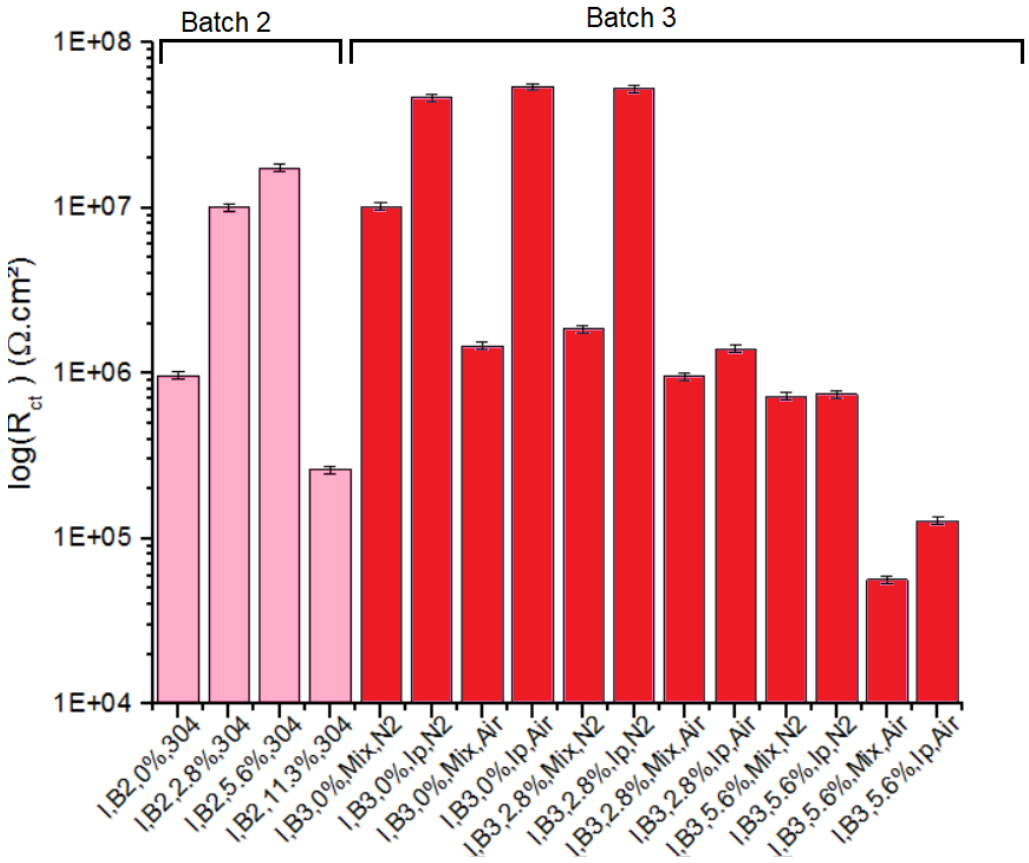

Figure 8.6 Comparison of R_{ct} at Day 30 of immersion for Batch 2 and 3

A reduction in water uptake would be expected as the percentage of titanium precursor added increases since it is supposed to lower the defects within the coating and increase its protective properties. This would reduce the ingress of electrolyte, thus the water uptake and accordingly the corrosion process [251-255] . A decrease in water uptake values leading to improved corrosion resistance can be related to other works which presented an improvement in resistive properties due to reduced coating capacitance [248-250]. However the values of capacitance for $I_{,B2,0\%,304}$, $I_{,B2,2.8\%,304}$ and $I_{,B2,5.6\%,304}$ are close to 1.10^{-8}F/cm while $I_{,B2,2.8\%,304}$ and $I_{,B2,5.6\%,304}$ have a resistance of $10^{7}\Omega.cm^{2}$ and $I_{,B2,0\%,304}$ closer to $10^{6}\Omega.cm^{2}$. On another hand $I_{,B2,11.3\%,304}$ has a higher capacitance (2.10^{-8}F/cm) and a lower resistance ($10^{5}\Omega.cm^{2}$). Contrary to the other doped samples, its protective properties are less effective, even compared to $I_{,B2,0\%,304}$ which has not been doped.

Among the samples of Batch 3, the samples with isopropanol as a solvent appear to have a higher resistance than their counterparts with the mixture as solvent. However apart from $I_{,B3,2.8\%,Mix,N2}$ and $I_{,B3,2.8\%,Ip,N2}$ the values of capacitance of the samples from Batch 3 also have a more importance values for the samples with isopropanol as a solvent.

The samples from Batch 3 whose curing process is in N_2 have a lower capacitance and a higher resistance compared to the samples cured in air which means that the performance of samples cured in N_2 has improved and the samples have better protective properties.

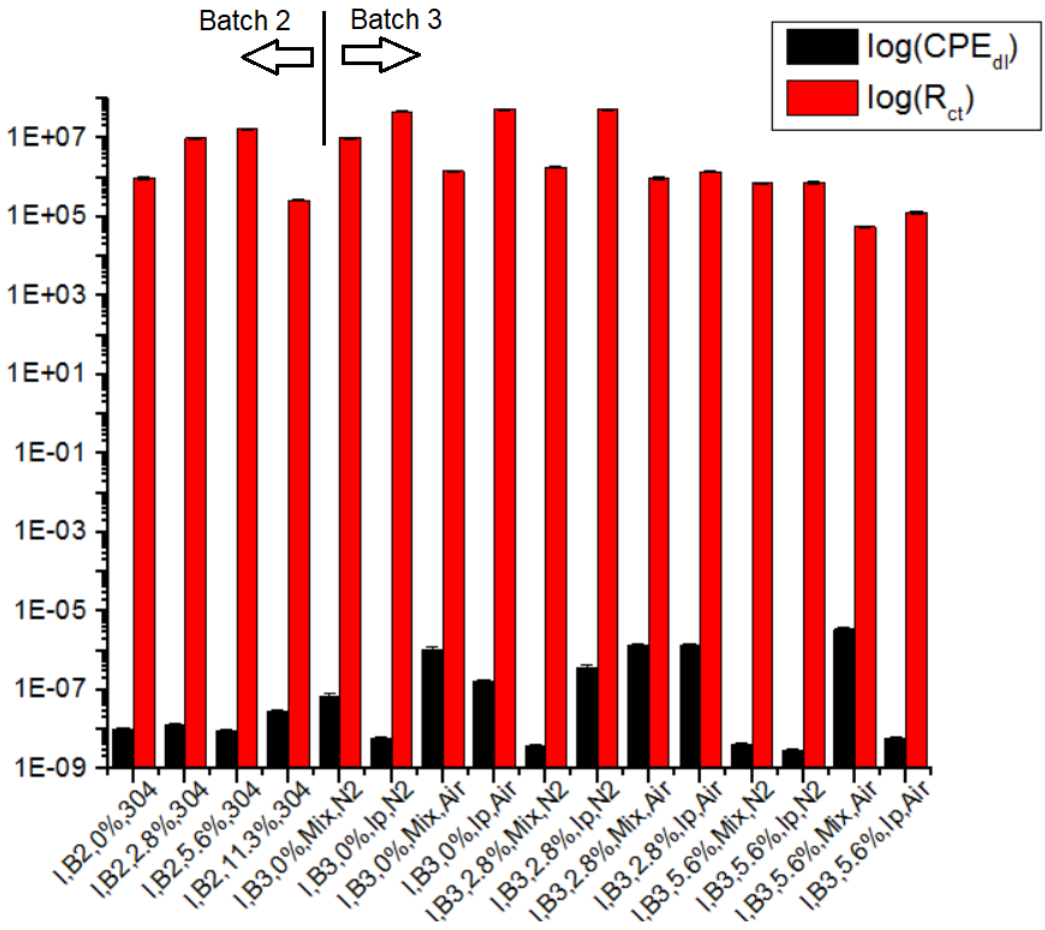

Figure 8.7 Comparison of the samples from Batch 2 and Batch 3

8.4 Role of Substrate

After the experiment of 30 days, the samples from the first batch are sorted in three categories: barely corroded, damaged but may be improved and delaminated (too damaged to be improved).

- Barely corroded represents 3 samples ($O_{,B1,2,X65,Yes}$, $O_{,B1,2,316L,No}$, and $O_{,B1,2,316L,Yes}$) which is 10.7% of all the samples tested. Moreover, all of those samples are from organic systems (especially system 2), none from the inorganic/hybrid nor hybrid/composites systems. On those 3 samples, 2 are on stainless steel and 1 on carbon steel.

- Damaged samples include 9 samples ($I_{,B1,2,316L,Yes}$, $I_{,B1,3,316L,No}$, $I_{,B1,3,316L,No}$, $I_{,B1,4,316L,No}$, $I_{,B1,4,316L,No}$, $I_{,B1,5,316L,No}$, $I_{,B1,5,316L,No}$, $H_{,B1,2,X65,Yes}$, and $H_{,B1,2,316L,No}$) which represent 32.1% of the first batch. Amongst those samples, 8 had for substrate stainless steel and 1 on carbon steel.

- Delaminated coatings are the remaining samples ($I_{,B1,1,X65,No}$, $O_{,B1,1,X65,No}$, $O_{,B1,1,X65,Yes}$, $O_{,B1,1,316L,No}$, $O_{,B1,1,316L,Yes}$, $O_{,B1,2,X65,No}$, $H_{,B1,1,X65,No}$, $H_{,B1,1,X65,Yes}$, $H_{,B1,1,316L,No}$, $H_{,B1,1,316L,Yes}$, $H_{,B1,2,X65,No}$, and $H_{,B1,2,316L,Yes}$) which represent 42.9% of the first batch. Of the 12 samples, 7 are on carbon steel while 5 are on stainless steel. For those samples data could not be measured as the samples are too damaged.

Overall, the samples which are the most corroded and damaged are the ones with a carbon steel X65 substrate. For a same coating, the X65 sample is more damaged than the 316L sample: as an example there is the sample $O_{,B1,1,X65,Yes}$ on X65 compared to the sample $O_{,B1,1,316L,No}$ on 316L in Figure 8.8. The sample $O_{,B1,1,316L,No}$ is shown with a totally delaminated coating but the sample $O_{,B1,1,X65,Yes}$ has no coating at all and the metal is deeply corroded.

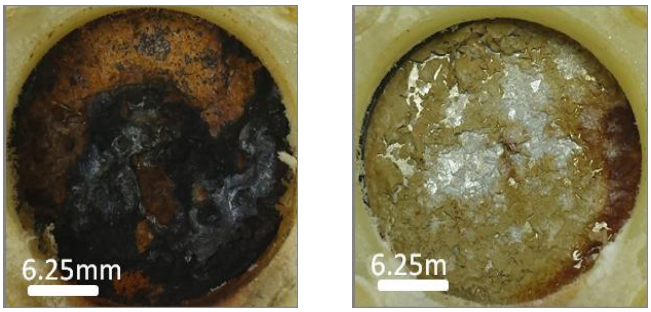

$O_{,B1,1,X65,Yes}$ after 30 days

$O_{,B1,1,316L,No}$ after 30 days

Figure 8.8 Sample $O_{,B1,1,X65,Yes}$ and sample $O_{,B1,1,316L,No}$ after 30 days (same coating: organic system 1).

Even if one of the barely damaged samples, $O_{,B1,2,X65,Yes,}$ has a carbon steel X65 substrate, the corrosion process at the coating/substrate interface depends strongly on the nature of the substrate. The barrier properties of the sol-gel coating are weakened by the corrosion rate of the metal substrate, which leads to the delamination of the coating.

Except for $O_{,B1,2,X65,Yes}$, the carbon steel X65 substrate gave poor results. For a same coating, the result on X65 would be worse than on stainless steel. It is known that the resistance of stainless steel is stronger than the resistance of carbon steel, but even coated the final results show this difference. The characteristics of the stainless steel being precisely a high chromium content that forms an invisible layer on the steel to prevent corrosion.

Except for $I_{,B1,1,X65,No}$, $O_{,B1,1,316L,Yes}$, $O_{,B1,2,316L,Yes}$ and $H_{,B1,1,316L,Yes}$ whose value tend to 0V, the samples tested have an OCP tending to the value of the OCP of their bare substrates with time (about -0.200V for 316L stainless steel and -0.500V for X65 carbon steel).

For Batch 2, when comparing the values obtained for the bare substrate and the coated sample on the same substrate, it is presented that the corrosion rate of the stainless steel substrate is reduced with the application of the sol-gel coating as expected [256] while the resistance is increased: about $10^6\Omega.cm^2$ for the bare 304 stainless steel to 10^7-$10^8\Omega.cm^2$ for $I_{,B2,0\%,304}$. However the values obtained for $I_{,B2,0\%,A1008Q}$ go from $10^6\Omega.cm^2$ at Day 1 (same order of magnitude than for bare 304 stainless steel) to $10^4\Omega.cm^2$ at the end of the experiment, which is lower than the measurements made on stainless steel and coated steel.

During the period of immersion, the shape of the impedance response for the uncoated sample remains almost unchanged with time, which suggests a stable structure of the passive film [169].

Figure 8.9 presents and compares the evolution of R_{tot} as a function of time for the same undoped inorganic/hybrid sol-gel coating but on two different substrates: 304 stainless steel and A1008Qpanel as well as the evolution for the bare substrate 304 stainless steel.

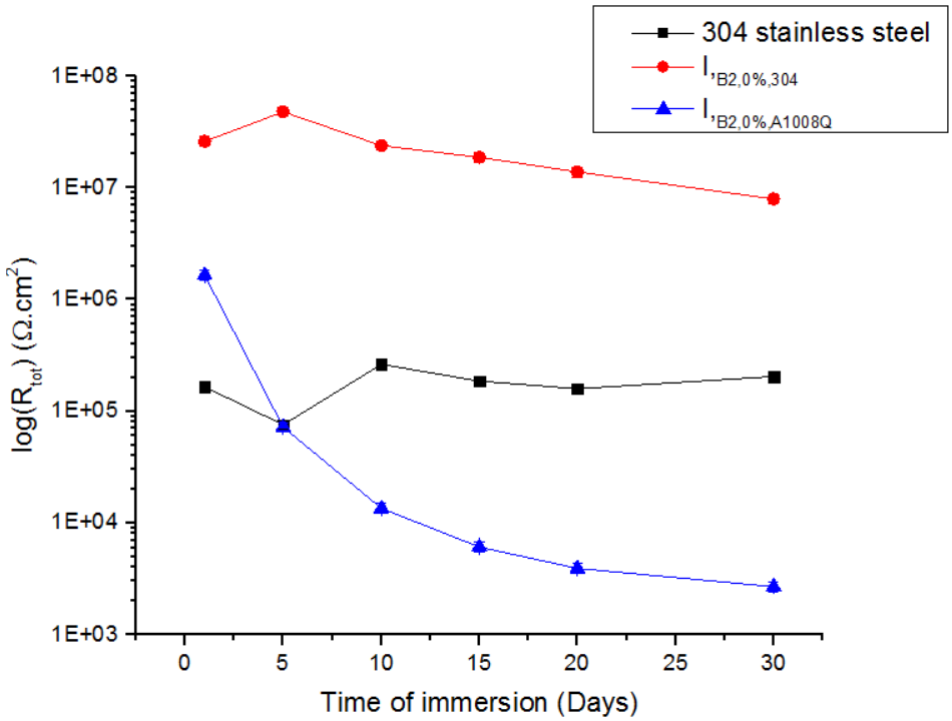

Figure 8.9 Time dependence of R_{tot} for uncoated 304 stainless steel, $I_{,B2,0\%,304}$ and $I_{,B2,0\%,A1008Q}$ in 3.5% NaCl

The substrate can be seen as having an effect on the performance of the sample as the value of R_{tot} for the sample on A1008Qpanel decreases with time through more than 2 orders of magnitude compared to the sample having for substrate 304 stainless steel. This sample has a higher value of resistance from the start of the experiment and has a slight decrease lower than one order of magnitude.

As the sample with A1008Qpanel as a substrate has a value lower than $10^4 \Omega.cm^2$ it can be considered as having poor resistance to corrosion and Figure 8.10 which is SEM images of the surface after the experiment shows the damage.

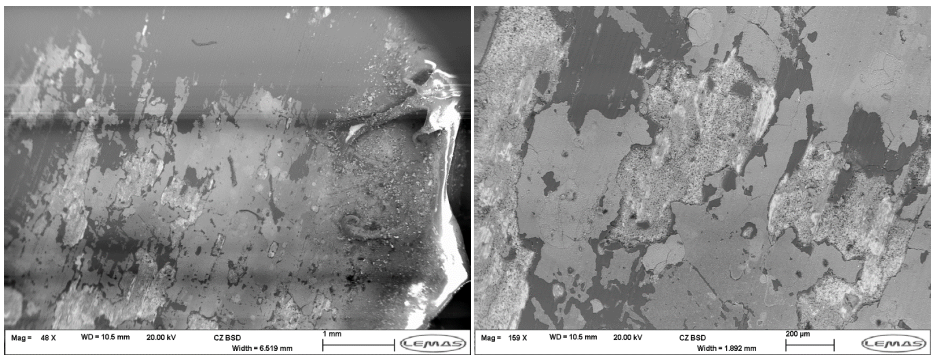

Figure 8.10 SEM images of $I_{,B2,0\%,A1008Q}$

R_s denotes a measure of the ionic film resistance [222] as the actual solution resistance in electrolytes such as seawater is negligible [257]. If the coating is thin enough, these values can give an indirect estimation of the coating protective properties. High values of R_s hint to better resistance especially in what is described as the areas of rapid solution uptake due to defects such as lack of polymerisation or other [257]. Its variation can be correlated to the coating degradation level. A decrease in R_s value with time of immersion indicates a deterioration in the ability of the coating to protect the substrate [222]. Figure 8.11 presents R_s as a function of time for the coated sample on 304 stainless steel.

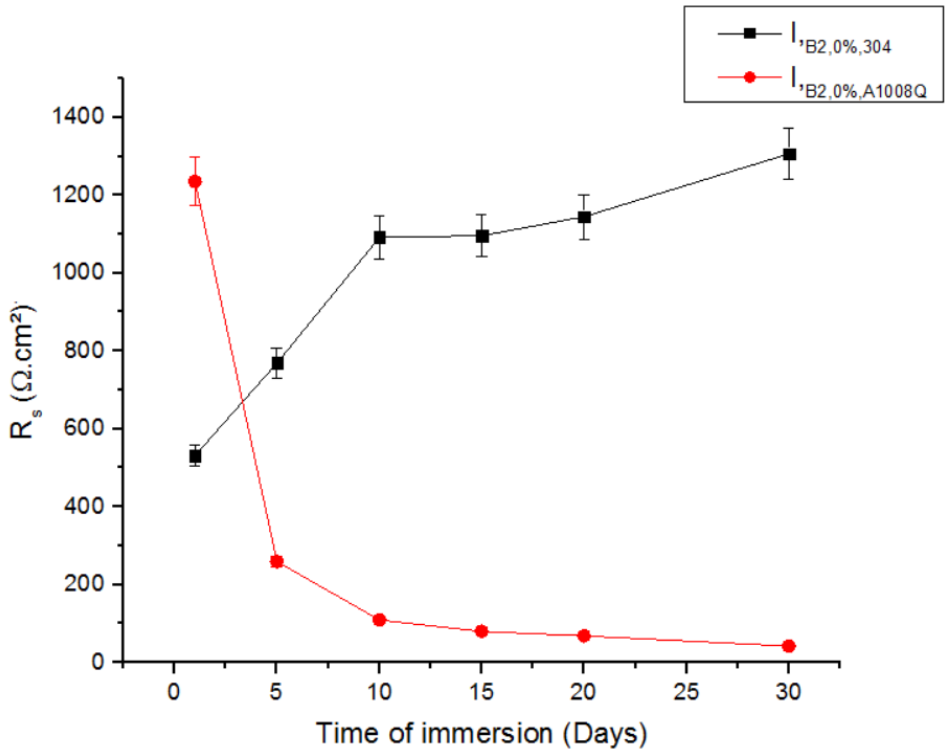

Figure 8.11 Comparison of R_s as a function of time for a same coating on different substrates over 30 days of immersion (Batch 2)

The coated sample on stainless steel is stable since the solution resistance R_s values increase with time during the experiment (from 500Ω.cm² to 1300Ω.cm²). The coating on A1008Qpanel shows a strong decrease in its R_s value after 5 days (from 1200Ω.cm² to less than 50Ω.cm²).

The capacitance of those samples in Chapter VI presented a stable evolution for bare 304 stainless steel and $I_{,B2,0\%,304}$ with values of the same order of magnitude throughout the experiment (10^{-5} F/cm for 304 stainless steel, 10^{-8} F/cm for $I_{,B2,0\%,304}$) while $I_{,B2,0\%,A1008Qp}$ presented an important increase, from 10^{-6} F/cm at Day 1 of the experiment, to 10^{-3} F/cm at Day 30, meaning a substantial water uptake while the resistances decrease the first days than appear to stabilize. However both bare 304 steel and $I_{,B2,0\%,304}$ have a higher resistance than the sample on A1008Qpanel.

The choice of substrate is important because it affects the structure and properties of the thin coatings [258]. When comparing carbon steel and stainless steel there are differences: for the stress-strain behaviour for instance, carbon steel presents a sharply defined yield point followed by a plateau while stainless steel displays a rounded curve [259]. For corrosion resistance, the higher chromium content of stainless steel enables a higher corrosion resistance compared to carbon steel

[259]. The addition of a sol-gel coating in environment where corrosion resistance is needed can improve this property.

8.5 Surface Chemistry Changes in the Coatings

8.5.1 Influence of Percentage of Titanium Precursor

Before any experiment the FTIR data presented the same spectra for all samples. For $I_{,B2,0\%,304}$, no clear additional peaks at 3400cm^{-1}, assigned to O-H stretch band in water, are detected after exposure of the coating to sea water. This implies that water does not contribute to the chemical structure of the coating following the immersion in sea-water. Water is detected and does not affect the coating as the functional groups present on Day 0 are still present at Day 30. All the other samples present at least some water on their surface as peaks attributed to water are detected.

These results can be linked to the EIS results: water is detected through FTIR analyses but the Nyquist plots from EIS showing a capacitive behaviour confirms that the coating is intact. The water is not penetrated through the coating in either case as the coating has high barrier properties and strong corrosion resistance.

The coating is visibly intact, however it lets water penetrate through the coating and once the water reaches the surface, the steel corrodes and this contributes to delamination.

Total resistance R_{tot} and SEM results of the hybrid/composites sample $H_{,B2,0\%,304}$ are presented respectively in Figure 8.12 and Figure 8.13 show low effectiveness of corrosion protection which led the focus of the study to be on the samples doped with titanium butoxide as a precursor.

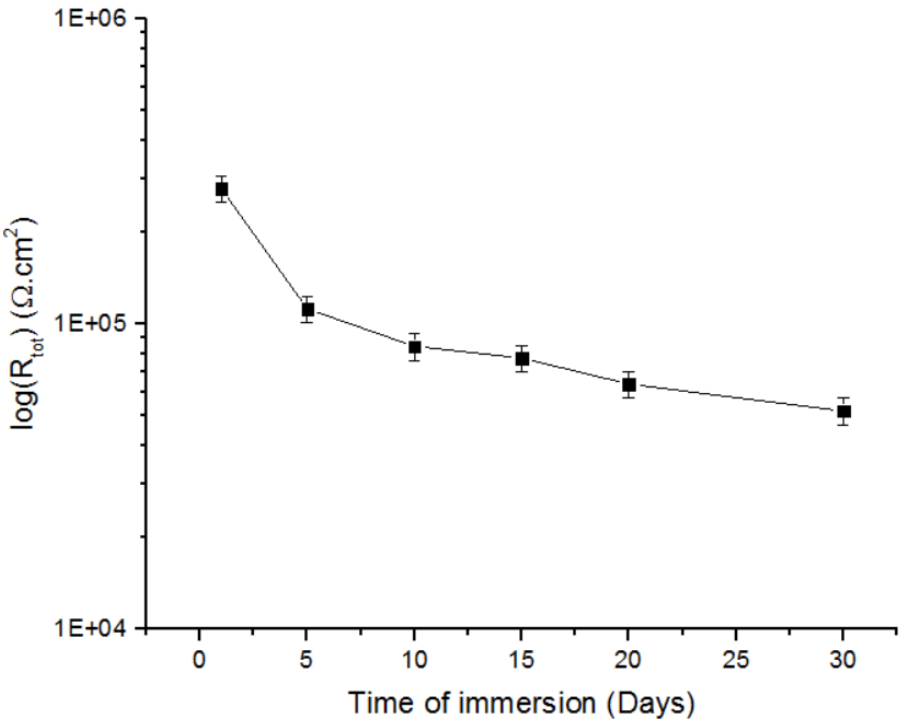

Figure 8.12 Time dependence of R_{tot} for $H_{,B2,0\%,\ 304}$ in 3.5% NaCl

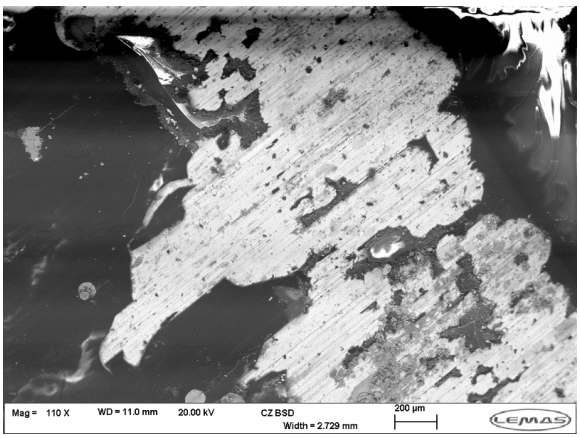

Figure 8.13 SEM image of the surface of $H_{,B2,0\%,\ 304}$ at Day 30 of immersion

Figure 8.14 presents and compares the evolution of R_{tot} as a function of time for the samples with different percentages of doping precursor while Figure 8.15 presents the values of R_s as a function of time.

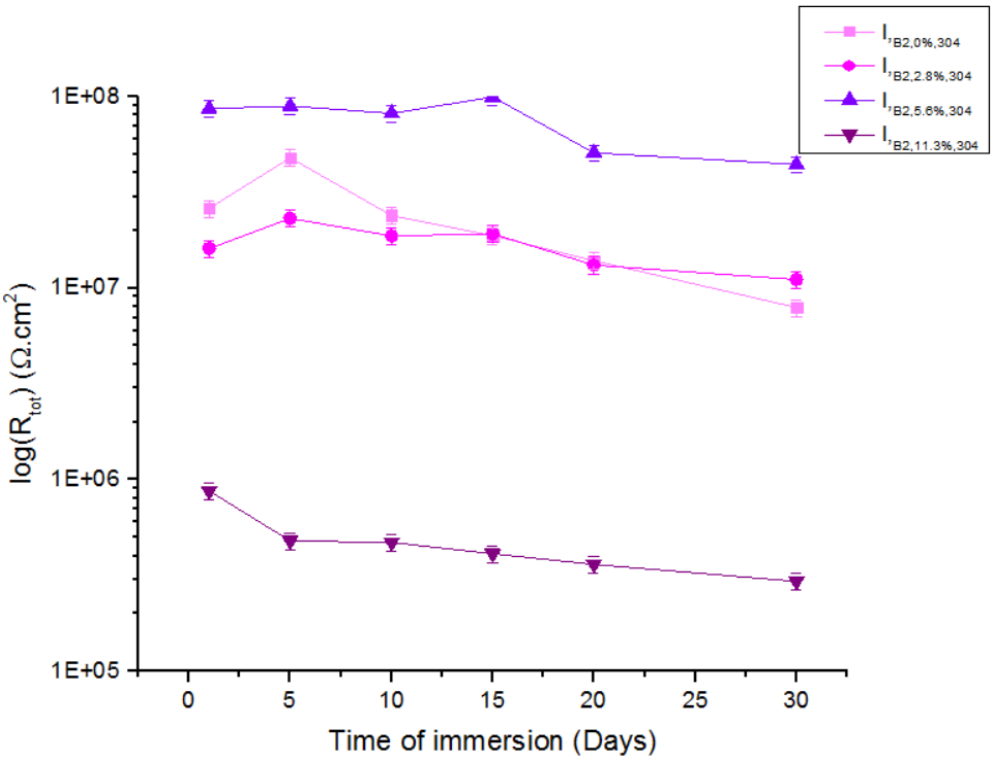

Figure 8.14 Time dependence of R_{tot} for inorganic/hybrid coatings of Batch 2 with different amounts of precursor in 3.5% NaCl

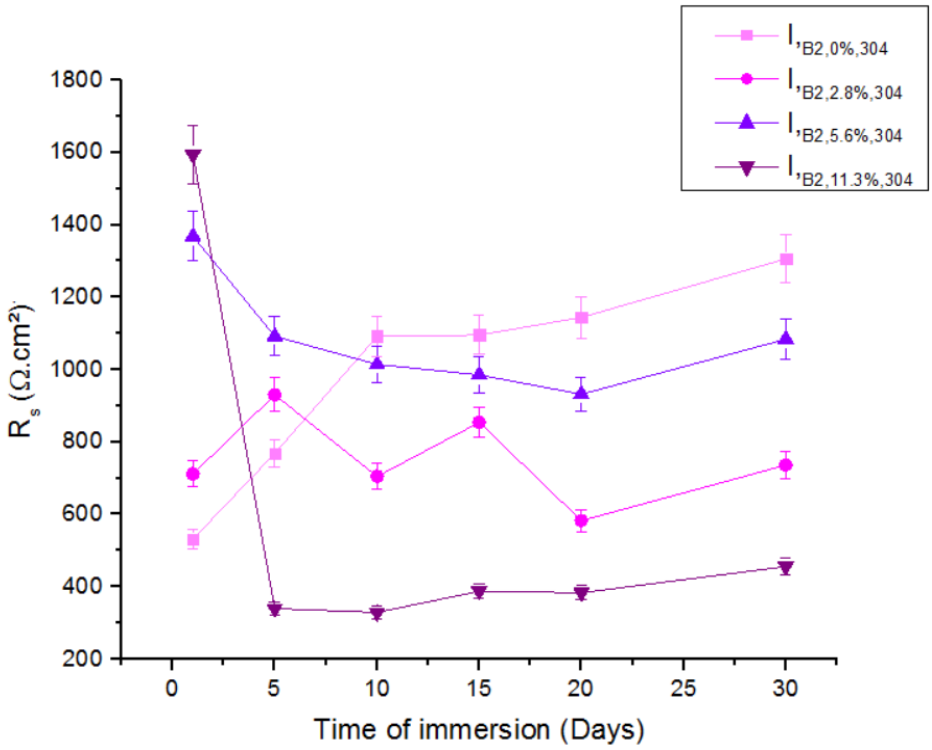

Figure 8.15 R_s as a function of time for the samples of Batch 2 with different percentages of titanium precursor in 3.5% NaCl over 30 days of immersion

From both graphs the sample with 11.3%w/w of titanium precursor appears to have the lowest values in resistance below $10^6\Omega.cm^2$ throughout the duration of the immersion, meaning the lowest resistance to corrosion among the 4 samples presented. There is a drop in R_s value after 5 days from $1600\Omega.cm^2$ to $300\Omega.cm^2$, hinting at low performance shortly after the start of the immersion. As its value of total resistance is lower than $10^6\Omega$ and keeps decreasing it is considered as having poor resistance to corrosion. This is also the sample with more additional peaks in its FTIR spectra after the experiment, peaks from the damaged coating: $3400cm^{-1}$ as damage from the water and $950cm^{-1}$ which can be ascribed to Si-OH as a deterioration of the coating.

The samples with 2.8%w/w and 5.6%w/w have stable R_{tot} values within $10^7\Omega.cm^2$ while the sample without doping has an increasing R_s value and a stable R_{tot} value as well, close to $10^8\ \Omega.cm^2$ at Day 1 to $5.10^7\ \Omega.cm^2$ at Day 30. Those three samples are considered as having good resistance to corrosion since they have high resistance values (R_{tot}, R_s and R_{ct}), low capacitance values and none ($I_{,B2,0\%,304}$) to barely any additional peaks in FTIR data ($2400cm^{-1}$ ascribed to CO_2 for $I_{,B2,5.6\%,304}$ and $3400cm^{-1}$ ascribed to water for $I_{,B2,2.8\%,304}$).

However, it can be seen from the FIB images Chapter V that the thickness of a coating is not the same over the surface of the sample and that can lead to faster corrosion of the substrate in places where the coating is thinner. This depends on the coating process and can differ from one sample to another even if all conditions and parameters are similar.

Generally, coatings with resistance over $10^8\Omega.cm^2$ provide good corrosion protection, while those with resistance evolving under $10^6\Omega.cm^2$ provide poor corrosion protection [221].

Other coatings are also used in the oil and gas industry for corrosion protection, for example epoxy coatings. According to some publications [221, 245, 260-264] even if they are considered efficient as protective coatings, their resistance value R_{ct} can be about 10^6-$10^5\ \Omega.cm^2$ for Day 1, decreases to be about $10^3\Omega.cm^2$ after experiment. The sol-gel coatings studied in this project, while being thinner, gave similar results even higher for the resistance values after experiment. The incorporation of organic inhibitors within the sol-gel matrix can increase the barrier properties of the hybrid coatings from $10^5\Omega.cm^2$ to $10^6\Omega.cm^2$ after 10 days in chloride solution [171].

The increase of the immersion time leads to the decrease of the pore resistance of the sol-gel coating due to formation and growth of new cracks and pores [171]. Another coating formulation is TiO_2 nanoparticle coating on steel, which compared with bare steel increases its corrosion resistance up to 100 times (up to $10^6 \Omega.cm^2$) [123].

8.5.2 Influence of Solvent and Curing Process

For the third batch, new changes in parameters are introduced: solvents and curing processes. The samples were either prepared with a solvent mixture (EtOH, IpOH, BuOH) or with isopropanol as solvent leading to differences in composition of the final coatings. The samples were either cured in N_2 or in air in order to find a combination improving the corrosion resistance properties of the sol-gel coatings.

In the FTIR data, samples $I_{,B3,0\%,Mix,N2}$ and $I_{,B3,2.8\%,Mix,N2}$ present no clear additional peaks at $3400cm^{-1}$, meaning that there is no water uptake after experiment. This correlates to the values of capacitances in Chapter VI. All the other samples present at least some water on their surface as peaks attributed to water are detected at $3400cm^{-1}$. The samples with isopropanol as solvent especially present additional peaks from the degradation of the coating such as $1250cm^{-1}$ C-O and $800cm^{-1}$ C-C-O symmetric stretch. Figure 8.16 presents the evolution of R_{tot} as a function of time for all the different samples with an undoped coating, thus 0%w/w of precursor.

Those four samples have a R_{tot} value higher than $10^6 \Omega.cm^2$ and are thus considered as having valuable corrosion resistance. The sample having the lower value from the four different samples is the one having a combination of solvent mixture and curing in air.

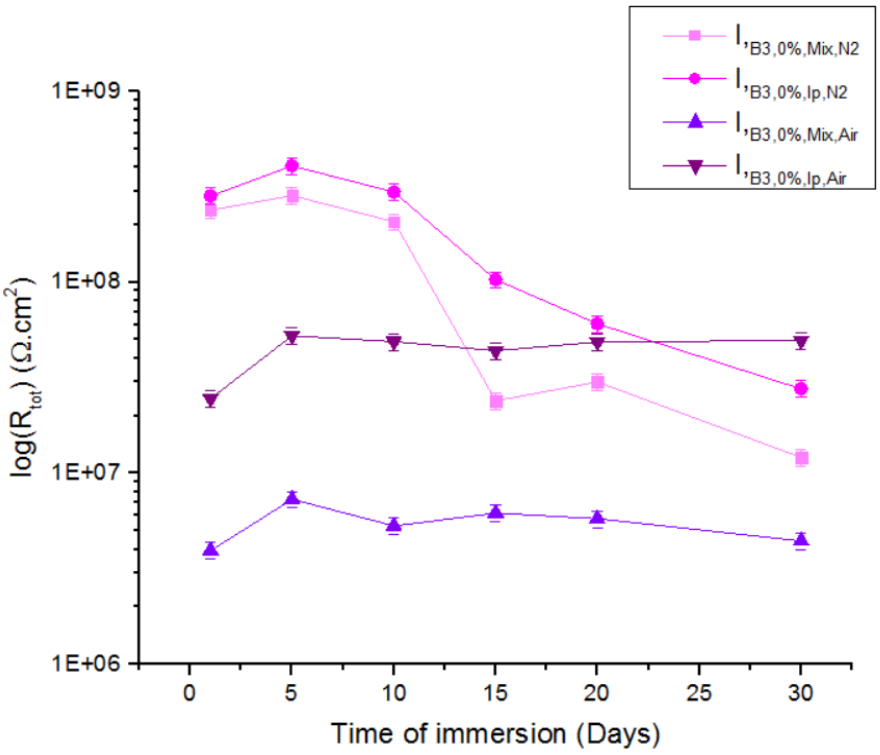

Figure 8.16 Time dependence of R_{tot} for inorganic/hybrid coatings without doping and with different solvents and curing process from Batch 3 in 3.5% NaCl

The samples with different solvent but same curing process can be seen as having the same shape of curve: $I_{,B3,0\%,Mix,N2}$ and $I_{,B3,0\%,Ip,N2}$ have both more fluctuation depending on the time while $I_{,B3,0\%,Mix,Air}$ and $I_{,B3,0\%,Ip,Air}$ have more stable values.

After the immersion the values of R_{tot} are included between 10^6 and 10^8 Ω.

Figure 8.17 presents the evolution of R_{tot} as a function of time for all the different samples with 2.8%w/w of precursor.

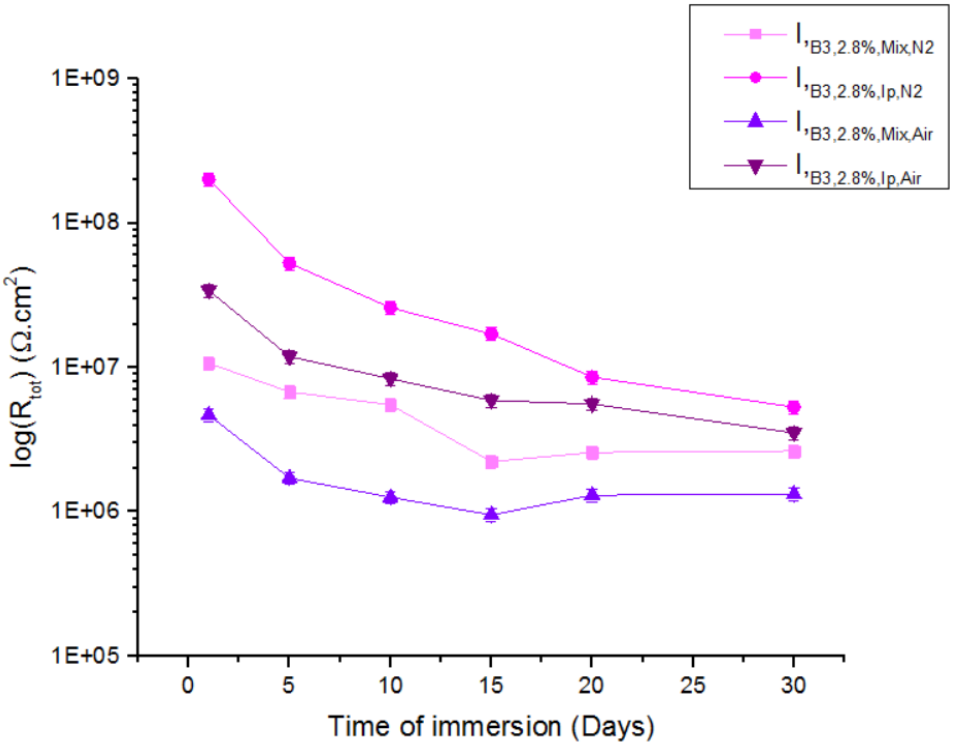

Figure 8.17 Time dependence of R_{tot} for inorganic/hybrid coatings doped with 2.8%w/w of precursor with different solvents and curing process from Batch 3 in 3.5% NaCl

All the samples here have the same evolution depending on the time of immersion.

The sample having the lower value is still the one having a combination of solvent mixture and curing in air. After 30 days of immersion all the values are included between 10^6 and $10^7\Omega$ and are considered as having good corrosion protection. The nature of the solvent has an influence on the structure and thickness of the coatings: an aprotic solvent enhances corrosion resistance while the use of alcohols as an opposite effect [72]. The solvents used in this study are isopropanol and a mixture of alcohols.

As opposition to the samples without any doping, these samples have the same evolution, their resistance values decreases for a few days and then seem to reach a plateau.

Figure 8.18 presents the evolution of R_{tot} as a function of time for all the different samples with 5.6%w/w of precursor.

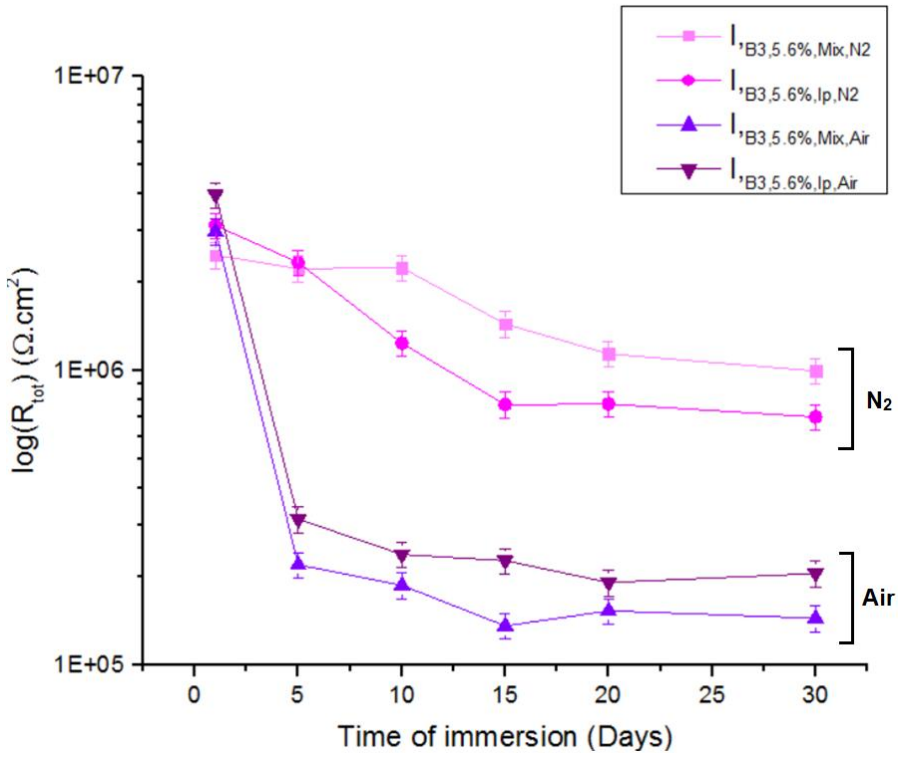

Figure 8.18 Time dependence of R_{tot} for inorganic/hybrid coatings doped with 5.6%w/w of precursor with different solvents and curing process from Batch 3 in 3.5% NaCl

The overall values of resistance are lower than the samples presented until now. The starting values for the first day are similar, the samples with different solvents but same curing process have the same evolution with time, with a drop in value for the samples cured in air then the values stabilize. The values of the samples cured in N_2 decrease slightly but stay within the order of $10^6\Omega.cm^2$. Here for the samples with 5.6%w/w of precursor, the values of R_{tot} decrease during the first days and then tend to the value of the substrate 304 stainless steel as presented in Figure 8.9, especially for $I_{,B3,5.6\%,Mix,Air}$ and $I_{,B3,5.6\%,Ip,Air}$ but after the experiment all the values of the resistance are lower than $10^6\Omega$. Moreover, those four samples either have a relative high value of CPE_c throughout the experiment or increasing with time according to Figure 6.46 which means that the protective properties of the coating are low and that there is an uptake of water during the immersion.

There is little information in the literature about the curing process other than the time and temperature. It can be suggested in this project that curing the samples in air decreases the barrier and protective properties while the curing in N_2 gives more satisfactory results.

The performance of the samples seems to decrease when the amount of titanium butoxide added is higher than 5%w/w for Batch 3.

Comparing the hardness and adhesion results, it can be said that the addition of precursor has an influence on the stiffness and adhesion of the coating but almost no influence on the hardness. The erosion results follow this path with the weight loss being approximately the same for the samples with or without any doping.

The combination better suited to have high protective properties seem to be when the solvent is the mixture, cured in N_2 with either no doping or a concentration of 2.8%w/w precursor.

While comparing the results of EIS and salt spray test, it can be observed that the coatings with poorest performance are the one with combination of mixture as a solvent and cured in air, regardless of the amount of titanium but their results worsen when the percentage is higher than 5%. The coatings with better performance in EIS and through spray test are the coatings with the combination isopropanol as a solvent and cured in N_2.

8.6 Permeability of the Coatings

Permeability as defined in Chapter III is a property of coatings. As inorganic coatings are supposed to have high mechanical strength, they should present low permeability. The permeability of liquids of the samples can be assessed with the help of several parameters: the day of failure of coatings for Batch 1 and the evolution of R_{ct} for the other batches as the samples provided improved results.

Figure 8.19 presents the time to failure as a function of thickness for the samples of Batch 1 while presents an enlargement for days 0 to 15. Only one system has a thickness more important than 12µm, which is the organic system 2. This coating, deposited on X65 carbon steel, fails in 4 days while the same coating but deposited on stainless steel 316L, present little damage at the end of the experiment of 30days. The time to failure for Batch 1 depends on the substrate. The pre-treatment seems to have some influence on the degradation but only for the inorganic/hybrid systems.

None of the hybrid/composites samples lasted until the end of the experiment. Thus it can be said that the hybrid/composites coatings are the samples which have the highest permeability.

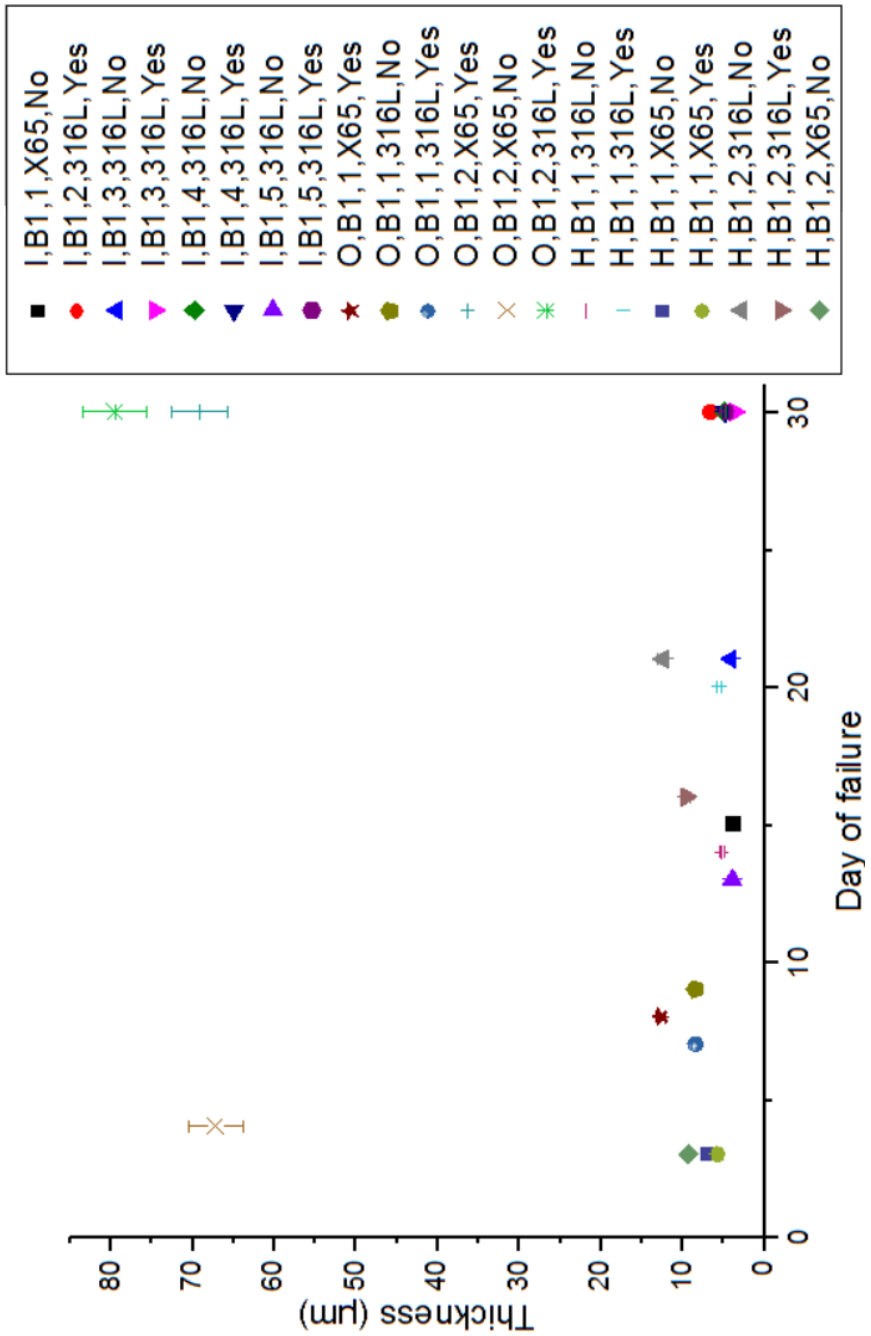

Figure 8.19 Time to failure as a function of thickness for Batch 1

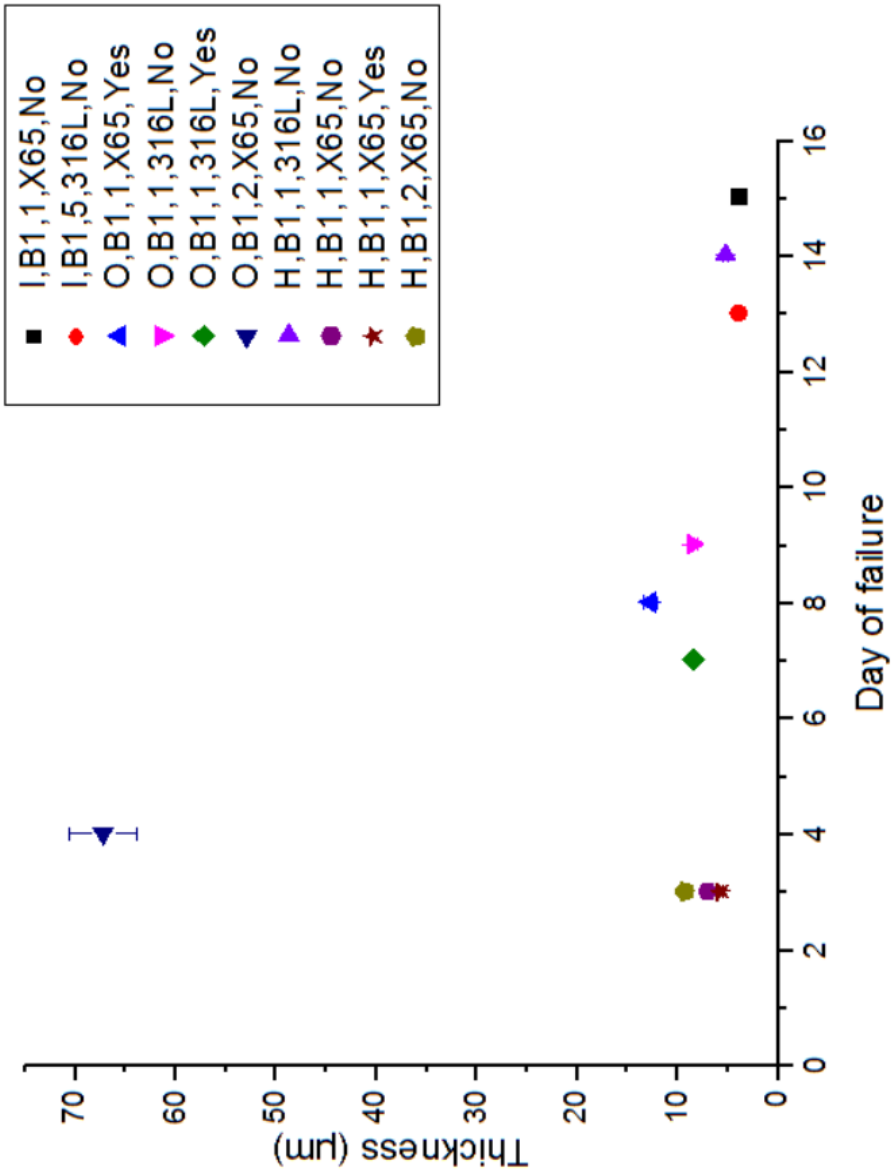

Figure 8. 20 Time to failure Day 0 to Day 15 as a function of thickness for Batch 1

Figure 8.21 presents the values of R_{ct} at Day 30 of immersion as a function of the thickness. This gives information about the permeability as well. A low resistance leads to high permeability. The water permeation is suppressed by the coatings.

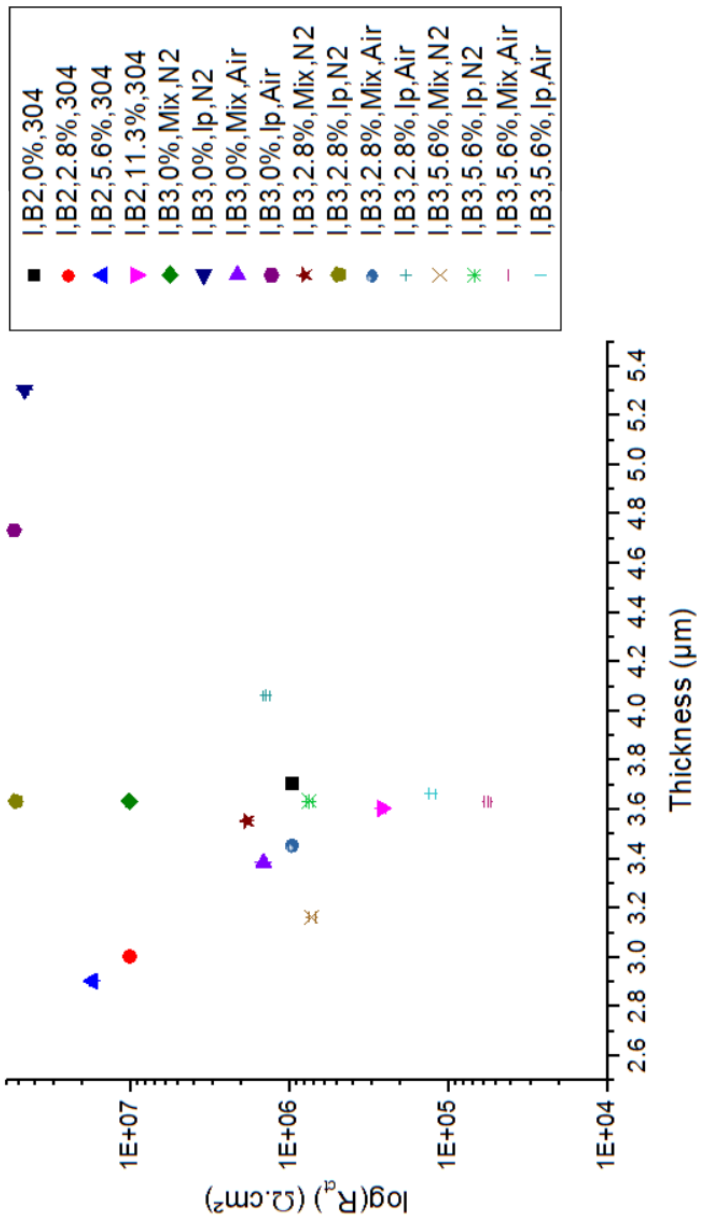

Figure 8.21 log(R_{ct}) of Day 30 as a function of thickness for Batch 2 and 3

It can be noted that the samples containing 5.6%w/w of titanium precursor presented better performance in Batch 2 compared to Batch 3. They had a higher resistance to corrosion. Moreover, the differences in curing process and solvents used have no effect on the thickness of the coatings.

Chapter IX. Conclusions and Future Work

9.1. Conclusions

This chapter summarises the project, its findings and conclusions from the work undertaken during the project. It ends on ideas for relevant future work

The main objective of this project was to analyse the sol-gel coatings from the sponsor company, EPG-AG. To achieve this goal there were several steps: a first batch containing organic, inorganic/hybrid and hybrid/composites coatings on two different steels. The purpose of this batch was to study which type of samples had a stronger resistance to corrosion in a mildly aggressive environment and presents improved protective and barrier properties as well as better mechanical properties. A methodology was developed with this batch which would be used for the following batches. The environment of the static experiment for Batch 1 was too aggressive thus the conditions were changed for Batch 2 and Batch 3. The purpose being the comparison of samples to determine their resistance properties, the conditions were changed to room temperature, CO_2 saturated in 3.5%NaCl solution. The organic coatings from Batch 1 were discarded to focus on sol-gel coatings (inorganic/hybrid and hybrid/composites coatings) for further analysis. In Batch 1, the inorganic/hybrid coatings seem to be more resistant to corrosion than the hybrid/composites coatings.

Then the focus of the project was changed with Batch 2 to be on samples with inorganic/hybrid and hybrid/composites coatings with or without doping. There was a change in metal substrate as well (from 316L stainless steel and X65 carbon steel for Batch 1 to 304 stainless steel and A1008Qpanel due to company restrictions for stainless steel, because of lack of adhesion for carbon steel). Different amounts of doping were introduced: 0%w/w (no doping), 2.8%w.w, 5.6%w.w and 11.3%w.w of titanium butoxide used as a precursor. Different percentages were chosen to gain information about the influence of its amount on the properties of the coatings: while there is an increase in resistance of the coatings, there is a threshold which weakens the coating once exceeded (above 10%w.w).

The last batch (Batch 3) consisted of inorganic/hybrid samples without doping or with different amounts of doping precursor (same as Batch 2) and different parameters modified during the sol-gel process: curing process (in N_2 or in air) and solvent used (isopropanol or mixture) in order to define the best combination leading

to the most resistant samples. The substrate was the same for all the samples for this batch (304 stainless steel).

The sol-gel coating degradation was studied for 30days of immersion in corrosive environment. The results of different methods could be linked between themselves and allow further understanding of the degradation mechanism. Several techniques are needed to evaluate and to optimize the coatings and thus giving a global view of the system.

The EIS data, while exposing the values of the resistance of the coatings also revealed the differences of order of magnitude which is linked to the corrosion progress. EIS method is useful for characterizing the coatings and the corrosion protection properties. It also gives possibility to determine the equivalent circuit which compare the most to the behaviour of the coating/metal interface. From this the capacitance of the coating can be determined, which is linked to the water uptake. The EIS data allowed the comparison of the samples and the influence that the parameters: nature of the coating, substrate, amount of precursor, solvent and curing process have on the barrier properties and corrosion resistance. This is correlated to the salt spray test which is an accelerated corrosion test as well as the erosion-corrosion test.

In the case of electrochemical measurements the coatings would be defined as failed when the resistance measured by EIS is equal to the value resistance of the bare substrate metal. While it is difficult to use EIS only by itself, when combined to other techniques details on the evolution of corrosion are obtained.

The results obtained for the samples of Batch 1 are considered as poor. Then the conditions were changed in order to focus on comparing the behaviour of the samples. Some of the coatings from Batch 2 and Batch 3 are found to be efficient for the amount of time tested as protective sol-gel coatings against corrosion as the corrosion resistance of the substrate is found to be improved by the tested coatings. The sample: coating + substrate is considered as a whole system. The samples with inorganic/hybrid coatings were more efficient especially for undoped and doped with 2.8% and 5.6%w/w precursor and with stainless steel as a substrate. The evolution of Bode and Nyquist plots help to prove the resistance of the samples, as a decrease in the impedance response indicates a decrease in the ability to protect and resistance of the system. Moreover the water uptake is linked to the capacitance and an increase in the capacitance value leads to an increase in water

uptake. This resistance was supported with the results of salt-spray and erosion tests, especially for undoped samples which had better corrosion protection.

The FTIR results presented the evolution of the surface composition with time as well, showing that some Si-OH bonds are formed. The FTIR spectra show that the hybrid/composites samples present peaks from both organic and inorganic/hybrid systems. The addition of doping element, with different percentages, do not change the basic structure of the functional groups detected on the surface of the samples. The spectra also present the evolution of the functional groups of the surface of the coating with additional peaks being added in case of damage. Some similarities can be found depending on the percentage of titanium precursor.

There is no direct degradation of the substrate as seen with FTIR where the water uptake found with EIS does not change the performance of the coating or with the SEM which shows no evidence of corrosion. It can be concluded that EIS measurements and results can be useful to help predicting the lifespan of coatings while immersed. However there seem to be a limit to the amount of titanium allowing the anti-corrosive properties to protect the substrate. The samples with coatings containing less than 10% of precursor give the optimum results for corrosion protection.

The corrosion process at the coating/substrate interface is strongly dependent on the nature of substrates. The barrier properties of the coating can be weakened by the corrosion rate of the active metal substrate, leading to the damaging of the coating.

The nanoindentation tests of the coatings showed that the hardness of the coating is not influenced by the concentration of the doping precursor but that it is a parameter to be considered regarding the Young modulus and the stiffness of the sample. The addition of titanium precursor makes the coating stiffer while having little to no influence on the hardness.

A thick and well-adhered coating provides good corrosion resistance to the substrate. However there is limitation of the coating which is the problem of defects that could be generated at higher coating thickness due to the internal stress within the coating and the properties of the coating itself. An optimum thickness, depending on the purpose of the coatings, should be investigated to avoid the onset of the coating defect as well as the homogeneity of the coating itself in order to have an even thickness all over the surface of the coating. The fluctuation of the thickness

as presented with FIB-SEM lead to faster corrosion when the substrate is barely protected. The nature of coating selected depends on the purpose of its use of coatings. Organic coatings were proven to have a greater thickness and thus a higher critical load. In Batch 1 the coatings with the greater thicknesses were organic and had the higher critical load with a ductile-type of failure. They can be of better use for areas where coatings with a greater critical load and strong adhesion are needed (the load can be linked to the adhesion) but due to their thermal weakness they cannot be used in certain areas of research. The inorganic/hybrid coatings presented a lower critical load but higher resistance properties and thus can be of use in mildly aggressive environment to protect substrates.

The addition of titanium butoxide has led to an improvement in the barrier properties and durability of the coatings. However there is an optimum concentration since an amount of more than 10% decreases these properties. Different amounts: 0%w/w, 2.8%w/w, 5.6%w/w and 11.3%w/w were studied. Samples from Batch 1 gave poor results as well as hybrid/composites systems from Batch 2, while inorganic/hybrid systems from Batch 2 and Batch 3 gave results which can be considered as acceptable. Most of the post-test investigations showed little signs of corrosion for the inorganic/hybrid coatings, (undoped and doped up to 5.6%w/w) with high values of resistance which indicate good anti-corrosion performance of the coatings.

The choice of substrate depending on the nature of the coating has to be taken into account has it was demonstrated once again with the experiments in this project that inorganic/hybrid sol-gel coatings do not adhere well on carbon steel. The adhesion of coatings on the substrate is the most important key characteristics as there would be no protection without the coating.

In a CO_2 environment, mildly aggressive, the inorganic/hybrid coatings undoped or with less than 10% of dopant can be used for corrosion protection. However only the undoped coating could be of use for erosion resistance. The coatings with a higher thickness can be of use for areas where strong critical load is needed while the other types of coatings are thinner and thus could be of use in other areas of protection. The coatings studied presented acceptable results for mildly aggressive environment at room temperature on flat surfaces. For experiments in similar conditions, the inorganic/hybrid coatings of this project (with a percentage of precursor less than 10%w/w) presented comparable results of corrosion resistance to epoxy coatings used for oil and gas pipelines. This is one area of research where the coatings could be applied as their resistance to corrosion can be considered as

acceptable; thus they can be applied on surfaces where the tolerance of sections is critical to ensure the proper functioning.

9.2 Relevance of the Research

Sol-gel coatings, despite decades of research and several advantages are still not as employed as they could. Thus it is hoped that by providing a better understanding of the mechanism of corrosion, corrosion performance, mechanical durability and influence of composition of coatings, this study will contribute to the path where the sol-gel coatings approach can be further developed and optimised.

This study, by combining electrochemical impedance spectroscopy with FTIR, offers an insight into the evaluation of the performance of the coatings. Those two techniques, while being frequently used in the field of corrosion and coatings, have been barely used together.

The characterisation of different types of coatings (inorganic/hybrid, organic and hybrid/composites) with different formulations and different amounts of precursor with EIS, FTIR, SEM/EDX, adhesion, nano-hardness and erosion present many point of views of the systems studied and information on the corrosion of these specific samples. Even when poor results are obtained, information is collected to improve the systems and literature.

When it comes to titanium and silica sol-gel coatings, most results include titanium nanoparticles as doping precursor. This study is about titanium butoxide as a dopant. The results presented showed that even without precursor the coating is considered as providing good resistance to corrosion with the addition of titanium butoxide increasing slightly this resistance but within a definite range of amount added.

9.3 Recommendations for Future Work

The experiments done during this project revealed a connection between the composition of the sol-gel coatings and the properties of the coatings. From there, there can be several directions for this work:

- Dope inorganic/hybrid samples with titanium butoxide with percentages below 10% and closer to 5% to determine the optimum concentration.
- Doping with titanium butoxide into different coatings
- Investigation into the porosity of the coatings.
- A detailed study of the functionalisation process and its impact on behavior.
- Determining the coating most resistant to corrosion; the concentration of various chemical compounds in the solution of the coating can be varied.
- Ascertain on what can make the coatings crack during the heating step and how to prevent it.
- Experiments with elevated temperature and pressure to examine the stability and adhesion properties of the coatings.
- Field testing as final qualification of coatings since laboratory testing cannot reproduce all conditions occurring in the field.
- Experiments on the same sol-gel coatings but with several layers deposited on substrates.

List of References

1. Barker, R., *Erosion-Corrosion of Carbon Steel Pipework on an Offshore Oil and Gas Facility*, Thesis, in *Mechanical Engineering*. 2012, University of Leeds: Leeds.
2. Chinedu, O.I., *Advances in asset management techniques: an overview of corrosion mechanisms and mitigation strategies for oil and gas pipelines.* International Scholarly Research Network - Corrosion, 2012. **2012**.
3. Davis, J.R., *Corrosion: understanding the basics*. 2000, Materials Park, OH: ASM International.
4. *Corrosion Resistant Coatings*. Coating applications 2011; [Online] Available from: https://www.metcoat.com/corrosion-resistant-coatings.htm.
5. Chemtronics *Conformal coatings guide*. 2018.
6. Pierre, A.C., *Introduction to sol-gel processing*. The Kluwer International Series in Sol-Gel Processing: Technology and Applications. Vol. 1. 1998, Boston/Dordrecht/London: Kluwer Academic Publishers.

.

7. Dimitriev, Y., Y. Ivanova, and R. Iordanova, *History of sol-gel science and technology*. Vol. 43. 2008. 181-192.
8. Zhong, X., et al., *A novel approach to heal the sol–gel coating system on magnesium alloy for corrosion protection.* Electrochimica Acta, 2010. **55**(7): p. 2424-2429.
9. Birch, W.R. and e. al., *The Molecular and Microscopic Structure of Precursing Thin Films of Anionic Surfactant on the Silicon Oxide/ Silicon surface.* Langmuir, 1995(11): p. 48.
10. Pepe, A., et al., *Sol-gel coatings on carbon steel: Electrochemical evaluation.* Surface and Coatings Technology, 2006. **200**(11): p. 3486-3491.
11. Saravanan, P., K. Jayamoorthy, and S. Ananda Kumar, *Design and characterization of non-toxic nano-hybrid coatings for corrosion and fouling resistance.* Journal of Science: Advanced Materials and Devices, 2016. **1**(3): p. 367-378.
12. Zheng, S. and J. Li, *Inorganic–organic sol gel hybrid coatings for corrosion protection of metals.* J Sol-Gel Sci Technol, 2010. **54**: p. 174-187.
13. Oyeneyin, B., *Integrated sand management for effective hydrocarbon flow assurance*. Vol. 62.;62;. 2014, Amsterdam: Elsevier.
14. Schweitzer, P.A., *Paint and coatings: applications and corrosion resistance*. 2006, Boca Raton, FL: Taylor & Francis.
15. Perez, N., *Electrochemistry and Corrosion Science*. 2004, Boston: Kluwer Academic Publishers.
16. Revie, R.W., *Uhlig's Corrosion Handbook*. 3rd Edition ed, ed. J.W. Sons. 2011, New York.
17. Fink, J.K., *Oil Field Chemicals*, in *Oil Field Chemicals*, J.K. Fink, Editor. 2003, Gulf Professional Publishing: Burlington. p. 1-33.
18. Lenntech. *Water Conductivity*. [Online] Available from: https://www.lenntech.com/applications/ultrapure/conductivity/water-conductivity.htm.
19. Kozhukharov, S.V., *Advanced Multifunctional Corrosion Protective Coating Systems for Light-Weight Aircraft Alloys—Actual Trends and Challenges*. Thin Film Processes - Artifacts on Surface Phenomena and Technological Facets. 2017.
20. Kharchenko, M.P., *Increased reliability bus system to transport gas environments*. 2013, Donetsk National Technical University: Unpublished master's thesis.
21. Roberge, P.R., *Corrosion engineering, principles and practice*. 2008: McGraw Hill Professional.

22. Curkovic, L., et al., *Enhancement of corrosion protection of AISI 304 stainless steel by nanostructured sol-gel TiO2 films.* CORROSION SCIENCE, 2013. **77**: p. 176-184.
23. Giourntas, L., T. Hodgkiess, and A.M. Galloway, *Comparative study of erosion–corrosion performance on a range of stainless steels.* Wear, 2015. **332–333**: p. 1051-1058.
24. Trethewey, K.R., *Corrosion for science and engineering*. 2nd ed. 1995, Harlow: Longman Scientific & Technical.
25. Uhlig, H.H., *Corrosion and corrosion control : an introduction to corrosion science and engineering*. 2nd ed ed. 1971, New York: Wiley.
26. Craig, B.D., *Fundamental aspect of corrosion films in corrosion science*. 1991, New York: Plenum.
27. Marcus, P., *Corrosion mechanisms in theory and practice*. 3rd ed. Corrosion technology. 2012, New York: Marcel Dekker.
28. Schutze, M., *Corrosion and environmental degradation*. Materials science and technology : a comprehensive treatment ; v. 19. Vol. Vol. 1. 2000, Weinheim ; Chichester: Wiley-VCH.
29. Scully, J.C., *The fundamentals of corrosion*. 3rd ed ed. 1990, Oxford: Pergamon Press.
30. Tait, W.S., *An Introduction to Electrochemical Corrosion Testing for Practicing Engineers and Scientists*. 1994, Racine, Wis: PairODocs Publications.
31. Jones, D.A., *Principles and prevention of corrosion*. 2nd Edition ed. 1996, Englewood Cliffs, NJ: Prentice Hall.
32. Papavinasam, S., *Corrosion control in the oil and gas industry*. 2014, Amsterdam: Elsevier/ Gulf Professional.
33. Ukpai, J.I., *Erosion-Corrosion Characterisation for Pipeline Materials Using Combined Acoustic Emission and Electrochemical Monitoring*, in *Mechanical Engineering*. 2014, University of Leeds: UK.
34. Steel, A., *Galvanic Corrosion*, in *Atlas Tech Note No.7*. 2010.
35. Bhandari J, et al., *Modelling of pitting corrosion in marine and offshore steel structures – A technical review.* Journal of Loss Prevention in the Process Industries, 2015. **37**: p. 39-62.
36. Treseder, R.S. and R.N. Tuttle, *Corrosion control in oil and gas production*. Vol. 1998. 1998, Houston, Texas CORUPDATE for NACE International.
37. Cole, I.S., et al., *Corrosion of pipelines used for CO2 transport in CCS: Is it a real problem?* International Journal of Greenhouse Gas Control, 2011. **5**(4): p. 749-756.
38. Nace. *Testing for Localized Corrosion*. [Online] Available from: https://www.nace.org/Corrosion-Central/Corrosion-101/Testing-for-Localized-Corrosion/.
39. Aribo, S., *Corrosion and Erosion-Corrosion Behaviour of Lean Duplex Stainless Steels in Marine and Oilfield Environments*, Thesis, in *Mechanical Engineering*. 2014, University of Leeds: Leeds.
40. Levy, A.V., *Solid particle erosion and erosion-corrosion of materials*. 1995, Materials Park: ASM International.
41. Zhao, Y., et al., *Erosion–corrosion behavior and corrosion resistance of AISI 316 stainless steel in flow jet impingement.* Wear, 2015. **328–329**: p. 464-474.
42. Stansbury, E.E. and R.A. Buchanan, *Fundamentals of Electrochemical Corrosion*. 2000: ASM International.
43. Brett, C.M.A., Brett Oliveira, Ana Maria, *Electrochemistry - Principles, Methods, and Applications*. 1993, Oxford: Oxford University Press.
44. Shreir, L.L., Burstein, G. T., Jarman, R. A., *Corrosion*. Vol. 3rd;3.;. 1994, Oxford;Boston;: Butterworth-Heinemann.
45. Oldham, K. and J. Myland, *Fundamentals of electrochemical science*, ed. Elsevier. 1993.

46. Kruger, J., *Electrochemistry of Corrosion*, in *Electrochemistry Encyclopedia*, [Online] Available from : http://electrochem.cwru.edu/ed/encycl/, Editor. 2001.
47. Shaw, B.A. and R.G. Kelly, *"What is corrosion?"* Electrochemical Society Interface, 2006. **15**(1): p. 24-26.
48. Roberge, P.R., *Handbook of Corrosion Engineering*. 2000, New York;London: McGraw-Hill.
49. Callegaro, L., *Electrical impedance: principles, measurement, and applications*. Vol. 10. 2013, Boca Raton, FL: CRC Press.
50. Wang, C., *Erosion-corrosion mitigation using chemicals*, in *School of Mechanical Engineering*. 2007, University of Leeds: Leeds.
51. Pharr, G. and W. Oliver, *Measurement of Thin Film Mechanical Properties Using Nanoindentation.* MRS Bulletin, 1992. **17**(7): p. 28-33.
52. Bard, A.J. and L.R. Faulkner, *Electrochemicals methods: Fundamentals and applications*. 2nd ed ed. 2001, United States of America: John Wiley & Sons,.
53. Nešić, S., *Key issues related to modelling of internal corrosion of oil and gas pipelines – A review.* Corrosion Science, 2007. **49**(12): p. 4308-4338.
54. Kermani, M.B. and A. Morshed, *Carbon dioxide corrosion in oil and gas production - A compendium.* Corrosion, 2003. **59**(8): p. 659-683.
55. Mishra, B., et al., *Development of a Predictive Model for Activation-Controlled Corrosion of Steel in Solutions Containing Carbon Dioxide.* Corrosion, 1997. **53**(11): p. 852-860.
56. Sun, W. and S. Nesic, *Kinetics of Corrosion Layer Formation: Part 1-Iron Carbonate Layers in Carbon Dioxide Corrosion.* Corrosion, 2008. **64**(4): p. 334-346.
57. Wang, D. and G.P. Bierwagen, *Sol–gel coatings on metals for corrosion protection.* Progress in Organic Coatings, 2009. **64**(4): p. 327-338.
58. Fabes B.D., e.a., *Sol-gel derived ceramic coatings in: Ceramic films and coatings*. 1993, New Jersey: Noyes publications.
59. Brinker, C.J. and G.W. Scherer, *THE PHYSICS AND CHEMISTRY OF SOL-GEL PROCESSING* Materials and Manufacturing Processes, ed. I. Academic Press. Vol. 8. 1990, San Diego, CA Taylor & Francis. 391-392.
60. Livage, J. and J. Lemerle, *TRANSITION-METAL OXIDE GELS AND COLLOIDS.* Annual Review of Materials Science, 1982. **12**: p. 103-122.
61. ChematTechnology. *A Total Sol-Gel Solution*. 2009; [Online] Available from: http://www.chemat.com/chemattechnology/news.aspx.
62. Stern, K.H., *Metallurgical and ceramic protective coatings*. 1996, London: Chapman & Hall.
63. Metroke, T.L., R.L. Parkhill, and E.T. Knobbe, *Passivation of metal alloys using sol–gel-derived materials — a review.* Progress in Organic Coatings, 2001. **41**(4): p. 233-238.
64. Yerokhin, A.L., et al., *Plasma electrolysis for surface engineering.* Surface and Coatings Technology, 1999. **106**: p. 167-173.
65. Gogotsi, G.A., *Fracture toughness of ceramics and ceramic composites.* Ceramics International, 2003. **29**(7): p. 777-784.
66. Bagheri, S., et al., *Nanocomposites in Electrochemical Sensors*. 2016: CRC Press.
67. Berg, J.C., *An introduction to interfaces & colloids : the bridge to nanoscience*. 2010, Singapore, London: World Scientific.
68. Cosgrove, T., *Colloid science: principles, methods and applications*. 2005, Oxford: Blackwell Pub.
69. Tadros, T.F., *Colloid stability: the role of surface forces*. Vol. 1, 2. 2007, Weinheim: Wiley-VCH Verlag.
70. Pope, E.J.A., S. Sakka, and L.C. Klein, *Sol-gel science and technology*. Vol. 55. 1995, Westerville, Ohio: American Ceramic Society.

71. Gallardo, J., A. Durán, and J.J. de Damborenea, *Electrochemical and in vitro behaviour of sol–gel coated 316L stainless steel.* Corrosion Science, 2004. **46**(4): p. 795-806.
72. Zheludkevich, M.L., I.M. Salvado, and M.G.S. Ferreira, *Sol-gel coatings for corrosion protection of metals.* Journal of Materials Chemistry, 2005. **15**(48): p. 5099-5111.
73. Brinker, C.J., *Hydrolysis and condensation of silicates: Effects on structure.* Journal of Non-Crystalline Solids, 1988. **100**(1–3): p. 31-50.
74. Livage, J., M. Henry, and C. Sanchez, *Sol-gel chemistry of transition metal oxides.* Progress in Solid State Chemistry, 1988. **18**(4): p. 259-341.
75. Hench, L.L., *Sol-Gel Silica: Properties, Processing and Technology Transfer*. 1998, Westwood, New Jersey: Noyes publications.
76. Hench, L.L. and J.K. West, *The Sol-Gel Process.* Chem. Rev., 1990. **90**: p. 33-72.
77. Komarneni, S. *Sol-gel synthesis and processing*. in *American Ceramic Society*. 1998. Westerville, Ohio: American Ceramic Society.
78. Aegerter M.A., M.M., *Sol-gel technologies for glass producers and users*. 2004, New York: Kluwer Academic Publishers.
79. Chou, T.P., et al., *Organic–inorganic hybrid coatings for corrosion protection.* Journal of Non-Crystalline Solids, 2001. **290**(2–3): p. 153-162.
80. Fallet, M., et al., *Electrochemical behaviour of ceramic sol–gel coatings on mild steel.* Journal of Non-Crystalline Solids, 2001. **293–295**: p. 527-533.
81. Ruhi, G., et al., *Effect of sintering temperatures on corrosion and wear properties of sol–gel alumina coatings on surface pre-treated mild steel.* Corrosion Science, 2008. **50**(3): p. 639-649.
82. Twite, R.L. and G.P. Bierwagen, *Review of alternatives to chromate for corrosion protection of aluminum aerospace alloys.* Progress in Organic Coatings, 1998. **33**(2): p. 91-100.
83. Guglielmi, M., *Sol-Gel Coatings on Metals.* Journal of Sol-Gel Science and Technology, 1997. **8**(1-3): p. 443-449.
84. El Hadad, A.A., et al., *Biocompatibility and Corrosion Protection Behaviour of Hydroxyapatite Sol-Gel-Derived Coatings on Ti6Al4V Alloy.* Materials 2017. **10**(2).
85. Alcantara-Garcia, A., A. Garcia-Casas, and A. Jiménez-Morales, *Electrochemical study of the synergic effect of phosphorus and cerium additions on a sol-gel coating for Titanium manufactured by powder metallurgy.* Progress in Organic Coatings, 2018. **124**: p. 267-274.
86. Zhang, Q.H., et al., *Comparative study on cracking behavior of sol-gel silica antireflective coating for high-powered laser system.* Engineering Failure Analysis, 2017. **82**: p. 64-71.
87. Babhu Vignesh, R., J. Balaji, and M.G. Sethuraman, *Surface modification, characterization and corrosion protection of 1,3-diphenylthiourea doped sol-gel coating on aluminium.* Progress in Organic Coatings, 2017. **111**: p. 112-123.
88. Gobara, M., *Effects of TiO2/SiO2 reinforced nanoparticles on the mechanical properties of green hybrid coating.* International Letters of Chemistry, Physics and Astronomy, 2015. **47**: p. 56-66.
89. Akid, R., M. Gobara, and H. Wang, *Corrosion protection performance of novel hybrid polyaniline/sol–gel coatings on an aluminium 2024 alloy in neutral, alkaline and acidic solutions.* Electrochimica Acta, 2011. **56**(5): p. 2483-2492.
90. Kermadi, S., et al., *Sol-gel synthesis of xTiO2(100 − x)SiO2 nanocomposite thin films: Structure, optical and antireflection properties.* Thin Solid Films, 2014. **564**: p. 170-178.
91. Xu, J., W. Pang, and W. Shi, *Synthesis of UV-curable organic–inorganic hybrid urethane acrylates and properties of cured films.* Thin Solid Films, 2006. **514**(1-2): p. 69-75.

92. Zhang, H., et al., *Comparative study on the optical, surface mechanical and wear resistant properties of transparent coatings filled with pyrogenic and colloidal silica nanoparticles.* Composites Science and Technology, 2011. **71**(4): p. 471-479.
93. Atanacio, A.J., et al., *Mechanical properties and adhesion characteristics of hybrid sol–gel thin films.* Surface and Coatings Technology, 2005. **192**(2–3): p. 354-364.
94. Kittel, J., et al., *New methods for the study of organic coatings by EIS: New insights into attached and free films.* Progress in Organic Coatings, 2001. **41**(1-3): p. 93-98.
95. Krakow, U.o.S.a.T.S.S., *Organic coatings*, in *Corrosion and corrosion protection*. 2014.
96. Fedrizzi, L., et al., *The use of electrochemical techniques to study the corrosion behaviour of organic coatings on steel pretreated with sol–gel zirconia films.* Electrochimica Acta, 2001. **46**(24–25): p. 3715-3724.
97. Khobaib, M., L.B. Reynolds, and M.S. Donley, *A comparative evaluation of corrosion protection of sol–gel based coatings systems.* Surface and Coatings Technology, 2001. **140**(1): p. 16-23.
98. Vasconcelos, D.C.L., et al., *Corrosion resistance of stainless steel coated with sol–gel silica.* Journal of Non-Crystalline Solids, 2000. **273**(1–3): p. 135-139.
99. Di Maggio, R., et al., *Dry and wet corrosion behaviour of AISI 304 stainless steel coated by sol-gel ZrO2-CeO2 films.* Thin Solid Films, 1996. **286**(1-2): p. 127-135.
100. Menning, M., et al., *Investigation of Glass-Like Sol-Gel Coatings for Corrosion Protection of Stainless Steel Against Liquid and Gaseous Attack.* Journal of Sol-Gel Science and Technology, 1998. **13**(1-3): p. 717-722.
101. Zheng, H., et al., *An alternative to anodization: Sol-gel solutions for metal finishing.* Metal Finishing, 1998. **96**(12): p. 35-38.
102. Aliofkhazraei, M., *Anti-abrasive nanocoatings : current and future applications*. Materials, ed. Woodhead. Publishing. 2015, Amsterdam.
103. Kalidindi, R.S.R. and R. Subasri, *5 - Sol-gel nanocomposite hard coatings*, in *Anti-Abrasive Nanocoatings*, M. Aliofkhazraei, Editor. 2015, Woodhead Publishing. p. 105-136.
104. Misli, Z.H., et al. *Inorganic Coatings*. Coating Failures 2013; Available from: https://bengforensic.wordpress.com/different-types-of-coatings/inorganic-coatings/.
105. Mackenzie, J.D. and E. Bescher, *Some Factors Governing the Coating of Organic Polymers by Sol-Gel Derived Hybrid Materials.* Journal of Sol-Gel Science and Technology, 2003. **27**(1): p. 7-14.
106. *Nanocoatings and Ultra-Thin Films: Technologies and Applications*. Metals and Surface Engineering, ed. W.P. Series. Elsevier.
107. Ono, S., et al., *Improvement of Corrosion Resistance of Metals by an Environmentally Friendly Silica Coating Method.* Journal of Sol-Gel Science and Technology, 2004. **29**(3): p. 147-153.
108. M.F., M., *Functional and smart coatings for corrosion protection: A review of recent advances.* Surface & Coatings Technology, 2014. **258**: p. 17-37.
109. Ahmad, S., et al., *Synthesis, characterization and development of high performance siloxane-modified epoxy paints.* Progress in Organic Coatings, 2005. **54**(3): p. 248-255.
110. Qian, M., et al., *Two-part epoxy-siloxane hybrid corrosion protection coatings for carbon steel.* Thin Solid Films, 2009. **517**(17): p. 5237-5242.
111. Diaz, I., et al., *Corrosion resistance of new epoxy–siloxane hybrid coatings. A laboratory study.* Progress in Organic Coatings, 2010. **69**(3): p. 278-286.
112. Lavollee, C., et al., *New architectured hybrid sol-gel coatings for wear and corrosion protection of low-carbon steel.* Progress in Organic Coatings, 2016. **99**: p. 337-345.

113. Maia, F., et al., *Corrosion protection of AA2024 by sol–gel coatings modified with MBT-loaded polyurea microcapsules.* Chemical Engineering Journal, 2016. **283**: p. 1108-1117.
114. Zheludkevich, M.L., et al., *Nanostructured sol-gel coatings doped with cerium nitrate as pre-treatments for AA2024-T3 Corrosion protection performance.* Electrochimica Acta, 2005. **51**(2): p. 208-217.
115. Seok, S.I., et al., *Preparation of corrosion protective coatings on galvanized iron from aqueous inorganic–organic hybrid sols by sol–gel method.* Surface and Coatings Technology, 2006. **200**(11): p. 3468-3472.
116. Schottner, G., *Hybrid Sol-Gel-Derived Polymers: Applications of Multifunctional Materials.* Chem. Mater, 2001. **13**: p. 3422-3435.
117. Figueira, R.B., C.J.R. Silva, and E.V. Pereira, *Organic-inorganic hybrid sol-gel coatings for metal corrosion protection: a review of recent progress.* Journal of Coatings Technology and Research, 2015. **12**(1): p. 1-35.
118. Alibakhshi, E., et al., *Evaluation of the corrosion protection performance of mild steel coated with hybrid sol-gel silane coating in 3.5 wt.% NaCl solution.* Progress in Organic Coatings, 2018. **123**: p. 190-200.
119. Danks, A.E., S.R. Hall, and Z. Schnepp, *The evolution of 'sol–gel' chemistry as a technique for materials synthesis.* Materials Horizons, 2016. **3**(2): p. 91-112.
120. Aries, L., et al., *Conversion coating on stainless steel as a support for electrochemically induced alumina deposit.* Electrochimica Acta, 1996. **41**(18): p. 2799-2803.
121. Marx, J., et al., *Rheological and Coating Properties of Modified Silica Sols.* Journal of Sol-Gel Science and Technology, 1998. **13**(1-3): p. 89-94.
122. Thim, G.P., et al., *Sol–gel silica film preparation from aqueous solutions for corrosion protection.* Journal of Non-Crystalline Solids, 2000. **273**(1–3): p. 124-128.
123. Shen, G.X., Y.C. Chen, and C.J. Lin, *Corrosion protection of 316 L stainless steel by a TiO2 nanoparticle coating prepared by sol–gel method.* Thin Solid Films, 2005. **489**(1–2): p. 130-136.
124. Zheludkevich, M.L., et al., *Corrosion protective properties of nanostructured sol–gel hybrid coatings to AA2024-T3.* Surface and Coatings Technology, 2006. **200**(9): p. 3084-3094.
125. Hofacker, S., et al., *Sol–gel: a new tool for coatings chemistry.* Progress in Organic Coatings, 2002. **45**(2–3): p. 159-164.
126. Zhou, Y., C. Chiu, and H. Liang, *Interfacial Structures and Properties of Organic Materials for Biosensors: An Overview.* Sensors, 2012. **12**(11): p. 15036-15062.
127. Mackenzie, J.D. and E.P. Bescher, *Structures, Properties and Potential Applications of Ormosils.* Journal of Sol-Gel Science and Technology, 1998. **13**(1-3): p. 371-377.
128. AerogelTechnologies. *Production of Silica Gels: Alkoxide Method*. [Online] Available from: http://www.aerogel.org/?p=90.
129. Tushinsky, L., et al., *Coated Metal: Structure and Properties of Metal-Coating Compositions*. Engineering Materials. 2002, Berlin: Springer-Verlag Berlin Heidelberg.
130. Oliver, W. and G. Pharr, *An improved technique for determining hardness and elastic modulus using load and displacement sensing indentation experiments.* Journal of Materials Research, 1992. **7**(6): p. 1564-1583.
131. Malzbender, J., et al., *Measuring mechanical properties of coatings: a methodology applied to nano-particle-filled sol–gel coatings on glass.* Materials Science & Engineering R, 2002. **36**(2): p. 47-103.
132. Loveday, D., P. Peterson, and B. Rodgers, *Evaluation of organic coatings with electrochemical impedance spectroscopy Part 1: Fundamentals of Electrochemical Impedance Spectroscopy.* Journal of Coatings Technology and Research, 2004.

133. Fischer-Cripps, A.C., *A review of analysis methods for sub-micron indentation testing.* Vacuum, 2000. **58**: p. 569-585.
134. Piens, M. and H. De Deurwaerder, *Effect of coating stress on adherence and on corrosion prevention.* Progress in Organic Coatings, 2001. **43**(1–3): p. 18-24.
135. Miszczyk, A. and T. Schauer, *Electrochemical approach to evaluate the interlayer adhesion of organic coatings.* Progress in Organic Coatings, 2005. **52**(4): p. 298-305.
136. Amirudin, A. and D. Thieny, *Application of electrochemical impedance spectroscopy to study the degradation of polymer-coated metals.* Progress in Organic Coatings, 1995. **26**(1): p. 1-28.
137. Deflorian, F., et al., *Organic coating capacitance measurement by EIS: ideal and actual trends.* Electrochimica Acta, 1999. **44**(24): p. 4243-4249.
138. Soutar, A.M., Q. Chen, and R.E. Raja Khalif, *Evaluation of commercially available transparent hard coating for polycarbonate*, in *SIMTech technical report* 2008. p. 161-165.
139. Sheffer, M., A. Groysman, and D. Mandler, *Electrodeposition of sol–gel films on Al for corrosion protection.* Corrosion Science, 2003. **45**(12): p. 2893-2904.
140. Voevodin, N., et al., *Characterization of pitting corrosion in bare and sol–gel coated aluminum 2024-T3 alloy.* Surface & Coatings Technology, 2001. **140**(1): p. 29-34.
141. Viitala, R., et al., *Surface properties of in vitro bioactive and non-bioactive sol–gel derived materials.* Biomaterials, 2002. **23**(15): p. 3073-3086.
142. ChematTechnology. *Advances in Sol-Gel Technology*. 2001; [Online] Available from: https://www.ceramicindustry.com/articles/83256-advances-in-sol-gel-technology.
143. Yusoff, M.F.M., et al., *Dipcoating of poly (ε-caprolactone)/hydroxyapatite composite coating on Ti6Al4V for enhanced corrosion protection.* Surface and Coatings Technology, 2014. **245**: p. 102-107.
144. Conde, A., A. Durán, and J.J. de Damborenea, *Polymeric sol–gel coatings as protective layers of aluminium alloys.* Progress in Organic Coatings, 2003. **46**(4): p. 288-296.
145. Masalski, J., et al., *Improvement in corrosion resistance of the 316l stainless steel by means of Al2O3 coatings deposited by the sol-gel method.* Thin Solid Films, 1999. **349**(1–2): p. 186-190.
146. Riboni, N., et al., *Sol-gel coated ion sources for liquid chromatography-direct electron ionization mass spectrometry.* Analytical Chimica Acta, 2017. **978**: p. 35-41.
147. *Applications of sol-gel technology*. Handbook of sol-gel science and technology. , ed. S. Sakka. Vol. 3. 2005: Springer Science & Business Media.
148. Castro, Y., et al., *Silica Sol-Gel Coatings on Metals Produced by EPD.* Journal of Sol-Gel Science and Technology, 2003. **26**(1-3): p. 735-739.
149. Low, J. *Electrodeposition of Nanostructured Metallic Coatings*. Electrochemical Coatings.
150. Leidheiser, H.J., *Corrosion of Painted Metals—A Review.* Corrosion, 1982. **38**(7): p. 374-383.
151. Yasakau, K.A., et al., *Influence of sol-gel process parameters on the protection properties of sol-gel coatings applied on AA2024.* SURFACE & COATINGS TECHNOLOGY, 2014. **246**: p. 6-16.
152. Liu, B., et al., *Blistering failure analysis of organic coatings on AZ91D Mg-alloy components.* Engineering Failure Analysis, 2014. **42**: p. 231-239.
153. Sorensen, P.A., et al., *Cathodic delamination: Quantification of ionic transport rates along coating–steel interfaces.* Progress in Organic Coatings, 2010. **68**(1-2): p. 70-78.
154. Kuchinski, F.A., *Corrosion resistant thick films by enamelling*, in *Ceramic films and coatings.* 1993, Noyes Publications: New Jersey.

155. García-Alonso, M.C., et al., *Effect of substrate roughness on the corrosion behaviour of the Al2O3/MA 956 system.* Biomaterials, 2000. **21**(1): p. 79-87.
156. Bamoulid, L., et al., *An efficient protection of stainless steel against corrosion: Combination of a conversion layer and titanium dioxide deposit.* Surface and Coatings Technology, 2008. **202**(20): p. 5020-5026.
157. GamryInstruments. *Basics of Electrochemical Impedance Spectroscopy*. 1997; [Online] Available from: https://www.gamry.com/application-notes/EIS/basics-of-electrochemical-impedance-spectroscopy/.
158. Thai, T.T., et al., *Influence of the sol-gel mesoporosity on the corrosion protection given by an epoxy primer applied on aluminum alloy 2024 –T3.* Progress in Organic Coatings, 2018. **121**: p. 53-63.
159. Mansfeld, F., et al., *Analysis of electrochemical impedance and noise data for polymer coated metals.* Corrosion Science, 1997. **39**(2): p. 255-279.
160. Geenen, F.M., J.H.W. De Wit, and E.P.M. Van Westing, *An impedance spectroscopy study of the degradation mechanism for a model epoxy coating on mild steel.* Progress in Organic Coatings, 1990. **18**(3): p. 399-312.
161. Van Westing, E.P.M., G.M. Ferrari, and J.H.W. De Wit, *The determination of coating performance with impedance measurements-I. Coating polymer properties.* Corrosion Science, 1993. **34**(9): p. 1511-1530.
162. Van Westing, E.P.M., et al., *In situ determination of the loss of adhesion of barrier epoxy coatings using electrochemical impedance spectroscopy.* Progress in Organic Coatings, 1993. **23**(1): p. 89-103.
163. Van Westing, E.P.M., G.M. Ferrari, and J.H.W. De Wit, *The determination of coating performance using electrochemical impedance spectroscopy.* Electrochimica Acta, 1994. **39**(7): p. 899-910.
164. Souto, R.M., M.M. Laz, and R.L. Reis, *Degradation characteristics of hydroxyapatite coatings on orthopaedic TiAlV in simulated physiological media investigated by electrochemical impedance spectroscopy.* Biomaterials, 2003. **24**(23): p. 4213-4221.
165. Balaji, J. and M.G. Sethuraman, *Improved corrosion resistance by forming multilayers over a copper surface by electrodeposition followed by a novel sol–gel coating method.* RSC Advances, 2016. **6**(98): p. 95396-95404.
166. Aparicio, M., et al., *Corrosion Protection of AISI 304 Stainless Steel with Melting Gel Coatings.* Electrochimica Acta, 2016. **202**: p. 325-332.
167. Ge, H.H., G.D. Zhou, and W. Wu, *Passivation model of 316 stainless steel in simulated cooling water and the effect of sulfide on the passive film.* Applied Surface Science, 2003. **211**(1-4): p. 321-334.
168. Ismail, K.M., et al., *The influence of bacteria on the passive film stability of 304 stainless steel.* Electrochimica Acta, 1999. **44**(26): p. 4685-4692.
169. Thammachart, M., *Corrosion Mechanisms On Composite Sol-Gel (CSG) Coating Systems*. 2005, Heriot-Watt University: Edinburgh, U.K.
170. Olivier, M.G. and M. Peolman, *Use of Electrochemical Impedance Spectroscopy (EIS) for the Evaluation of Electrocoatings Performances*, in *Recent researches in corrosion evaluation and protection*, R.S. Razavi, Editor. 2012.
171. Zheludkevich, M.L., et al., *Nanostructured sol-gel coatings doped with cerium nitrate as pre-treatments for AA2024-T3 corrosion protection performance.* Electrochimica Acta, 2005. **51**: p. 208-217.
172. Suppliers, P.I. *5L Specification for Line Pipe*. API 2004.
173. Montemor, M.F., et al., *Chemical composition and electronic structure of the oxide films formed on 316L stainless steel and nickel based alloys in high temperature aqueous environments.* Corrosion Science, 2000. **42**(9): p. 1635-1650.
174. Hanna, J.S., *Understanding Corrosion Protection and Failure Through Model Polymers in Thin Films*, in *Polymers and High Performance Materials*. 2012, The University of Southern Mississippi

175. *Q-Panel Steel and Iron Phosphated Panels*, Q.-L. Corporation, Editor. 2007, [Online] Available from: Q-Lab Corporation: www.q-lab.com.
176. De, A.K., et al., *Quantitative measurement of deformation-induced martensite in 304 stainless steel by X-ray diffraction.* Scripta Materialia, 2004. **50**(12): p. 1445-1449.
177. Kundu, S., et al., *Diffusion bonding of commercially pure titanium to 304 stainless steel using copper interlayer.* Materials Science and Engineering: A, 2005. **407**(1-2): p. 154-160.
178. T, N. *Perkin Elmer Spectrum 100 with Universal ATR*. 2007; [Online] Available from: http://eqdb.nrf.ac.za/equipment/spectrometers/perkin-elmer-spectrum-100-universal-atr.
179. Hering, N., et al., *Synthesis of polymeric precursors for the formation of nanocrystalline Ti-C-N/amorphous Si-C-N composites.* Applied Organometallic Chemistry, 2001. **15**(10): p. 879-886.
180. Hong, J.-K., H.-R. Kim, and H.-H. Park, *The effect of sol viscosity on the sol–gel derived low density SiO2 xerogel film for intermetal dielectric application.* Thin Solid Films, 1998. **332**(1–2): p. 449-454.
181. Jeon, H.-J., S.-C. Yi, and S.-G. Oh, *Preparation and antibacterial effects of Ag–SiO2 thin films by sol–gel method.* Biomaterials, 2003. **24**(27): p. 4921-4928.
182. Yoldas, B.E., *Modification of polymer-gel structures.* Journal of Non-Crystalline Solids, 1984. **63**(1): p. 145-154.
183. Rodic, P., et al., *Corrosion behaviour and chemical stability of transparent hybrid sol-gel coatings deposited on aluminium in acidic and alkaline solutions.* Progress in Organic Coatings, 2018. **124**: p. 286-295.
184. Patel, S., et al., *Transparent TiO 2 nanotubes on zirconia for biomedical applications.* RSC Advances 2017. **7**(48): p. 30397-30410.
185. Al-Amin, M., et al., *Solar Assisted Photocatalytic Degradation of Reactive Azo Dyes in Presence of Anatase Titanium Dioxide.* International Journal of Latest Research in Engineering and Technology, 2016. **2**(3): p. 14-21.
186. Schneider, R., *Scanning Electron Microscopy Studies of Nafion Deformation into Silicon Micro Trenches for Fuel Cell Applications*. 2008.
187. Brundle, C.R., et al., *Encyclopedia of materials characterization: surfaces, interfaces, thin films*. 1992, Boston;Greenwich, CT;: Butterworth-Heinemann.
188. Atteberry, J. *How Scanning Electron Microscopes Work*. How stuff works 2009; Available from: https://science.howstuffworks.com/scanning-electron-microscope2.htm.
189. McSwiggen, P. *WDS VS EDS*. TechNotes 2005; [Online] Available from: http://www.mcswiggen.com/TechNotes/WDSvsEDS.htm.
190. *Nanoindentation*. Techniques; [Online] Available from: https://www.micromaterials.co.uk/techniques/nanoindentation/.
191. Oliver, W.C. and G.M. Pharr, *An improved technique for determining hardness and elastic modulus using load and displacement sensing indentation experiments.* Journal of Materials Research, 1992. **7**(6): p. 1564-1583.
192. Oliver, W.C. and G.M. Pharr, *Measurement of hardness and elastic modulus by instrumented indentation: Advances in understanding and refinements to methodology.* Journal of Materials Research, 2004. **19**(1): p. 3-20.
193. Blees, M.H., et al., *The effect of friction on scratch adhesion testing: application to a sol–gel coating on polypropylene.* Thin Solid Films, 2000. **359**(1): p. 1-13.
194. Kareer, A., *Nano-scratch hardness and the Lateral Size Effect (LSE)*, in *Department of Engineering*. 2015, University of Leicester.
195. Lu, N.D., J. Cai, and L.L. Li, *Dependence of interfacial adhesion of Co-P film on its microstructure.* SURFACE & COATINGS TECHNOLOGY, 2012. **206**(23): p. 4822-4827.

196. Koumoulos, E.P., et al., *Nanomechanical and nanotribological properties of hydrophobic fluorocarbon dielectric coating on tetraethoxysilane for electrowetting applications.* SURFACE & COATINGS TECHNOLOGY, 2012. **206**(19-20): p. 3823-3831.
197. Barshilia, H.C., et al., *Ar + H-2 plasma etching for improved adhesion of PVD coatings on steel substrates.* VACUUM, 2012. **86**(8): p. 1165-1173.
198. Bull, S.J., *Failure modes in scratch adhesion testing.* Surface and Coatings Technology, 1991. **50**(1): p. 25-32.
199. Bull, S.J., *Failure mode maps in the thin film scratch adhesion test.* Tribology International, 1997. **30**(7): p. 491-498.
200. *Scratch tester*. [Online] Available from: https://www.pvd-coatings.co.uk/pvd-coating-technology/testing-equipment/scratch-tester/.
201. Li, D., *Understanding Coating Failure Using Scratch Testing*. 2013, Nanovea.
202. Tribotechnic. *Milli scratch tester*. 2009 [Online] Available from; http://www.tribotechnic.com/contenu.php?page=milliscratch].
203. Li. D. *Understanding Coating Failures Using Scratch Testing*. 2013; [Online] Available from: http://nanovea.com/App-Notes/coating-failure-scratch.pdf.
204. Wang, H., R. Akid, and M. Gobara, *Scratch-resistant anticorrosion sol–gel coating for the protection of AZ31 magnesium alloy via a low temperature sol–gel route.* Corrosion Science, 2010. **52**(8): p. 2565-2570.
205. Raghavendra, G., et al., *Evaluation of mechanical and tribological properties of bamboo-glass hybrid fiber reinforced polymer composite.* Journal of Industrial Textiles, 2015. **46**(1).
206. Buchheit, R.G., et al., *A Correlation Between Salt Spray and Electrochemical Impedance Spectroscopy Test Results for Conversion-Coated Aluminum Alloys.* Corrosion, 1998. **54**(1): p. 61-72.
207. *Salt Spray Test Chamber*. Environment test Chamber 2016; [Online] Available from: http://www.haidatestequipment.com/products/salt-spray-test-chamber.htm.
208. G Aldrich-Smith, N.M.J.J.H., *A Round Robin to Measure the Adhesion of Thin Coatings*, in *Mechanical Property Measurement of Thin Films and Coatings*, VAMAS, Editor. 2004, Materials Performance National Physical Laboratory: United Kingdom.
209. Voevodin, A.A., C. Rebholz, and A. Matthews, *Comparative tribology studies of hard ceramic and composite metal-DLC coatings in sliding friction conditions.* Tribology Transactions, 1995. **38**(4): p. 829-836.
210. Pierson, E.S. *Electron microscopy (EM)*. 2011; [Online] Available from: http://www.vcbio.science.ru.nl/en/fesem/eds/.
211. Benjamin, P. and C. Weaver, *Measurement of Adhesion of Thin Film.* Proceedings of the Royal Society, 1960. **254**: p. 163-176.
212. Vasconcelos, D.C.L., et al., *Infrared Spectroscopy of Titania Sol-Gel Coatings on 316L Stainless Steel* Materials Sciences and Applications, 2011. **2**: p. 1375-1382.
213. Kiele, E., et al., *Sol-gel derived coatings for the conservation of steel.* Processing and Application of Ceramics, 2015. **9**(2): p. 81-89.
214. Romero-Gavilán, F., et al., *Control of the degradation of silica sol-gel hybrid coatings for metal implants prepared by the triple combination of alkoxysilanes.* Journal of Non-Crystalline Solids, 2016. **453**: p. 66-73.
215. White, R.G., *Handbook of industrial infrared analysis*. 1964, New York: Plenum Press.
216. Griffiths, P.R. and J.A. De Haseth, *Fourier transform infrared spectrometry*. Vol. 83;83.;. 1986, Chichester;New York;: Wiley.
217. Malzbender, J., G. de With, and J.M.J. den Toonder, *Determination of the elastic modulus and hardness of sol–gel coatings on glass: influence of indenter geometry.* Thin Solid Films, 2000. **372**(1–2): p. 134-143.

218. Ioffe Institute Database., *Physical properties of Silicon (Si)* http://www.ioffe.ru/SVA/NSM/Semicond/Si/.
219. Boyd, E.J. and D. Uttamchandani, *Measurement of the Anisotropy of Young's Modulus in Single-Crystal Silicon.* Journal of Microelectromechanical Systems 2012. **21**(1): p. 243-249.
220. Wortman, J.J. and R.A. Evans, *Young's Modulus, Shear Modulus, and Poisson's Ratio in Silicon and Germanium.* Journal of Applied Physics, 1965. **36**: p. 153-156.
221. Bierwagen, G.P., et al., *Studies of a new accelerated evaluation method for coating corrosion resistance — thermal cycling testing.* Progress in Organic Coatings, 2000. **39**(1): p. 67-78.
222. Nicholson, J., *Evaluation of the anti-corrosion performance of water-borne ionomer coatings using AC impedance.* Surface coatings international 1994. **77**: p. 472-476.
223. Siva, T. and S. Sathiyanarayanan, *Cationic surfactant assisted synthesis of poly o-methoxy aniline (PoMA) hollow spheres and their self healing performance.* RSC ADVANCES, 2016. **6**(4): p. 2944-2950.
224. Santana, I., et al., *Corrosion protection of carbon steel by silica-based hybrid coatings containing cerium salts: Effect of silica nanoparticle content.* SURFACE & COATINGS TECHNOLOGY, 2015. **265**: p. 106-116.
225. Sarmento, V.H.V., et al., *Corrosion protection of stainless steel by polysiloxane hybrid coatings prepared using the sol–gel process.* Surface & Coatings Technology, 2010. **204**(16): p. 2689-2701.
226. Kirtay, S., *Preparation of hybrid silica sol–gel coatings on mild steel surfaces and evaluation of their corrosion resistance.* Progress in Organic Coatings, 2014. **77**(11): p. 1861-1866.
227. Liu, C., et al., *An electrochemical impedance spectroscopy study of the corrosion behaviour of PVD coated steels in 0.5 N NaCl aqueous solution: Part II. EIS interpretation of corrosion.* Corrosion Science, 2003. **45**(6): p. 1243-1256.
228. Lin, C., T. Nguyen, and M.E. McKnight, *Relation between AC impedance data and degradation of coated steel.* Progress in Organic Coatings, 1992. **20**(2): p. 169-186.
229. Resources, R.S.a. *Fitting EIS Data - Diffusion Elements - Warburg*. 2001; [Online] Available from: http://www.consultrsr.net/resources/eis/diffusion.htm.
230. Thompson, I. and D. Campbell, *Interpreting Nyquist responses from defective coatings on steel substrates.* Corrosion Science, 1994. **36**(1): p. 187-198.
231. Smith, B.C. *Alcohols—The Rest of the Story*. Spectroscopy, 2017. **32**, 19-23.
232. Kennepohl, D., S. Farmer, and W. Reusch *Infrared Spectra of Some Common Functional Groups*. Chemistry, 2016.
233. Bautista, Y., et al., *Relation between the scratch resistance and the chemical structure of organic–inorganic hybrid coatings.* Progress in Organic Coatings, 2011. **70**(4): p. 358-364.
234. Phani, A.R., et al., *Enhanced corrosion resistance by sol-gel-based ZrO2-CeO2coatings on magnesium alloys.* Materials and Corrosion 2005. **56**(2): p. 77-82.
235. Amerio, E., et al., *Scratch resistance of nano-silica reinforced acrylic coatings.* Progress in Organic Coatings, 2008. **62**(2): p. 129-133.
236. Bondioli, F., R. Taurino, and A.M. Ferrari, *Functionalization of ceramic tile surface by sol–gel technique.* Journal of Colloid And Interface Science, 2009. **334**(2): p. 195-201.
237. Toselli, M., et al., *Sol–gel derived hybrid coatings for the improvement of scratch resistance of polyethylene.* Journal of Sol-Gel Science and Technology, 2007. **43**(1): p. 73-83.
238. Aldrich-Smith, G., N. Jennett, and J. Housden, *Adhesion of thin coatings—the VAMAS (TWA 22-2) interlaboratory exercise.* Surface and Coatings Technology, 2005. **197**(2-3): p. 336-344.

239. Aldrich-Smith, G., N.M. Jennett, and J. Housden, *A Round Robin to Measure the Adhesion of Thin Coatings*, in *Mechanical Property Measurement of Thin Films and Coatings*. 2004, VAMAS: United Kingdom.
240. Musil, J. and M. Jirout, *Toughness of hard nanostructured ceramic thin films.* Surface & Coatings Technology, 2007. **201**(9-11): p. 5148-5152.
241. Berriche, R. and R.T. Holt, *Effect of Load on the Hardness of Hot Isostatically Pressed Silicon Nitride.* Journal of the American Ceramic Society, 1993. **76**(6): p. 1395-1400.
242. Yurkov, A.L. and Bradt, *Fracture Mechanics of Ceramics*, ed. D. Munz. 1996, New York: Plenum.
243. Quinn, J.B. and G.D. Quinn, *Indentation brittleness of ceramics: a fresh approach.* Journal of Materials Science, 1997. **32**: p. 4331-4346.
244. Takadoum, J. and H.H. Bennani, *Influence of substrate roughness and coating thickness on adhesion, friction and wear of TiN films.* Surface & Coatings Technology, 1997. **96**(2-3): p. 272-282.
245. Brasher, D.M. and A.H. Kingsbury, *Electrical measurements in the study of immersed paint coatings on metal. I. Comparison between capacitance and gravimetric methods of estimating water-uptake.* Journal of Applied Chemistry, 1954. **4**(2): p. 62-72.
246. Santágata, D.M., et al., *Evaluation of the surface treatment effect on the corrosion performance of paint coated carbon steel.* Progress in Organic Coatings, 1998. **33**(1): p. 44-54.
247. Rakesh N. Patil, B.V.S., Prakash A. Mahanwar, *Electrochemical Impedance Spectroscopy of Hybrid Epoxy Resin Emulsion Coatings* Journal of Minerals and Materials Characterization and Engineering, 2012. **11**: p. 1012-1019.
248. Huang, K.Y., et al., *Preparation and anticorrosive properties of hybrid coatings based on epoxy-silica hybrid materials.* Journal of Applied Polymer Science, 2009. **112**: p. 1933-1942.
249. Lakshmi, R.V., et al., *Effect of the size of silica nanoparticles on wettability and Surface chemistry of sol-gel superhydrophobic and oleophobic nanocomposite coatings.* Applied Surface Science, 2014. **320**: p. 780-786.
250. Peres, R.N., et al., *Influence of the addition of SiO2 nanoparticles to a hybrid coating applied on an AZ31 alloy for early corrosion protection.* Surface & Coatings Technology, 2016. **303**: p. 372-384.
251. Philipp, G. and H. Schmidt, *New materials for contact lenses prepared from Si- and Ti- alkoxides by the sol-gel process.* Journal of Non-Crystalline Solids, 1984. **63**: p. 283-292.
252. Hoebbel, D., M. Nacken, and H. Schmidt, *On the Existence and Hydrolytic Stability of Titanosiloxane Bonds in the System: Glycidoxypropyltrimethoxysilane-Water-Titaniumtetraethoxide.* Journal of Sol-Gel Science and Technology, 1998. **13**: p. 37-43.
253. Doslu, S.T., B.D. Mert, and B. Yazici, *Polyindole top coat on TiO2 sol–gel films for corrosion protection of steel.* Corrosion Science, 2013. **66**: p. 51-58.
254. Hu, Y.W., et al., *A corrosion-resistance superhydrophobic TiO2 film.* APPLIED SURFACE SCIENCE, 2012. **258**(19): p. 7460-7464.
255. Aliofkhazraei, M., et al., *Enhancement of corrosion protection of micro-arc oxidation by applying nanostructured TiO2 thin film via the "sol-gel" method.* Anti-Corrosion Methods and Materials, 2010. **2**: p. 75-82.
256. Messaddeq, S.H., et al., *Microstructure and corrosion resistance of inorganic-organic (ZrO2-PMMA) hybrid coating on stainless steel.* Journal of Non-Crystalline Solids, 1999. **247**(1-3): p. 164-170.
257. Chuter, J.C.R.a.D.J., in *Proc. 8th Int. Congr. Metallic Corrosion*. 1981: Mainz. p. 1068.
258. Cimieri, I., *Sol-gel preparation and characterization of titanium dioxide films for degradation of organic pollutants*, in *Physics*. 2013-2014, Ghent University.

259. Gardner, L., *The use of stainless steel in structures.* Progress in Structural Engineering and Materials, 2005. **7**: p. 45-55.
260. Rajasekharan, V., et al., *Electrochemical Evaluation of Anticorrosive Performance of Organic Acid Doped Polyaniline Based Coatings.* INTERNATIONAL JOURNAL OF ELECTROCHEMICAL SCIENCE, 2013. **8**(9): p. 11327-11336.
261. Santana, J.J., et al., *Evaluation of Ecological Organic Paint Coatings via Electrochemical Impedance Spectroscopy.* INTERNATIONAL JOURNAL OF ELECTROCHEMICAL SCIENCE, 2012. **7**(7): p. 6489-6500.
262. Shi, X., et al., *Effect of nanoparticles on the anticorrosion and mechanical properties of epoxy coating.* Surface & Coatings Technology, 2009. **204**(3): p. 237-245.
263. Suegama, P.H., et al., *Corrosion behavior of carbon steel protected with single and bi-layer of silane films filled with silica nanoparticles.* Surface & Coatings Technology, 2008. **202**(13): p. 2850-2858.
264. Dolatzadeh, F., S. Moradian, and M.M. Jalili, *Influence of various surface treated silica nanoparticles on the electrochemical properties of SiO2/polyurethane nanocoatings.* Corrosion Science, 2011. **53**(12): p. 4248-4257.

Appendices

Appendix A: Sample with inorganic/hybrid sol-gel coating doped with 5.6% of titanium precursor – Second batch: $I_{,B2,5.6\%,304}$

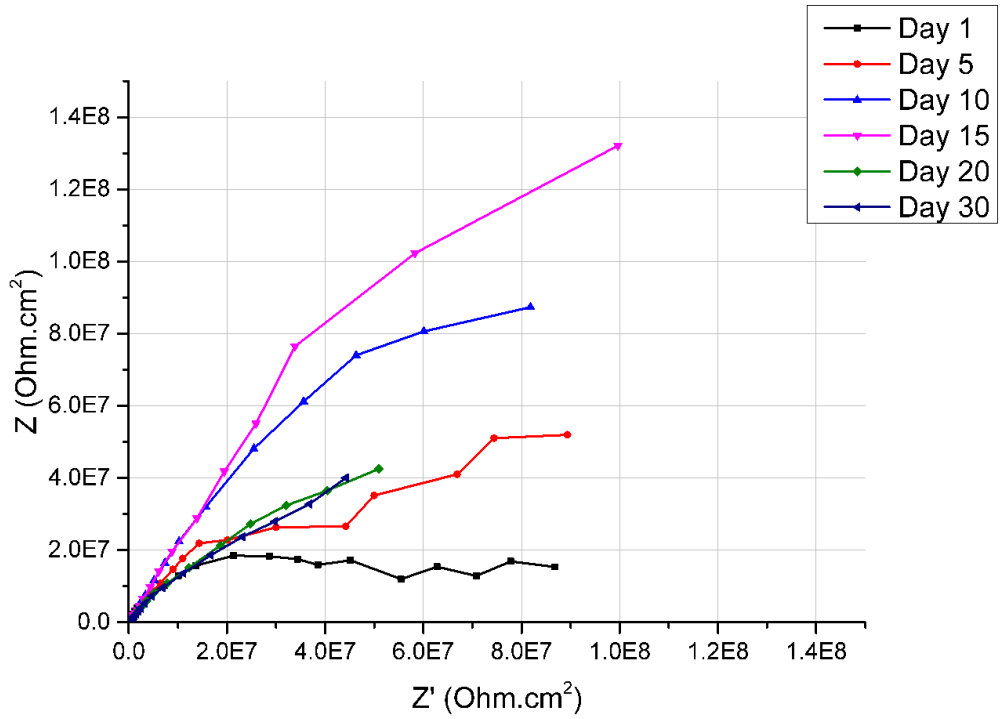

Nyquist plot of inorganic/hybrid sol-gel coated sample doped with 5.6% of titanium precursor

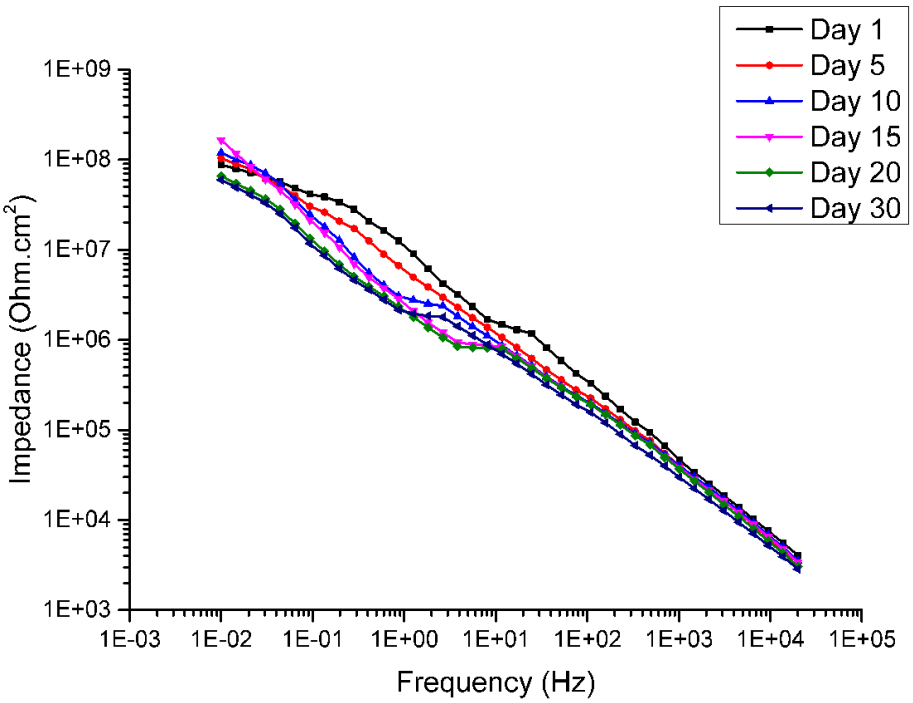

Bode impedance plot of inorganic/hybrid sol-gel coated sample doped with 5.6% of titanium precursor

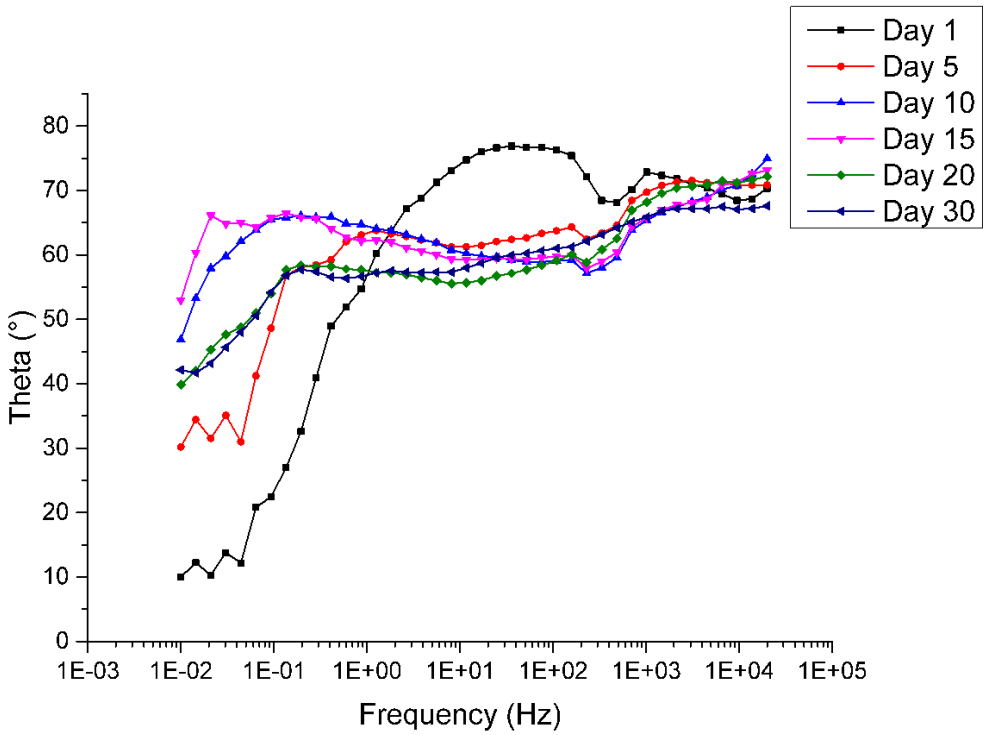

Bode phase plot of inorganic/hybrid sol-gel coated sample doped with 5.6% of titanium precursor

Appendix B: Sample with inorganic/hybrid sol-gel coating doped with 11.3% of titanium precursor – Second batch: $I_{,B2,11.3\%,304}$

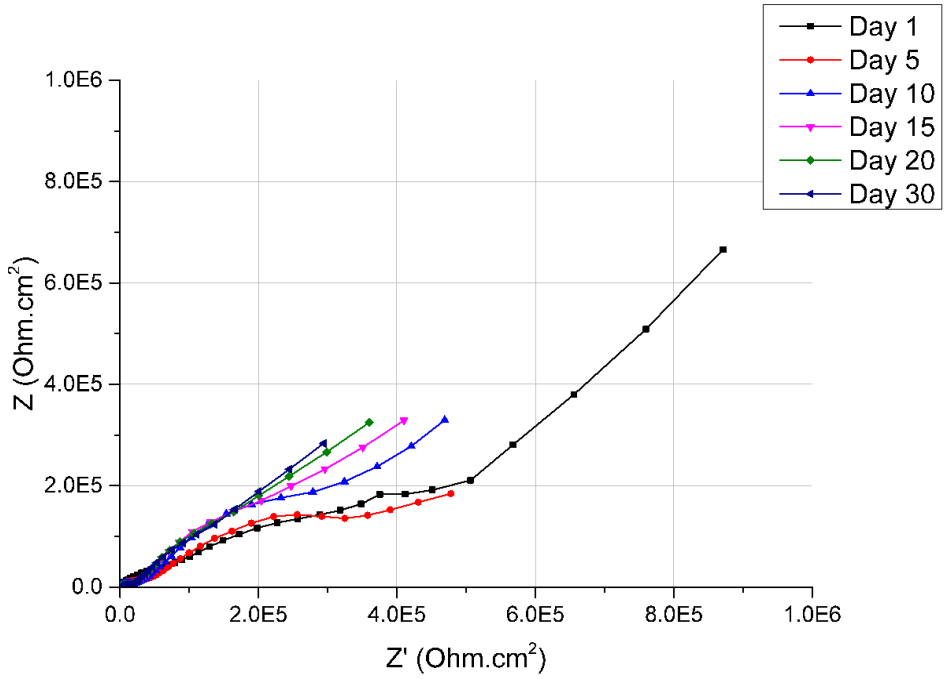

Nyquist plot of inorganic/hybrid sol-gel coated sample doped with 11.3% of titanium precursor

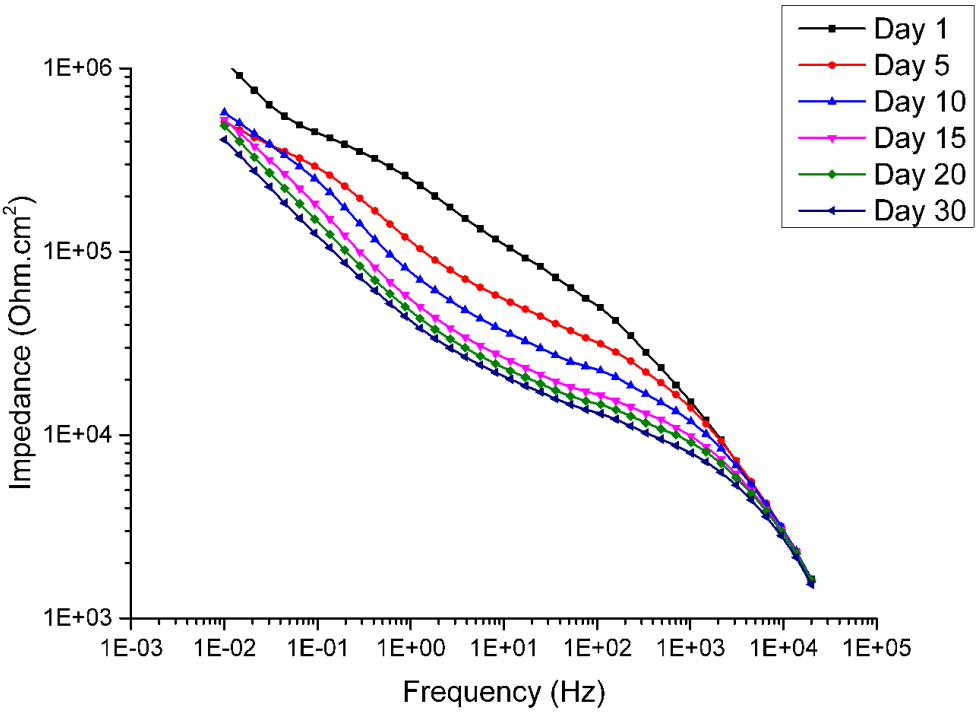

Bode impedance plot of inorganic/hybrid sol-gel coated sample doped with 11.3% of titanium precursor

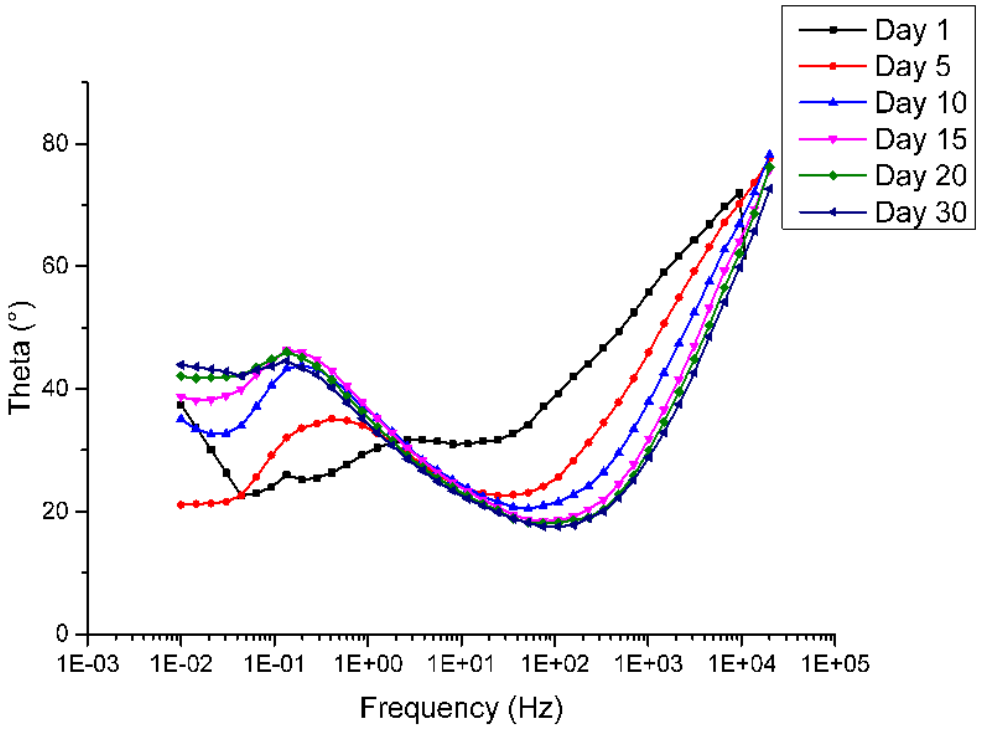

Bode phase plot of inorganic/hybrid sol-gel coated sample doped with 11.3% of titanium precursor

Appendix C: Sample with hybrid/composites coating – Second batch: $H_{,B2,0\%,304}$

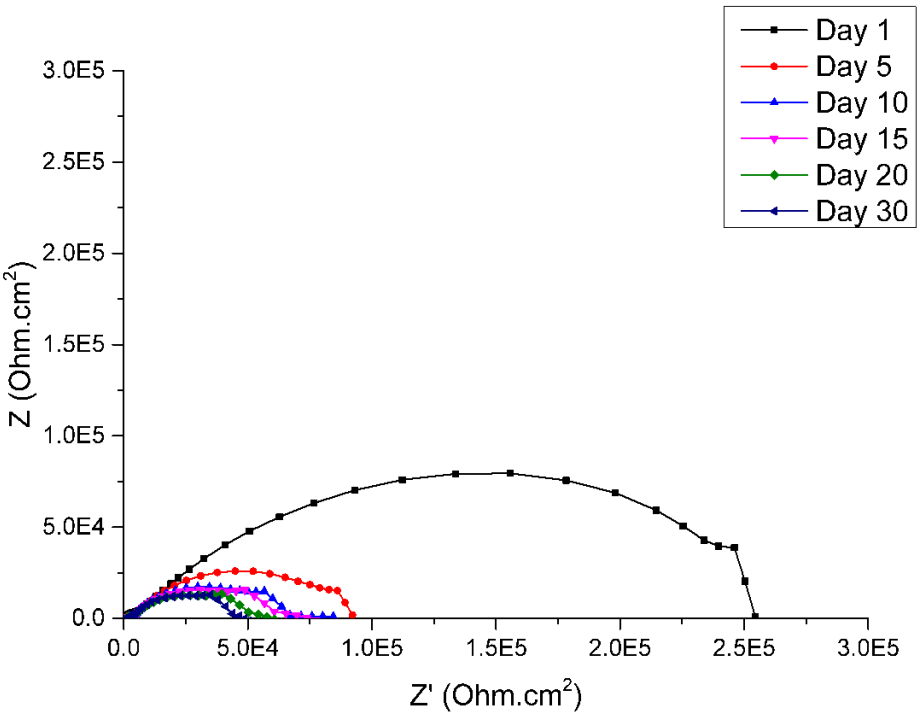

Nyquist plot of hybrid/composites sol-gel coating sample

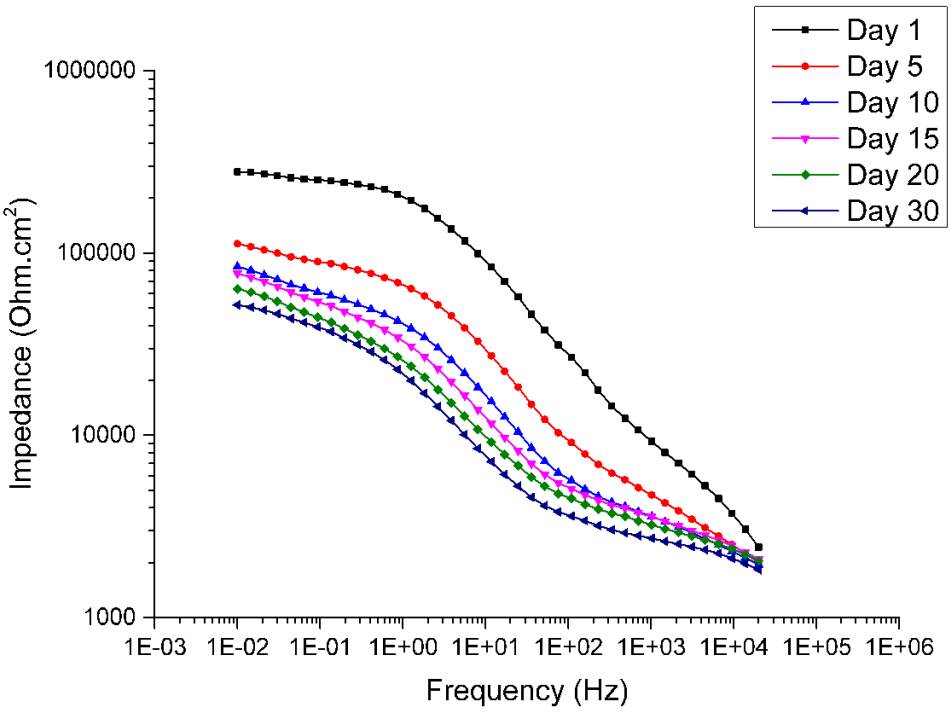

Bode impedance plot of hybrid/composites sol-gel coating sample

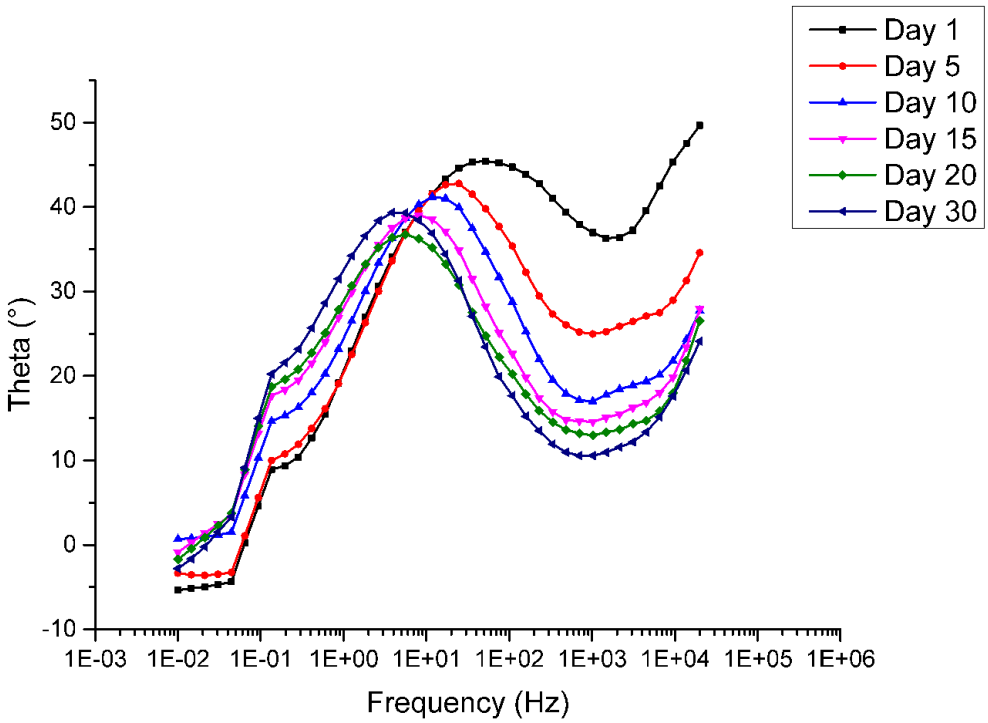

Bode phase plot of hybrid/composites sol-gel coating sample

Appendix D: Nyquist and Bode plots of samples from Batch 3

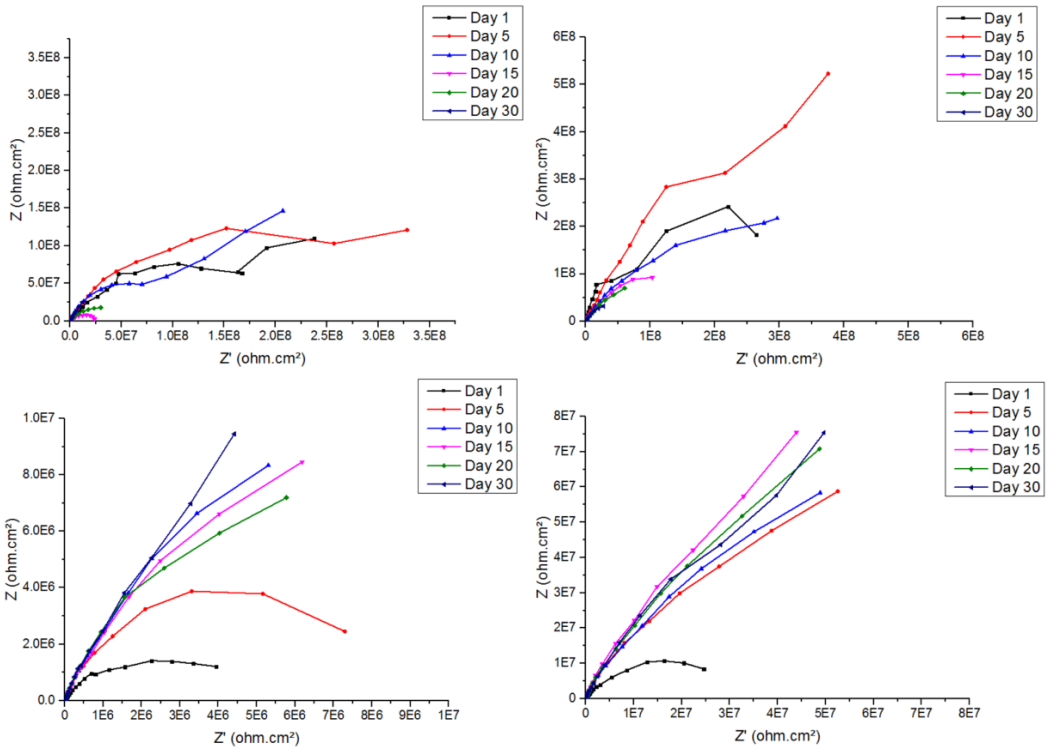

Nyquist plot of the sample a) $I_{B3,0\%,Mix,N2}$ b) $I_{B3,0\%,Ip,N2}$ c) $I_{B3,0\%,Mix,Air}$ d) $I_{B3,0\%,Ip,Air}$ over 30 days of immersion

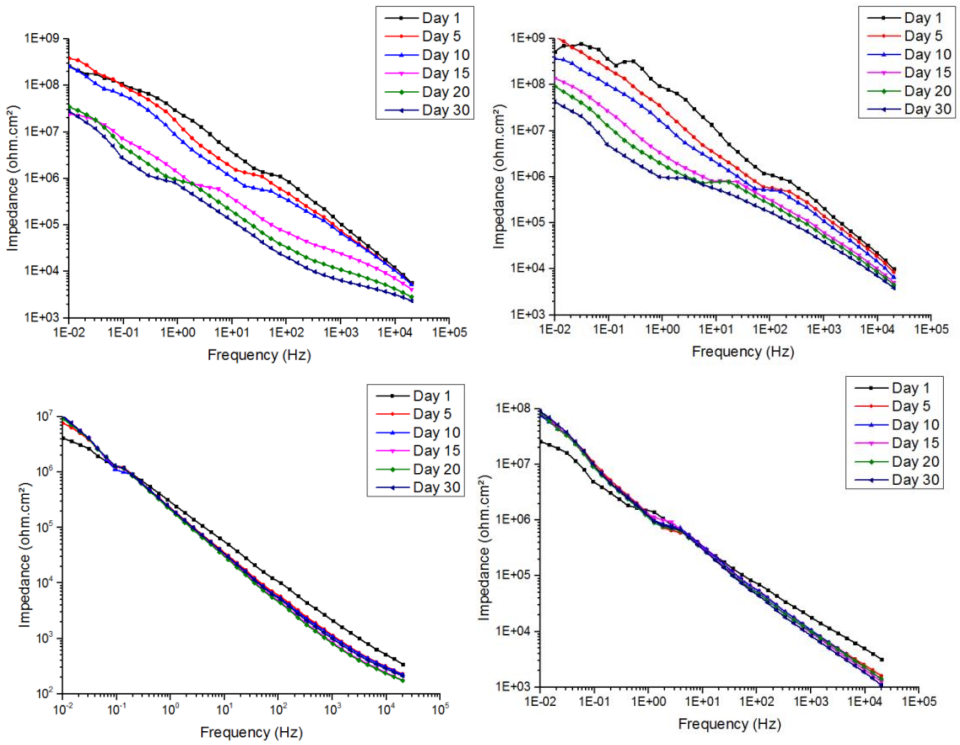

Bode impedance plot of the sample a) $I_{B3,0\%,Mix,N2}$ b) $I_{B3,0\%,Ip,N2}$ c) $I_{B3,0\%,Mix,Air}$ d) $I_{B3,0\%,Ip,Air}$ over 30 days of immersion

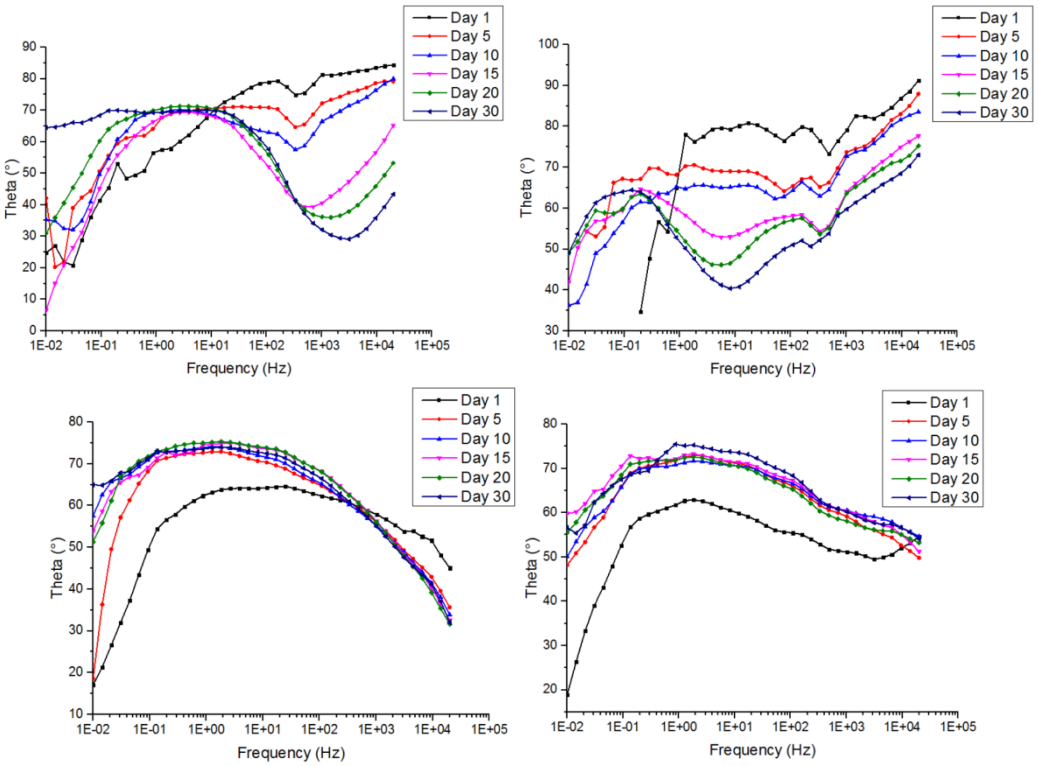

Bode phase shift plot of the sample a) $I_{,B3,0\%,Mix,N2}$ b) $I_{,B3,0\%,Ip,N2}$ c) $I_{,B3,0\%,Mix,Air}$ d) $I_{,B3,0\%,Ip,Air}$ over 30 days of immersion

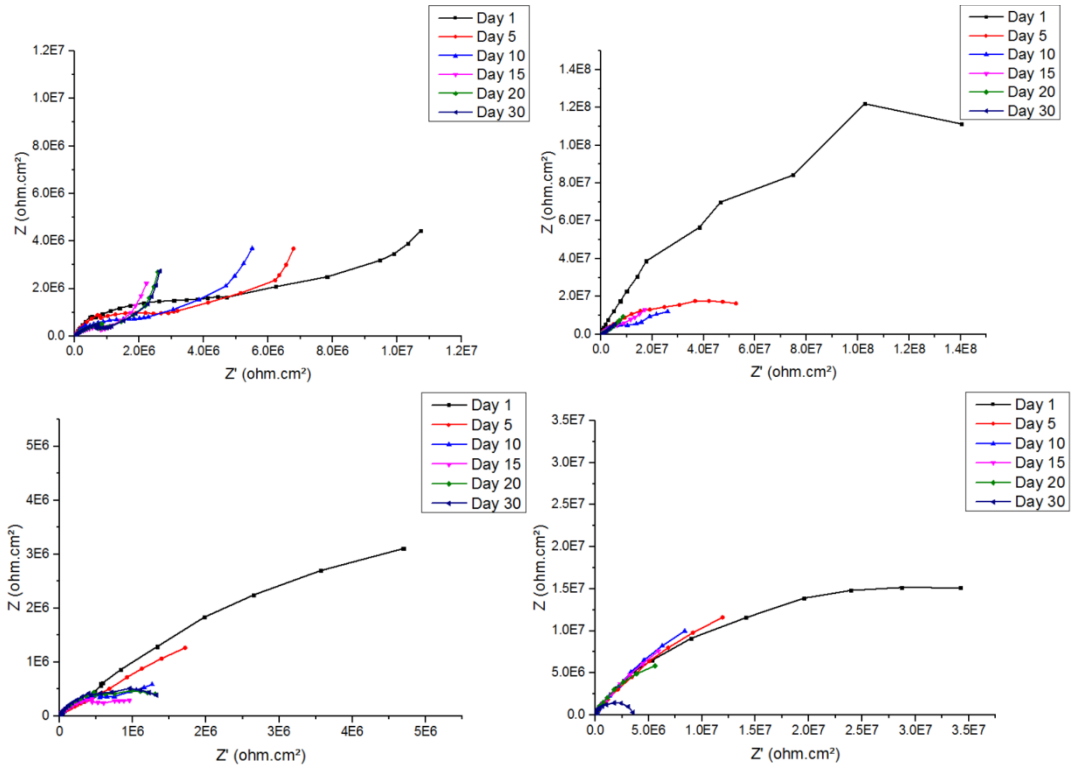

Nyquist plot of the sample a) $I_{,B3,2.8\%,Mix,N2}$ b) $I_{,B3,2.8\%,Ip,N2}$ c) $I_{,B3,2.8\%,Mix,Air}$ d) $I_{,B3,2.8\%,Ip,Air}$ over 30 days of immersion

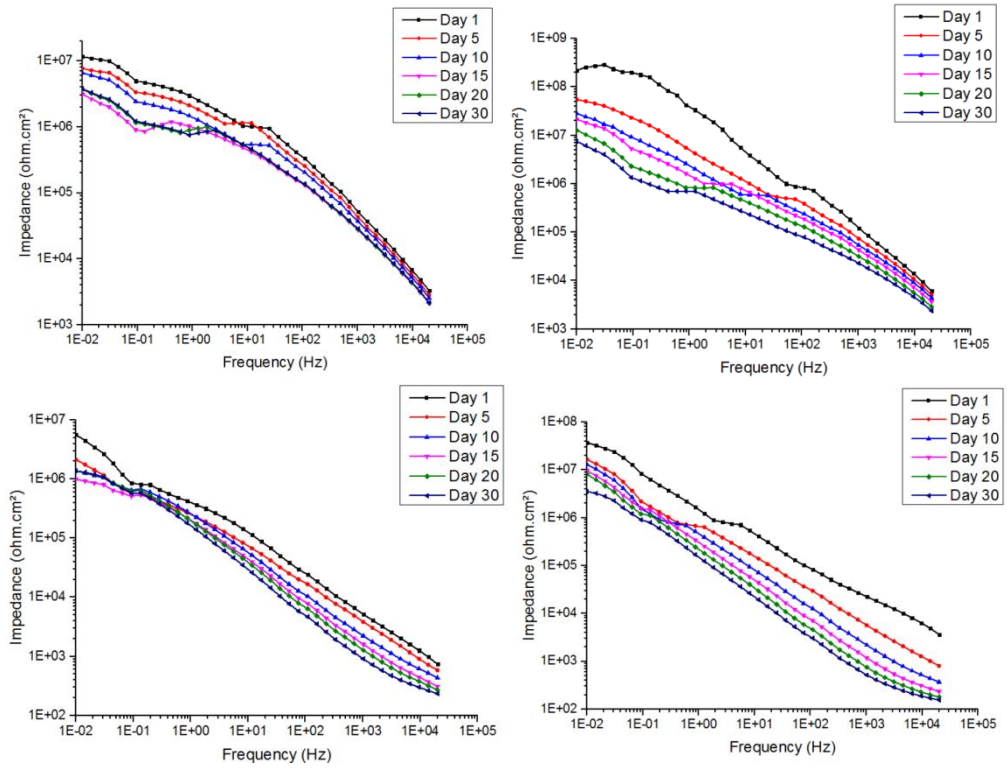

Bode impedance plot of the sample a) $I_{,B3,2.8\%,Mix,N2}$ b) $I_{,B3,2.8\%,Ip,N2}$ c) $I_{,B3,2.8\%,Mix,Air}$ d) $I_{,B3,2.8\%,Ip,Air}$ over 30 days of immersion

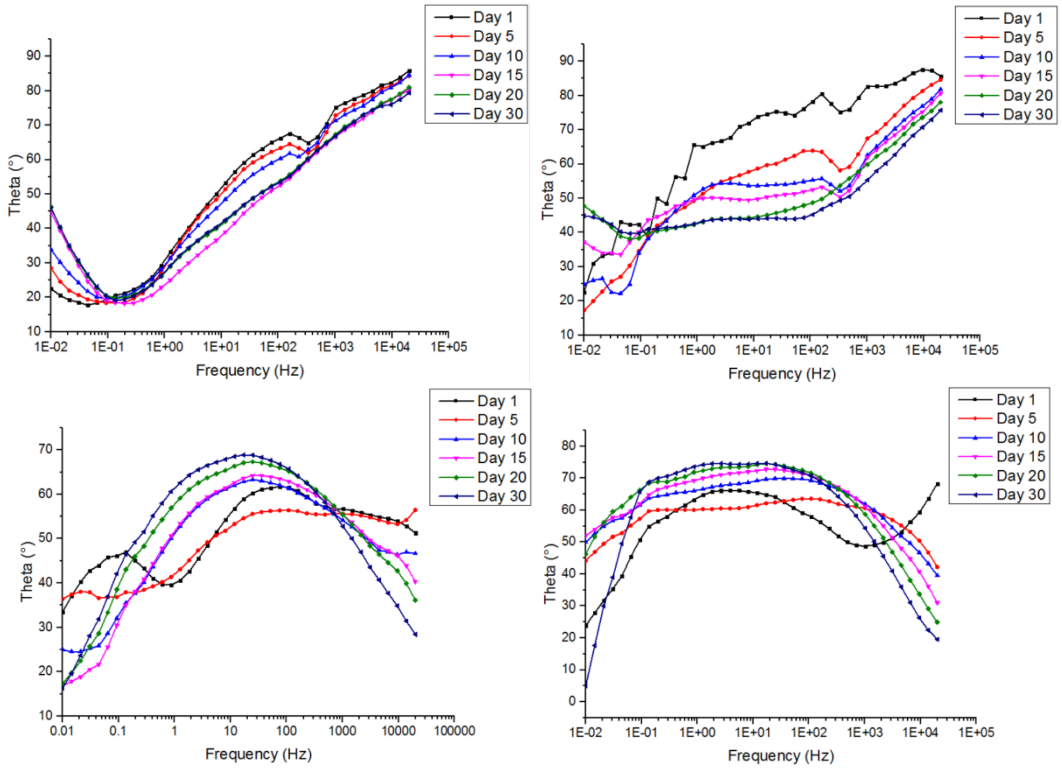

Bode phase shift plot of the sample a) $I_{,B3,2.8\%,Mix,N2}$ b) $I_{,B3,2.8\%,Ip,N2}$ c) $I_{,B3,2.8\%,Mix,Air}$ d) $I_{,B3,2.8\%,Ip,Air}$ over 30 days of immersion

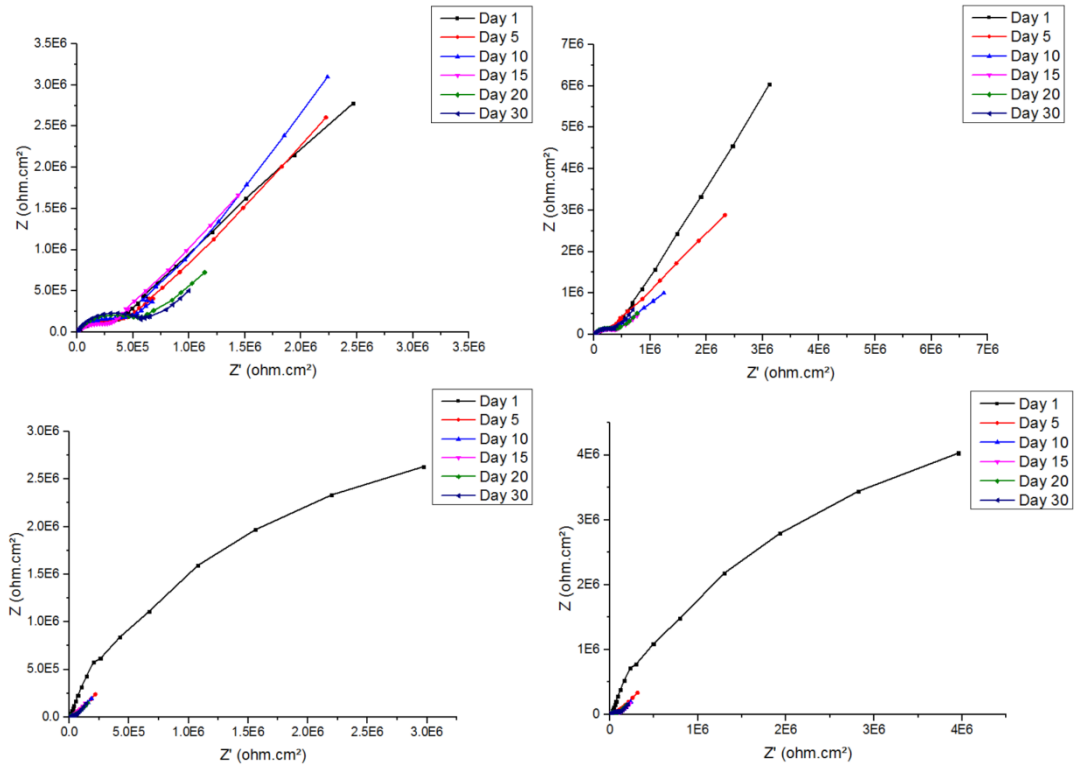

Nyquist plot of the sample a) $I_{B3,5.6\%,Mix,N2}$ b) $I_{B3,5.6\%,Ip,N2}$ c) $I_{B3,5.6\%,Mix,Air}$ d) $I_{B3,5.6\%,Ip,Air}$ over 30 days of immersion

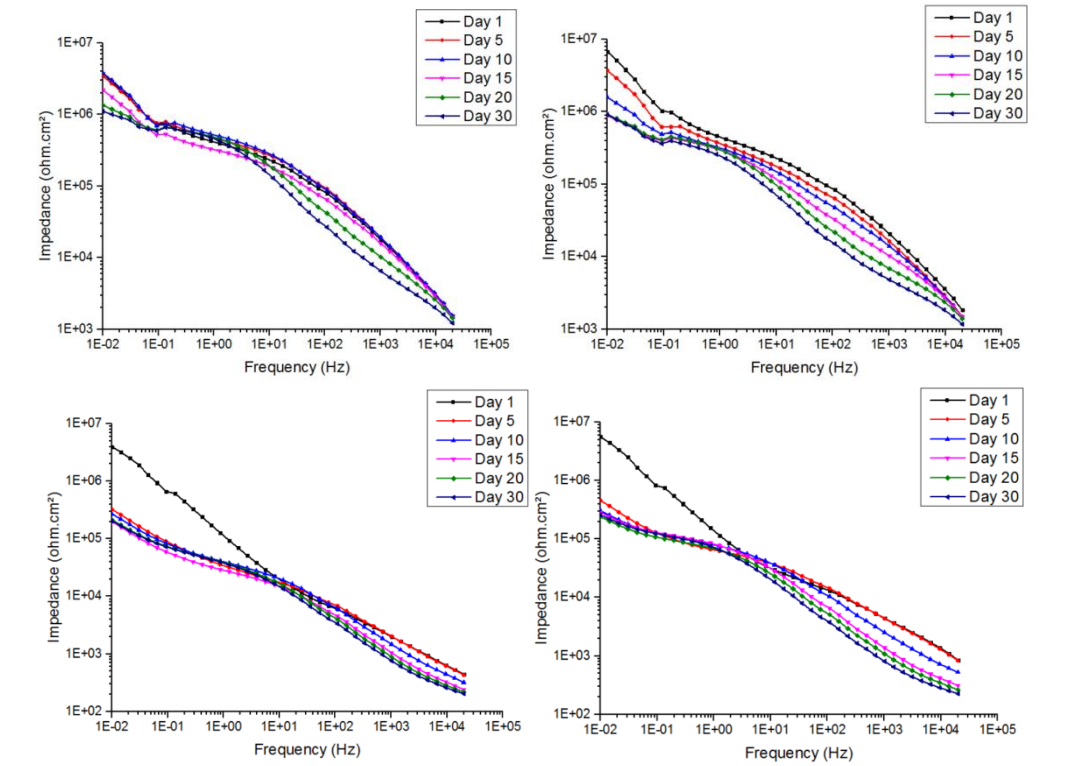

Bode impedance plot of the sample a) $I_{B3,5.6\%,Mix,N2}$ b) $I_{B3,5.6\%,Ip,N2}$ c) $I_{B3,5.6\%,Mix,Air}$ d) $I_{B3,5.6\%,Ip,Air}$ over 30 days of immersion

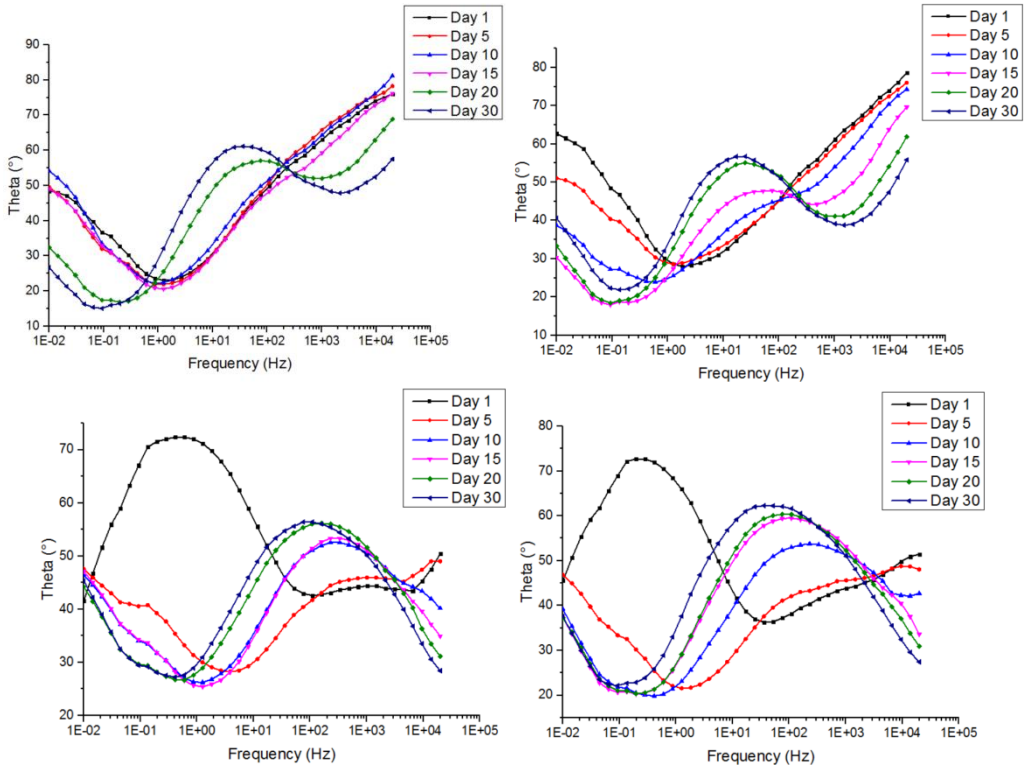

Bode phase shift plot of the sample a) $I_{,B3,5.6\%,Mix,N2}$ b) $I_{,B3,5.6\%,Ip,N2}$ c) $I_{,B3,5.6\%,Mix,Air}$ d) $I_{,B3,5.6\%,Ip,Air}$ over 30 days of immersion